School of Doctoral Studies in Biological Sciences
University of South Bohemia in České Budějovice
Faculty of Science

Function of the Type IV pili proteins in the cyanobacterium *Synechocystis* sp. PCC 6803

Ph.D. Thesis

Mgr. Markéta Linhartová

Supervisor: doc. Ing. Roman Sobotka, Ph.D.
Institute of Microbiology, CAS, Centre Algatech Třeboň
University of South Bohemia, Faculty of Science

České Budějovice 2021

This thesis should be cited as:

Linhartová, M., 2021: Function of the Type IV pili proteins in the cyanobacterium *Synechocystis* sp. PCC 6803. Ph.D. Thesis, University of South Bohemia, Faculty of Science, School of Doctoral Studies in Biological Sciences, České Budějovice, The Czech Republic, 150 pp.

Annotation

The thesis is focused on the function of the Type IV pili machinery in the cyanobacterium *Synechocystis* sp. PCC. 6803. In my work, I provided evidence that in phototrophs, some pilin proteins have acquired a novel function related to metal transport and assembly of photosynthetic complexes. The tight connection between the synthesis of the major pilin PilA1 and the biogenesis of photosynthetic complexes has been demonstrated in the *pilD* mutant lacking prepilins peptidase. I isolated and characterized *pilD* suppressor strains, which revealed the important role of the minor pilin PilA2 in the glycosylation of PilA1 and the restricted mobility of PilA1 prepilin in the membrane. My unpublished data indicate that the retraction mode of pili, driven by the PilT1 molecular motor, facilitates manganese uptake and the activity of this machine is critically important during the regulation from the exponential to the linear growth phase.

Declaration

I hereby declare that I am the author of this dissertation and that I have used only those sources and literature detailed in the list of references.

České Budějovice, 24.6.2021 Markéta Linhartová

This thesis originated from a partnership of the **Faculty of Science, University of South Bohemia**, and **Institute of Microbiology, CAS, Centre Algatech**, supporting doctoral studies in the **Molecular and Cell Biology and Genetics** study programme.

Přírodovědecká fakulta
Faculty of Science

Financial support

This work was financially supported by PhD student grant project GAJU 084/2011/P of the Grant Agency of the University of South Bohemia. Further, it was supported by Algatech and by project 14-13967S of the Grant Agency of the Czech Republic.

Acknowledgements

My biggest thanks go to Roman Sobotka who supervised me with patience for all the years although it sometimes was out of the lab scope. He is more than inspiring and I am grateful to be a member of his lab and happy to watch the progress. Consulting with Josef Komenda was an excellent way to learn a lot about science and life and I appreciate his sense of humour and forgiveness. I would like to thank Martin Tichý for processing the sequencing data, answering my questions and directing me occasionally. I thank Prof. Annegret Wilde and Prof. Taina Tyystjärvi for the opportunity to study and work in their labs. I am grateful to Radek Kaňa and his group for confocal microscopy and motivating scientific conversations. There are many past and recent lab colleagues whom I sincerely thank for exceptional help, inspiring chatting, and having fun. Thanks go to Adéla Kaňová, Jana Talbot, Lenka Moravcová, Martina Bečková, Jana Zahradníková, Lucie Kovářová, Parisa Rahimzadeh, and Anna Wysocka. I thank Jana Konoppová for many good advices, precious processing of labelled samples and oxgen evolution measurements. Eva Prachová has always been so friendly and does great technical support similar to Jan Pilný who is also a perfect officemate. I thank my friend Lenka 'Agnes' Bučinská for the electron microscopy results and support. Petra Skotnicová is a great mate who helped with my experiments during the time I stayed off the lab with my children and who cheers me up every day since I've come back. I'm extremely indebted to Vendula Krynická for being so close, open-minded and challenging friend and colleague.
Many thanks go to Amie Wheeldon for English proofreading. I am also indebted to my parents for supporting my studies (Mami a tati, díky, že jsem mohla studovat!). Dearest Pavel survives all times with me and gives me time for work since we've become parents. As well, I must thank my children Hynek and Astrid who made me more patient and sometimes furious enough to finish this long journey.

List of papers and author's contribution

Linhartová, M., Bučinská, L., Halada, P., Ječmen, T., Šetlík, J., Komenda, J., Sobotka, R. 2014. Accumulation of the Type IV prepilin triggers degradation of SecY and YidC and inhibits synthesis of Photosystem II proteins in the cyanobacterium *Synechocystis* PCC 6803. Molecular Microbiology 93:1207-1223. (IF = 4.419)
M.L. participated in the design of this study and prepared all data except for protein MS analyses, electron microscopy, and the measurement of oxygen evolution. Together with R.S., M.L. wrote the manuscript. The study was co-funded by a GAJU project obtained by M.L.

Chidgey, J.W., **Linhartová, M.**, Komenda, J., Jackson, P.J., Dickman, M.J., Caniffe, D.P., Pilný, J., Hunter, N., Sobotka, R. 2014. A cyanobacterial chlorophyll synthase-HliD complex associates with the Ycf39 protein and the YidC/Alb3 insertase. Plant Cell 26(3): 1267-1279. (IF = 9.338)
M.L. was involved in the purifications and analysis of ChlG complexes, and the manuscript revision.

Linhartová, M., Petra Skotnicová, P., Hakkila, K., Tichý, M., Komenda, J., Knoppová, J., Gilabert, J. F., Guallar V., Tyystjärvi,T., Sobotka, R. Manuscript. Mutations suppressing the lack of prepilin peptidase provide insights into the maturation of the major pilin protein in cyanobacteria. (Manuscript)
M.L. and R.S. designed together the study and wrote the manuscript. M.L. performed all experiments except for the molecular dynamics simulations, [35S] labelling, and genome sequencing.

Roman Sobotka, the supervisor of this Ph.D. thesis and corresponding author of these three publications fully acknowledges the stated contribution of Markéta Linhartová to these manuscripts.

doc. Ing. Roman Sobotka, Ph.D.

Contents

List of abbreviations

Chl	Chlorophyll
PCC	Pasteur Culture collection of Cyanobacteria
PSI	Photosystem I
PSI[1]	Monomeric photosystem I
PSI[3]	Trimeric photosystem I
PSII	Photosystem II
PSII[1]	Monomeric photosystem II
PSII[2]	Dimeric photosystem II
RC47	Photosystem II assembly complex lacking the inner antenna CP43
RCII	Photosystem II assembly complex lacking CP43 and CP47
RCIIa	A form of RCII containing Ycf48 and CyanoP
RCII*	A form of RCII containing Ycf48, CyanoP, and Ycf39/Hlip complex
RCCII	Reaction centre complex of photosystem II
Synechocystis	*Synechocystis* sp. PCC 6803
TM	Thylakoid membrane
WT	Wild type

1. Preface

1.1 Cyanobacteria – bacterial (blue-green) cousins of plants

Cyanobacteria form one of the largest and the most important bacterial phyla that emerged no later than 3.5 billion years ago (Schopf, 2006). A trait that makes cyanobacteria distinct from other bacteria is, first of all, a unique type of metabolism known as oxidative photosynthesis. Powered by the energy of photons, specialized cyanobacterial protein complexes oxidize water molecules and, utilizing obtained electrons, generate the power required for cell proliferation. Switching to such a unique metabolic strategy led to extensive modifications of the original bacterial cell, and thus these cyanobacteria have been inaccurately termed blue-green algae (eukaryotic) for many decades. However, it is without question that cyanobacteria are a distinct group of prokaryotes of Gram-negative type. Although more than a hundred protein families universally shared among cyanobacteria have no counterparts in other bacteria (Mulkidjanian et al., 2006).

The subject linking together research communities working on cyanobacteria, algae and plants is oxygenic photosynthesis. Although modern plants and cyanobacteria have evolved independently for a billion years, the photosynthetic apparatus has remained highly conserved and results obtained using cyanobacteria are often directly applicable to the understanding of processes in algal and plant chloroplasts. Despite the fact that the recent interest in cyanobacterial biotechnology moved the whole research field closer to microbiology, even nowadays, the cyanobacterial community is closer to algal and plant biologists rather than with ‘classical’ microbiologists. On the other hand, given the conservation of photosynthetic apparatus in all groups of oxygenic phototrophs, it is tempting to hold back the fact that the cyanobacterial photosynthesis occurs in a bacterial cell - a different and probably more complex environment than can be found in plastids. Indeed, the evolution of cyanobacterial cells towards oxygenic photosynthesis had to result in adaptation and remodelling of the original bacterial structures and one should be aware that photosynthesis in cyanobacteria can highly depend on typical bacterial structures absent in recent chloroplasts.

Type IV pili filaments are an example of a bacterial structure that have remained well preserved in cyanobacteria since their evolutionary branching from other bacteria. These hair-like appendages are found on the cell surface but they are anchored in the plasma membrane and undergo dynamic polymerization and depolymerization. Pili serve in a diverse spectrum of functions including cell motility, DNA uptake and secretion, and

therefore pili apparatus are being called a bacterial Swiss Army knife (Berry and Pelicic, 2015). Given the trophic strategy, it is not surprising that the pili-mediated cell motility in cyanobacteria is highly dependent on light signals (Bhaya et al., 2001a); a range of photoreceptors can trigger phototactic signalling in the cyanobacterial cell (Yoshihara et al., 2001). Even so, a functional connection between pili fibres anchored in the plasma membrane, and the photosynthetic apparatus embedded in the endogenous thylakoid membrane, appears unlikely. Surprisingly, in the model cyanobacterium *Synechocystis* PCC 6803 (hereafter *Synechocystis*) the major pilin protein (PilA1), a key subunit of pili fibres, has been localized in both the plasma membrane and the thylakoid membrane (Selão et al., 2016). In addition, enigmatic defects (related to photosynthesis) have been described in this cyanobacterium after deletion of *pilA1* gene. Such a mutant strain exhibits enhanced photobleaching of photosynthetic apparatus after light exposure and releases UV-absorbing pigments into the growth media (Bhaya et al., 1999; Bhaya et al., 2000). Regarding the function of pilin proteins, even more intriguing is the report on a *Synechocystis* strain engineered to deplete photosystems in the dark. After shifting such a mutant back from darkness to light, the re-synthesis of chlorophyll (Chl) and the accumulation of photosystems can be studied in details. In a report from He & Vermaas (1999; see later) there was evidence that further deletion of *pilA* genes in such a genetic background causes a clear defect in the re-synthesis of Chl-binding complexes. The object of this thesis is to shed more light on the observed functional link between Type IV pili proteins and the photosynthetic apparatus.

1.2 Oxygenic photosynthesis and thylakoid membrane

Cyanobacteria are capable of utilizing light as their exclusive source of energy for their production. Like all other phototrophs, they convert the energy of photons into chemical energy (typically in form of organic molecules like sugars or lipids) in their photosynthetic apparatus localized in the thylakoid membrane. Of course, they also have an outer membrane and a plasma membrane as is common for all Gram-negative bacteria. From the point of view of energy metabolism (Figure 1), the plasma membrane mostly hosts the respiratory complexes (type 1 NADPH dehydrogenase, succinate dehydrogenase, and terminal oxidase) while the TM contains both respiratory and photosynthetic complexes, particularly photosystem I (PSI) and photosystem II (PSII) (Vermaas, 2001). Both the plasma membrane and thylakoid membrane (TM) contain the electron carrier plastoquinone and its oxidase, cytochrome b_6f, plastocyanin, and ATP synthetase.

Cyanobacterial TM is not, however, a homogenous mixture of complexes. In particular, the content of PSI or PSII varies in different segments of the TM, which indicates that the TM contains functional membrane microdomains (Strašková et al., 2019).

PSI and PSII are large pigment-protein assemblages working as two functionally coupled light-powered oxidoreductases (Figure 1). After absorbing the energy of photons, PSII oxidizes water using a cluster of manganese atoms attached to its lumenal side; oxygen is a by-product of this reaction. Protons released from the split water molecules acidify lumen whereas electrons from the same reaction are utilized by PSII to reduce plastoquinone to plastoquinol. This reduced lipidic compound donates electrons further to cytochrome b_6f, a membrane complex working as a proton pump powered by oxidation of plastoquinol. The proton-motive force at the lumenal side of the TM, established by PSII and cytochrome b_6f complexes, is finally utilized by ATP synthase to synthesize ATP. Meanwhile, electrons from cytochrome b_6f can be transferred to PSI by soluble plastocyanin or cytochrome c. These two metalloproteins are finally oxidized by the PSI complex, which utilizes the energy of photons to achieve a strong reducing power needed for the reduction of ferredoxin. Utilizing ferredoxin as an electron donor, enzyme ferredoxin-NADP+ reductase converts NADP+ to its reduced form NADPH. Most of ATP and NADPH produced are directly used for the fixation of carbon dioxide in the Calvin-Benson cycle.

PSII captures light using its inner antenna subunits (CP43 and CP47, see later) containing a total of 30 molecules of Chl. However, unless the illumination is very intense, the number of photons harvested by the PSII inner antennae are not sufficient and so PSII needs an external light-harvesting system. Unlike green algae and plants, which possess Chl-containing light-harvesting complexes, cyanobacteria harvest photons for PSII by phycobilisomes (PBS) – huge pigment-protein structures responsible for the typical blue tinge of cyanobacteria culture. During light exposure, the energy of photons is transferred from phycobilisomes to molecules of Chl associated with PSII. The number of light-harvesting Chls in PSI is much higher than in PSII (~100 Chl molecules per monomeric PSI) and, at least in cyanobacteria, PSI might not need any additional antenna. A potential attachment of PSB to PSI under limiting light intensities is a long-standing open question (Liu and Scheuring, 2013; Watanabe et al., 2014).

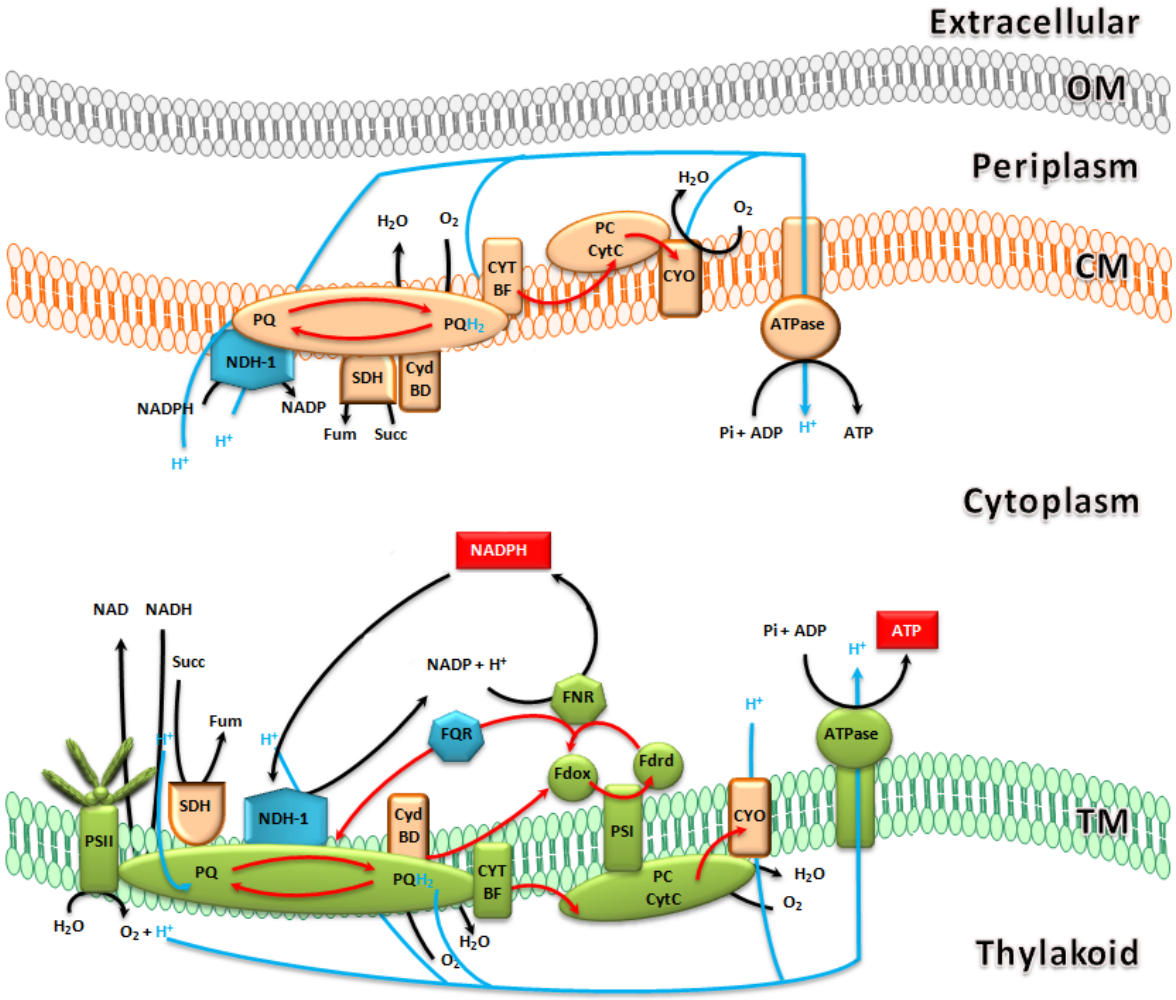

Figure 1. Model of the distribution of energy metabolism complexes in cyanobacteria. The scheme shows the localization of the photosynthetic pathway (depicted in green shapes) and the respiratory pathway (orange-coloured) as well as the accessory complexes (in blue) in the outer (OM), plasma (PM), and thylakoid membranes (TM). Fluxes of electrons and protons through both pathways are indicated by red and blue arrows, respectively. ATP and NADPH, generated by photosynthetic complexes, are represented by red squares. The abbreviations used are SDH (succinate dehydrogenase complex); PQ (plastoquinone); CYTBF (cytochrome *b6f)*; PC (plastocyanin); CytC (cytochrome *c*6); CYO (cytochrome oxidase); CYTBD (plastoquinone oxidase); PSI (photosystem I); Fdox/rd (oxidized/reduced ferredoxin); FNR (ferredoxin NADP+ reductase); FQR (ferredoxin plastoquinone reductase); ATPase (ATP synthetase) and NDH-1 (type 1 NADPH dehydrogenase complexes). Adapted from Nogales et al. (2012).

1.3 *Synechocystis* as a model cyanobacterium

The unicellular cyanobacterium *Synechocystis* became an organism of choice in studies related to photosynthesis and later as a model species for cyanobacterial biotechnology. The original *Synechocystis* Berkeley strain was isolated from freshwater in California (Stanier et al., 1971) and deposited in the Pasteur Culture Collection. About thirty years later (1996), the genome of a glucose tolerant *Synechocystis* substrain was fully sequenced; thus, this cyanobacterium belongs to the first sequenced organisms in the world (Kaneko et al., 1996). *Synechocystis* contains a circular chromosome and seven plasmids containing approximately 3700 genes (~4 Mbp). As in many other cyanobacteria, the chromosome is present in several (7 – 11) identical copies per cell depending on the growth phase and environmental conditions (Tichý et al., 2016). One of the important features of *Synechocystis* is the ability to uptake and integrate exogenous DNA into its genome via efficient homologous recombination. This mechanism allows easy and quick production of mutated strains with modified genes of choice (Labarre et al., 1989).

The original *Synechocystis* strain deposited in the Pasteur collection was strictly photoautotrophic. However, glucose-tolerant strains, which can also be cultivated under mixotrophic or heterotrophic regimes, have been generated by spontaneous mutagenesis. This plasticity of *Synechocystis* metabolism is a great advantage in the construction of site-directed mutants defective in the function of the photosynthetic apparatus (Williams, 1988).

2. Introduction

2.1 Structure and biogenesis of photosystems

PSI and PSII are large assemblages of proteins and a high number of different cofactors – Chl, carotenoids, heme, or iron-sulphur clusters among others. Chl molecules are very abundant in photosystems - there are about 100 and 35 Chl molecules per monomeric PSI and PSII, respectively. The core of the PSI is formed by a heterodimer of PsaA and PsbB Chl-binding proteins and is joined with nine smaller subunits (Figure 2.1B). The unique feature of the cyanobacterial PSI is its trimeric structure (PSI[3]) of a total molecular weight ~1 MDa (Netzer-El et al., 2019). Plant and algal PSI complexes are exclusively monomeric and surrounded by light-harvesting antennae (Jordan et al., 2001). As noted above, PSI complexes are very rich in Chl as each PSI[3] binds ~300 Chl molecules. Under stress-free laboratory conditions, the absolute majority (>85%) of cellular Chl in *Synechocystis* is located in PSI[3] and this complex is also the main sink for *de novo* synthesized Chl molecules (Kopečná et al., 2012). The PSII complexes, organized in cyanobacteria mostly as dimers, are assembled from four large Chl-binding proteins (D1, D2, CP43 and CP47) and surrounded by 13 transmembrane and 3 peripheral subunits giving a total molecular weight of ~ 350 kDa per monomer (Figure 2.1A).

The biogenesis of photosystems, the translation of individual subunits, attachment of cofactors and the subsequent assembly of all subunits into large complexes, requires complicated machinery (Komenda and Sobotka, 2019). The large Chl-binding subunits of PSI (PsaA and PsaB) and PSII (CP43, CP47, D1, and D2) are transmembrane multi-helical proteins that are co-translationally inserted into the TM. As for the majority of transmembrane proteins in bacteria, membrane insertion is facilitated by Sec translocase, a sophisticated pore in the membrane. The major component of translocase, the SecY channel-like protein, is associated with the transmembrane SecG and SecE proteins. The SecYEG trimer can either translocate a protein across the membrane into lumen/periplasm or integrate nascent membrane-spanning segments into the membrane bilayer. In the latter case, the hydrophobic segments of the membrane protein exit sideways through the lateral gate into the lipid phase (Van den Berg et al., 2004). YidC foldase (and its plastid homologue Alb3) is a membrane protein that physically associates with SecYEG and assists in partitioning many different transmembrane proteins into the membrane (Sachelaru et al., 2017). In oxygenic phototrophs, SecYEG is known to interact with D1

and CP47 subunits of PSII (Zhang et al., 2000; Bučinská et al., 2018) and the D1 protein is integrated into TM under the assistance of YidC/Alb3 (Ossenbuhl et al., 2006).

Membrane insertion via Sec translocon is coupled with the insertion of Chl molecules from the Chl synthase enzyme (ChlG), the last enzyme of the Chl biosynthetic pathway, which is physically attached to YidC (Chidgey et al., 2014). This arrangement is expected to be the same for the synthesis of Chl-binding subunits for both photosystems as reviewed in Komenda and Sobotka (2019). Therefore, the production of *de novo* photosystems needs to be tightly balanced with the biosynthesis of all cofactors, but especially with Chl molecules synthesized in cells in high amounts. Chl is readily excited by light and, if the absorbed energy is not quenched by carotenoids or passed promptly to the photosystem reaction centre, excited Chl molecules can switch into the triplet excited state and generate damaging reactive oxygen species. However, how the tight coordination between the syntheses of Chl-binding apoproteins and Chl/heme is organized in the photosynthetic cell is an unresolved question.

Large Chl-binding subunits of photosystems are probably synthesized with the majority of pigment cofactors bound and then assembled into larger sub-complexes (Komenda et al., 2012b). Assembly of PSII happens in a stepwise manner from four so-called modules, each containing one large Chl-binding protein (D1, D2, CP43, CP47; Figure 2.1A) associated with a few small subunits. The D1 protein is nonetheless synthesized as a longer precursor (pD1) with a C-terminal extension that is cleaved out during later assembly steps. In the current model, PSII assembly starts with the attachment of the pD1 module and D2 module, together creating the reaction centre of PSII (RCII). After the formation of RCII, the pD1 undergoes its maturation catalysed by a dedicated CtpA protease (Takahashi et al., 1988; Nixon et al., 1992; Komenda et al., 2004; Komenda et al., 2008; Dobáková et al., 2009; Knoppová et al., 2014). Then the CP47 module associates with the RCII, which results in the RC47 complex (Boehm et al., 2011; Boehm et al., 2012) and the additional step is the association of the CP43 module to the RC47 to form the reaction centre complex II (RCCII; Komenda et al., 2012b). RCCII binds the manganese cluster and lumenal extrinsic subunits while becoming PSII[1] (reviewed by Bricker et al., 2012). As the final step, the monomeric PSII dimerizes. The quality of PSII assembly is controlled by FtsH proteases (Komenda et al., 2006; Krynická et al., 2015).

Many protein factors have been identified in assisting the process of PSII assembly. These so-called auxiliary factors interact with PSII subunits at various steps of the assembly but are not present in the final structure of PSII (Figure 2.1A). The role of PSII assembly

factors is not fully explained, however, there are recent studies strongly indicating that some factors promote insertion of Chl into the newly-synthesized subunits of PSII. Ycf48 is a lumenal protein that has been localized in the vicinity of SecY translocon and probably stabilizes the folding of Chl proteins to allow Chl insertion (Komenda et al., 2008; Yu et al., 2018). Another assembly factor, Pam68, seems to have a similar role in the biogenesis of CP47. Ycf39 assists differently, working as a shuttle for small Chl-binding High light-inducible proteins (Hlips); the whole Ycf39-Hlips subcomplex is attached to the nascent D1. Hlips are single-helix proteins able to bind Chl and β-carotene that have got an apparent function in re-utilization of Chl molecules released from the degraded proteins (Vavilin et al., 2007; Yao et al., 2012; Knoppová et al., 2014; Staleva et al., 2015). In a proposed mechanism, Ycf39 controls the delivery of Chl (Hlips) to D1 from Chl synthase, which also interacts with the Ycf39-Hlip subcomplex (Chidgey et al., 2014). There are additional PSII auxiliary factors like Psb28, CyanoP and Psb27 proteins interacting with D2, CP43, and CP47 modules (Dobáková et al., 2009; Komenda et al., 2012a; Bečková et al., 2017).

The mechanism of PSI assembly is much less explored than the biogenesis of PSII, however, it is believed to begin with the formation of the heterodimeric PsaA-PsaB core (Figure 2.1B). Then the stromal (cytoplasmic) proteins PsaC, PsaD, and PsaE bind to stabilize the PSI acceptor site, and finally the other small membrane subunits associate to generate the active PSI[1] complex (Nellaepalli et al., 2018). PsaL and PsaI polypeptides are responsible for the trimerization of cyanobacterial PSI (Chitnis and Chitnis, 1993). Only a few factors assisting the PSI assembly are known and only two factors (Ycf3, Ycf4) have been studied in detail (Figure 2.1B); still, the role of these proteins is unclear.

Unlike PSI complexes, which appear quite stable, the PSII is a vulnerable component of the photosynthetic electron transport chain. In particular, the PSII core D1 subunit is readily damaged by radical oxygen species. Damaged D1 causes photoinhibition and the pool of inhibited PSII grows with the exposition of cells to higher light intensities. To deal with this problem, cyanobacteria evolved a sophisticated PSII repair cycle involving a specific replacement of the damaged D1 subunit. Briefly, this multi-step process comprises de-attachment of the CP43 subunit, presumably also the release of extrinsic proteins, the degradation of the damaged D1 by FtsH and Deg proteases, and a consequent fast co-translational insertion of the new D1 copy via SecYEG translocon (reviewed in Komenda and Sobotka, 2019) . Therefore, PSII undergoes a frequent process of disassembly, reassembly, and quality control, which requires specific structural dynamics and transport.

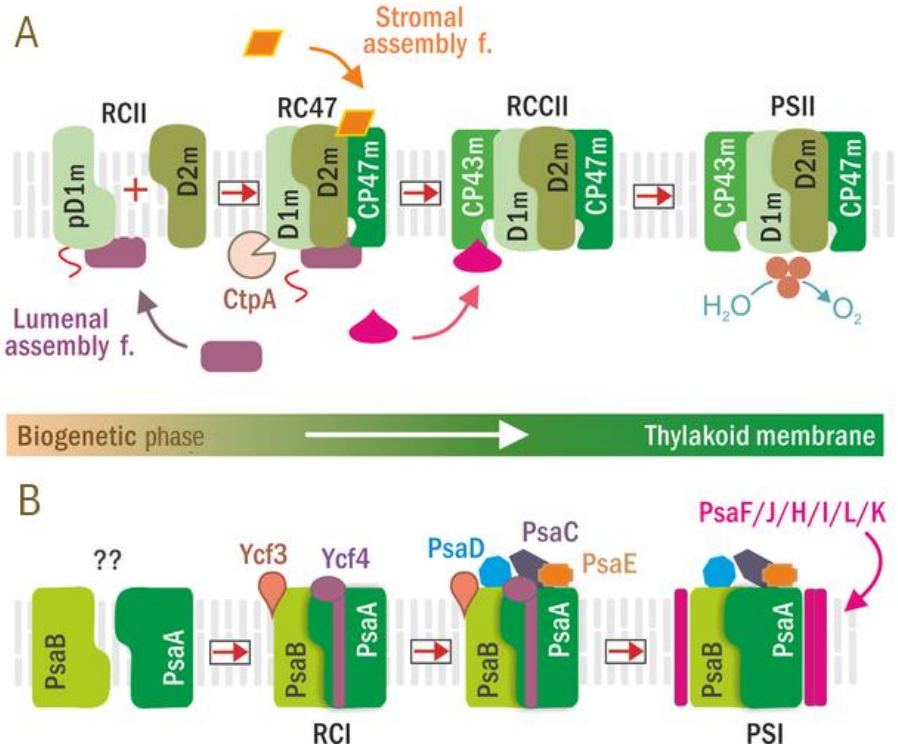

Figure 2.1. The scheme of the *de novo* stepwise assembly of PSII (A) and PSI (B) complexes in cyanobacteria. A) PSII assembly starts with the synthesis and insertion of the pD1 module (pD1m) and continues with the sequential attachment of D2, CP47 and CP43 modules. It leads to the formation of RCII, RC47, RCCII, and PSII[1] complexes, respectively. Formation of individual PSII intermediates is assisted by lumenal and stromal assembly factors. B) PSI assembly is most likely initiated by the formation of the PsaA-PsaB heterodimer under the assistance of Ycf3 and Ycf4 assembly factors. Later, the stromal proteins that create the PSI acceptor site are attached, and finally the other small subunits associate to generate the fully active PSI complex. Adapted from Komenda and Sobotka (2019).

2.2 Structure and biogenesis of Type IV pili apparatus

2.2.1 Bacterial pili

Cell surface appendages, usually called pili, are widespread in the bacterial world. These nano-filaments were historically classified into distinct types according to their function but nowadays are classified by their immunological characteristics or by comparing the amino acid sequences of their structural subunits. At least four different groups of pili can be recognized in Gram-negative bacteria: i) chaperone-usher (CU) pili with their adhesive tip that can be further subdivided into classical CU and alternative Type 1 and P-pili; ii) curli pili; iii) Type IV pili (T4P); and iv) conjugative F-pili (Werneburg et al., 2018).

Appendages in Gram-positive bacteria are less well-studied though they have become an active area of research in the last 15 years. Gram-positive bacteria display fibres homologous to T4P and sortase-mediated covalently linked pili (Melville and Craig, 2013; Khare and Narayana, 2017).

T4P are thus present on the cell surface of nearly all bacterial and archaeal phyla species using structurally modified types of machinery (Varga et al., 2006; Imam et al., 2011; Berry and Pelicic, 2015). During the evolution, T4P apparatus achieved a variety of seemingly unrelated functions: adhesion, cell aggregation, colony formation, twitching and social motility, virulence, natural competence for exogenous DNA uptake, conjugation machinery for DNA exchange, secretion, and electrical conductivity (Strom and Lory, 1993; Lee and Shimkets, 1994; Yoshida et al., 1998; Wolfgang et al., 1999; Friedrich et al., 2003; Hélaine et al., 2005; Bonner et al., 2006; Chen et al., 2006; Hélaine et al., 2007; Laurenceau et al., 2013; Berry and Pelicic, 2015) Although the spectrum of functions connected with T4P is broad, they still share a well-conserved mechanism of assembly, elongation and retraction (Vignon et al., 2003; Köhler et al., 2004; Jarrell and Albers, 2012; Korotkov et al., 2012).

2.2.2 The structure of bacterial Type IV machinery

According to the current knowledge, T4P assembly machinery requires direct interaction of at least 15 proteins (reviewed in Chang et al., 2016). Each pilus stem, a polymer of major pilin subunit, is anchored in a cell envelope-spanning complex which comprises a cytoplasmic motor joined with the outer membrane pore by a set of rings in the periplasm (Figure 2.2A, B). During the process of pilus biogenesis, pilin proteins (designated PilA in *Synechocystis*) are extracted from the plasma membrane and polymerised into the growing filament. The cytoplasmic motor complex comprising PilB, PilC and the PilM ring is responsible for the pilin extraction, assembly and anchoring of the pilus into the membrane (Figure 2.2C, D). PilB is a hexameric ATP-driven motor producing force needed for the extraction of pilin proteins from the membrane and for the pilus extension. In addition, a structurally similar ATPase motor PilT facilitates pilus retraction if the PilB in the basal part of the T4P machinery is replaced (Jakovljevic et al., 2008). The transmembrane protein PilC may coordinate the activity of the cytoplasmic motor while the PilM protein, exposed to cytoplasm, provides contact with other cytoplasmic components of pilin apparatus (Takhar et al., 2013). The growing pilus passes through a lower-periplasmic ring most likely made of PilN and PilO heterodimers (Sampaleanu et al., 2009) and a mid-periplasmic

ring containing PilP. The outer membrane pore for pilus is created by a large PilQ protein (also called secretin), which partially spans into the mid-periplasmic ring (Figure 2.2C, D). All individual periplasmatic rings appear to be linked together forming a semi-rigid structure; the only components free to rotate are PilC and potentially the pilus itself. Apart from the major PilA pilins, virtually all bacteria contain several minor pilins, which are present in lower amounts than the major pilin protein. The function of minor pilins is still not fully clarified but they form a complex with the major pilin and most likely lower the energetic barrier needed for the extraction of pilus from the membrane (Giltner et al., 2010; Cisneros et al., 2012; Nguyen et al., 2015).

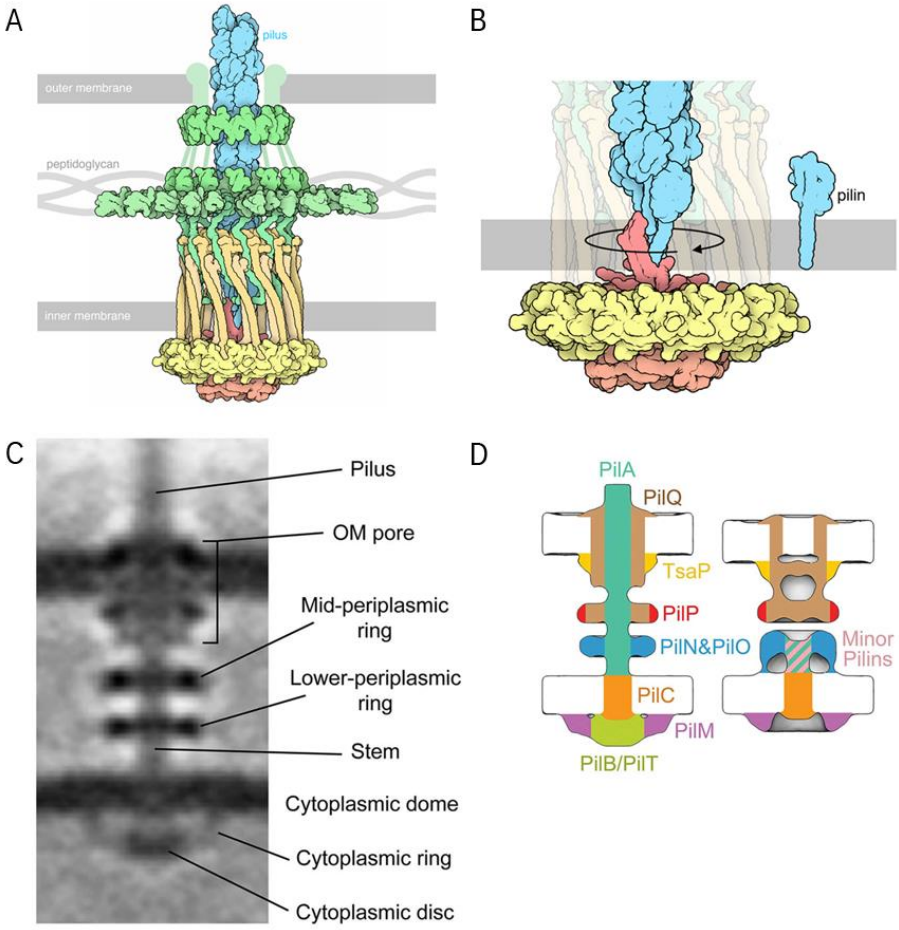

Figure 2.2. Structural models of Type IV machinery. A) A structural model of the entire machinery with the part of the pilus fibre passing through the outer membrane. B) Mechanism of the pilus assembly into the stem (blue) powered by the cytoplasmic AAA-type ATPase (pink). C) Visualization of an anchored pilus in intact *Myxococcus xanthus* cells using cryo-electron tomography. OM – outer membrane. D) Schematics showing protein subunits of the Type IV machinery in the piliated (left) and empty (right) basal body. A) and B) - Berman et al. (2000); C) and D) - Chang et al. (2016).

2.2.3 Type IV pili in cyanobacteria

T4P have traditionally received the most attention in pathogens but scientists have just recently revealed novel functions in non-pathogenic species (Reguera et al., 2005; Gorby et al., 2006) including cyanobacteria (Lamb et al., 2014; Sure et al., 2016; Lamb and Hohmann-Marriott, 2017). Cyanobacteria possess several different surface fibres according to their various locomotion strategies (Hoiczyk and Hansel, 2000). Apart from the T4P, cyanobacteria can form oscilin fibrils and probably also CU pili (Schuergers and Wilde, 2015). T4P are best studied in *Synechocystis* (reviewed in Chen et al., 2020) and only a few publications deal, in detail, with T4P in other cyanobacteria, such as unicellular *Microcystis aeruginosa* PCC 7806 (Nakasugi and Neilan, 2005), *Thermosynechococcus elongatus* BP-1 (Iwai et al., 2004), and filamentous *Nostoc punctiforme* (Duggan et al., 2007).

Two types of fibres can be distinguished on the surface of *Synechocystis* cells using electron microscopy (Figure 2.3) - thick pili with a diameter of 5-8 nm and a length of 1-2 μm and more abundant, thinner pili with a diameter of 2-4 nm and a shorter length of 0.5-1 μm (Bhaya et al., 2000; Yoshihara et al., 2001; Nakane and Nishizaka, 2017). Thick pili, essential for DNA uptake and twitching motility, match most of the functional and morphological characteristics of the T4P group (reviewed in Schuergers and Wilde, 2015; Nakane and Nishizaka, 2017). In contrast to thick pili, which are flexible and often appear twisted or knotted, the more abundant thin pili are much shorter, wavy or stretched straight and uniformly distributed (Bhaya et al., 2000). Thin pili might represent CU pili, however, experimental evidence is missing (Schuergers and Wilde, 2015). In contrast to the motile PCC-WT, cells of the GT-P and GT-W non-motile substrains (Tichý et al., 2016) display one type of pili that resembles the thin pili morphotype (compare Figure 2.3 and Figure 2.4).

According to the current knowledge, the aforementioned ‘canonical’ model of T4P apparatus in *Myxococcus xanthus* (Figure 2.2) may be structurally close to the organization of T4P in cyanobacteria, though there are some differences. T4P subunits from *Synechocystis* that refer to the model of Chang et al. (2016) are summarized in Table 1. Reverse genetics in *Synechocystis* led to the identification of around 300 *Synechocystis* genes, which are essential for the biogenesis of T4P apparatus or functioning and regulation of motility (Bhaya et al., 2001b; Chen et al., 2020). Although being of Gram-negative type, cyanobacteria possess certain features similar to Gram-positive bacteria including a thicker peptidoglycan cell layer (Hoiczyk and Hansel, 2000). It might be related to a different organization of the T4P periplasmic ring in cyanobacteria, which appears to lack the PilP

and TsaP proteins (Schuergers and Wilde, 2015). Absence of PilP and TsaP together with PilC, PilQ and PilW proteins are characteristic for Gram-positive bacteria due to the absence of the outer membrane (Berry and Pelicic, 2015). Notably, pilB and pilT genes coding for the motor ATPases powering pilus extension and retraction are duplicated in many cyanobacterial genomes (Schuergers and Wilde, 2015). PilB1 and PilT1 variants appear to house the motor functions, as disruption of their coding genes impaired motility with the expected non- or conversely hyper-piliated phenotypes, respectively (Bhaya et al., 2000; Okamoto and Ohmori, 2002). Motility and phototaxis in *Synechocystis* require interaction between PilB1 and an RNA chaperone Hfq (Dienst et al., 2008; Schuergers et al., 2014). Moreover, the localization of PilB1 on the plasma membrane correlates with the leading pole and the direction of motility (Schuergers et al., 2015). The negative direction of phototaxis was reported in the ΔpilT2 strain (Bhaya et al., 2000). So far, the role of PilB2 is not clear but its deletion caused about a one-third lower transformation efficiency when compared to WT (Yoshihara et al., 2001).

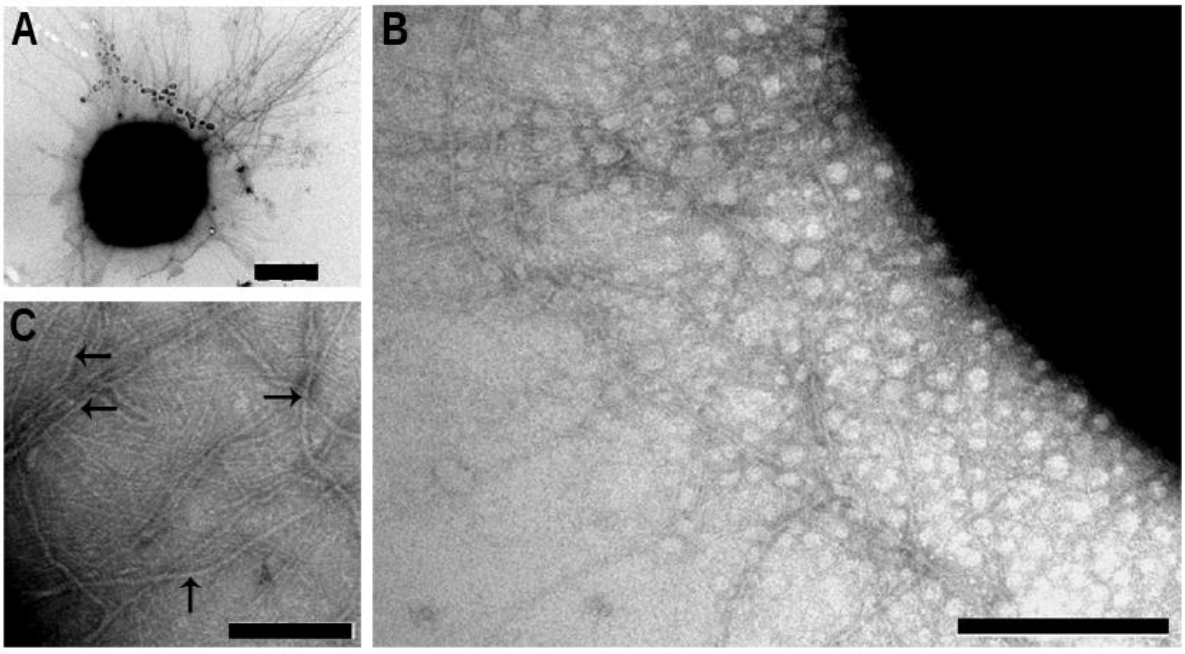

Figure 2.3. Electron microscopy micrographs of pili on the surface of motile WT *Synechocystis* cells. A) A cell with pili fibres on its surface; long thick pili are distinguishable in the right top of the picture (B) and (C). Thick and thin types of fibres can be distinguished after negative staining (1% uranyl acetate); thick pili are indicated with black arrows. Black bars represent 750, 200, and 100 nm in panels A, B, and C, respectively.

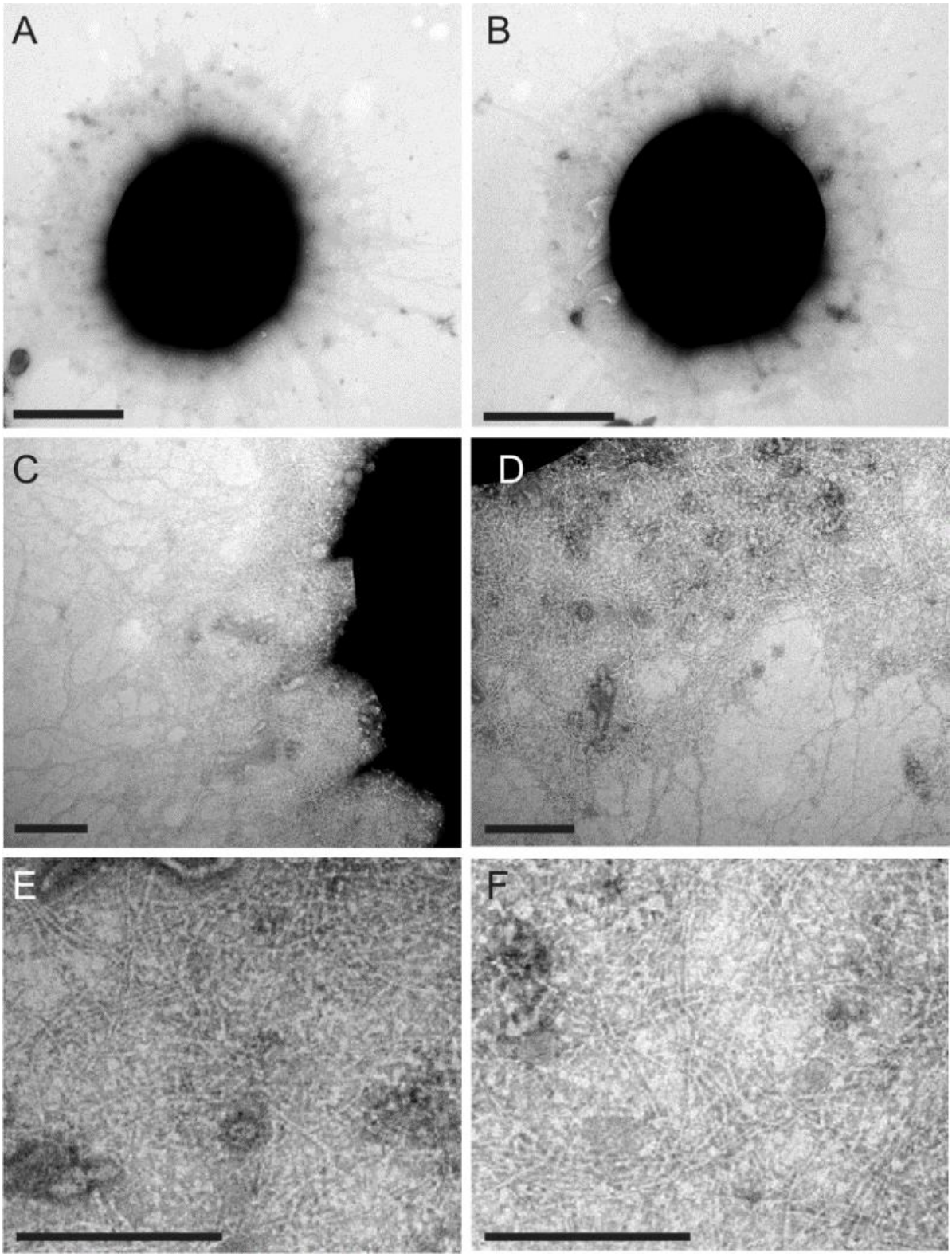

Figure 2.4. Electron microscopy micrographs of pili on the surface of non-motile WT-W *Synechocystis* cells. A, B) A cell with pili fibres on its surface; a corona of thin pili is distinguishable around the black body of the cell. C, D) A dense structure of thin pili. E, F) Only a thin type of fibres can be recognized in non-motile cells after negative staining with 1% uranyl acetate. Bars represent 1 μm in panels A, B; 200 in panels C, D and 100 nm in panels E, F.

Table 1. List of Type IV pili structural genes and proteins in *Synechocystis*

	Protein	Gene	ORF	Cluster	Annotation
Pilins	PilA1	*pilA1*	*sll1694*	*sll1693 - 96*	1, 2, 3, 4
	PilA2	*pilA2*	*sll1695*	*sll1693 - 96*	1, 2, 3, 4
	PilA4	*pilA4*	*slr1456*		1, 3, 4
	PilA5	*pilA5*	*slr1928*	*slr1928 - 31*	1, 4
	PilA6	*pilA6*	*slr1929*	*slr1928 - 31*	1, 3, 4
	PilA7	*pilA7*	*slr1930*	*slr1928 - 31*	1, 3, 4
	PilA8	*pilA8*	*slr1931*	*slr1928 - 31*	1, 4
	PilA9	*pilA9*	*slr2015*	*slr2015 - 18*	1, 5
	PilA10	*pilA10*	*slr2016*	*slr2015 - 18*	1, 3, 5
	PilA11	*pilA11*	*slr2017*	*slr2015 - 18*	1, 5
	PilA12	*pilA12*	*slr2018*	*slr2015 - 18*	7
Peptidase/ Methylase	PilD	*pilD*	*slr1120*		3, 4, 6
Cytoplasmic motor and ring	PilB1	*pilB1*	*slr0063*		4
	PilB2	*pilB2*	*slr0079*		4
	PilC	*pilC*	*slr0162*		3
	PilC´	*pilC´*	*slr0163*		3
	PilT1	*pilT1*	*slr0161*		3
	PilT2	*pilT2*	*sll1533*		3
	PilM	*pilM*	*slr1274*		4
Lower periplasmic ring	PilN	*pilN*	*slr1275*		4
	PilO	*pilO*	*slr1276*		4
Outer membrane ring	PilQ	*pilQ*	*slr1277*		4

Key to annotations. 1. He and Vermaas (1999); 2. Bhaya et al. (1999); 3. Bhaya et al. (2000); 4. Yoshihara et al. (2001); 5. Yoshimura et al. (2002); 6. Linhartová et al. (2014); 7. Chandra et al. (2017).

2.2.4 Synthesis and maturation of *Synechocystis* PilA (pilin) proteins

Bacterial genomes contain variable numbers of genes coding for pilin (PilA) proteins (Imam et al., 2011). In *Synechocystis* the number is relatively high (12 genes) although *pilA3* is probably not a true pilin gene (Foldynová, 2009). Apart from *pilA4*, other *pilA* genes are organized in three gene clusters (*pilA1-2*; *pilA5-7*, *pilA8-12*; Table 1). As shown by reverse genetics, the PilA1 pilin, which has high similarity to major PilA proteins of *Pseudomonas aeruginosa* and *Myxococcus xanthus* (Foldynová, 2009) represents the major pilin in *Synechocystis* (Bhaya et al., 2000). PilA2 and PilA4 proteins are also similar to

canonical pilins; however, their roles are not known (see below). Mature PilA1 and PilA4 are also the most abundant and can be detected in the cell membrane fraction, on the cell surface, and among secreted proteins in the growth medium (He and Vermaas, 1999; Sergeyenko and Los, 2000; Linhartová et al., 2014; Cengic et al., 2018). The display of PilA4 on the cell surface is however, dependent on the PilA1 and PilT1. This indicates that PilA4 is a true minor subunit of pili which is also considered to affect the retraction of pili (Cengic et al., 2018). Exact roles of other pilin homologues are not known. Only *pilA1*, *pilA9*, *pilA10*, *pilA11*, and *pilA12* genes are essential for motility and only *pilA1* is crucial for the formation of thick pili (Bhaya et al., 2000; Yoshihara et al., 2001; Yoshihara and Ikeuchi, 2004; Chandra et al., 2017). However, PilA1 also seems to be implicated in the biogenesis of thin pili as these structures are less abundant in the *Synechocystis* Δ*pilA1* mutant (Yoshihara et al., 2001). A little attention has been paid to the function of the *pilA2* gene that is located downstream of the *pilA1* gene in the *Synechocystis* genome. Lower transformability relative to the WT strain is the only known phenotype of the Δ*pilA2* mutant (Yoshihara et al., 2001). However, PilA2 was detected on the cell surface, although present in lower densities than PilA1 and PilA4 (Cengic et al., 2018). Yoshihara et al. (2001) reported that the *pilA2* gene is highly expressed, which is contradicting the result of Bhaya et al. (2000) who found no detectable expression of *pilA2*. According to the CyanoEXpress database, the expression of *pilA2* is increased under most of the stress conditions with maximum values under cold stress or the stationary phase (Hernández-Prieto and Futschik, 2012; Hernández-Prieto et al., 2016).

As already noted, PilA proteins are synthesized as precursors (prepilins) and undergo cleavage and trimethylation by PilD protease. Other post-translational modifications of pilins like glycosylation, phosphorylation, or acetylation have also been reported (Kim et al., 2011; Linhartová et al., 2014; Chen et al., 2015; Mo et al., 2015). A deletion of the *Synechocystis slr1443* (*pknA*) gene abolished the formation of thick pili although a matured PilA1 accumulated in the cell. Interestingly, immunoblot analysis revealed a faster (~ 4 kDa) electrophoretic mobility of the PilA1 in the *slr1443* mutant strain, indicating a missing post-translational modification (Kim et al., 2004). These lower-mass PilA1 proteins were less abundant in the membrane and not assembled into pili but rather released into cultivation media. A similar gel mobility shift of PilA1 was observed in the *pilD* mutant, accumulating a non-glycosylated form of PilA1 prepilin (Linhartová et al., 2014). Another example of the shifted gel mobility of PilA1, in this case to a ~ 4 kDa higher mass, has been observed in the *sll0899* mutant and was caused by an excessive O-

glycosylation of PilA1 (Kim et al., 2009). Interestingly, the maturation of *Synechocystis* prepilins by *PilD* is an essential step not just for the biogenesis of T4P (Bhaya et al., 2000; Yoshihara et al., 2001) but also for the photoautotrophic growth. *Synechocystis* Δ*pilD* cells, which accumulate unprocessed PilA1, and its non-glycosylated derivative, also suffered by abolished biogenesis of PSII (Linhartová et al., 2014).

2.2.5 The role of Type IV pili in cyanobacteria

As in many bacteria, T4P in cyanobacteria aid in gliding motility, natural competence, secretion, biofilm formation and flocculation (Sergeyenko and Los, 2000; Bhaya et al., 2001b; Yoshihara et al., 2001; Sergeyenko and Los, 2003; Cengic et al., 2018; Allen et al., 2019; Conradi et al., 2019). Gliding (twitching) motility is the ability of cells to move on a solid surface by the mechanism of pili attachment and reversible extension (Strom and Lory, 1993). Motility enables random or directed surface exploration and, specifically in cyanobacteria, it is not only driven by the chemical environment but also by phototaxis. It means that motility is highly dependent on phototactic signals triggered by a range of photoreceptors (Yoshihara et al., 2000; Wilde et al., 2002; Yoshihara and Ikeuchi, 2004; Okajima et al., 2005; Song et al., 2011; Sugimoto et al., 2017). This regulatory cascade results in positive or negative motility towards the light (Bhaya et al., 2000; Nakane and Nishizaka, 2017). Negative phototactic gliding is typically provoked by UV irradiation (Choi et al., 1999). To localize the position of the light source the *Synechocystis* cell works as a spherical microlens focusing the light beam from the source into a spot on the plasma membrane (Schuergers et al., 2016). If other cells are nearby, pilus-pilus contacts can lead to the formation of cell aggregates or colonies, as described in unicellular cyanobacteria. Particularly in *Synechocystis*, colony motility induced by phototaxis might be divided into three phases (Bhaya et al., 2006). In the first (preparative) phase, lasting for several hours, cells are still not visibly motile. During the second phase (16-48 hours later) cells aggregate and those growing nearest the light source start to move, the front edge of the moving cells forms a characteristic crescent shape. In the last phase, finger-like projections extend from the crescent, moving rapidly and reaching 4-10 mm within 2 to 4 days. Alternatively, the fronts of the aggregated cells move towards the moderate light source. The rates and characteristics of movement directly depend on the cell density, doubling times, surface wetness and light quality. Moreover, motility is locally enhanced by trails left by other cells, which suggests that *Synechocystis* secretes an unknown extracellular substance altering surface properties and increasing the colony motility (Ursell et al., 2013).

In the case of multicellular filamentous strains like *Nostoc punctiforme*, colony motility combines T4P with extracellular slime deposition (Khayatan et al., 2015; Wilde and Mullineaux, 2015); however, the mechanism remains mostly unknown. T4P appear only in hormogonia, a motile type of trichomes, into which cells transform under stressful conditions (Duggan et al., 2007). Surprisingly, T4P subunits were localized in hormogonia in cell junctions, which excrete gliding slime (Hoiczyk and Baumeister, 1998), indicating that the junctional pore complex could be a modified T4P structure (Risser et al., 2014).

Apart from motility, the T4P in cyanobacteria serves for the uptake of the exogenous DNA and secretion machinery. In the first case, pilins, together with the specialized ComA/ComF proteins, bind and transport extracellular DNA into the cell across the cell wall and the plasma membrane (Yura et al., 1999; Yoshihara et al., 2001; Nakasugi et al., 2006). Subunits of T4P are structurally and functionally related to the Type II secretion system (T2SS) and is also referred to as the General secretory pathway in Gram-negative bacteria (Nunn, 1999; Py et al., 2001). Proteins secreted by the T2SS pathway are synthesized with a typical leader N- terminal peptide (similarly to pilins) and transported into the periplasmic space by Sec or Tat pathways. This process is often followed by post-translation modifications such as glycosylation (Dalbey and Kuhn, 2012). Matured proteins are then exported via the T2SS across the plasma membrane and outer membrane into extracellular space (reviewed in Nivaskumar and Francetic, 2014). The mechanism of crossing the outer membrane relies on the selective recognition of the cargo by the homomeric (PilQ) secretin channel (Filloux, 2004; Korotkov and Sandkvist, 2019). T2SS pseudopilus is a short variant of the T4P pilus and functions either as a retractable "plug" for the outer membrane PilQ secretin and/or as a "piston" that actively pushes secreted proteins through the pore (Hobbs and Mattick, 1993). Functional similarity between T4P and T2SS is high and PilD methylase/peptidase, PilB motor ATPase, and the PilQ secretin channel are often shared in the cell by both types of machinery. The functioning of T2SS in *Synechocystis* is not characterized well, however, the leader peptide of PilA1 was successfully used for the secretion of the reporter protein. In addition, artificial leader peptides with an overall positive charge were recognized by the secretion system in a sequence-non-specific manner (Sergeyenko and Los, 2003).

Type IV pili can mediate an electron donation to extracellular electron acceptors such as iron oxides (e.g. in *Geobacter sulfurreducens*; Lovley and Malvankar, 2015). However, the conductivity mechanism is still not fully clarified and, according to Bouhenni et al. (2010), the surface reduction of iron and manganese oxides is facilitated by outer-

membrane cytochromes *c* (MtrC/OmcA) of which the presence in outer membrane depends on T4P subunits. These bacterial electro-conductive nanowires are one of the most interesting microbial structures discovered within the last decade. T4P of a cyanobacterium *Nostoc punctiforme* appear to be electrically conductive (Sure et al., 2016). T4P of *Synechocystis* has also been subjected to testing for conductivity (Gorby et al., 2006; Lamb et al., 2014; Sure et al., 2015) but it has been rebutted recently (Thirumurthy et al., 2020). Nonetheless, the presence of T4P on the *Synechocystis* cell surface enhances the ability to grow on iron and manganese oxides (Lamb et al., 2014; Lamb and Hohmann-Marriott, 2017).

Enigmatic is the role of pilin proteins in the biogenesis or regulation of the photosynthetic apparatus. As noted earlier, the major PilA1 protein is abundant in *Synechocystis* TM (Pisareva et al., 2011; Selão et al., 2016). According to He and Vermaas (1999), later steps of Chl biosynthesis were delayed in the *pilA1/2/4 Synechocystis* mutant. In this work, the authors utilized strains that lacked PSI and the *chlL* gene encoding for the L subunit of light-independent protochlorophyllide reductase, an enzyme in the Chl biosynthetic pathway. Due to the *chL* mutation, the PSI-less/*chL*- strain produced Chl only in light and, instead of Chl, protochlorophyllide accumulates in cells shifted to darkness. After re-exposition to light, Chl is synthesized at the expense of accumulated protochlorophyllide (Wu and Vermaas, 1995). The authors analysed 'green' Chl-protein complexes that first appeared during the process of re-greening by native electrophoresis and they co-localized this with PilA1 protein. Also, the deletions of the *pilA1/2/4* genes in the PSI-less/*chL*- strain resulted in a 30% decrease in the Chl synthesis rate during the first six hours of illumination (He and Vermaas, 1999). This led to speculation that PilA proteins are involved in the delivery of Chl to nascent subunits of photosystems. A link between T4P and photosynthetic apparatus is further supported by analysis of the *Synechocystis* Δ*pilD* strain. As shown by Linhartová et al. (2014), accumulation of PilA1 prepilin (pPilA1) led to the degradation of Sec translocons, impaired synthesis of PSII subunits and an aberrant TM ultrastructure. Interestingly, the pPilA1 prepilin physically interacted with SecY in vivo and thus the proteolytic degradation of SecY and YidC was most likely triggered by the jamming of the SecY translocon by prepilins. The synthesis of membrane proteins was consitstently more strongly diminished in the Δ*pilD* strain. Strikingly, the synthesis of PSI trimers and ATP synthase remained on the WT level, contrasting to the abolished synthesis of subunits of PSII complex. This indicates that there is a specific pool

of Sec translocons dedicated to the synthesis of PSII subunit(s) but not for the subunits of PSI, and that this pool might be more sensitive to jamming by pPilA1.

3. Unpublished results - The essential role of Synechocystis pilin proteins in the transition from the exponential to the linear growth phase

This chapter presents unpublished data on the role of pilin proteins in the biogenesis of the photosynthetic apparatus and metal uptake in *Synechocystis*, in particular, under long-term cultivation. The growth of typical heterotrophic bacteria can be divided into three phases: lag, exponential, and stationary phase. In cyanobacteria, there is, however, an additional (linear) phase that probably results from the limited availability of light when cell density reaches a certain point (Schuurmans et al., 2017). During the transition from the exponential to the linear phase, cyanobacteria slow down their growth and accumulate more biomass but do not change the PSI-PSII ratio. The linear phase can be further characterized by downregulated transcription of photosynthesis-related genes such as carbon uptake systems, more efficient energy transfer from phycobilisomes to PSII, and a less oxidized plastoquinone pool (Foster et al., 2007; Schuurmans et al., 2017).

3.1 Bleaching of pilin mutant cells cultivated on agar plates

The loss of pigments during cultivation on a BG11 agar plate in a *Synechocystis* Δ*pilA1* strain was first reported by Bhaya et al. (1999). I observed the bleaching phenotype in Δ*pilA1*/*2* and Δ*pilA1*/*2*/*4* mutants after three weeks of cultivation in our standard laboratory conditions (40 µmol of photons m^{-2} s^{-1} at 28 °C; Figure 3.1A). Interestingly, the Δ*pilA2* (minor pilin) strain showed a similar bleaching phenotype but the Δ*pilA4* mutant behaved as WT (Figure 3.1 A). According to the whole-cell absorption spectra, the plate-grown Δ*pilA2*, Δ*pilA1*/*2*, Δ*pilA1*/*2*/*4* had a significantly lower content of phycobilisomes than WT and Δ*pilA4* cells whereas the level of Chl remained similar (Figure 3.1B). The loss of phycobilisomes was not prevented when the strains were grown on agar plates supplemented with increased concentrations of iron or nitrogen (data not shown).

To understand the changes in pilin mutants, I scraped off WT and Δ*pilA1*/*2*/*4* cells that were cultivated on an agar plate for three weeks and analysed the content of protein complexes by 2D Clear Native/SDS-PAGE (Figure 3.2). Although the content of both photosystem complexes was comparable in the WT and pilin mutant (Figure 3.2), the intensity of several protein spots on the stained 2D gel differed markedly (Figure 3.2 arrows). These spots were cut from the gel and analysed by protein MS (Peter Koník, Department of Chemistry, University of South Bohemia; Table 3.1). Notably, the Sll1693

protein, a product of the upstream gene of *pilA1*, accumulated only in the mutant. Additionally, the stress-induced Orange carotenoid-binding protein (OCP) and the Heat shock protein 17 (Hsp17) together with glucose-6-phosphate isomerase were more abundant in the membrane fraction of the Δ*pilA1*/*2*/*4* cells.

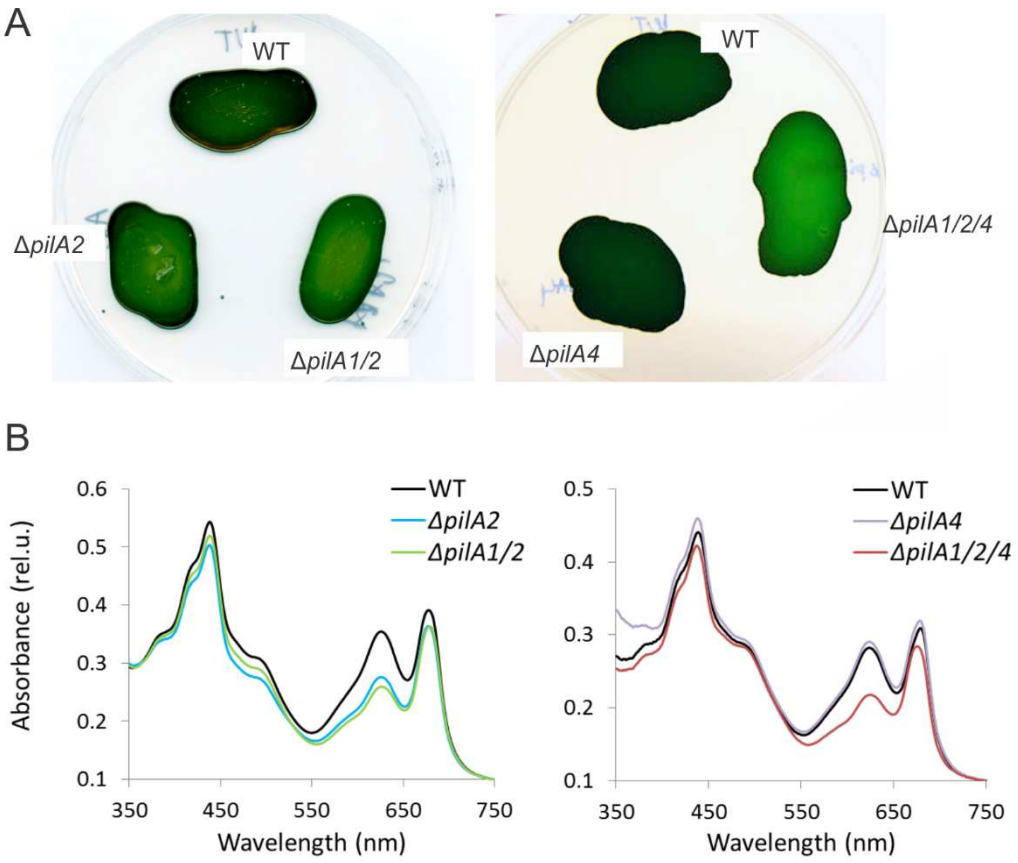

Figure 3.1. Bleaching of pilin mutant cells cultivated on agar plates. A) Appearance of indicated strains grown for three weeks on a BG11 plate under standard laboratory conditions (see Methods). B) Identical cells as shown in (A) were resuspended in BG11, their absorption spectra were measured and normalized to light scattering at 750 nm; absorbance peaks at 625 nm and 681 nm represent phycobilisomes and Chl, respectively.

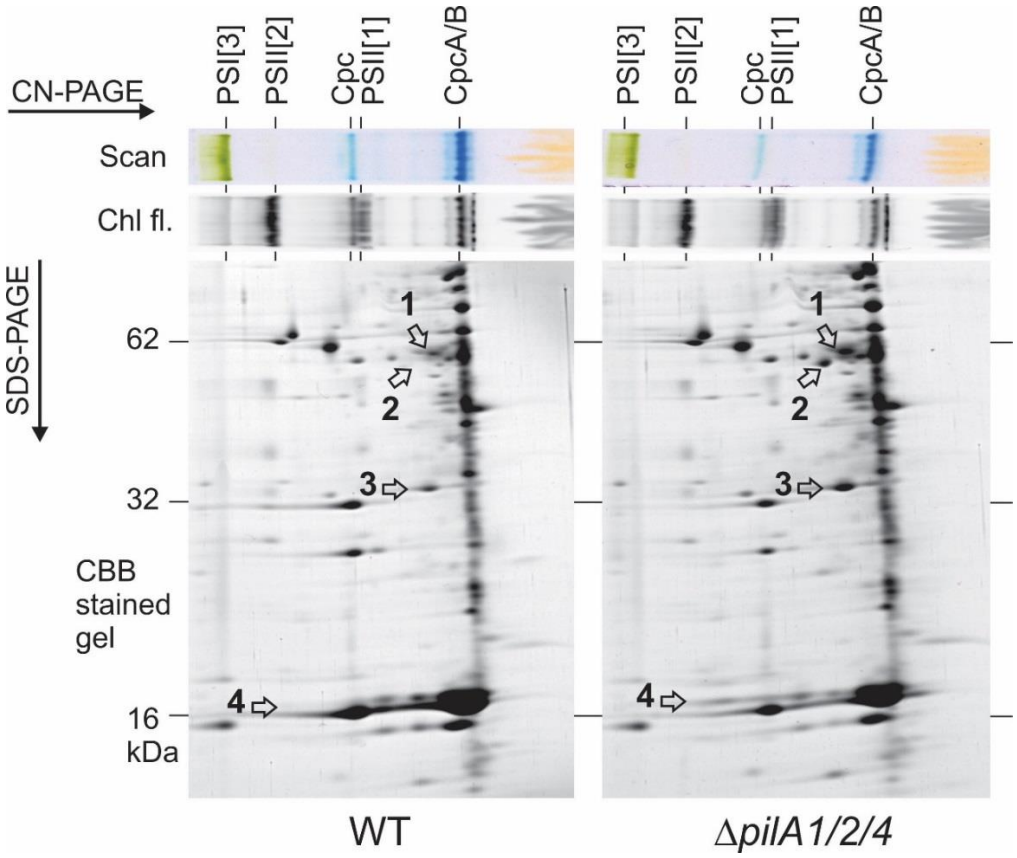

Figure 3.2 The content of membrane proteins in WT and Δ*pilA1/2/4* pilin mutant after prolonged cultivation on agar plates. 2D CN/SDS-PAGE of the isolated protein samples from cells cultivated on the identical agar plate as shown in Figure 3.1A. Each loaded sample contained 4 μg of Chl. The gel was stained with Coomassie blue and the marked spots were analyzed by protein MS (Table 3.1). Designation of complexes and subunits: PSI[3] - Photosystem I trimer, PSII[2] - Photosystem II dimer, Cpc – phycobilisome rod linkers, PSII[1] - Photosystem II monomer, CpcA/B – phycocyanin α and β subunits. Black arrows represent 1. Slr1349/G6PI, 2. Sll1693, 3. Slr1963/OCP, 4. HspA/Hsp17. Chl fl. - Chl fluorescence after excitation with blue light.

Table 3.1. A list of membrane proteins, with levels differing markedly in the WT and the Δ*pilA1/2/4* cells when cultivated on an agar plate for three weeks. See Figure 3.2 for spot intensity. *PLGS score represents peptide assignment accuracy calculated using the Protein Lynx Global Server (PLGS 2.2.3) software (Waters).

Spot	Protein	Coverage (%)	kDa	PLGS Score*	Function
1	G6PI	66.5	58.3	1811	Glucose-6-phosphate isomerase
2	Sll1693	40.0	50.6	2299	Unknown, upstream gene to *pilA1*
3	OCP	71.0	34.6	2541	Orange carotenoid-binding protein
4	Hsp17	65.1	16.6	879	16.6 kDa small heat shock protein

3.2 Arrested proliferation of pilin mutants in late growth phases

Under our standard laboratory conditions the liquid cultures of *Synechocystis*, starting at low OD_{730} (~ 0.1), grow exponentially for 3-4 days up to OD_{730} ~ 1 (equivalent to 5.5 µg of Chl ml^{-1}). After this point, the proliferation rate (doubling time) declines but the growth continues as a linear growth phase. Finally, after an additional 8 to 14 days, the number of cells remains constant with the onset of the stationary phase (Esteves-Ferreira et al., 2017; Schuurmans et al., 2017). Although the growth rate of WT cells can significantly vary from the 5th day, WT continues in proliferation for an additional 10 - 15 days reaching OD_{730nm} > 5. This is in sharp contrast with the Δ*pilA1/2* mutant, the growth of which is arrested around the 6th day at OD_{730nm} ~ 1.3 (8.5 µg of Chl ml^{-1}, Figure 3.3).

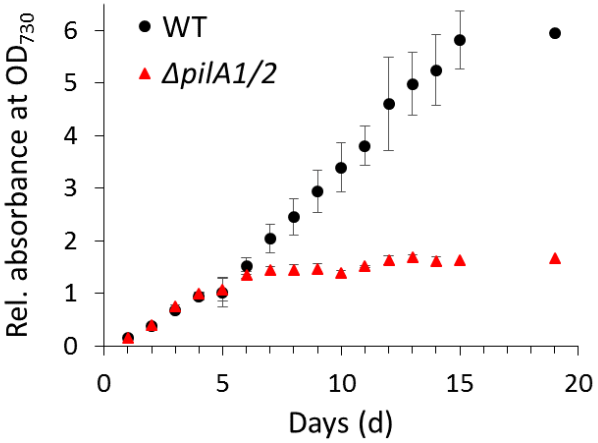

Figure 3.3. Growth curves of WT and Δ*pilA1/2* cultures under our standard laboratory conditions. Liquid cultures of WT and Δ*pilA1/2* strains were grown in triplicates and their optical density was measured at 730 nm at the indicated time points.

To clarify, when assessing the inhibited growth of the Δ*pilA1/2*, I compared its absorbance spectra with WT during the exponential (day 1), linear (day 5), late linear (day 10 and 15), and stationary growth phases (day 20; Figure 3.3). On the 5th day, the cell spectra of both strains were similar with a decrease in phycobilisomes in Δ*pilA1/2* (Figure 3.4). Nonetheless, the content of phycobilisomes in the Δ*pilA1/2* decreased more after 10 days along with a substantial increase in the level of carotenoids, consistent with the phenotype described for cells grown on agar plates (Figure 3.2B). After 20 days, the phycobilisome level in the mutant further decreased and there was also a significant reduction in the content of Chl (57.4 ± 8.7 % of WT level, n=6).

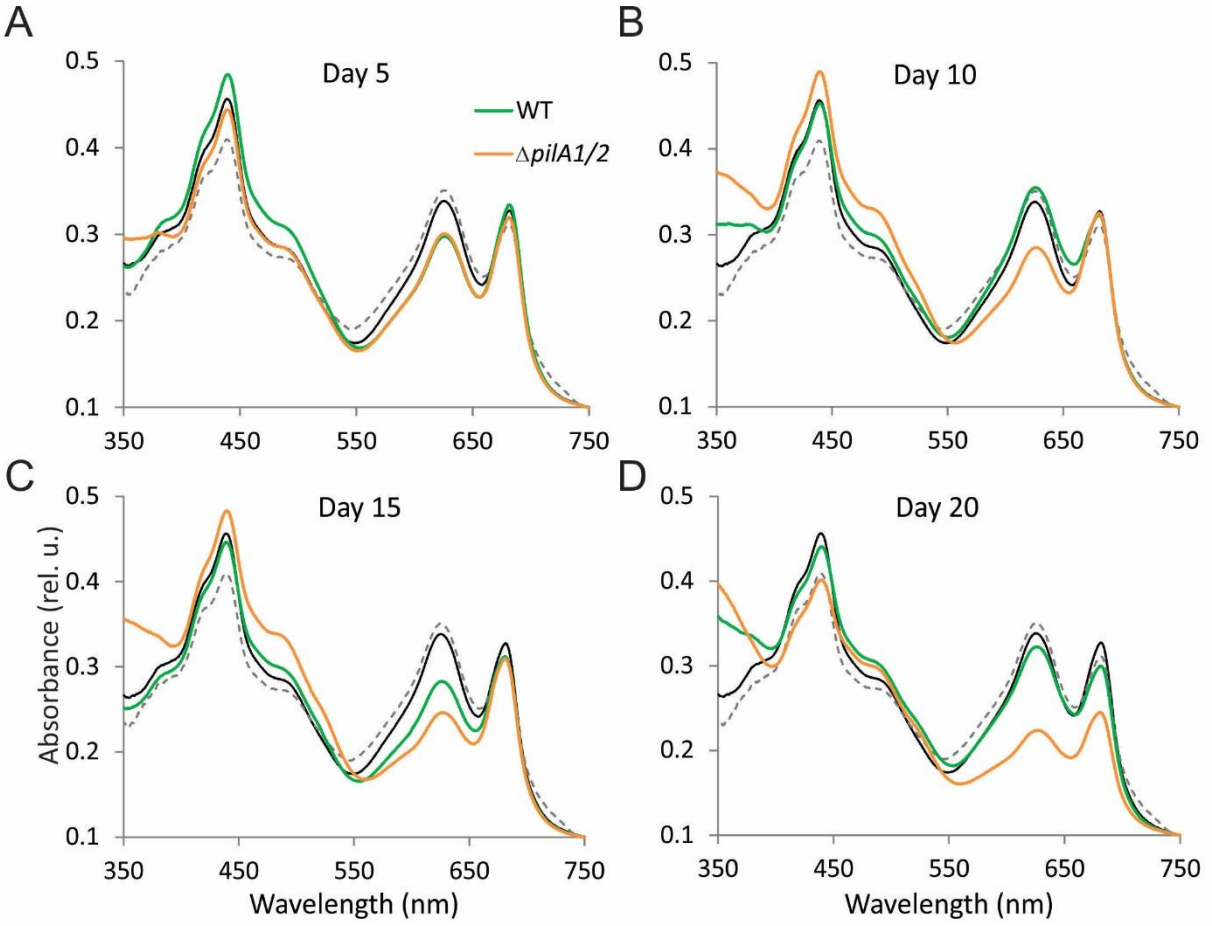

Figure 3.4. Whole-cell absorption spectra of the WT and Δ*pilA1/2* mutant measured in different growth phases. Cells were grown photoautotrophically in liquid cultures and their absorption spectra were measured during 20 days. The exponential phase of growth (Day 1) is compared with A) Day 5 (early linear phase), B) Day 10, C) Day 15 (late linear phase), and D) Day 20 (stationary phase). Full black and dashed grey lines represent WT and Δ*pilA1/2* at Day1, respectively. Green and orange lines represent WT and Δ*pilA1/2*, respectively, at the day indicated in the title of each chart. Spectra were normalized to light scattering at 750 nm, wavelengths between 450 and 500 nm are absorbed by carotenoids, peaks at 625 nm and 682 nm represent phycobilisomes and Chl, respectively. The absorbance in the UV region might be increased due to accumulated extracellular polymeric substances (see below).

PSI complexes bind most of Chl in the *Synechocystis* cell (>80%) and also represent the main sink for *de novo* Chl (Kopečná et al., 2012). The observed loss of phycobiliproteins and Chl (PSI) in pilin mutants during the senescent phase of growth thus signalled a potential defect in the tetrapyrrole pathway. I therefore analysed metabolites of the tetrapyrrole pathway during long-term cultivation of the WT and the pilin mutant according to Pilný et al. (2015). When compared to the exponential phase (1d, Table 3.2), WT cells increased the levels of most of the Chl precursors on the 5th day but they dropped down on the 10th day and the *de novo* pathway seems to be blocked after 15 days of

cultivation. The persisting high level of the monovinyl chlorophyllide present in WT after 10 and 15 days should originate from Chl catabolism (Chl recycling) rather than from the *de novo* Chl pathway (Kopečná et al., 2015). The Δ*pilA1/2* strain accumulated similar levels of Chl precursors as WT in the exponential phase (1d). However, unlike in the WT, the content of Chl precursors had already diminished on the 5th day in the mutant and only the level of monovinyl chlorophyllide remained high on the 10th and 15th day. Downregulation of tetrapyrrole biosynthesis at the transition from the exponential to the linear phase could explain the observed gradual decrease in the content of phycobilisomes (Figure 3.4).

Table 3.2. A relative level of heme/Chl precursors in the WT and Δ*pilA1/2* strains during the 15 days of cultivation. All values refer to a peak area of fluorescence peaks measured by HPLC fluorescence detectors Pilný et al. (2015) and were normalized to the WT 1d sample. d = days, CoPP = coproporphyrin III, PPIX = protoporphyrin IX, MgP = Mg-protoporphyrin IX, MgPME = Mg-protoporphyrin IX monomethyl ester, DV Pchlide = divinyl protochlorophyllide, MV Chlide = monovinyl chlorophyllide.

	Chl precursors (% of WT 1d)					
Strain	**CoPP**	**PPIX**	**MgP**	**MgPME**	**DV Pchlide**	**MV Chlide**
WT 1d	100	100	100	100	100	100
WT 5d	382	406	318	197	92	189
WT 10d	32	22	18	79	11	227
WT 15d	10	2	3	15	2	207
Δ*pilA1/2* 1d	91	111	91	123	90	82
Δ*pilA1/2* 5d	34	38	6	14	11	287
Δ*pilA1/2* 10d	9	0	2	10	7	561
Δ*pilA1/2* 15d	22	3	3	13	9	413

The growth *defect* in the Δ*pilA1/2* strain is already obvious during the early linear phase (day 5, Figure 3.3) correlating with the downregulated levels of heme/Chl precursors (Table 3.2). However, significant changes in Chl and phycobilin content are detectable later, after 10 days (Figure 3.4). To obtain a detailed view on the content and stoichiometry of photosynthetic complexes, I harvested cells at the 1st, 5th, 15th, and 20th days referring to the exponential, early linear, late linear and stationary phase, respectively. Membrane protein fractions isolated from cells were solubilized and separated on CN-PAGE (Figure 3.5). The PSI to PSII ratio as well as the ratio of dimeric and monomeric PSII (PSII[2] and PSII[1]) can be assessed from the comparison of the colour scan of the gel (Figure 3.5 A) and the Chl fluorescence detection 'in gel' after excitation with blue light (Figure 3.5 B). The level of PSI trimer (PSI[3]) in WT visibly decreased between the 1st and the 15th days

and then remained constant, consistent with the cell spectra (Figure 3.5 A). WT cells also gradually reduced the level of PSII during the whole time-course of the growth experiment but a sharp drop in the PSII[2] occurred on the 5th day greatly lowering the PSII[2]/PSII[1] ratio (Figure 3.5 B). Although the Δ*pilA1*/*2* mutant contained virtually the same levels of PSI and PSII as WT on the 1st day, it maintained significantly more PSII, in particular its dimeric form, than WT on the 5th day. The PSI content was reduced in the later stages of the growth with a sharp decrease in the PSI[3] after 20 days of cultivation (Figure 3.5 A).

Interestingly, despite the mutant containing a higher level of PSII than WT after 5 days of growth, the PSII activity (oxygen evolution) was lower (370 ± 20 µmol of O_2 mg Chl^{-1} h^{-1}; n=3) than in WT (532 ± 41 µmol of O_2 mg Chl^{-1} h^{-1}; n=3). The reduced activity of PSII in the mutant can also be detected on the 10th day of the experiment (175 ± 35 to 351 ± 121 µmol of O_2 mg Chl^{-1} h^{-1}; n=3). This data indicates that PSII complexes in the pilin mutant are not fully active or there is a large pool of inactivated PSII. Moreover, after 15 days, membrane-attached ribosomes were almost absent in WT cells but present in the mutant (Fig 3.6), well detectable also in the ultrastructure of the cells (compact black spots, Fig 3.9), indicating higher protein biosynthetic activity of the mutant. An interesting trait of WT cells was the accumulation of iron transporter FutA1 and phosphate-binding periplasmic PstS protein indicating nutrient limitation after 15 days which is absent in the mutant (see Discussion, Figure 3.6).

To clarify the lower activity but higher content of PSII complexes in the Δ*pilA1*/*2* mutant during the early linear growth phase (day 5), I analyzed the rate of *de novo* synthesis of photosynthetic complexes by protein [^{35}S] radiolabelling. As a control, the same experiment was performed with WT and Δ*pilA1*/*2* cells harvested in the mid-exponential phase, which showed no obvious differences. Cells were pulse-labelled for 30 minutes by a mixture of [^{35}S] cysteine and methionine and the isolated membranes were separated on SDS-PAGE (Figure 3.7). The gel was stained with Coomassie Blue, dried and the radioactivity was visualized using a phosphorimager plate. The exponentially-grown WT and Δ*pilA1*/*2* cells had a comparable synthesis of membrane proteins except for the missing PilA1 protein in the mutant (Figure 3.7 B). Intriguingly, WT cells from the early linear growth phase (5th day) contained a much higher level of the labelled precursor of D1 (pD1) than cells harvested during exponential growth. This finding contrasted to the weakly labelled pD1 and iD1 in the mutant; the later protein is a partially matured D1 subunit (intermediate D1; Figure 3.7 B). Additionally, the FtsH2/FtsH3 protease complex was less

labelled in the Δ*pilA1/2* strain during linear growth as well as an unknown <10 kDa protein (labelled by an asterisk on Figure 3.7 B).

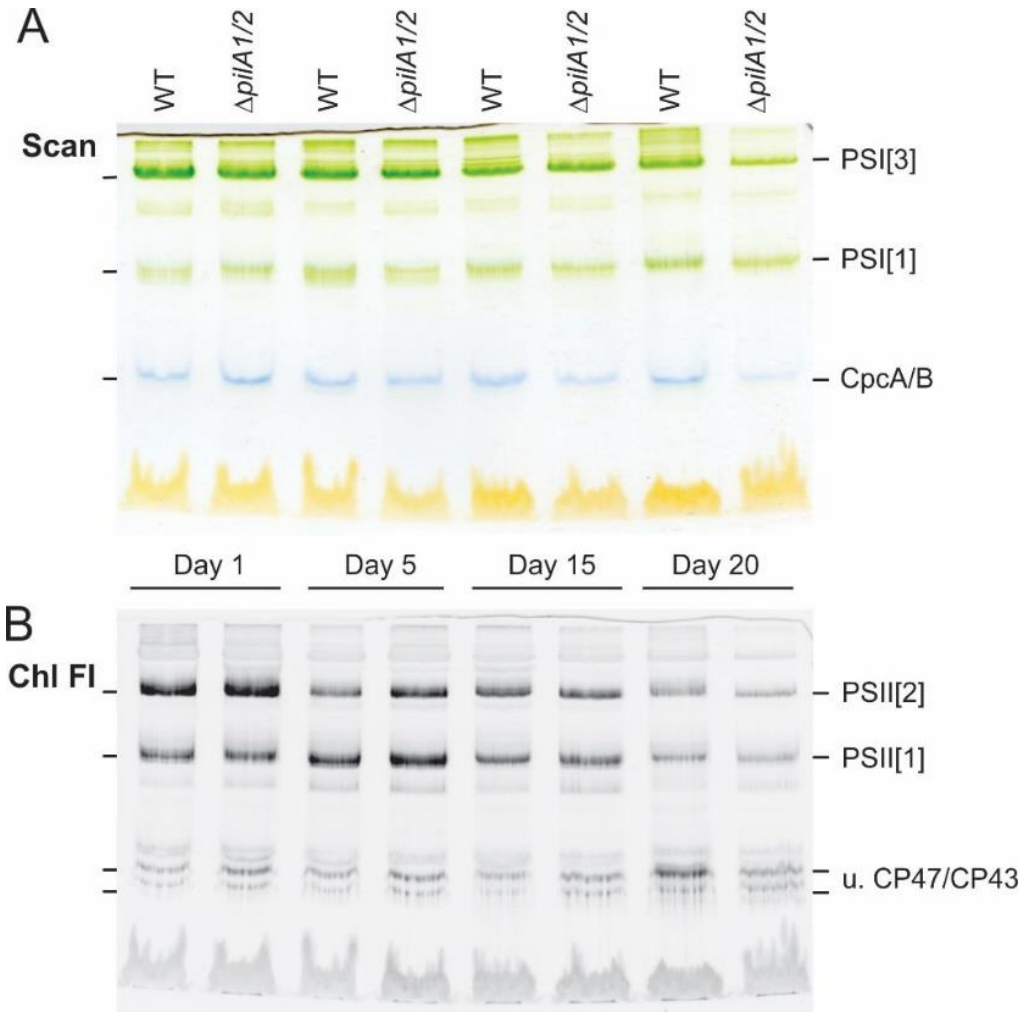

Figure 3.5. Composition of membrane protein complexes in WT and Δ*pilA1/2* cells harvested at different growth stages. Cells were harvested on the indicated day, broken and the isolated membranes were solubilized by dodecyl-β-maltoside. Each sample was loaded per a similar number of cells (the same optical density at 730 nm). The gel was scanned in true colours (A) and the Chl fluorescence of PSII complexes was measured after excitation by blue light (B). Abbreviations used: Photosystem I trimer (PSI[3]); Photosystem I monomer (PSI[1]); α and β subunits of phycobilisomes (CpcA/B); Photosystem II dimer (PSII[2]); Photosystem II monomer (PSII[1]); unassembled subunits of PSII (u. CP47/CP43).

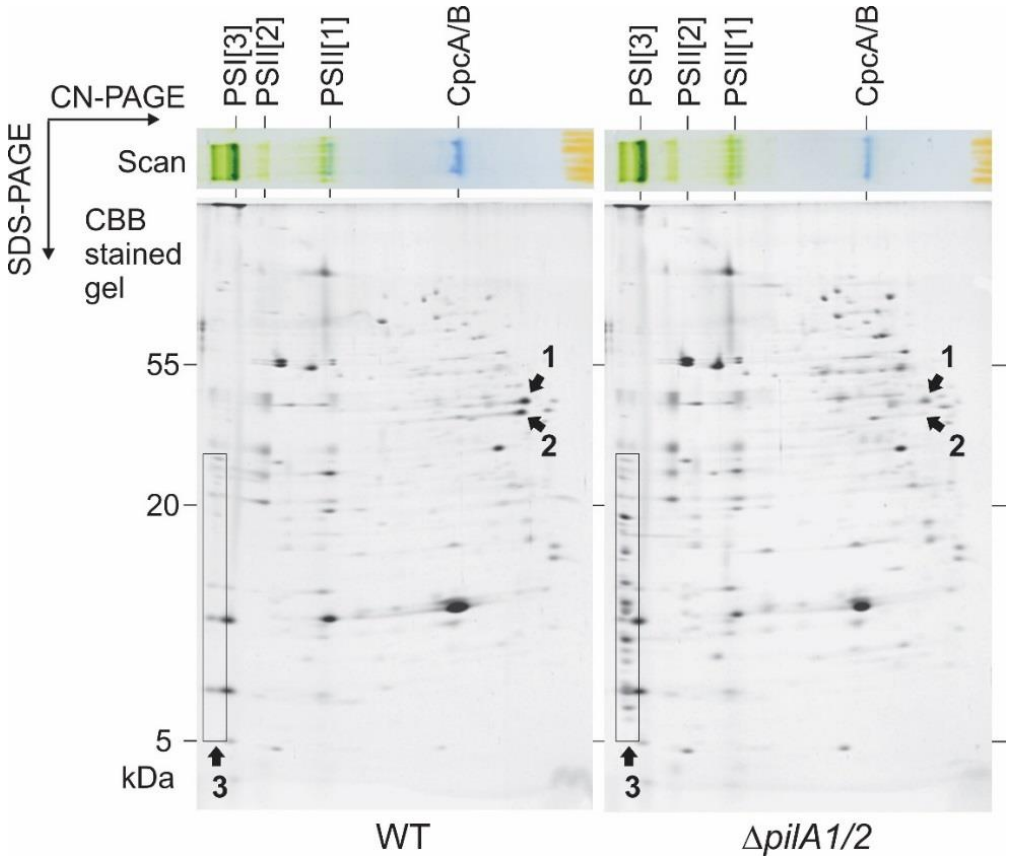

Figure 3.6. Membrane fractions of the WT and Δ*pilA1/2* mutant grown for 15 days in a liquid medium. Isolated membrane proteins, loaded to a similar number of cells (the same optical density at 730 nm), were separated using 2D CN/SDS-PAGE. The gel was stained with Coomassie blue and the spots marked with arrows were identified by protein MS. Designation of complexes and subunits: Photosystem I trimer (PSI[3]); Photosystem II dimer (PSII[2]); Photosystem II monomer (PSII[1]); α and β subunits of phycobilisomes (CpcA/B). Black arrows represent 1) PstS; 2) FutA1; 3) ribosomal subunits.

The identical radiolabelled samples as described above were further separated by 2D CN/SDS-PAGE (Figure 3.8). Most of the observed protein spots on the Coomassie-stained gel, including subunits of PSII, appeared very similar in both analysed strains (not shown). However, consistent with the result of the 1D SDS-gel, the mutant differed in the labelling of the D1 subunit (Figure 3.8). Remarkably, the majority of the newly synthesized (labelled) D1 in the mutant was already incorporated into monomeric and dimeric PSII complexes, whereas a large pool of the unassembled D1 can be detected in WT. The fast protein maturation and incorporation into PSII in the mutant became particularly prominent during the linear growth phase (see Figure 3.8) where it also visibly concerns D2 and CP43 subunits. These data strongly indicate that the PSII complexes undergo faster turn-over in the pilin mutant and need to be synthesized and repaired more actively.

In summary, the results shown so far have indicated that the 'overgrown' pilin mutant is impaired in maintaining the active PSII and the content of PSI. In a five-day old culture, the mutant can synthesize enough of the D1 subunit (Figure 3.8) and assemble new PSII complexes even more intensively than WT (Figure 3.9), but a large portion of PSII complexes in the mutant are either less active or non-active (see Discussion).

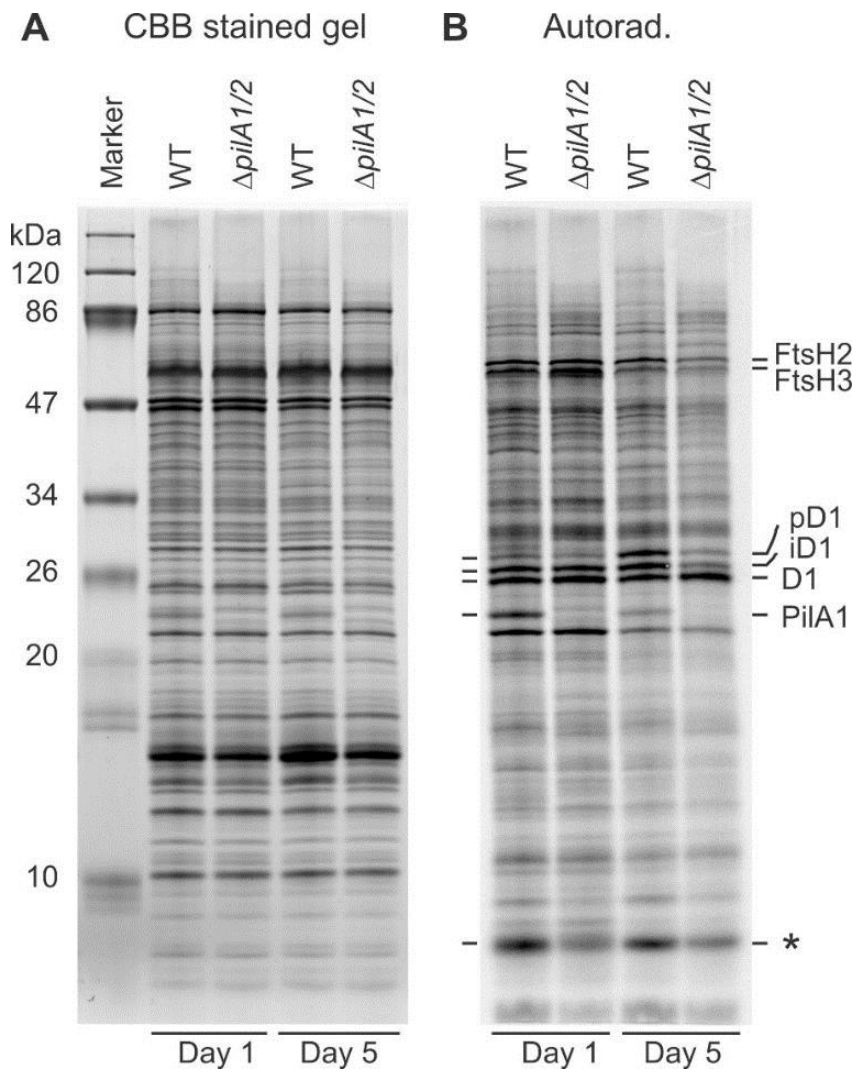

Figure 3.7. Synthesis of membrane proteins in WT and Δ*pilA1/2* mutant grown for one and five days in a liquid medium. Cells were pulse-labelled for 30 min with a mixture of [^{35}S] labelled Met/Cys, and the isolated membrane proteins corresponding to 2 μg Chl were separated using denaturing SDS-PAGE. The gel was stained with Coomassie blue (A), dried and then exposed to a Phosphorimager plate (Autorad.; B). All three forms of the D1 protein are marked, a precursor of D1 (pD1); an intermediate of D1 maturation (iD1); matured D1 subunit of PSII (D1).

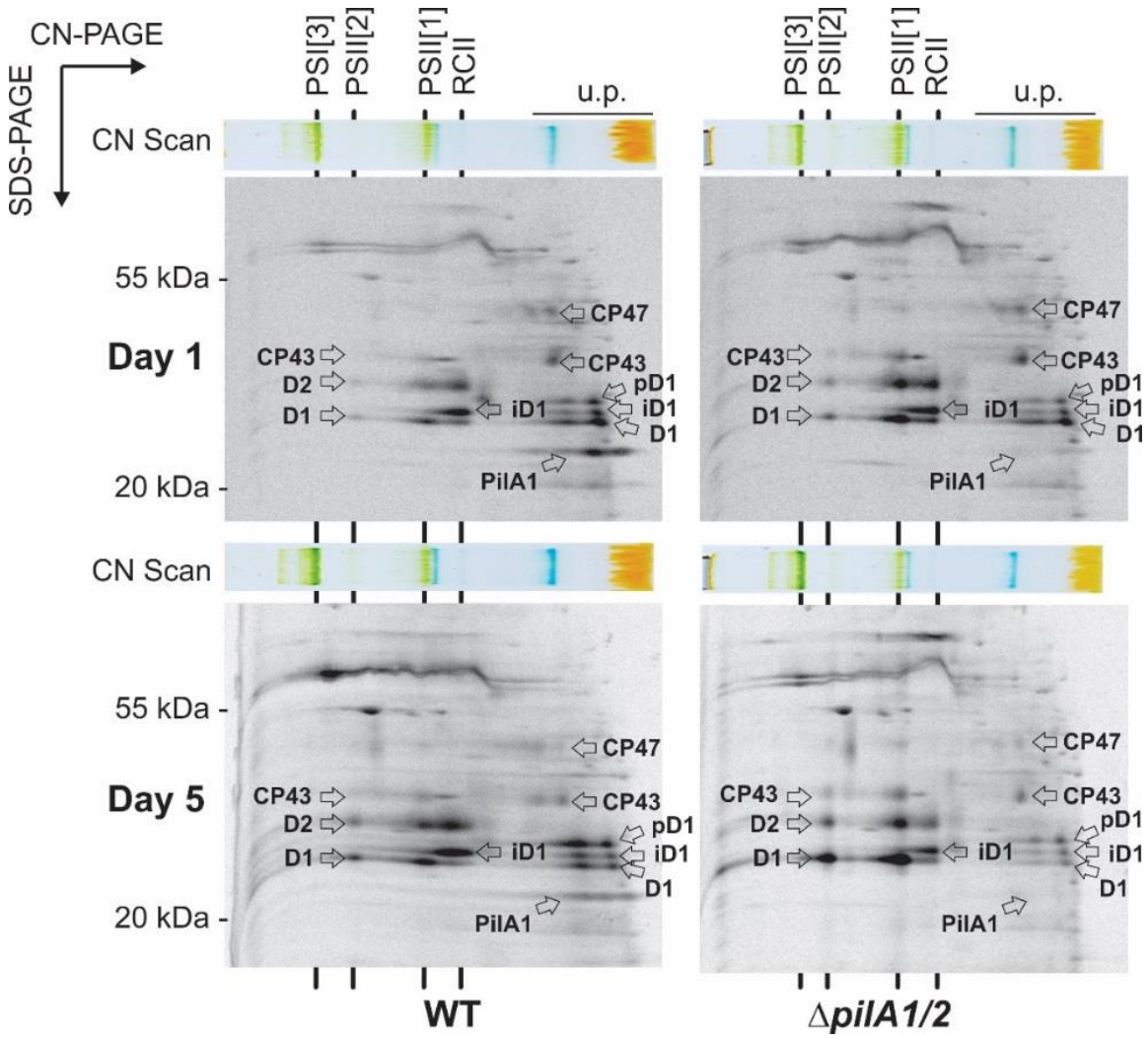

Figure 3.8. Synthesis and assembly of membrane protein complexes in WT and Δ*pilA1/2* in the exponential and linear phases of the growth. Isolated membrane proteins from [^{35}S] radiolabelled cells described in Figure 3.7 were first separated by CN-PAGE (4 µg per sample) and then in the second dimension by SDS-PAGE. The gel was stained with Coomassie blue (not shown), dried and exposed to a Phosphorimager plate. All three forms of the unassembled D1 protein are marked with transparent arrows, 1 - pD1, 2 - iD1, 3 - D1, D2, CP43, and CP47 are subunits of PSII.

Apart from changes in pigmentation of the Δ*pilA1/2* mutant I observed an increase in UV-A absorbance (350-400 nm) during the late growth phases accompanied by higher viscosity of the growth medium. This absorbance was higher for the mutant culture (Fig 3.4 and 3.9 A). As cyanobacteria can secrete extracellular polymeric substances (Li and Yu, 2014), I measured the content of these compounds in a filtered growth medium according to Thornton et al. (2007). The result suggested that both strains were releasing a similar amount of polysaccharides until the 5th day of cultivation (Figure 3.9 B). However, the concentration of excreted polysaccharides were significantly reduced in the WT cell

culture between the 5th and 15th day of cultivation, while it remained constant in the mutant culture. A potentially relevant observation is that the mutant cells accumulate glycogen granules after long-term incubation meaning that although they were no dividing, the cells fixed carbon and stored glycogen in a large quantity (Fig 3.9 C).

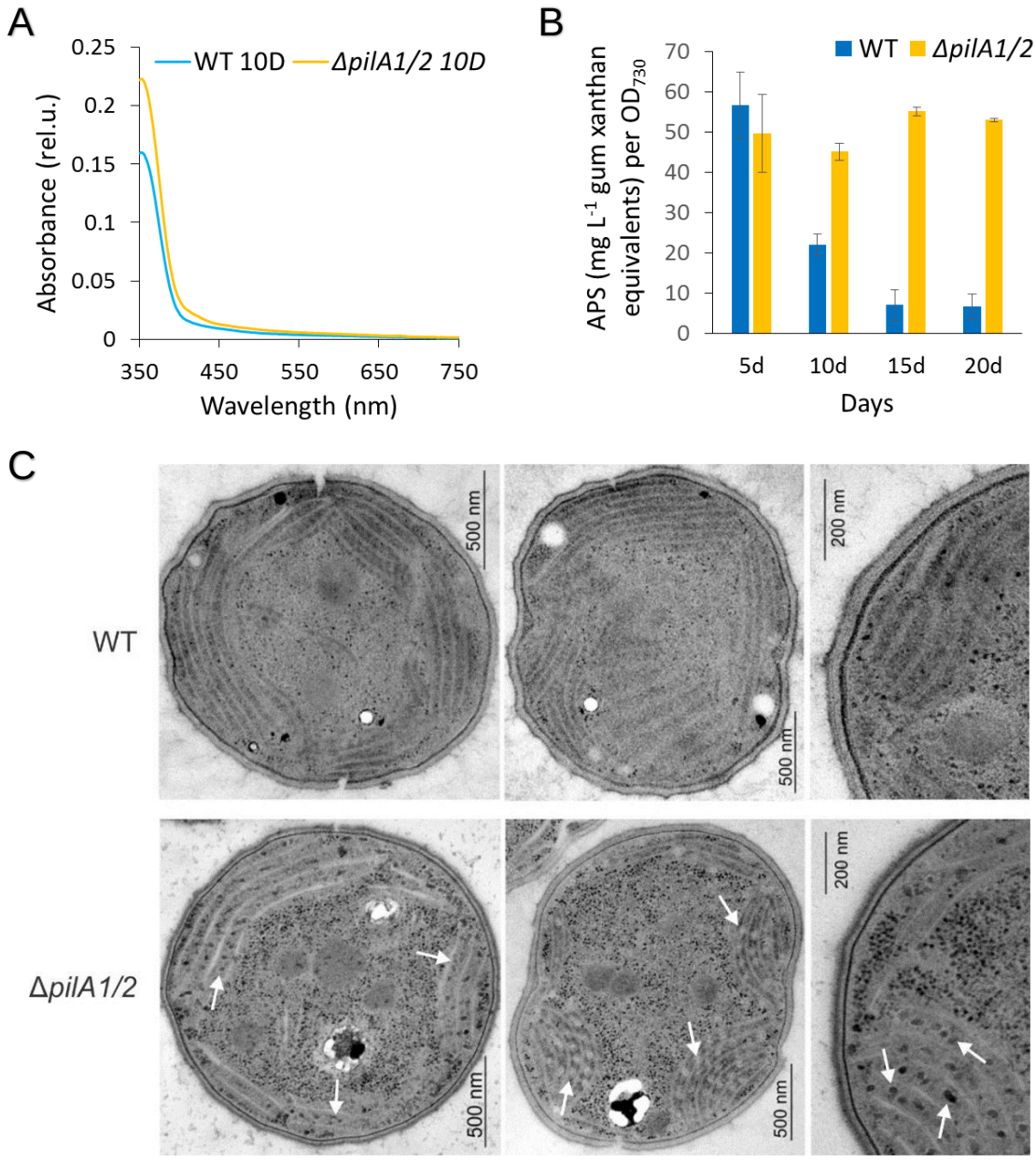

Figure 3.9. Detection and quantification of acid polysaccharides (APS) in growth media and glycogen granules in long-term cultivated WT and Δ*pilA1/2*. A) Absorbance of filtered media after 10 days of cultivation normalized to the same OD_{730nm}. B) Content of acid polysaccharides in the growth media measured with an Alcian assay and normalized to the optical density of cells at 730 nm. The bars show standard deviations (n=3). C) Ultrastructure of the cells after 15 days of cultivation. Ultrathin sections were analyzed with transmission electron microscopy (Bučinská L., unpublished data). Vesicle-like structures (indicated with white arrows) surrounding the thylakoid membrane only in the mutant cells are glycogen granules (appear white or black, depends on reaction with the contrasting agent). Tiny black spots spread all over the cells are ribosomes.

3.3 The minor PilA2 pilin is required for the accumulation of glycosylated PilA1

The *pilA2* gene is located downstream of the *pilA1* in the *Synechocystis* genome but both genes are expressed as separated transcripts (He and Vermaas, 1999; Yoshihara et al., 2001). Contradictory data on the expression level of *pilA2* range from a high expression (Yoshihara et al., 2001), an expression similar to other *pilA* genes, *e.g.* to *pilA1* (Orf et al., 2016), or to an undetectable expression (Bhaya et al., 2000). Although the role of PilA2 minor pilin is unknown, down-regulation of *pilA2* and *sigF* were among the strongest expression responses under very high illumination (Ogawa et al., 2018). I found that the level of PilA1 protein in the *Synechocystis* Δ*pilA2* mutant is significantly lowered (Figure 3.10 A; B). In addition, the *pilA2* cells harvested during the linear growth phase contained a detectable amount of an unknown PilA1 form with mobility that would correspond to non-glycosylated PilA1(Figure 3.10 B). During the late growth phases, the Δ*pilA2* strain also exhibited a similar pigment bleaching as I described earlier for the Δ*pilA1*/*2* strain (Figure 3.1-A and 3.11). A most dramatic change in the Δ*pilA2* cell absorption can be observed between 14 and 20 days of cultivation. However, the Δ*pilA2* mutant showed a somewhat better performance than Δ*pilA1*/*A2* in the linear growth phase reaching a higher OD_{730} between the 5^{th} and the 10^{th} day of cultivation, typically around 2 (Figure 3.11.).

Finally, I analyzed the content of membrane proteins isolated from Δ*pilA2* cells by 2D CN/SDS-PAGE. Notably, the Δ*pilA2* mutant accumulated quantities of a large protein (Figure 3.12) identified as Slr0442 (62.9 kDa, coverage 33.4%, PLGS score 2444); high levels of Slr0442 can also be observed in Δ*pilA1*/*2* or Δ*pilA1*/*2*/*4* mutants (not shown). The Slr0442 is predicted to be a bait-chain like protein with an N-terminal transmembrane segment and an unusual 60 amino-acid long Ser/Pro-rich region at its C-terminus (see Figure 3.13). The *slr0442* gene is a known target of the cAMP-regulated pathway and it is worth noting that the cAMP messenger stimulates motility in *Synechocystis* and mediates blue-light sensing for phototaxis (Terauchi and Ohmori, 1999, 2004; Dienst et al., 2008; Hedger et al., 2009). I prepared a *Synechocystis* Δ*slr0442* strain and tested its growth characteristics under photoautotrophic (medium and low light) conditions or mixotrophic conditions (with 10 mM glucose) but there was no obvious difference from WT (data not shown). Similarly, the phenotypes of Δ*pilA1*/*2 and* Δ*slr0442*/*pilA1*/*2* strains showed no observable differences.

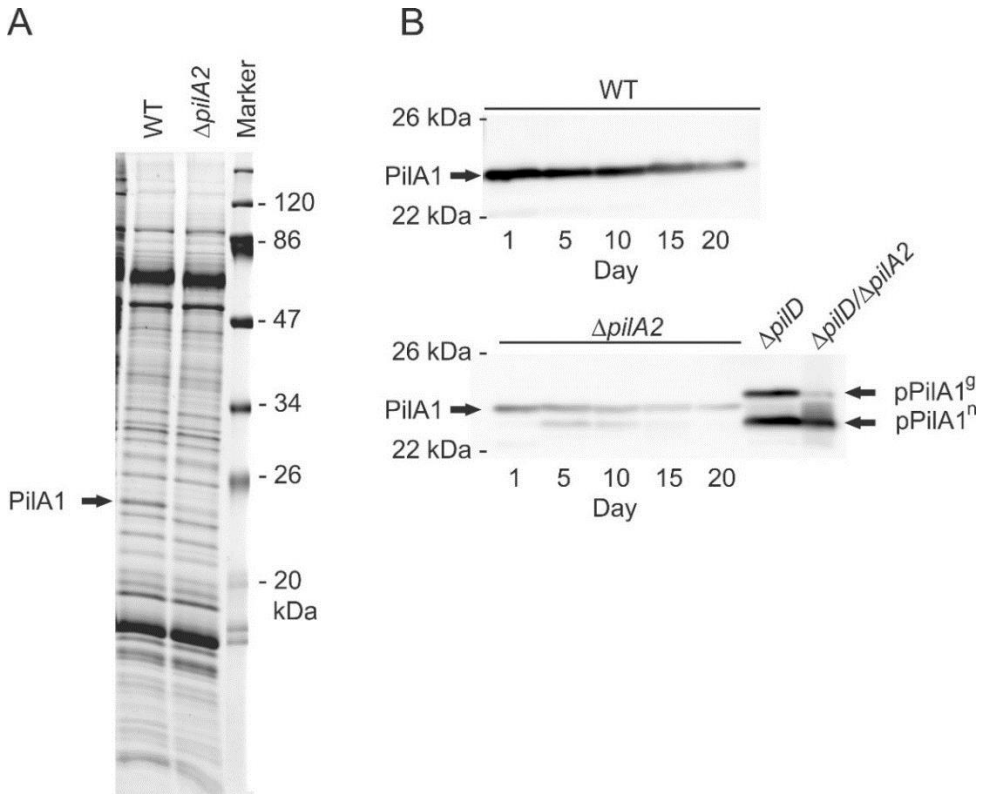

Figure 3.10. Impaired biogenesis of PilA1 in the Δ*pilA2* strain. A) Membrane proteins isolated from the exponentially grown WT and Δ*pilA2* strains separated by SDS-PAGE and stained with Coomassie blue; 1 µg of Chl loaded per each sample. The PilA1 protein is indicated with an arrow. B) Membrane protein fractions isolated during the aforementioned time-course experiment were separated using SDS-PAGE, electroblotted and PilA1 was detected with the specific antibody. The PilA1 signals for WT and Δ*pilA2* come from the same exposition of the blot. The Δ*pilD* strain was included as a control; a non-glycosylated form of the PilA1 prepilin (pPilA1^{n}); glycosylated prepilin PilA1 (pPilA1^{g}).

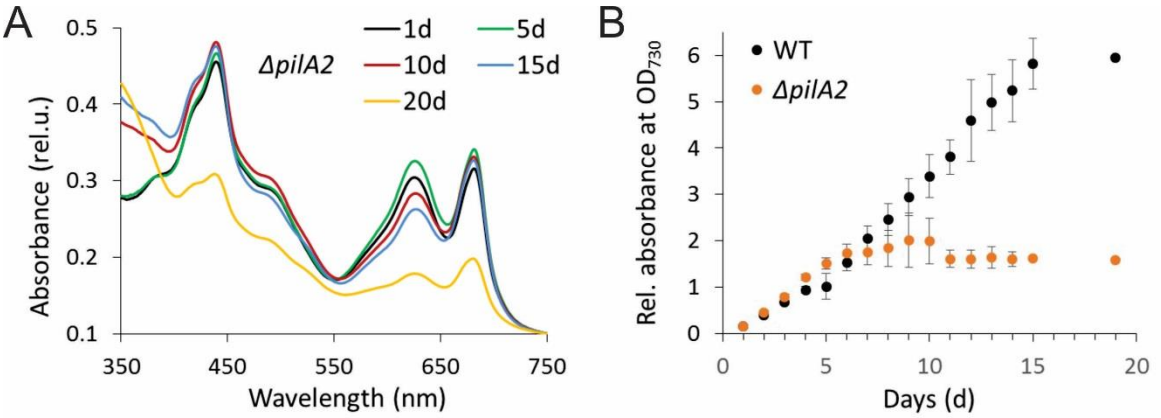

Figure 3.11. The pigment content and growth rate of the Δ*pilA2* strain during different phases of growth. A) Whole-cell absorption spectra of Δ*pilA2* strain normalized to light scattering at 750 nm. Starting with exponential cultures at OD_{750} ~ 0.3, the strain was cultivated for 20 days in liquid BG11. B) Growth curves of WT and Δ*pilA2* strains under standart laboratory contitions. OD_{730} were measured in the indicated time points. The bars show standard deviations (n=3).

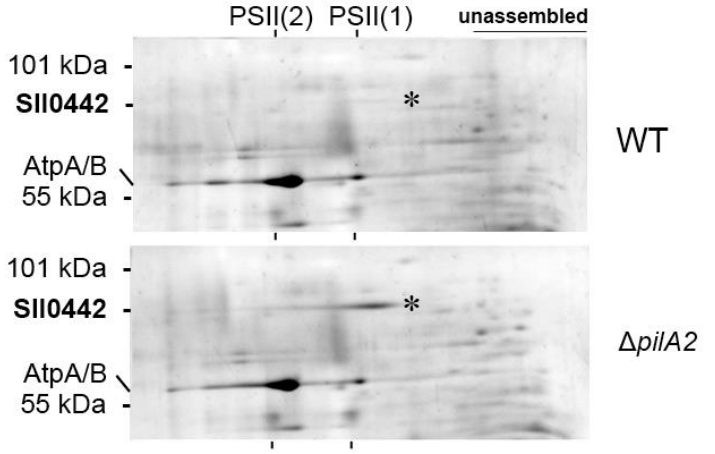

Figure 3.12. Accumulation of the Slr0442 protein in the Δ*pilA2* strain. Membrane proteins isolated from the stationary grown WT and Δ*pilA2* strains were separated on the 2D CN/SDS-PAGE and then stained with SYPRO Orange; 4 µg of Chl was loaded per each sample.

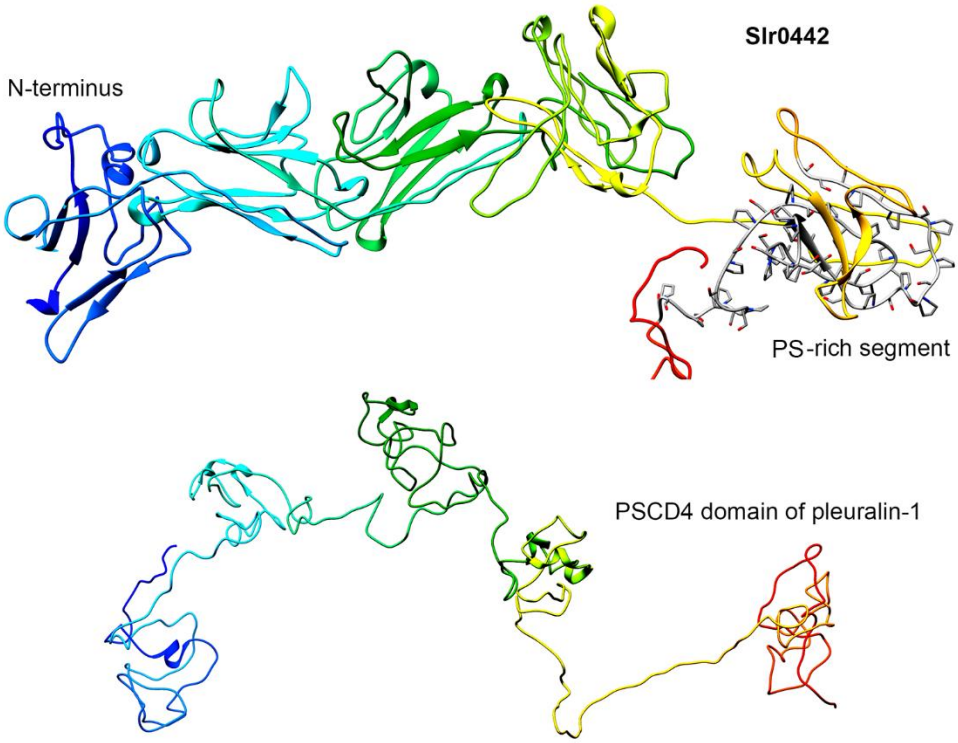

Figure 3.13. A structural model of the *Synechocystis* Slr0442 protein. A) 3D structure of the Slr0442 has been predicted using iTASSER, the beat-chain like region of Slr0442 is highlighted by different colours (from blue to yellow) for each beat domain. C-terminal Pro-Ser -rich domain is in grey. B) The structure of Pleuralin 1 from *Cylindrotheca fusiformis* (diatoms, PBD code - 2NBI, 2MK0) is shown as an example of a beat-chain protein with a Pro-Ser -rich domain (De Sanctis et al., 2016).

3.4 Purification of the PilA1 protein using Flag-tag

To identify proteins interacting with PilA1, I prepared a *Synechocystis* strain expressing PilA1 fused at its C-terminus with 3xFlag tag (PilA1-Flag). The accumulation of the PilA1-Flag in the membrane fraction was confirmed with specific PilA1 and Flag antibodies (data not shown). The purification of PilA1-Flag was performed from the membrane fraction isolated from either exponentially grown or late-linear growth phase PilA1-Flag cells (15 days). To exclude proteins interacting in a non-specific way with the resin, a control purification was performed with WT membranes and these hits were subtracted from the list. A list of unique proteins co-eluted from the resin with PilA1-Flag contains prohibitin 2 (Slr1768), a protein implicated in the maintenance of thylakoid membrane after light damage (Bryan et al., 2011), an ABC transporter involved in motility (Bhaya et al., 2001b), and two unknown proteins. Of them, Sll1696 is a downstream gene of *pilA2* while Sll1106 is a glycine zipper protein, which deletion affects ferrochelatase activity and Chl biosynthesis (Skotnicová, 2019). Interestingly, PilA1 has been previously co-eluted with Sll1106-Flag used as bait (Skotnicová, 2019).

Table 3.3. A list of proteins co-eluted with PilA1-Flag protein isolated from exponentially and linearly grown *pilA1*-Flag cells. Proteins were identified using protein MS and proteins grey highlighted were present in PilA1-Flag preparations from both exponentially and linearly (15 days) grown cultures. Proteins identified in eluates from WT cells were subtracted. * The PLGS score is a statistical measure of peptide assignment accuracy; it is calculated with Protein Lynx Global Server (PLGS 2.2.3) software (Waters).

Protein	Coverage (%)	kDa	PLGS Score*	Function
PilA1	17.3	17.6	459.3	Major pilin – bait
Slr1768	22.8	32.8	399.1	Prohibitin 2
Sll0415	21.2	39.5	386.8	ABC transporter
Sll1106	33.9	18.0	351.0	Unknown
Sll1696	18.1	30.3	237.9	Unknown, downstream of the *pilA2* gene

3.5 Iron and manganese limitations

PilA1 and pili in *Synechocystis* have already been connected with manganese or iron uptake (Lamb et al., 2014; Lamb and Hohmann-Marriott, 2017). My experiments with long-term cultivations (Chapters 3.1 and 3.2) revealed a defect in PSII activity and a block in the tetrapyrrole pathway, which could indeed be connected with the uptake of metals. I tested the impact of iron and manganese limitations in liquid cultures of WT and Δ*pilA1*/*2* cells (Figure 3.14). Δ*pilA1*/*2* cells were markedly bleached when grown in a modified BG11

lacking iron and manganese ions. Importantly, a 5 µmol L^{-1} concentration of $MnCl_2$ prevented bleaching and the growth retardation of Δ*pilA1/2* cells in modified BG11 (0Fe/5Mn; Figure 3.14). Nonetheless, the WT cultures reached higher OD_{730} than the mutant in both limited BG11 media (compare Fig 3.14). In another experiment, I supplemented cultures, already stressed by depletion in both metals (0Fe/0Mn), either with 5 µmol L^{-1} of $FeCl_3$ or $MnCl_2$ (Figure 3.14). In contrast to manganese, the supplementation with iron almost fully restored the growth and pigmentation of Δ*pilA1/2* cells.

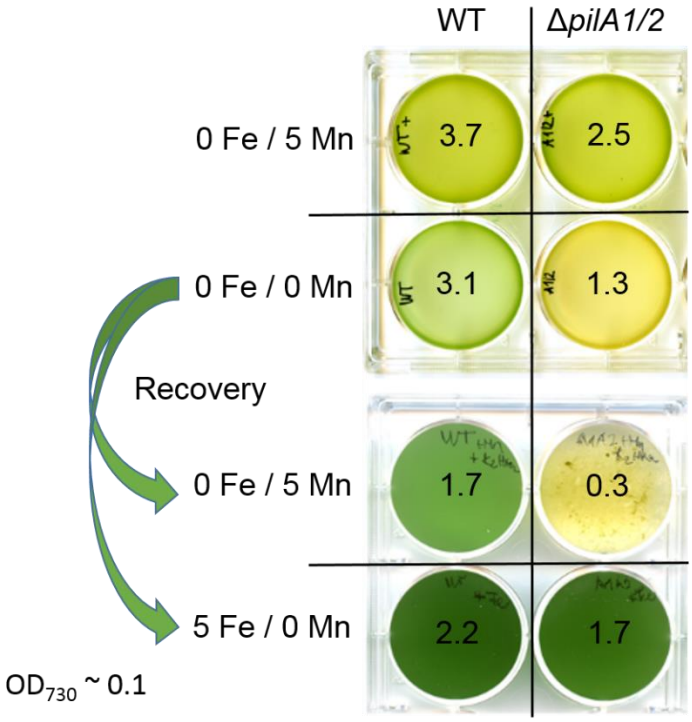

Figure 3.14. The effect of iron and manganese limitation on the Δ*pilA1/2* mutant. WT and Δ*pilA1/2* cells starting at OD_{730} ~ 0.15 were cultivated in a modified liquid BG11 without ferric citrate (0 Fe/5 Mn) or ferric citrate and manganese chloride (0 Fe/0 Mn) at 25 °C for two weeks. Then the optical density of the cultures (OD_{730}) was measured (indicated in each well) to assess the growth under deprivation. At this point, the cultures were diluted to OD_{730} ~ 0.1 with modified BG11 containing either: i) 5 µmol L^{-1} of $FeCl_3$ (5 Fe) or ii) 5 µmol L^{-1} of $MnCl_2$ (5 Mn). The recovery after metal re-supplementation (indicated as OD_{730}) was evaluated after 7 days.

To clarify what other subunits of the pilus apparatus are also essential for the metal homeostasis in *Synechocystis*, individual mutants lacking components of the pilus plasma membrane complex (Δ*pilC*, Δ*pilB1*, or Δ*pilT1*) or the outer membrane pore Δ*pilQ*, were cultivated on a BG11 plate for 15 days (Figure 3.15). Intriguingly, only the Δ*pilT1* strain, lacking a pilus retraction motor, differed in absorption cell spectra when accumulating more

carotenoids and fewer phycobilins than WT (Figure 3.15 A, C). I also tested whether the phenotype of Δ*pilT1* is comparable with Δ*pilA1/2* when cultivated in iron and manganese deprivation. Indeed, the bleaching phenotype is present for Δ*pilT1* cells although it is less severe than in Δ*pilA1/2* (Figure 3.15 B).

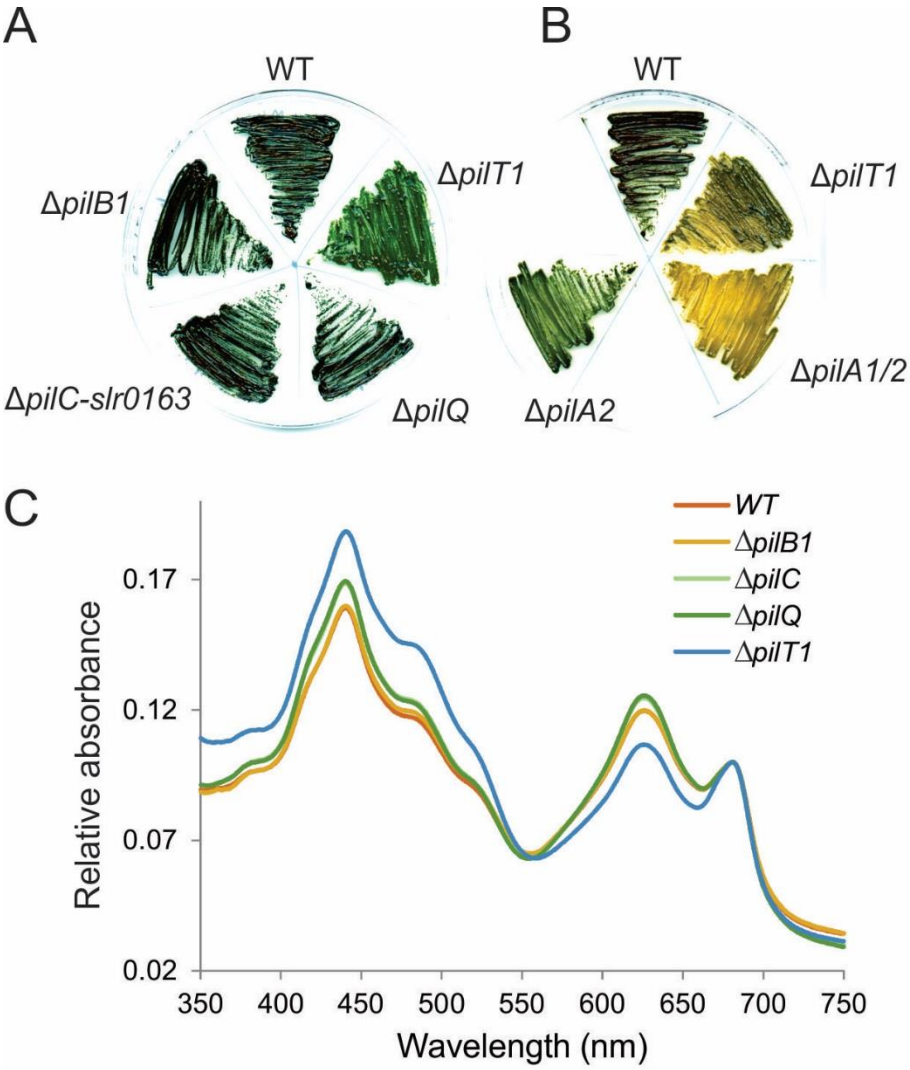

Figure 3.15. The effect of prolonged cultivation of *pil* mutants on agar plates. BG11 plates with indicated strains were scanned after three weeks of incubation under standard laboratory conditions (A) or iron and manganese deprivation (B, see Methods). C) Cells from the plate (A) were resuspended in BG11 and their absorption spectra measured and normalized to light scattering at 681 nm; the peak at 625 nm represents phycobilisomes and 681 nm Chl.

4. Discussion

4.1 Is the pilus basal complex active in the non-motile *Synechocystis* WT?

The original *Synechocystis* strain, deposited in 1968 into the Pasteur Culture collection of Cyanobacteria (PCC), is motile but decades of passaging on agar plates in laboratories worldwide generated many 'WT' sub-strains and variants with no functional motility which are commonly used now (Ding et al., 2015; Zavřel et al., 2017). Our standard laboratory strains are non-motile glucose-tolerant GT-P and GT-W sub-strains that lack thick pili on their cell surface. The responsibility for this defect was assigned to mutated *slr0332* (*cheA*) and *spkA* genes that regulate the activity of pili machinery (Kamei et al., 2001; Ding et al., 2015). Nonetheless, it is likely that even in the non-motile sub-strains, the apparatus for the elongation and retraction of the thick pilus is functional. Although thick pili are not present on the surface of GT-P and GT-W, both strains are capable of nutrients uptake and natural competence, tasks widely believed to rely on Type IV pili (Yura et al., 1999; Yoshihara et al., 2001; Nakasugi et al., 2006; Lamb et al., 2014; Lamb and Hohmann-Marriott, 2017). It raises the question of whether the extracellularly-displayed thick pili are essential for DNA or nutrient uptake.

I am tempted to speculate that the Type IV assembly machinery, perhaps with basally assembled pilins, is a functional unit (Figure 4.1). My unpublished data (Figure 3.3; 3.11; 3.15) demonstrate that the loss of outer membrane secretin PilQ and pili elongation motor PilB1 does not limit the growth capacity of non-motile *Synechocystis*, but the pili-retraction motor PilT1 and pilins are needed. This is consistent with the recent identification of PilT in unpiliated basal pili complexes in *Pseudomonas aeruginosa* and with the finding that displacement of PilB with PilT in Type IV basal complexes abolished the assembly of pili fibres (Koch et al., 2021). I hypothesize that the basal pili complexes in non-motile *Synechocystis* strains operate exclusively in the retraction mode. Mature pilins can form spontaneous (hetero)oligomers and then interact with PilC protein priming the basal pili complex but the pilus is not elongated due to the absence of PilB in the pili apparatus. Indeed, this inability of PilB to replace PilT may be caused by *cheA* and *spkA* mutations. Nonetheless, even though the motility is lost, the basal complex with membrane-bound pilin proteins could still facilitate the nutrient or DNA uptake (see later). If this is true, one would expect that the deletion of PilC, an essential structural protein for the assembly of the basal complex, results in a similar phenotype as the missing PilT1 (Figure 2.2). However, the annotation of *pilC* in *Synechocystis* is confusing; there may be two *pilC*

copies (*slr0162*, *slr0163*) and the published Δ*pilC* strain (Δ*slr0163*; Bhaya et al., 2000) could still express the second PilC homologue (Slr0162).

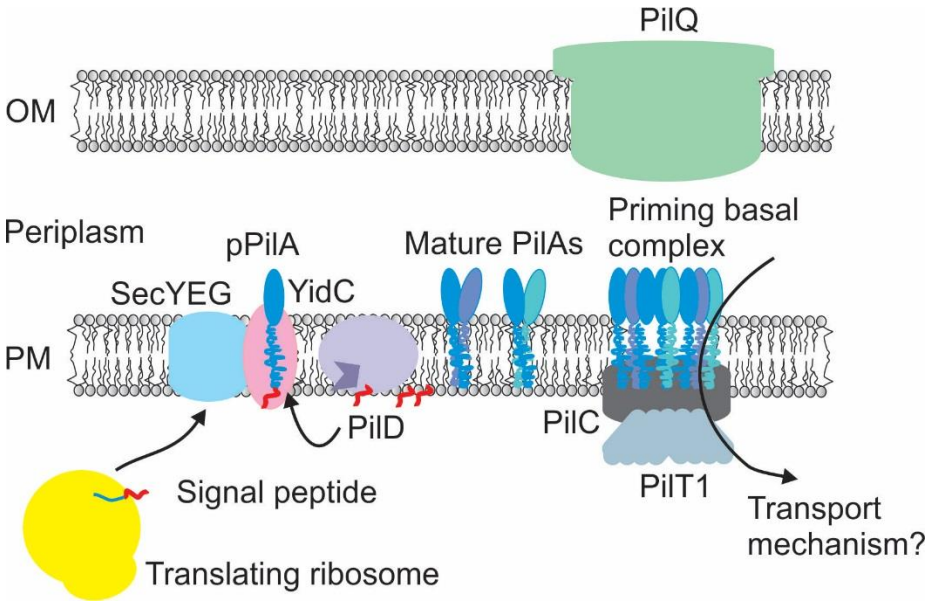

Figure 4.1. A model of the Type IV pili machinery in non-motile *Synechocystis* WT strains. Ribosomes translating PilA1 are targeted via the SRP pathway (omitted in the picture) to the SecYEG/YidC holotranslocon that facilitates pilin insertion into the membrane. Released from the translocon, the PilA1 prepilin is processed by PilD peptidase/methylase. Next, PilA1 forms heterooligomers with minor pilins promoting the formation of the priming basal pili complex (Nguyen et al., 2015). Attachment of the PilT1 to the basal complex activates the retractive function of the priming complex and blocks the pilus elongation. This basal complex with PilT1 might be involved in the transport of nutrients from the periplasm into the cytoplasm (see later).

4.2 Function of the minor pilin PilA2

As shown in Figure 3.9, the Δ*pilA2* strain accumulates less PilA1 under various growth conditions. These results strongly indicate that the minor pilin PilA2 protein is required for the synthesis or stability of PilA1. Interestingly, a fraction of PilA1 in the Δ*pilA2* migrated faster in an electrophoretic gel (Figure 3.9 B), similar to non-glycosylated PilA1 prepilin in the Δ*pilD* strain (Linhartová et al., 2014). The limited transformability (Yoshihara et al., 2001), loss of pigments, and impaired growth of the Δ*pilA2* strain could be thus explained by lower content of the maturated (glycosylated) PilA1. The phenotype of Δ*pilA2* is indeed less severe than that observed for the Δ*pilA1*/*2* containing no PilA1 (Fig 3.11). Given the decreased content of PilA1 in Δ*pilA2*, one would expect that the deletion of *pilA2* improves, at least partially, the phenotype of the Δ*pilD* strain, analogously to mutations in sigma

factor SigF (Linhartová et al., 2014; manuscript). However, the additional deletion of *pilA2* in the Δ*pilD* background did not restore the photoautotrophy of Δ*pilD* although it significantly lowers the amount of glycosylated PilA1 prepilin (Figure 3.9 B). This result supports the model that the non-glycosylated form of prepilin is specifically deleterious for *Synechocystis* (Linhartová et al., manuscript). Deletion of PilA2, a protein facilitating the PilA1 glycosylation, thus cannot improve the Δ*pilD* phenotype even the total content of pPilA1 is reduced. On the contrary, the stronger expression of *pilA2* (resulting in faster prepilin glycosylation) most likely suppresses the lack of PilD (see Linhartová et al., manuscript).

The tandem arrangement of two *pilA* genes is common in many bacterial groups; the promoter-proximal *pilA* gene is required for the surface piliation, while the second *pilA* gene appears to have a negligible effect on the piliation or motility (Giltner et al., 2012). I propose a functional link between genes of the whole *sll1693-pilA1-pilA2-sll1696* cluster. Sll1693 protein, belonging to SAM-dependent methyltransferases (Singh et al., 2005), accumulates in the Δ*pilA1/2/4* strain (Figure 3.2). Pilins are frequently N-terminal methylated by PilD after removal of the signal sequence; however, peptidase and methylase activities of PilD are independent, and not all PilDs possess the methylation activity (Giltner et al., 2012). It is not known whether the *Synechocystis* PilD is a methylase thus, the Sll1693 may play a role in the methylation of pilin proteins. The Sll1696 protein, coded by the downstream gene of the '*pilA1/2*' cluster, was co-purified with the FLAG-tagged PilA1 protein (Table 3.3). The role of Sll1696, possessing a tetratricopeptide repeat is, however, unknown. Participation of 'border' genes in pilin biogenesis is supported by their synchronized transcription with the *pilA1-pilA2* couple under various cultivation conditions (CyanoEXpress - Hernández-Prieto and Futschik, 2012; Hernández-Prieto et al., 2016).

Synechocystis strains lacking *pilA2* or *pilA1/2* genes contain high levels of Slr0442 protein, which might be a response to the restricted production of pilin proteins. The *slr0442* gene is a positively regulated target of the Sycrp1 transcription factor that participates in cAMP-regulated blue-light sensing and stimulation of various motility genes during phototaxis (Terauchi and Ohmori, 1999, 2004; Dienst et al., 2008; Hedger et al., 2009). The Slr0442 was identified among soluble proteins (Gao et al., 2009) but I can also detect it in the membrane fraction (Figure 3.12). The Slr0442 C-terminus possesses an unusual Ser/Pro-rich segment SS[SP]32 that is similar to mammalian proline-rich salivary protein, which huge surface area helps to precipitate tannins and polyhydroxylated phenols (Delimont et al., 2017). These antioxidant compounds are known to chelate metals e.g. iron

(Khokhar and Owusu Apenten, 2003) and, given this similarity, the Slr0442 could also participate in the binding of chelated metals or metal homeostasis.

4.3 PilA1 is required for the transition from the exponential to the linear growth phase

Motility enables cells to survey their surroundings to reach nutrients. Non-motile *Synechocystis* grows quickly into dense colonies on BG11 plates probably until reaching a certain limit in light and nutrients. When cells overgrow or deplete nutrients, they execute a genetic program to remodel their cell content and enter the stationary phase (Esteves-Ferreira et al., 2017). Cells of the Δ*pilA1* strain grow into lower densities and differ from WT in the content of protein-pigment complexes (Lamb et al., 2014). As shown here, a three-week-old culture of the Δ*pilA1*/*2*/*4* cells contains a high level of glucose-6-phosphate isomerase (Table 3.1), which signifies intensive glycogen catabolism (You et al., 2015). Moreover, they accumulated heat shock protein Hsp17 and orange carotenoid protein OCP (Table 3.1); both these proteins are involved in a stress-response regulated by histidine kinase Hik34. It is worth noting that the overexpression of the Hik34 enhances the expression of the whole *sll1693-pilA1-pilA2-sll1696* cluster (Suzuki et al., 2005). Interestingly, many Hik34-regulated genes, including the *sll1693-pilA1-pilA2-sll1696* genes, are up-regulated in a photoautotrophic revertant of the Δ*psbO*/*U* strain (Summerfield et al., 2007). The original mutant is impaired in the stability of PSII due to loss of lumenal PSII subunits and does not evolve oxygen (Eaton-Rye et al., 2003). Future work on the Hik34 regulation could help to clarify the role of pilins during the stationary growth phase.

In liquid cultures, the proliferation of Δ*pilA1*/2 is almost arrested from the 5th day of cultivation (Figure 3.3) when cells enter the linear phase (Esteves-Ferreira et al., 2017) while WT cells continue growing. However, at day 5, WT shows an unusually high content of the unprocessed D1 subunit of PSII (pD1), which is otherwise matured quickly (Komenda et al., 2006; Figure 3.8). Similarly, the unassembled D2 subunit is also relatively abundant (Figure 3.8). These results indicate that, at the beginning of the linear phase, the process of PSII assembly becomes somehow difficult for WT cells though plenty of D1 and D2 core subunits are synthesized. The situation in the pilin mutant is different. Although the Δ*pilA1*/*2* cells are no longer dividing, the rate of PSII assembly and the incorporation of *de novo* produced D1/D2 subunits is high. This intensive PSII biogenesis contrasts to low PSII activity in the pilin mutant; the newly synthesized PSIIs are either not

(fully) active from the beginning or are quickly inactivated. Cells might compensate for the low PSII activity by enhanced *de novo* PSII biogenesis or by PSII repair.

Although transcription of photosystem genes is downregulated during long-term cultivation (CyanoEXpress - Hernández-Prieto and Futschik, 2012; Hernández-Prieto et al., 2016) the specific loss of PSI and the lack of activity (but not the content) of PSII observed in the mutant is very unusual; typically, both photosystems are lost during cell bleaching induced by a lack of Chl (Kopečná et al., 2012; 2013; Bučinská et al., 2018). This may be the reason that the rate of *de novo* chlorophyll biosynthesis appears very weak at day 5 in Δ*pilA1/2* cells (Table 3.2), as the PSII content in pilin mutants might be maintained at the expense of Chl from PSI. Nonetheless, cell growth collapses anyway due to the low activity of PSII. My unpublished data are consistent with Lamb et al. (2014; 2017) whose spectroscopical analysis of the Δ*pilA1* strain indicated a problem with the biogenesis of PSII and low content of PSI. Based on the fact that the linear phase is explained as a response to light limitation (Esteves-Ferreira et al., 2017) one could conclude that the PilA1 has an important role in coping with light conditions. But, as discussed later, it seems to be an oversimplification, and factors of high cell density or the availability of mineral nutrients need to be considered.

4.4 A role of pili subunits in iron and manganese acquisition

The Δ*pilA1/2* mutant is severely affected by deficiency in iron and manganese, which are both critical cofactors for the functioning of photosynthetic complexes (Figure 3.14). The mutant cells also grow slower than WT on insoluble ferric iron oxides or manganese oxides. As an explanation of this phenotype, pili were suggested to transport electrons from the electron transport chain to reduce (and dissolve) Mn^{3+}, Mn^{4+}, and iron oxides (Lamb et al., 2014; Lamb and Hohmann-Marriott, 2017). However, there is no support for the function of pilins as electric wires in *Synechocystis* (Thirumurthy et al., 2020).

Almost sudden growth inhibition of the Δ*pilA1/2* at the 5^{th} day can be hardly explained by a depletion of iron from the growth media (Singh and Sherman, 2006). It led me to speculation that, rather than iron, manganese is much more likely the limiting nutrient at the beginning of the linear phase (Keren et al., 2002). An interesting finding is that virtually all manganese from the BG-11 medium is transported into *Synechocystis* cells within a day and then stored in the periplasm. Mn^{2+} circulates between TM and periplasm and this turnover in the cell is very fast and strictly regulated; 70% of the Mn^{2+} from TM is

released back to the periplasm in 1 hour (Brandenburg et al., 2017). The initial periplasmatic pool of manganese provides, however, a sufficient supply for exponentially-growing cells for no more than six cycles of cell division (Keren et al., 2002). Indeed, the loss of phycobiliproteins in the Δ*pilA1*/*A2* somewhat resembles bleaching during manganese starvation (Salomon and Keren, 2011). Moreover, the supplementation with 5 μmol L^{-1} $MnCl_2$ prevents bleaching and the growth arrest of Δ*pilA1*/*A2* in an iron-limited medium (Fig 3.14).

The uptake of Mn^{2+} can be inhibited by either vast excess or lack of iron, which is an important fact suggesting that the transport of $Fe^{3+/2+}$ ions mutually affects the transport of Mn^{2+} into the cell or cytoplasm (Keren et al., 2002; Sharon et al., 2014). According to our current knowledge, the TonB-ExbB-ExbD pathway activates outer membrane channels for the uptake of Fe^{3+} and Mn^{2+} into the periplasm (Jiang et al., 2015). Similarly, both Fe^{3+} and Mn^{2+} metals are imported into the cytoplasm by the identical FutABC (ABC-type) transporters (Eisenhut, 2020). The idea that Fe^{3+} and Mn^{2+} share a set of metal transporters is based on the low selectivity of transporters for Fe^{3+} and Mn^{2+} ions (Sharon et al., 2014). Only a severe Mn^{2+}-deficiency triggers a specific expression of the MntCAB (Mn^{2+} high-affinity ABC-like) plasma membrane transporter (Yamaguchi et al., 2002).

Chlorophyll-binding IsiA protein and the iron uptake protein FutA1 are well-established markers of iron limitation in *Synechocystis* (Krynická et al., 2014). These two proteins, however, do not accumulate during long-term cultivation of the Δ*pilA1*/*A2* strain (Figure 3.6), which means that the mutant has enough iron. In a control experiment, Δ*pilA1*/*A2* cells produced IsiA and FutA1, if grown in an iron-depleted BG11 (data not shown). In WT the FutA1 level is also low until the 15^{th} day of cultivation when the density of the culture is approximately five times higher than that of the mutant. How can bleaching and slower growth of Δ*pilA1* cells under iron deficiency reported by Lamb et al. (2014) be explained? I assume that iron deprivation limits the manganese transport over the plasma membrane which is operated by FutABC. Therefore, manganese is accumulated in the periplasm where it binds to ManS sensor kinase and effectively blocks the expression of manganese-starvation induced MntCAB transporters. If basal pili complexes are functioning, they are involved in manganese transport from the periplasm to PSII-biogenic centers (specified below in the text). This alternative pathway is, however, missing in pilin mutants, which results in the observed bleaching phenotype.

4.5 Do pilin proteins play an alternative role in the thylakoid membrane?

PilA1 subunits are the main building blocks of the extracellular thick pili fibers and, like in other bacteria, PilA1 pilins are indeed present in the plasma membrane of *Synechocystis* (Selão et al., 2016). Interestingly, a pool of PilA1 (~ 30%) is localized in TM (Srivastava et al., 2005; Liberton et al., 2016; Selão et al., 2016). PilA1 can even be co-purified with typical TM complexes such as is the RCII* assembly intermediate of PSII (Knoppová J., unpublished - Figure 4.2). These results open a question on the role of the major pilin protein in TM and, more specifically, on the function of PilA1 during PSII biogenesis.

The plasma membrane and TM converge at some areas of the cell creating so-called thylapses. According to the current model, biogenesis of photosystems is initiated in thylapses – specialized membrane domains devoid of phycobilisomes but occupied with ribosomes (Rast et al., 2019). PilA1-translating ribosomes are most likely targeted to SecYEG/YidC holotranslocons present in both plasma membrane and TM. Indeed, the accumulation of PilA1 prepilin abolishes the function of translocons engaged in the biosynthesis of TM proteins (Linhartová et al., 2014) linking the pilin synthesis to thylapses. Furthermore, a protein complex composed of PilA1 and TM proteins Sll1106 and CurT can be isolated from *Synechocystis*, using any of these three proteins as bait (Skotnicová, 2019; Table 3.3). Transmembrane CurT protein is crucial for the biosynthesis and curvature of TM (Heinz et al., 2016) while the function of Sll1106, a glycine zipper protein, is unknown. The lack of the latter protein however affects the ferrochelatase activity (Skotnicová, 2019) and it is worth noting that the ferrochelatase - CurT - Sll1106 complex can be also isolated using Flag-tagged ferrochelatase (Pazderník, 2019). Another result supporting a functional connection between CurT and PilA1 is the loss of competence for DNA uptake in the *curT* deletion strain (Heinz et al., 2016). I speculate that the PilA1 - Sll1106 - CurT complex, directly or indirectly, facilitates the manganese delivery to the PSII complexes produced in thylapses. Alternatively, these proteins somehow interconnect the plasma membrane and thylapses. The proximity of plasma membrane and thylapses could be essential for the delivery of metals for the assembled PSII.

Future work should focus on the TM-specific role of pilins in cyanobacteria. Prepilin signal peptide could be tracked after fusion with a fluorescent protein, and a comprehensive localization of the pilin biogenic machinery is required. Various omics studies should help to better understand the transition between the exponential and linear growth phases – the process impaired in the Δ*pilA1*/*A2* cells. A careful characterization of the PilA1 - CurT - Sll1106 complex isolated from different growth phases and metal-

limited conditions could be another promising direction. Finally, understanding the role of PilA1 in manganese uptake will require the employment of a set of *Synechocystis* mutants defective in metal transporters and advanced techniques such as high-res nanoSIMS for the localization of metals in the cell.

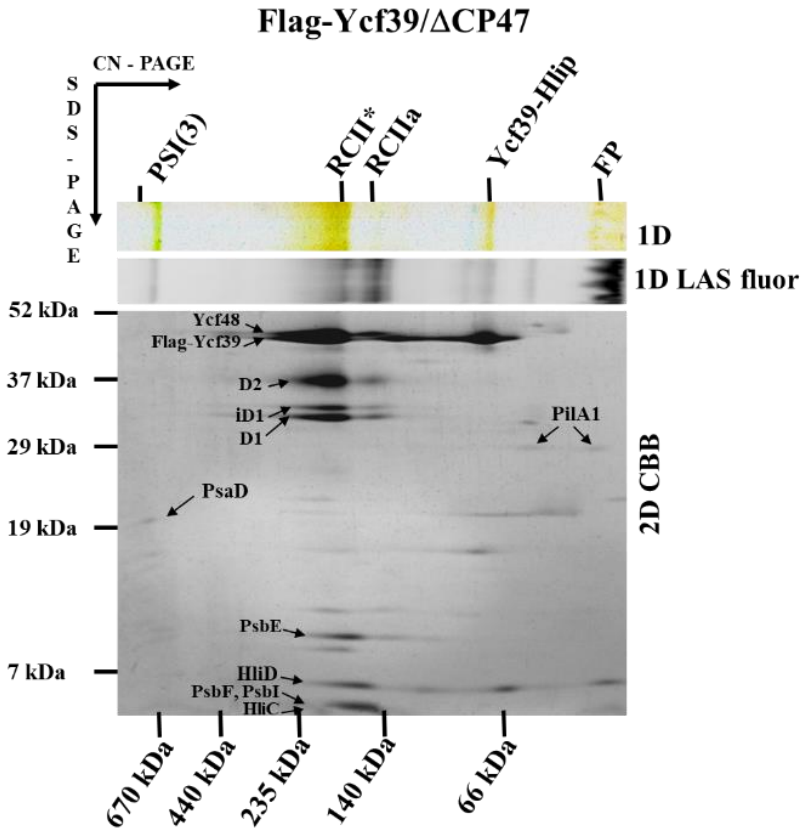

Figure 4.2. Two-dimensional Clear Native/SDS-PAGE of Flag-Ycf39 eluate. The Flag-Ycf39 complex from the ΔCP47 mutant was isolated and separated using 2D gel according to Selão et al. (2016). The gel was stained with Coomassie blue stain. Designation of complexes: PSI(3) – Photosystem I trimer, RCII* and RCIIa – two forms of the reaction center complex of PSII, Ycf39-Hlip – a complex of Flag-Ycf39 and HliD/C proteins, FP – free proteins (Knoppová J., unpublished data). Proteins indicated with arrows were identified using protein MS.

5. Material and Methods

5.1 Construction of *Synechocystis* mutants

Synechocystis mutants described in this work were produced in either WT-P or WT-W non-motile sub-strains (Tichý et al., 2016), as indicated in the text. Constructions of Δ*pilA2*, Δ*pilA1*/*2*, Δ*pilA4*, Δ*pilA1*/*2*/*4*, Δ*pilB1*, Δ*pilD*, and Δ*pilQ* strains are described in Linhartová et al. (2014). To prepare the *slr0442* mutant, a part (38-1813 bp) of the *slr0442* gene was replaced with a spectinomycin-resistance cassette (1359 bp; Prentki and Krisch, 1984) using the mega-primer PCR method (Lee et al., 2004). The Δ*slr0442*/*pilA1*/*2* strain was constructed by transformation of the Δ*slr0442* strain by chromosomal DNA isolated from the Δ*pilA1*/*2* mutant. To prepare the Δ*pilC* strain, chromosomal DNA was isolated from the previously reported Δ*pilC* mutant (Bhaya et al., 2000), which was a generous gift from Professor Devaki Bhaya (Carnegie Institution for Science, Stanford, USA). To prepare the Δ*pilT1* strain, chromosomal DNA was isolated from the previously reported Δ*pilT1* mutant (Conradi et al., 2019), which was a generous gift from Professor Annegret Wilde (University of Freiburg, Freiburg, Germany). Isolated DNA was used to transform the WT-V sub-strain and transformants were selected using spectinomycin (Δ*slr0442* or Δ*pilC*) or apramycin (Δ*pilT1*). To achieve full segregation, transformants were re-streaked several times on BG11 agar plates with increasing concentrations of the respective antibiotic up to 50 µg mL^{-}1 of apramycin or 100 µg mL^{-}1 of spectinomycin.

To prepare a *Synechocystis* strain expressing the PilA1 protein with a 3xFLAG tag at the C-terminus, the *pilA1* gene was cloned into the pPD-*C*FLAG plasmid (Chidgey et al., 2014) and the construct was transformed into the GT-P WT. The pPD-*C*FLAG plasmid contains the *Synechocystis psbAII* promoter, a sequence encoding the FLAG-tag, kanamycin resistance cassette, and flanking sequences for the replacement of the *psbAII* gene by homologous recombination. Transformants were selected and segregated with increasing concentrations of the antibiotic up to 50 µg mL^{-1}.

5.2 Cultivation of *Synechocystis* strains

All strains were grown photoautotrophically in the BG11 medium at 28 °C and irradiance of 40 µmol photons m^{-2} s^{-1}, either on agar plates or in liquid medium in Erlenmayer´s flasks on a rotary shaker. To mimic manganese or iron-depleted conditions ferric citrate or $MnCl_2$ were omitted in the BG11 medium, and if indicated, supplied additionally in micromolar concentrations of $MnCl_2$ or $FeCl_3$.

5.3 Electron microscopy

Cells were harvested at OD_{730} ~ 0.4. For negative contrast, the cells were fixed in 1% glutaraldehyde, resuspended in fresh BG11, applied to grids, and then stained with 1% uranyl acetate. Ultra-thin sections were prepared and examined as described in Linhartová et al. (2014). Negative contrast and ultra-thin sections were examined in a JEOL 1010 transmission electron microscope equipped with a Mega View III camera (Olympus – SIS).

5.4 Whole-cell absorption spectra, Chl content, and oxygen evolution

Whole-cell absorption spectra of intact cells were measured using Shimadzu UV-3000 spectrophotometer. To quantify the Chl content per cell, cell cultures at OD_{750} ~ 0.4 were harvested, the pigments were extracted with 100% methanol, and the Chl concentration was determined spectrophotometrically as described in Porra et al. (1989). The rate of oxygen evolution was measured using Hansatech Instruments Oxygraph+ System according to Knoppová and Komenda (2019). The data are averages ± SD of the triplicates with two biological experiments each.

5.5 Content of polysaccharides and proteins excreted into the growth medium

The content of polysaccharides was determined using the Alcian blue assay (Thornton et al., 2007) as follows: 5µL of the stock solution of 1% Alcian blue in 3% acetic acid was mixed with 1 mL of control BG11 or filtered (0.22 µm syringe filter) growth medium of a *Synechocystis* culture, and vortexed for 1 minute. Each sample was centrifuged at 14 000 rpm per 5 minutes at room temperature to remove the Alcian blue precipitates before the absorbance measurements. Absorbance spectra were measured within a range of 350-750 nm using Shimadzu UV-3000 spectrophotometer. Gum xanthan (1 g L^{-1} in BG11) was used as the standard for the assay and the calibration curve of gum xanthan was measured for a range of 0-100 mg L^{-1} in nine points. Sucrose, glucose, and maltose served as negative controls.

5.6 Analysis of cellular tetrapyrroles

The relative level of Chl precursors was determined from 2 mL of harvested cells and normalized to OD_{730} = 1. Chl precursors were extracted with 70 % methanol. Extracted

pigments were analyzed using high-performance liquid chromatography (HPLC), as described in Pilný et al. (2015).

5.7 Radiolabelling and preparation of TMs

Synechocystis cells were pulse-labelled for 30 minutes using a mixture of [^{35}S]Met and [^{35}S]Cys (Hartmann Analytics) as described in Dobáková et al. (2009). Cells were harvested by 6000 x g for 10 min, washed with, and resuspended in a thylakoid buffer containing 25mM MES/NaOH, pH 6.5, 10mM $MgCl_2$, 10mM $MgCl_2$, and 25% glycerol. Cell membranes were isolated by breaking cells with glass beads by Mini-Beadbeated-16 (Biospec, USA).

5.8 Electrophoresis and immunoblotting

The protein composition of membrane samples was analyzed either by one-dimensional SDS-electrophoresis (SDS-PAGE) or by two-dimensional clear native (CN)/SDS-PAGE. 1D PAGE was performed in a denaturing 12% polyacrylamide gel or 12-20% gradient gel containing 7M urea (Dobáková et al., 2009). To carry out CN-PAGE, membrane protein complexes were solubilized with 1% n-dodecyl-β-D-maltosite and separated in 4-14% gradient gel (Komenda et al., 2012a). For the second dimension, the cut CN gel strip was first incubated in 2% SDS and 1% dithiothreitol for 20 minutes at room temperature, and the denatured proteins were separated in a 12-20% or 16-20% polyacrylamide gel containing 7M urea. The protein gel was stained with Coomassie Brilliant Blue (G-250) or SYPRO Orange. Mass spectrometry identification of Coomassie-stained protein bands/spots from the SDS-PAGE gels was accomplished as described by Linhartová et al. (2014). Gels containing pulse-labelled proteins were dried, exposed overnight to a Phosphorimager plate (GE Healthcare), and scanned by Storm (Molecular Dynamics). For immunodetection, proteins were transferred from the SDS gel to a PVDF membrane (Immobilon-P, Merck Millipore) that was incubated first with a primary antibody and then with a secondary antibody conjugated with horseradish peroxidase (Sigma-Aldrich). The primary antibody against the *Synechocystis* PilA1 was raised in a rabbit using the synthetic peptide fragment that contained amino acids 147–160 (GenScript, USA).

5.9 PilA1-FLAG purification

Membrane proteins were isolated in a thylakoid buffer (see above) from 1.2 L of the culture at OD_{730} ~ 0.4 and solubilized for 1 hour at 4 °C in 5mL of the same buffer containing 1.5% n-dodecyl-β-D-maltosite. An unsolubilized fraction was pelleted by centrifugation at 18 000 g for 20 minutes at 4 °C and the obtained supernatant containing 1.6-2 mg of Chl was loaded directly onto the column with 200 µL of the Anti-FLAG-M2 agarose resin (Sigma-Aldrich). Before the loading, the column was equilibrated with 0.04% n-dodecyl-β-D-maltosite in the thylakoid buffer and the same buffer was used during the rest of the protocol. The supernatant was applied three times to the column and collected as a flow-through fraction, then the resin was intensively washed with 20 mL of the buffer. FLAG-tagged PilA1 was finally eluted with 300 µg/ml of 3xFLAG peptide (Sigma-Aldrich) in the 200 µL of the buffer. The elution was twice repeated to obtain about 400 µL of the eluate.

6. Summary

Gliding cyanobacteria can move towards or away from a variety of stimuli such as nutrients or light. Cell movement thus efficiently optimizes metabolic homeostasis to external conditions. This thesis aimed to explore the function of Type IV pili, the molecular apparatus responsible for the motility, using the model cyanobacterium *Synechocystis* sp. PCC 6803. In contrast to other studies focused on the role of various pilin proteins in motility, I investigated alternative and cyanobacteria-specific tasks of Type IV pili proteins. I used a spectrum of molecular, biochemical, and biophysical methods to demonstrate that the Type IV pili machinery fulfils a new role in cyanobacteria important for the biogenesis of Photosystem II, most likely the transport of manganese ions. I propose a model that the pilin machinery located in biogenic domains (thylapses) of the thylakoid membrane facilitates the delivery of manganese to the assembling Photosystem II.

The publication of Linhartová et al. (2014) provides an in-depth analysis of the *Synechocystis pilD* mutant lacking prepilin peptidase (PilD). The mutant accumulates an unprocessed form (prepilins) of the major pili subunit PilA1. Intriguingly, the presence of PilA1 prepilin almost completely inhibited the synthesis of membrane proteins including the essential subunits of Photosystem II. We have found that SecYEG-YidC holo-translocons interact aberrantly with PilA1 prepilin and are prone to proteolytic degradation. This work is the first report that prepilins are lethal for the photoautotrophically-grown cyanobacteria.

The second publication (Chidgey et al., 2014) reveals a physical link between the chlorophyll biosynthesis and the Sec/YidC-driven insertion of nascent chlorophyll-binding proteins. We purified an enzymatically active chlorophyll synthase complex comprising YidC, SecY, and ribosome subunits. This complex implies an effective manner that works to minimize the risk of accumulation of unbound chlorophylls in the membrane.

In the manuscript of Linhartová et al. (unpublished) we identified suppressor mutations restoring the photoautotrophic capacity of the original mutant lacking the PilD peptidase. The identified suppressor mutations alternated either PilA1 mRNA or prepilin glycosylation. It confirmed our previous conclusions about the toxicity of non-glycosylated prepilins PilA1 (Linhartová et al., 2014). In this work, we discuss the consequences of the presence of PilA1 in the thylakoid membrane. Moreover, we present a model that the signal

peptide of PilA1 hinders the mobility of the prepilin in the membrane causing its accumulation in the vicinity of Sec/YidC translocons.

In the chapter on unpublished results, I analyse bleaching and growth phenotypes of several *Synechocystis* pili mutants. I discovered an important role of pili subunits for the transition from the exponential to the linear phase, most likely connected to metal homeostasis. My data shows that in cells lacking PilA1, PSII complexes are less active but are more intensively synthesized and that the chlorophyll synthesis is downregulated. I hypothesize that the major pilin PilA1 and the retraction pili motor PilT1 are involved in manganese transport across the plasma membrane to sites where the PSII biogenesis occurs. This model is supported by the identification of a protein complex comprising PilA1/CurT/Sll1106. Moreover, I show that the minor pilin PilA2 is required for the glycosylation of PilA1.

7. Conclusions

Type IV pili are universal and multipurpose filaments often described as prokaryotic Swiss Army knives. This Ph.D. thesis deals with a novel function of pilin proteins in the biogenesis of photosynthetic apparatus in cyanobacteria. In addition, I elucidate important aspects of the pilin synthesis, maturation, and post-translation modifications in the model cyanobacterium *Synechocystis* sp. PCC 6803. The thesis is composed of two first-author publications, one first-author manuscript, and a chapter of unpublished results. The main conclusions are as follows:

- *Synechocystis* PilD peptidase matures the major pilin PilA1 by cleaving off its signal sequence in the proximity of SecYEG-YidC holo-translocons. When PilD is absent, unprocessed PilA1 (prepilin) accumulates in biosynthetically active (Sec/YidC-rich) membrane domains, which attenuates translocation and depletes essential membrane proteins.
- The deleterious effect of the unprocessed prepilin in the *pilD* mutant can be compensated by either its lower expression or its more efficient glycosylation, and probably also by faster lateral diffusion of the PilA1 prepilin in the membrane (away from biogenic membrane domains).
- In *Synechocystis* mutants lacking major pilin PilA1, minor pilin PilA2, or the molecular retraction motor PilT1, the transition from the exponential to the linear phase of growth led to a growth defect. It seems that the PilA1 and PilT1 proteins are involved in manganese uptake while the PilA2 promotes the PilA1 glycosylation.
- Biosynthesis of chlorophyll-binding proteins (core photosystem subunits) on Sec/YidC translocons is co-translationally linked with chlorophyll biosynthesis and the chlorophyll delivery from the chlorophyll synthase enzyme.

8. Literature

Allen, R., Rittmann, B.E., and Curtiss, R., 3rd. (2019). Axenic biofilm formation and aggregation by *Synechocystis* sp. strain PCC 6803 are induced by changes in nutrient concentration and require cell surface structures. Appl Environ Microbiol **85:** e02192-02218.

Bečková, M., Gardian, Z., Yu, J., Koník, P., Nixon, P.J., and Komenda, J. (2017). Association of Psb28 and Psb27 proteins with PSII-PSI supercomplexes upon exposure of *Synechocystis* sp. PCC 6803 to high light. Mol Plant **10:** 62-72.

Berman, H.M., Westbrook, J., Feng, Z., Gilliland, G., Bhat, T.N., Weissig, H., Shindyalov, I.N., and Bourne, P.E. (2000). The Protein Data Bank. Nucleic Acids Res **28:** 235-242.

Berry, J.L., and Pelicic, V. (2015). Exceptionally widespread nanomachines composed of type IV pilins: the prokaryotic Swiss Army knives. FEMS Microbiol Rev **39:** 134-154.

Bhaya, D., Watanabe, N., Ogawa, T., and Grossman, A.R. (1999). The role of an alternative sigma factor in motility and pilus formation in the cyanobacterium *Synechocystis* sp. strain PCC6803. Proc Natl Acad Sci USA **96:** 3188-3193.

Bhaya, D., Bianco, N.R., Bryant, D., and Grossman, A. (2000). Type IV pilus biogenesis and motility in the cyanobacterium *Synechocystis* sp PCC6803. Mol Microbiol **37:** 941-951.

Bhaya, D., Takahashi, A., and Grossman, A.R. (2001a). Light regulation of type IV pilus-dependent motility by chemosensor-like elements in *Synechocystis* PCC6803. Proc Natl Acad Sci USA **98:** 7540-7545.

Bhaya, D., Takahashi, A., Shahi, P., and Grossman, A.R. (2001b). Novel motility mutants of *Synechocystis* strain PCC 6803 generated by in vitro transposon mutagenesis. J Bacteriol **183:** 6140-6143.

Bhaya, D., Nakasugi, K., Fazeli, F., and Burriesci, M.S. (2006). Phototaxis and impaired motility in adenylyl cyclase and cyclase receptor protein mutants of *Synechocystis* sp. strain PCC 6803. J Bacteriol **188:** 7306-7310.

Boehm, M., Romero, E., Reisinger, V., Yu, J.F., Komenda, J., Eichacker, L.A., Dekker, J.P., and Nixon, P.J. (2011). Investigating the early stages of Photosystem II sssembly in *Synechocystis* sp PCC 6803. Isolation of CP47 and CP43 complexes. J Biol Chem **286:** 14812-14819.

Boehm, M., Yu, J., Reisinger, V., Bečková, M., Eichacker, L.A., Schlodder, E., Komenda, J., and Nixon, P.J. (2012). Subunit composition of CP43-less photosystem II complexes of *Synechocystis* sp PCC 6803: implications for the assembly and repair of photosystem II. Philos Trans R Soc B Biol Sci **367:** 3444-3454.

Bonner, P.J., Black, W.P., Yang, Z., and Shimkets, L.J. (2006). FibA and PilA act cooperatively during fruiting body formation of *Myxococcus xanthus*. Mol Microbiol **61:** 1283-1293.

Bouhenni, R.A., Vora, G.J., Biffinger, J.C., Shirodkar, S., Brockman, K., Ray, R., Wu, P., Johnson, B.J., Biddle, E.M., Marshall, M.J., Fitzgerald, L.A., Little, B.J., Fredrickson, J.K., Beliaev, A.S., Ringeisen, B.R., and Saffarini, D.A. (2010).

The role of *Shewanella oneidensis* MR-1 outer surface structures in extracellular electron transfer. Electroanalysis **22:** 856-864.

Brandenburg, F., Schoffman, H., Kurz, S., Krämer, U., Keren, N., Weber, A.P.M., and Eisenhut, M. (2017). The *Synechocystis* manganese exporter Mnx is essential for manganese homeostasis in cyanobacteria. Plant Physiol **173:** 1798-1810.

Bricker, T.M., Roose, J.L., Fagerlund, R.D., Frankel, L.K., and Eaton-Rye, J.J. (2012). The extrinsic proteins of Photosystem II. Biochim Biophys Acta **1817:** 121-142.

Bryan, S.J., Burroughs, N.J., Evered, C., Sacharz, J., Nenninger, A., Mullineaux, C.W., and Spence, E.M. (2011). Loss of the SPHF homologue Slr1768 leads to a catastrophic failure in the maintenance of thylakoid membranes in *Synechocystis* sp. PCC 6803. PLOS ONE **6:** e19625.

Bučinská, L., Kiss, E., Koník, P., Knoppová, J., Komenda, J., and Sobotka, R. (2018). The ribosome-bound protein Pam68 promotes insertion of chlorophyll into the CP47 subunit of photosystem II. Plant Physiol **176:** 2931-2942.

Cengic, I., Uhlén, M., and Hudson, E.P. (2018). Surface display of small affinity proteins on *Synechocystis* sp. strain PCC 6803 mediated by fusion to the major Type IV pilin PilA1. J Bacteriol **200:** e00270-00218.

Chandra, A., Joubert, L.-M., and Bhaya, D. (2017). Modulation of Type IV pili phenotypic plasticity through a novel Chaperone-Usher system in *Synechocystis* sp. bioRxiv**:** 130278.

Chang, Y.-W., Rettberg, L.A., Treuner-Lange, A., Iwasa, J., Søgaard-Andersen, L., and Jensen, G.J. (2016). Architecture of the type IVa pilus machine. Science **351:** aad2001.

Chen, I., Provvedi, R., and Dubnau, D. (2006). A macromolecular complex formed by a pilin-like protein in competent *Bacillus subtilis*. J Biol Chem **281:** 21720-21727.

Chen, Z., Zhan, J., Chen, Y., Yang, M., He, C., Ge, F., and Wang, Q. (2015). Effects of phosphorylation of β subunits of phycocyanins on state transition in the model cyanobacterium *Synechocystis* sp. PCC 6803. Plant Cell Physiol **56:** 1997-2013.

Chen, Z., Li, X., Tan, X., Zhang, Y., and Wang, B. (2020). Recent advances in biological functions of thick pili in the cyanobacterium *Synechocystis* sp. PCC 6803. Front Plant Sci **11**.

Chidgey, J.W., Linhartová, M., Komenda, J., Jackson, P.J., Dickman, M.J., Canniffe, D.P., Koník, P., Pilný, J., Hunter, C.N., and Sobotka, R. (2014). A cyanobacterial chlorophyll synthase-HliD complex associates with the Ycf39 protein and the YidC/Alb3 insertase. Plant Cell **26:** 1267-1279.

Chitnis, V.P., and Chitnis, P.R. (1993). PsaL subunit is required for the formation of photosystem I trimers in the cyanobacterium *Synechocystis* sp. PCC 6803. FEBS Lett **336:** 330-334.

Choi, J.-S., Chung, Y.-H., Moon, Y.-J., Kim, C., Watanabe, M., Song, P.-S., Joe, C.-O., Bogorad, L., and Park, Y.M. (1999). Photomovement of the gliding cyanobacterium *Synechocystis* sp. PCC 6803. Photochem Photobiol **70:** 95-102.

Cisneros, D.A., Pehau-Arnaudet, G., and Francetic, O. (2012). Heterologous assembly of type IV pili by a type II secretion system reveals the role of minor pilins in assembly initiation. Mol Microbiol **86:** 805-818.

Conradi, F.D., Zhou, R.Q., Oeser, S., Schuergers, N., Wilde, A., and Mullineaux, C.W. (2019). Factors controlling floc formation and structure in the cyanobacterium *Synechocystis* sp. strain PCC 6803. J Bacteriol **201:** e00344-00319.

Dalbey, R.E., and Kuhn, A. (2012). Protein Traffic in Gram-negative bacteria – how exported and secreted proteins find their way. FEMS Microbiol Rev **36:** 1023-1045.

De Sanctis, S., Wenzler, M., Kröger, N., Malloni, Wilhelm M., Sumper, M., Deutzmann, R., Zadravec, P., Brunner, E., Kremer, W., and Kalbitzer, Hans R. (2016). PSCD domains of pleuralin-1 from the diatom *Cylindrotheca fusiformis*: NMR structures and interactions with other biosilica-associated proteins. Structure **24:** 1178-1191.

Delimont, N.M., Rosenkranz, S.K., Haub, M.D., and Lindshield, B.L. (2017). Salivary proline-rich protein may reduce tannin-iron chelation: a systematic narrative review. Nutrition & Metabolism **14:** 47.

Dienst, D., Dühring, U., Mollenkopf, H.J., Vogel, J., Golecki, J., Hess, W.R., and Wilde, A. (2008). The cyanobacterial homologue of the RNA chaperone Hfq is essential for motility of *Synechocystis* sp. PCC 6803. Microbiology (Read) **154:** 3134-3143.

Ding, Q., Chen, G., Wang, Y., and Wei, D. (2015). Identification of specific variations in a non-motile strain of cyanobacterium *Synechocystis* sp. PCC 6803 originated from ATCC 27184 by whole genome resequencing. International Journal of Molecular Sciences **16:** 24081-24093.

Dobáková, M., Sobotka, R., Tichý, M., and Komenda, J. (2009). Psb28 protein is involved in the biogenesis of the photosystem II inner antenna CP47 (PsbB) in the cyanobacterium *Synechocystis* sp. PCC 6803. Plant Physiol **149:** 1076-1086.

Duggan, P.S., Gottardello, P., and Adams, D.G. (2007). Molecular analysis of genes in *Nostoc punctiforme* involved in pilus biogenesis and plant infection. J Bacteriol **189:** 4547-4551.

Eaton-Rye, J.J., Shand, J.A., and Nicoll, W.S. (2003). pH-dependent photoautotrophic growth of specific photosystem II mutants lacking lumenal extrinsic polypeptides in *Synechocystis* PCC 6803. FEBS Lett **543:** 148-153.

Eisenhut, M. (2020). Manganese homeostasis in cyanobacteria. Plants **9:** 18.

Esteves-Ferreira, A.A., Inaba, M., Obata, T., Fort, A., Fleming, G.T.A., Araújo, W.L., Fernie, A.R., and Sulpice, R. (2017). A novel mechanism, linked to cell density, largely controls cell division in *Synechocystis.* Plant Physiol **174:** 2166-2182.

Filloux, A. (2004). The underlying mechanisms of type II protein secretion. BBA - Mol Cell Res **1694:** 163-179.

Foldynová, M. (2009). Analysis of the role of PilA proteins in the cyanobacterium *Synechocystis* sp. PCC 6803. Mgr. Thesis, in English. Faculty of Science, University of South Bohemia, České Budějovice, The Czech Republic.**:** 37pp.

Foster, J.S., Singh, A.K., Rothschild, L.J., and Sherman, L.A. (2007). Growth-phase dependent differential gene expression in *Synechocystis* sp strain PCC 6803 and regulation by a group 2 sigma factor. Arch Microbiol **187:** 265-279.

Friedrich, A., Rumszauer, J., Henne, A., and Averhoff, B. (2003). Pilin-like proteins in the extremely thermophilic bacterium *Thermus thermophilus* HB27: Implication in competence for natural transformation and links to type IV pilus biogenesis. Appl Environ Microbiol **69:** 3695-3700.

Gao, Y., Xiong, W., Li, X.-b., Gao, C.-F., Zhang, Y.-l., Li, H., and Wu, Q.-y. (2009). Identification of the proteomic changes in *Synechocystis* sp. PCC 6803 following prolonged UV-B irradiation. J Exp Bot **60:** 1141-1154.

Giltner, C.L., Habash, M., and Burrows, L.L. (2010). *Pseudomonas aeruginosa* minor pilins are incorporated into type IV pili. J Mol Biol **398:** 444-461.

Giltner, C.L., Nguyen, Y., and Burrows, L.L. (2012). Type IV pilin proteins: versatile molecular modules. Microbiol Mol Biol Rev **76:** 740-772.

Gorby, Y.A., Yanina, S., McLean, J.S., Rosso, K.M., Moyles, D., Dohnalkova, A., Beveridge, T.J., Chang, I.S., Kim, B.H., Kim, K.S., Culley, D.E., Reed, S.B., Romine, M.F., Saffarini, D.A., Hill, E.A., Shi, L., Elias, D.A., Kennedy, D.W., Pinchuk, G., Watanabe, K., Ishii, S.i., Logan, B., Nealson, K.H., and Fredrickson, J.K. (2006). Electrically conductive bacterial nanowires produced by *Shewanella oneidensis* strain MR-1 and other microorganisms. Proc Natl Acad Sci USA **103:** 11358-11363.

He, Q., and Vermaas, W.F.J. (1999). Genetic deletion of proteins resembling Type IV pilins in *Synechocystis* sp. PCC 6803: their role in binding or transfer of newly synthesized chlorophyll. Plant Mol Biol **39:** 1175-1188.

Hedger, J., Holmquist, P.C., Leigh, K.A., Saraff, K., Pomykal, C., and Summers, M.L. (2009). Illumination stimulates cAMP receptor protein-dependent transcriptional activation from regulatory regions containing class I and class II promoter elements in *Synechocystis* sp. PCC 6803. Microbiology **155:** 2994-3004.

Heinz, S., Rast, A., Shao, L., Gutu, A., Gügel, I.L., Heyno, E., Labs, M., Rengstl, B., Viola, S., Nowaczyk, M.M., Leister, D., and Nickelsen, J. (2016). Thylakoid membrane architecture in *Synechocystis* depends on CurT, a homolog of the granal CURVATURE THYLAKOID 1 proteins. Plant Cell **28:** 2238.

Hélaine, S., Carbonnelle, E., Prouvensier, L., Beretti, J.L., Nassif, X., and Pelicic, V. (2005). PilX, a pilus-associated protein essential for bacterial aggregation, is a key to pilus-facilitated attachment of *Neisseria meningitidis* to human cells. Mol Microbiol **55:** 65-77.

Hélaine, S., Dyer, D.H., Nassif, X., Pelicic, V., and Forest, K.T. (2007). 3D structure/function analysis of PilX reveals how minor pilins can modulate the virulence properties of type IV pili. Proc Natl Acad Sci U S A **104:** 15888-15893.

Hernández-Prieto, M.A., and Futschik, M.E. (2012). CyanoEXpress: A web database for exploration and visualisation of the integrated transcriptome of cyanobacterium *Synechocystis* sp. PCC6803. Bioinformation **8:** 634-638.

Hernández-Prieto, M.A., Semeniuk, T.A., Giner-Lamia, J., and Futschik, M.E. (2016). The transcriptional landscape of the photosynthetic model cyanobacterium *Synechocystis* sp. PCC6803. Scientific Reports **6:** 22168.

Hobbs, M., and Mattick, J.S. (1993). Common components in the assembly of type 4 fimbriae, DNA transfer systems, filamentous phage and protein-secretion apparatus: a general system for the formation of surface-associated protein complexes. Mol Microbiol **10:** 233-243.

Hoiczyk, E., and Baumeister, W. (1998). The junctional pore complex, a prokaryotic secretion organelle, is the molecular motor underlying gliding motility in cyanobacteria. Curr Biol **8:** 1161-1168.

Hoiczyk, E., and Hansel, A. (2000). Cyanobacterial cell walls: News from an unusual prokaryotic envelope. J Bacteriol **182:** 1191-1199.

Imam, S., Chen, Z., Roos, D.S., and Pohlschröder, M. (2011). Identification of surprisingly diverse type IV pili, across a broad range of gram-positive bacteria. PLoS One **6:** e28919.

Iwai, M., Katoh, H., Katayama, M., and Ikeuchi, M. (2004). Improved genetic transformation of the thermophilic cyanobacterium, *Thermosynechococcus elongatus* BP-1. Plant Cell Physiol **45:** 171-175.

Jakovljevic, V., Leonardy, S., Hoppert, M., and Søgaard-Andersen, L. (2008). PilB and PilT are ATPases acting antagonistically in type IV pilus function in *Myxococcus xanthus*. J Bacteriol **190:** 2411-2421.

Jarrell, K.F., and Albers, S.V. (2012). The archaellum: an old motility structure with a new name. Trends Microbiol **20:** 307-312.

Jiang, H.-B., Lou, W.-J., Ke, W.-T., Song, W.-Y., Price, N.M., and Qiu, B.-S. (2015). New insights into iron acquisition by cyanobacteria: an essential role for ExbB-ExbD complex in inorganic iron uptake. The ISME Journal **9:** 297-309.

Jordan, P., Fromme, P., Witt, H.T., Klukas, O., Saenger, W., and Ktrauss, N. (2001). Three-dimensional structure of cyanobacterial photosystem I at 2.5 A resolution. Nature **411:** 909-917.

Kamei, A., Yuasa, T., Orikawa, K., Geng, X.X., and Ikeuchi, M. (2001). A eukaryotic-type protein kinase, SpkA, is required for normal motility of the unicellular cyanobacterium *Synechocystis* sp. strain PCC 6803. J Bacteriol **183:** 1505-1510.

Kaneko, T., Sato, S., Kotani, H., Tanaka, A., Asamizu, E., Nakamura, Y., Miyajima, N., Hirosawa, M., Sugiura, M., Sasamoto, S., Kimura, T., Hosouchi, T., Matsuno, A., Muraki, A., Nakazaki, N., Naruo, K., Okumura, S., Shimpo, S., Takeuchi, C., Wada, T., Watanabe, A., Yamada, M., Yasuda, M., and Tabata, S. (1996). Sequence analysis of the genome of the unicellular cyanobacterium *Synechocystis* sp. strain PCC6803. II. Sequence determination of the entire genome and assignment of potential protein-coding regions. DNA research **3:** 109-136.

Keren, N., Kidd, M.J., PennerHahn, J.E., and Pakrasi, H.B. (2002). A light-dependent mechanism for massive accumulation of manganese in the photosynthetic bacterium *Synechocystis* sp PCC 6803. Biochemistry **41:** 15085-15092.

Khare, B., and Narayana, S.V.L. (2017). Pilus biogenesis of Gram-positive bacteria: Roles of sortases and implications for assembly. Protein Sci **26:** 1458-1473.

Khayatan, B., Meeks, J.C., and Risser, D.D. (2015). Evidence that a modified type IV pilus-like system powers gliding motility and polysaccharide secretion in filamentous cyanobacteria. Mol Microbiol **98:** 1021-1036.

Khokhar, S., and Owusu Apenten, R.K. (2003). Iron binding characteristics of phenolic compounds: some tentative structure–activity relations. Food Chem **81:** 133-140.

Kim, Y.H., Park, Y.M., Kim, S.J., Park, Y.I., Choi, J.S., and Chung, Y.H. (2004). The role of Slr1443 in pilus biogenesis in *Synechocystis* sp. PCC 6803: Involvement in post-translational modification of pilins. Biochem Biophys Res Commun **315:** 179-186.

Kim, Y.H., Kim, J.Y., Kim, S.Y., Lee, J.H., Lee, J.S., Chung, Y.H., Yoo, J.S., and Park, Y.M. (2009). Alteration in the glycan pattern of pilin in a nonmotile mutant of *Synechocystis* sp. PCC 6803. Proteomics **9:** 1075-1086.

Kim, Y.H., Park, K.H., Kim, S.Y., Ji, E.S., Kim, J.Y., Lee, S.K., Yoo, J.S., Kim, H.S., and Park, Y.M. (2011). Identification of trimethylation at C-terminal lysine of pilin in the cyanobacterium *Synechocystis* PCC 6803. Biochem Biophys Res Commun **404:** 587-592.

Knoppová, J., Sobotka, R., Tichý, M., Yu, J., Koník, P., Halada, P., Nixon, P.J., and Komenda, J. (2014). Discovery of a chlorophyll binding protein complex involved in the early steps of photosystem II assembly in *Synechocystis*. Plant Cell **26:** 1200-1212.

Knoppová, J., and Komenda, J. (2019). Sequential deletions of photosystem II assembly factors Ycf48, Ycf39 and Pam68 result in progressive loss of autotrophy in the cyanobacterium *Synechocystis* PCC 6803. Folia Microbiol (Praha) **64:** 683-689.

Koch, M.D., Fei, C., Wingreen, N.S., Shaevitz, J.W., and Gitai, Z. (2021). Competitive binding of independent extension and retraction motors explains the quantitative dynamics of type IV pili. Proc Natl Acad Sci USA **118:** e2014926118.

Köhler, R., Schäfer, K., Müller, S., Vignon, G., Diederichs, K., Philippsen, A., Ringler, P., Pugsley, A.P., Engel, A., and Welte, W. (2004). Structure and assembly of the pseudopilin PulG. Mol Microbiol **54:** 647-664.

Komenda, J., Reisinger, V., Muller, B.C., Dobáková, M., Granvogl, B., and Eichacker, L.A. (2004). Accumulation of the D2 protein is a key regulatory step for assembly of the photosystem II reaction center complex in *Synechocystis* PCC 6803. J Biol Chem **279:** 48620-48629.

Komenda, J., Barker, M., Kuviková, S., de Vries, R., Mullineaux, C.W., Tichý, M., and Nixon, P.J. (2006). The FtsH protease slr0228 is important for quality control of photosystem II in the thylakoid membrane of *Synechocystis* sp PCC 6803. J Biol Chem **281:** 1145-1151.

Komenda, J., Nickelsen, J., Tichý, M., Prášil, O., Eichacker, L.A., and Nixon, P.J. (2008). The cyanobacterial homologue of HCF136/YCF48 is a component of an early photosystem II assembly complex and is important for both the efficient assembly and repair of photosystem II in *Synechocystis* sp PCC 6803. J Biol Chem **283:** 22390-22399.

Komenda, J., Knoppová, J., Kopečná, J., Sobotka, R., Halada, P., Yu, J.F., Nickelsen, J., Boehm, M., and Nixon, P.J. (2012a). The Psb27 assembly factor binds to the CP43 complex of photosystem II in the cyanobacterium *Synechocystis* sp PCC 6803. Plant Physiol **158:** 476-486.

Komenda, J., Sobotka, R., and Nixon, P.J. (2012b). Assembling and maintaining the Photosystem II complex in chloroplasts and cyanobacteria. Curr Opin Plant Biol **15:** 245-251.

Komenda, J., and Sobotka, R. (2019). Chlorophyll-binding subunits of photosystem I and II: Biosynthesis, chlorophyll incorporation and assembly. In Metabolism, structure and function of plant tetrapyrroles: Control mechanisms of chlorophyll biosynthesis and analysis of chlorophyll-binding proteins, B. Grimm, ed (Elsevier), pp. 195-223.

Kopečná, J., Komenda, J., Bučinská, L., and Sobotka, R. (2012). Long-term acclimation of the cyanobacterium *Synechocystis* sp. PCC 6803 to high light is accompanied by an enhanced production of chlorophyll that is preferentially channeled to trimeric photosystem I. Plant Physiol **160:** 2239-2250.

Kopečná, J., Sobotka, R., and Komenda, J. (2013). Inhibition of chlorophyll biosynthesis at the protochlorophyllide reduction step results in the parallel depletion of Photosystem I and Photosystem II in the cyanobacterium *Synechocystis* PCC 6803. Planta **237:** 497-508.

Kopečná, J., Pilný, J., Krynická, V., Tomčala, A., Kis, M., Gombos, Z., Komenda, J., and Sobotka, R. (2015). Lack of phosphatidylglycerol inhibits chlorophyll biosynthesis at multiple sites and limits chlorophyllide reutilization in the cyanobacterium *Synechocystis* 6803. Plant Physiol **169:** 1307-1317.

Korotkov, K.V., Sandkvist, M., and Hol, W.G. (2012). The type II secretion system: biogenesis, molecular architecture and mechanism. Nat Rev Microbiol **10:** 336-351.

Korotkov, K.V., and Sandkvist, M. (2019). Architecture, function, and substrates of the type II secretion system. EcoSal Plus **8:** 10.1128.

Krynická, V., Tichý, M., Krafl, J., Yu, J., Kaňa, R., Boehm, M., Nixon, P.J., and Komenda, J. (2014). Two essential FtsH proteases control the level of the Fur repressor during iron deficiency in the cyanobacterium *Synechocystis* sp. PCC 6803. Mol Microbiol **94:** 609-624.

Krynická, V., Shao, S., Nixon, P.J., and Komenda, J. (2015). Accessibility controls selective degradation of photosystem II subunits by FtsH protease. Nat Plant **1:** 15168.

Labarre, J., Chauvat, F., and Thuriaux, P. (1989). Insertional mutagenesis by random cloning of antibiotic resistance genes into the genome of the cyanobacterium *Synechocystis* strain PCC 6803. J Bacteriol **171:** 3449-3457.

Lamb, J.J., Hill, R.E., Eaton-Rye, J.J., and Hohmann-Marriott, M.F. (2014). Functional role of PilA in iron acquisition in the cyanobacterium *Synechocystis* sp. PCC 6803. PLOS One **9:** e105761.

Lamb, J.J., and Hohmann-Marriott, M.F. (2017). Manganese acquisition is facilitated by PilA in the cyanobacterium *Synechocystis* sp. PCC 6803. PLOS One **12:** e0184685.

Laurenceau, R., Péhau-Arnaudet, G., Baconnais, S., Gault, J., Malosse, C., Dujeancourt, A., Campo, N., Chamot-Rooke, J., Le Cam, E., Claverys, J.P., and Fronzes, R. (2013). A type IV pilus mediates DNA binding during natural transformation in *Streptococcus pneumoniae*. PLoS pathogens **9:** e1003473.

Lee, J., Lee, H.J., Shin, M.K., and Ryu, W.S. (2004). Versatile PCR-mediated insertion or deletion mutagenesis. BioTechniques **36:** 398-400.

Lee, K., and Shimkets, L.J. (1994). Cloning and characterization of the *socA* locus which restores development to *Myxococcus xanthus* C-signaling mutants. J Bacteriol **176:** 2200-2209.

Li, W.-W., and Yu, H.-Q. (2014). Insight into the roles of microbial extracellular polymer substances in metal biosorption. Bioresour Technol **160:** 15-23.

Liberton, M., Saha, R., Jacobs, J.M., Nguyen, A.Y., Gritsenko, M.A., Smith, R.D., Koppenaal, D.W., and Pakrasi, H.B. (2016). Global proteomic analysis reveals an exclusive role of thylakoid membranes in bioenergetics of a model cyanobacterium. Molecular & cellular proteomics : MCP **15:** 2021-2032.

Linhartová, M., Bučinská, L., Halada, P., Ječmen, T., Šetlík, J., Komenda, J., and Sobotka, R. (2014). Accumulation of the Type IV prepilin triggers degradation of SecY and YidC and inhibits synthesis of Photosystem II proteins in the cyanobacterium *Synechocystis* PCC 6803. Mol Microbiol **93:** 1207-1223.

Liu, L.-N., and Scheuring, S. (2013). Investigation of photosynthetic membrane structure using atomic force microscopy. Trends Plant Sci **18:** 277-286.

Lovley, D.R., and Malvankar, N.S. (2015). Seeing is believing: novel imaging techniques help clarify microbial nanowire structure and function. Environ Microbiol **17:** 2209-2215.

Melville, S., and Craig, L. (2013). Type IV pili in Gram-positive bacteria. Microbiol Mol Biol Rev **77:** 323-341.

Mo, R., Yang, M., Chen, Z., Cheng, Z., Yi, X., Li, C., He, C., Xiong, Q., Chen, H., Wang, Q., and Ge, F. (2015). Acetylome analysis reveals the involvement of lysine acetylation in photosynthesis and carbon metabolism in the model cyanobacterium *Synechocystis* sp. PCC 6803. J Proteome Res **14:** 1275-1286.

Mulkidjanian, A.Y., Koonin, E.V., Makarova, K.S., Mekhedov, S.L., Sorokin, A., Wolf, Y.I., Dufresne, A., Partensky, F.d.r., Burd, H., Kaznadzey, D., Haselkorn, R., and Galperin, M.Y. (2006). The cyanobacterial genome core and the origin of photosynthesis. Proc Natl Acad Sci USA **103:** 13126-13131.

Nakane, D., and Nishizaka, T. (2017). Asymmetric distribution of type IV pili triggered by directional light in unicellular cyanobacteria. Proc Natl Acad Sci USA **114:** 6593-6598.

Nakasugi, K., and Neilan, B.A. (2005). Identification of pilus-like structures and genes in *Microcystis aeruginosa* PCC7806. Appl Environ Microbiol **71:** 7621-7625.

Nakasugi, K., Svenson, C.J., and Neilan, B.A. (2006). The competence gene, *comF*, from *Synechocystis* sp. strain PCC 6803 is involved in natural transformation, phototactic motility and piliation. Microbiology (Read) **152:** 3623-3631.

Nellaepalli, S., Ozawa, S.-I., Kuroda, H., and Takahashi, Y. (2018). The photosystem I assembly apparatus consisting of Ycf3–Y3IP1 and Ycf4 modules. Nature Communications **9:** 2439.

Netzer-El, S.Y., Caspy, I., and Nelson, N. (2019). Crystal structure of photosystem I monomer from *Synechocystis* PCC 6803. Front Plant Sci **9**.

Nguyen, Y., Sugiman-Marangos, S., Harvey, H., Bell, S.D., Charlton, C.L., Junop, M.S., and Burrows, L.L. (2015). *Pseudomonas aeruginosa* minor pilins prime type IVa pilus assembly and promote surface display of the PilY1 adhesin. J Biol Chem **290:** 601-611.

Nivaskumar, M., and Francetic, O. (2014). Type II secretion system: a magic beanstalk or a protein escalator. Biochim Biophys Acta **1843:** 1568-1577.

Nixon, P.J., Trost, J.T., and Diner, B.A. (1992). Role of the carboxy terminus of polypeptide-D1 in the assembly of a functional water-oxidizing manganese cluster in photosystem-II of the cyanobacterium *Synechocystis* sp. PCC 6803 - assembly requires a free carboxyl group at C-terminal position 344. Biochemistry **31:** 10859-10871.

Nogales, J., Gudmundsson, S., Knight, E.M., Palsson, B.O., and Thiele, I. (2012). Detailing the optimality of photosynthesis in cyanobacteria through systems biology analysis. Proc Natl Acad Sci USA **109:** 2678-2683.

Nunn, D. (1999). Bacterial type II protein export and pilus biogenesis: more than just homologies? Trends Cell Biol **9:** 402-408.

Ogawa, K., Yoshikawa, K., Matsuda, F., Toya, Y., and Shimizu, H. (2018). Transcriptome analysis of the cyanobacterium *Synechocystis* sp. PCC 6803 and mechanisms of photoinhibition tolerance under extreme high light conditions. J Biosci Bioeng **126:** 596-602.

Okajima, K., Yoshihara, S., Fukushima, Y., Geng, X., Katayama, M., Higashi, S., Watanabe, M., Sato, S., Tabata, S., Shibata, Y., Itoh, S., and Ikeuchi, M. (2005). Biochemical and functional characterization of BLUF-type flavin-binding proteins of two species of cyanobacteria. Journal of biochemistry **137:** 741-750.

Okamoto, S., and Ohmori, M. (2002). The cyanobacterial PilT protein responsible for cell motility and transformation hydrolyzes ATP. Plant & cell physiology **43 10:** 1127-1136.

Orf, I., Schwarz, D., Kaplan, A., Kopka, J., Hess, W.R., Hagemann, M., and Klähn, S. (2016). CyAbrB2 contributes to the transcriptional regulation of low CO_2 acclimation in *Synechocystis* sp. PCC 6803. Plant Cell Physiol **57:** 2232-2243.

Ossenbuhl, F., Inaba-Sulpice, M., Meurer, J., Soll, J., and Eichacker, L.A. (2006). The *Synechocystis* sp PCC 6803 Oxa1 homolog is essential for membrane integration of reaction center precursor protein pD1. Plant Cell **18:** 2236-2246.

Pazderník, M. (2019). Light-harvesting like domain of the cyanobacterial ferrochelatase, Ph.D. Thesis. University of South Bohemia, Faculty of Science, School of Doctoral Studies in Biological Sciences, České Budějovice, The Czech Republic.**:** 102pp.

Pilný, J., Kopečná, J., Noda, J., and Sobotka, R. (2015). Detection and quantification of heme and chlorophyll precursors using a High Performance Liquid Chromatography (HPLC) system equipped with two fluorescence detectors. Bio-protocol **5:** e1390.

Pisareva, T., Kwon, J., Oh, J., Kim, S., Ge, C.R., Wieslander, A., Choi, J.S., and Norling, B. (2011). Model for membrane organization and protein sorting in the cyanobacterium *Synechocystis* sp PCC 6803 inferred from proteomics and multivariate sequence analyses. J Proteome Res **10:** 3617-3631.

Porra, R.J., Thompson, W.A., and Kriedemann, P.E. (1989). Determination of accurate extinction coefficients and simultaneous equations for assaying chlorophylls *a* and *b* extracted with four different solvents: verification of the concentration of chlorophyll standards by atomic absorption spectroscopy. Biochim Biophys Acta **975:** 384-394.

Prentki, P., and Krisch, H.M. (1984). In vitro insertional mutagenesis with a selectable DNA fragment. Gene **29:** 303-313.

Py, B., Loiseau, L., and Barras, F. (2001). An inner membrane platform in the type II secretion machinery of Gram-negative bacteria. EMBO Rep **2:** 244-248.

Rast, A., Schaffer, M., Albert, S., Wan, W., Pfeffer, S., Beck, F., Plitzko, J.M., Nickelsen, J., and Engel, B.D. (2019). Biogenic regions of cyanobacterial thylakoids form contact sites with the plasma membrane. Nat Plant **5:** 436-446.

Reguera, G., McCarthy, K.D., Mehta, T., Nicoll, J.S., Tuominen, M.T., and Lovley, D.R. (2005). Extracellular electron transfer via microbial nanowires. Nature **435:** 1098-1101.

Risser, D.D., Chew, W.G., and Meeks, J.C. (2014). Genetic characterization of the *hmp* locus, a chemotaxis-like gene cluster that regulates hormogonium development and motility in *Nostoc punctiforme*. Mol Microbiol **92:** 222-233.

Sachelaru, I., Winter, L., Knyazev, D.G., Zimmermann, M., Vogt, A., Kuttner, R., Ollinger, N., Siligan, C., Pohl, P., and Koch, H.-G. (2017). YidC and SecYEG form a heterotetrameric protein translocation channel. Scientific Reports **7:** 101.

Salomon, E., and Keren, N. (2011). Manganese limitation induces changes in the activity and in the organization of photosynthetic complexes in the cyanobacterium *Synechocystis* sp strain PCC 6803. Plant Physiol **155:** 571-579.

Sampaleanu, L.M., Bonanno, J.B., Ayers, M., Koo, J., Tammam, S., Burley, S.K., Almo, S.C., Burrows, L.L., and Howell, P.L. (2009). Periplasmic domains of *Pseudomonas aeruginosa* PilN and PilO form a stable heterodimeric complex. J Mol Biol **394:** 143-159.

Schopf, J.W. (2006). Fossil evidence of Archaean life. Philos Trans R Soc B Biol Sci **361:** 869-885.

Schuergers, N., Ruppert, U., Watanabe, S., Nürnberg, D.J., Lochnit, G., Dienst, D., Mullineaux, C.W., and Wilde, A. (2014). Binding of the RNA chaperone Hfq to the type IV pilus base is crucial for its function in *Synechocystis* sp. PCC 6803. Mol Microbiol **92:** 840-852.

Schuergers, N., Nürnberg, D.J., Wallner, T., Mullineaux, C.W., and Wilde, A. (2015). PilB localization correlates with the direction of twitching motility in the cyanobacterium *Synechocystis* sp. PCC 6803. Microbiology (Read) **161:** 960-966.

Schuergers, N., and Wilde, A. (2015). Appendages of the cyanobacterial cell. Life **5:** 700-715.

Schuergers, N., Lenn, T., Kampmann, R., Meissner, M.V., Esteves, T., Temerinac-Ott, M., Korvink, J.G., Lowe, A.R., Mullineaux, C.W., and Wilde, A. (2016). Cyanobacteria use micro-optics to sense light direction. eLife **5:** e12620.

Schuurmans, R.M., Matthijs, J.C.P., and Hellingwerf, K.J. (2017). Transition from exponential to linear photoautotrophic growth changes the physiology of *Synechocystis* sp. PCC 6803. Photosyn Res **132:** 69-82.

Selão, T.T., Zhang, L., Knoppova, J., Komenda, J., and Norling, B. (2016). Photosystem II assembly steps take place in the thylakoid membrane of the cyanobacterium *Synechocystis* sp. PCC6803. Plant Cell Physiol **57:** 95-104.

Sergeyenko, T.V., and Los, D.A. (2000). Identification of secreted proteins of the cyanobacterium *Synechocystis* sp. strain PCC 6803. FEMS Microbiol Lett **193:** 213-216.

Sergeyenko, T.V., and Los, D.A. (2003). Cyanobacterial leader peptides for protein secretion. FEMS Microbiol Lett **218:** 351-357.

Sharon, S., Salomon, E., Kranzler, C., Lis, H., Lehmann, R., Georg, J., Zer, H., Hess, W.R., and Keren, N. (2014). The hierarchy of transition metal homeostasis: Iron controls manganese accumulation in a unicellular cyanobacterium. Biochim Biophys Acta **1837:** 1990-1997.

Singh, A.K., Li, H., Bono, L., and Sherman, L.A. (2005). Novel adaptive responses revealed by transcription profiling of a *Synechocystis* sp PCC 6803 Delta isiA mutant in the presence and absence of hydrogen peroxide. Photosyn Res **84:** 65-70.

Singh, A.K., and Sherman, L.A. (2006). Iron-independent dynamics of IsiA production during the transition to stationary phase in the cyanobacterium *Synechocystis* sp PCC 6803. FEMS Microbiol Lett **256:** 159-164.

Skotnicová, P. (2019). Proteins involved in the tetrapyrrole pathway in *Synechocystis* sp. PCC 6803 and their localization in the proximity of PSII biogenesis. Ph.D. Thesis, in English. University of South Bohemia, Faculty of Science, School of Doctoral Studies in Biological Sciences, České Budějovice, The Czech Republic**:** 118pp.

Song, J.-Y., Cho, H.S., Cho, J.-I., Jeon, J.-S., Lagarias, J.C., and Park, Y.-I. (2011). Near-UV cyanobacteriochrome signaling system elicits negative phototaxis in the cyanobacterium *Synechocystis* sp. PCC 6803. Proc Natl Acad Sci USA **108:** 10780-10785.

Srivastava, R., Pisareva, T., and Norling, B. (2005). Proteomic studies of the thylakoid membrane of *Synechocystis* sp PCC 6803. Proteomics **5:** 4905-4916.

Staleva, H., Komenda, J., Shukla, M.K., Šlouf, V., Kaňa, R., Polívka, T., and Sobotka, R. (2015). Mechanism of photoprotection in the cyanobacterial ancestor of plant antenna proteins. Nat Chem Biol **11:** 287-291.

Stanier, R.Y., Kunisawa, R., Mandel, M., and Cohen-Bazire, G. (1971). Purification and properties of unicellular blue-green algae (order Chroococcales). Bacteriological Reviews **35:** 171-205.

Strašková, A., Steinbach, G., Konert, G., Kotabová, E., Komenda, J., Tichý, M., and Kaňa, R. (2019). Pigment-protein complexes are organized into stable microdomains in cyanobacterial thylakoids. Biochim Biophys Acta Bioenerg **1860:** 148053.

Strom, M.S., and Lory, S. (1993). Structure-function and biogenesis of the type IV pili. Annu Rev Microbiol **47:** 565-596.

Sugimoto, Y., Nakamura, H., Ren, S., Hori, K., and Masuda, S. (2017). Genetics of the blue light-dependent signal cascade that controls phototaxis in the cyanobacterium *Synechocystis* sp. PCC6803. Plant Cell Physiol **58:** 458-465.

Summerfield, T.C., Eaton-Rye, J.J., and Sherman, L.A. (2007). Global gene expression of a Delta PsbO :Delta PsbU mutant and a spontaneous revertant in the cyanobacterium *Synechocystis* sp strain PCC 6803. Photosyn Res **94:** 265-274.

Sure, S., Torriero, A.A.J., Gaur, A., Li, L.H., Chen, Y., Tripathi, C., Adholeya, A., Ackland, M.L., and Kochar, M. (2015). Inquisition of *Microcystis aeruginosa* and *Synechocystis* nanowires: characterization and modelling. Antonie Leeuwenhoek **108:** 1213-1225.

Sure, S., Torriero, A.A., Gaur, A., Li, L.H., Chen, Y., Tripathi, C., Adholeya, A., Ackland, M.L., and Kochar, M. (2016). Identification and topographical characterisation of microbial nanowires in *Nostoc punctiforme*. Antonie Leeuwenhoek **109:** 475-480.

Suzuki, I., Kanesaki, Y., Hayashi, H., Hall, J.J., Simon, W.J., Slabas, A.R., and Murata, N. (2005). The histidine kinase Hik34 is involved in thermotolerance by regulating the expression of heat shock genes in *Synechocystis*. Plant Physiol **138:** 1409-1421.

Takahashi, M., Shiraishi, T., and Asada, K. (1988). Isolation of the D1 protein and a 28-kDa fragment of the D2 protein from spinach photosystem II membranes. Plant Cell Physiol **29:** 109-116.

Takhar, H.K., Kemp, K., Kim, M., Howell, P.L., and Burrows, L.L. (2013). The platform protein is essential for type IV pilus biogenesis. J Biol Chem **288:** 9721-9728.

Terauchi, K., and Ohmori, M. (1999). An adenylate cyclase, cyal, regulates cell motility in the cyanobacterium *Synechocystis* sp. PCC 6803. Plant Cell Physiol **40:** 248-251.

Terauchi, K., and Ohmori, M. (2004). Blue light stimulates cyanobacterial motility via a cAMP signal transduction system. Mol Microbiol **52:** 303-309.

Thirumurthy, M.A., Hitchcock, A., Cereda, A., Liu, J., Chavez, M.S., Doss, B.L., Ros, R., El-Naggar, M.Y., Heap, J.T., Bibby, T.S., and Jones, A.K. (2020). Type IV pili-independent photocurrent production by the cyanobacterium *Synechocystis* sp. PCC 6803. Frontiers in Microbiology **11**.

Thornton, D.C.O., Fejes, E.M., DiMarco, S.F., and Clancy, K.M. (2007). Measurement of acid polysaccharides in marine and freshwater samples using alcian blue. Limnol Oceanogr Meth **5:** 73-87.

Tichý, M., Bečková, M., Kopečná, J., Noda, J., Sobotka, R., and Komenda, J. (2016). Strain of *Synechocystis* PCC 6803 with aberrant assembly of photosystem II contains tandem duplication of a large chromosomal region. Front Plant Sci **7:** 648.

Ursell, T., Chau, R.M., Wisen, S., Bhaya, D., and Huang, K.C. (2013). Motility enhancement through surface modification is sufficient for cyanobacterial community organization during phototaxis. PLoS computational biology **9:** e1003205.

Van den Berg, B., Clemons, W.M., Jr., Collinson, I., Modis, Y., Hartmann, E., Harrison, S.C., and Rapoport, T.A. (2004). X-ray structure of a protein-conducting channel. Nature **427:** 36-44.

Varga, J.J., Nguyen, V., O'Brien, D.K., Rodgers, K., Walker, R.A., and Melville, S.B. (2006). Type IV pili-dependent gliding motility in the Gram-positive pathogen *Clostridium perfringens* and other *Clostridia*. Mol Microbiol **62:** 680-694.

Vavilin, D., Yao, D., and Vermaas, W.F.J. (2007). Small cab-like proteins retard degradation of photosystem II-associated chlorophyll in *Synechocystis* sp PCC 6803 - Kinetic analysis of pigment labeling with N-15 and C-13. J Biol Chem **282:** 37660-37668.

Vermaas, W. (2001). Photosynthesis and respiration in cyanobacteria. (In eLS: John Wiley & Sons Ltd, Chichester, United Kingdom).

Vignon, G., Köhler, R., Larquet, E., Giroux, S., Prévost, M.C., Roux, P., and Pugsley, A.P. (2003). Type IV-like pili formed by the type II secreton: specificity, composition, bundling, polar localization, and surface presentation of peptides. J Bacteriol **185:** 3416-3428.

Watanabe, M., Semchonok, D.A., Webber-Birungi, M.T., Ehira, S., Kondo, K., Narikawa, R., Ohmori, M., Boekema, E.J., and Ikeuchi, M. (2014). Attachment of phycobilisomes in an antenna–photosystem I supercomplex of cyanobacteria. Proc Natl Acad Sci USA **111:** 2512-2517.

Werneburg, G.T., Thanassi, D.G., and Donnenberg, M.S. (2018). Pili assembled by the chaperone/usher pathway in *Escherichia coli* and *Salmonella*. EcoSal Plus **8**.

Wilde, A., Fiedler, B., and Borner, T. (2002). The cyanobacterial phytochrome Cph2 inhibits phototaxis towards blue light. Mol Microbiol **44:** 981-988.

Wilde, A., and Mullineaux, C.W. (2015). Motility in cyanobacteria: polysaccharide tracks and Type IV pilus motors. Mol Microbiol **98:** 998-1001.

Williams, J.G.K. (1988). Construction of specific mutations in photosystem II photosynthetic reaction center by genetic engineering methods in *Synechocystis* 6803. Methods Enzymol **167:** 766-778.

Wolfgang, M., Van Putten, J.P.M., Hayes, S.F., and Koomey, M. (1999). The *comP* locus of *Neisseria gonorrhoeae* encodes a type IV prepilin that is dispensable for pilus biogenesis but essential for natural transformation. Mol Microbiol **31:** 1345-1357.

Wu, Q.G., and Vermaas, W.F.J. (1995). Light-dependent chlorophyll a biosynthesis upon chlL deletion in wild-type and photosystem I-less strains of the cyanobacterium *Synechocystis* sp PCC 6803. Plant Mol Biol **29:** 933-945.

Yamaguchi, K., Suzuki, I., Yamamoto, H., Lyukevich, A., Bodrova, I., Los, D.A., Piven, I., Zinchenko, V., Kanehisa, M., and Murata, N. (2002). A two-component Mn^{2+}-sensing system negatively regulates expression of the mntCAB operon in *Synechocystis*. Plant Cell **14:** 2901-2913.

Yao, D.C.I., Brune, D.C., Vavilin, D., and Vermaas, W.F.J. (2012). Photosystem II component lifetimes in the cyanobacterium *Synechocystis* sp. strain PCC 6803: small Cab-like proteins stabilize biosynthesis intermediates and affect early steps in chlorophyll synthesis. J Biol Chem **287:** 682-692.

Yoshida, T., Furuya, N., Ishikura, M., Isobe, T., Haino-Fukushima, K., Ogawa, T., and Komano, T. (1998). Purification and characterization of thin pili of IncI1 plasmids ColIb-P9 and R64: formation of PilV-specific cell aggregates by type IV pili. J Bacteriol **180:** 2842-2848.

Yoshihara, S., Suzuki, F., Fujita, H., Geng, X.X., and Ikeuchi, M. (2000). Novel putative photoreceptor and regulatory genes required for the positive phototactic movement of the unicellular motile cyanobacterium *Synechocystis* sp. PCC 6803. Plant Cell Physiol **41:** 1299-1304.

Yoshihara, S., Geng, X., Okamoto, S., Yura, K., Murata, T., Go, M., Ohmori, M., and Ikeuchi, M. (2001). Mutational analysis of genes involved in pilus structure, motility and transformation competency in the unicellular motile cyanobacterium *Synechocystis* sp. PCC6803. Plant Cell Physiol **42:** 63-73.

Yoshihara, S., and Ikeuchi, M. (2004). Phototactic motility in the unicellular cyanobacterium *Synechocystis* sp. PCC 6803. Photochem Photobiol Sci **3:** 512-518.

Yoshimura, H., Yoshihara, S., Okamoto, S., Ikeuchi, M., and Ohmori, M. (2002). A cAMP receptor protein, SYCRP1, is responsible for the cell motility of *Synechocystis* sp PCC 6803. Plant Cell Physiol **43:** 460-463.

You, L., He, L., Tang, Y.J., and Boer, P.d. (2015). Photoheterotrophic fluxome in *Synechocystis* sp. strain PCC 6803 and its implications for cyanobacterial bioenergetics. J Bacteriol **197:** 943-950.

Yu, J., Knoppová, J., Michoux, F., Bialek, W., Cota, E., Shukla, M.K., Strašková, A., Pascual Aznar, G., Sobotka, R., Komenda, J., Murray, J.W., and Nixon, P.J. (2018). Ycf48 involved in the biogenesis of the oxygen-evolving photosystem II complex is a seven-bladed beta-propeller protein. Proc Natl Acad Sci USA **115:** E7824-E7833.

Yura, K., Toh, H., and Go, M. (1999). Putative mechanism of natural transformation as deduced from genome data. DNA Research **6:** 75-82.

Zavřel, T., Očenášová, P., and Červený, J. (2017). Phenotypic characterization of *Synechocystis* sp. PCC 6803 substrains reveals differences in sensitivity to abiotic stress. PLOS ONE **12:** e0189130.

Zhang, L.X., Paakkarinen, V., van Wijk, K.J., and Aro, E.M. (2000). Biogenesis of the chloroplast-encoded D1 protein: Regulation of translation elongation, insertion, and assembly into photosystem II. Plant Cell **12:** 1769-1781.

9. Published results

9.1 Publication I: Accumulation of the Type IV prepilin triggers degradation of SecY and YidC and inhibits synthesis of Photosystem II proteins in the cyanobacterium *Synechocystis* PCC 6803.

Linhartová, M., Bučinská, L., Halada, P., Ječmen, T., Šetlík, J., Komenda, J., and Sobotka, R. (2014).

Mol. Microbiol. 93: 1207-1223.

Molecular Microbiology (2014) 93(6), 1207–1223 ■
doi:10.1111/mmi.12730
First published online 12 August 2014

Accumulation of the Type IV prepilin triggers degradation of SecY and YidC and inhibits synthesis of Photosystem II proteins in the cyanobacterium *Synechocystis* PCC 6803

Markéta Linhartová,[1,2] Lenka Bučinská,[1,2] Petr Halada,[3] Tomáš Ječmen,[4] Jiří Šetlík,[1] Josef Komenda[1,2] and Roman Sobotka[1,2]*

[1]*Institute of Microbiology, Academy of Sciences, Opatovický mlýn, 37981 Třeboň, Czech Republic.*
[2]*Faculty of Sciences, University of South Bohemia, Branišovská 31, 37005 České Budějovice, Czech Republic.*
[3]*Institute of Microbiology, Academy of Sciences, Vídeňská 1083, 14220 Prague 4, Czech Republic.*
[4]*Department of Biochemistry, Faculty of Science, Charles University in Prague, Hlavova 8, 128 43 Prague, Czech Republic.*

Summary

Type IV pilins are bacterial proteins that are small in size but have a broad range of functions, including motility, transformation competence and secretion. Although pilins vary in sequence, they possess a characteristic signal peptide that has to be removed by the prepilin peptidase PilD during pilin maturation. We generated a *pilD* (*slr1120*) null mutant of the cyanobacterium *Synechocystis* 6803 that accumulates an unprocessed form of the major pilin PilA1 (pPilA1) and its non-glycosylated derivative (NpPilA1). Notably, the *pilD* strain had aberrant membrane ultrastructure and did not grow photoautotrophically because the synthesis of Photosystem II subunits was abolished. However, other membrane components such as Photosystem I and ATP synthase were synthesized at levels comparable to the control strain. Proliferation of the *pilD* strain was rescued by elimination of the *pilA1* gene, demonstrating that PilA1 prepilin inhibited the synthesis of Photosystem II. Furthermore, NpPilA1 co-immunoprecipitated with the SecY translocase and the YidC insertase, and both of these essential translocon components were degraded in the mutant. We propose that unprocessed prepilins inactivate an identical pool of translocons that function in the synthesis of both pilins and the core subunits of Photosystem II.

Accepted 23 July, 2014. *For correspondence. E-mail sobotka@alga.cz; Tel. (+42) 384 340491; Fax (+42) 384 340415.

Introduction

Bacterial Type IV pilins, pseudopilins and the related archaeal flagellins form a large family of proteins with an extraordinary broad spectrum of functions. They are implicated in motility, genetic transformation, cell aggregation, secretion or even serve as electrically conductive nanowires (reviewed in Giltner *et al.*, 2012). The signature of Type IV pilins is a cleavable N-terminal signal peptide (SP) followed by a conserved hydrophobic segment (Fig. 1). The C-terminal domain forms a globular head faced to periplasmic space and, although its sequence is usually quite divergent, the available crystal structures are highly conserved and contain four-stranded anti-parallel β-sheets (Giltner *et al.*, 2012).

In the current model of pilin biogenesis, pilins are co-translationally inserted into the membrane by the Sec pathway (Arts *et al.*, 2007; Francetic *et al.*, 2007). The SP is then removed by a dedicated membrane-bound prepilin peptidase called PilD, and the same enzyme also methylates the amino-terminal residue (Holt *et al.*, 2005; reviewed in Dalbey and Kuhn, 2012). PilD belongs to a family of aspartyl proteases (Dalbey and Kuhn, 2012) and cleaves prepilins roughly proximal to the membrane surface, consistently with the recently published structure of the related presenilin protease (Li *et al.*, 2013). The cleavage of the SP is necessary for further processing of all known Type IV pilins into functional structures (Giltner *et al.*, 2012).

It is unclear how mature pilins are extruded from the lipid bilayer and polymerized into long fibres. According to the current knowledge, pilus assembly requires the interaction of at least 15 proteins (Carbonnelle *et al.*, 2006). The core components of the assembly machinery are the PilQ secretin, a channel in the outer membrane through which the pilus fibre (polymerized pilins) exits the cell, and PilC, which forms a platform in the inner membrane. PilQ is a large multimer exposed within the periplasm, and the other components of the assembly machinery are most likely arranged around the PilQ-PilC scaffold in a compact structure spanning the entire cell envelope (Burrows, 2012; Tammam *et al.*, 2013). The hexameric ATPase PilB associates with PilC (Takhar *et al.*, 2013) and generates force to move pilins from the inner membrane under

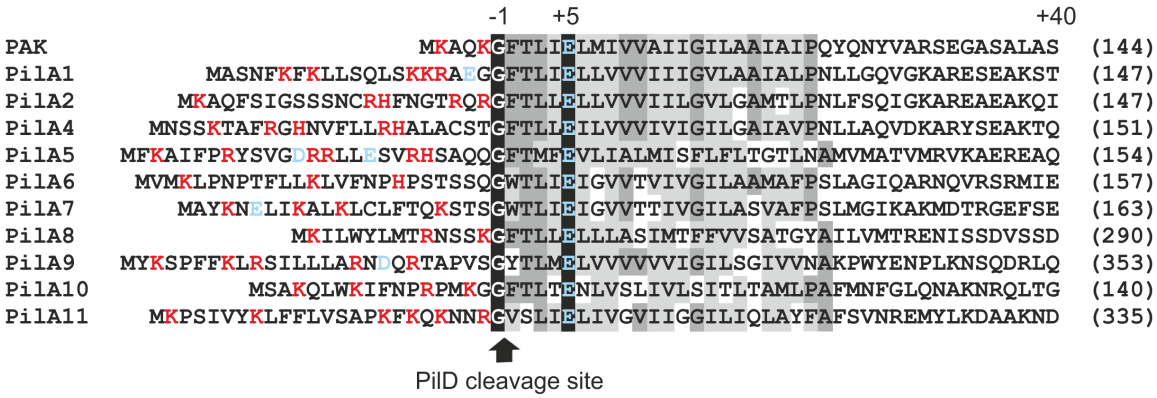

Fig. 1. Alignment of putative pilin proteins encoded in the *Synechocystis* genome and the canonical Type IV pilin (PAK) from *Pseudomonas aeruginosa*. The leader peptide and first 40 N-terminal residues were aligned based on the PilD peptidase cleavage site (marked by an arrow). The cleavage domain contains hydrophobic amino acids between the conserved glycine (– 1) and glutamic acid (+ 5) residues. The membrane segment is shown in grey, the positively and negatively charged amino acid residues in the leader peptide and in the membrane segment are highlighted in red and blue, respectively, and the total length of each mature protein is indicated on the right.

assistance of other critical components (PilM, PilN, PilO and PilP). Pilin polymerization is reversible, and cycles of pilus assembly and disassembly underlie twitching motility (Burrows, 2012).

Cyanobacteria form an important bacterial phylum that emerged at the dawn of life on Earth (Knoll, 2008). These organisms have evolved an efficient photoautotrophic metabolism based on oxidation of water molecules, which is powered by energy of photons. The evolution of cyanobacteria relying on oxygenic photosynthesis and possessing an endogenous thylakoid membrane system had to result in substantial remodelling of the original bacterial structures. Indeed, more than a hundred protein families universally shared by cyanobacteria have no counterparts in other bacteria (Mulkidjanian *et al.*, 2006). Although cyanobacteria are highly specialized, many typical bacterial structures have been preserved over billions of years after the branching of cyanobacteria and bacteria; an example is Type IV pilus-based motility (Bhaya *et al.*, 2000). However, genomic data show that cyanobacterial strains often contain unusually high numbers of type IV pilin-like genes (Table S1). For instance, the genome of the cyanobacterium *Acaryochloris marina* contains at least 16 genes with the typical pilin signature (Table S1). The genome of the best-studied cyanobacterium *Synechocystis* PCC 6803 (hereafter referred to as *Synechocystis*) encodes 10 putative Type IV pilin proteins (Fig. 1), and only four of these proteins (PilA1, PilA9, PilA10, PilA11) are essential for motility (Bhaya *et al.*, 2000; 2001; Yoshihara *et al.*, 2001). The functions of other pilin-like proteins remain unknown. Surprisingly, He and Vermaas (1999) observed that cyanobacterial pilins are implicated in the biogenesis of Photosystem II (PSII). They analysed a multiple *Synechocystis* mutant that synthesized chlorophyll only under light conditions and also lacked Photosystem I (PSI). After incubation in the dark, the mutant cells were almost entirely depleted of chlorophyll; therefore, these mutant cells enabled the study of early events in PSII biogenesis, which were unmasked by the absence of abundant chlorophyll complexes. Notably, the first observable green complex during re-greening contained typical pilin proteins (He and Vermaas, 1999). The authors also demonstrated that the appearance of this first chlorophyll complex was significantly delayed when two pilin genes (*pilA1, pilA2*) were inactivated (He and Vermaas, 1999).

In this study, we assessed the photosynthetic performance of *Synechocystis* mutants lacking pilins or proteins essential for the biogenesis of pilus fibres. Interestingly, unlike other tested strains that showed no obvious growth phenotypes, the *pilD* null strain lacking the prepilin peptidase proliferated only when the growth medium was supplemented with glucose. We demonstrated that the loss of photoautotrophy in *pilD* was caused exclusively by the toxicity of the unprocessed form (prepilin) of the major pilin PilA1. The presence of the prepilin in membranes strongly impaired the synthesis of PSII subunits but not PSI and induced the degradation of Sec translocons. These data suggest that the PilA1 prepilin interferes with the translocon machinery required for the synthesis of pilins and PSII.

Results

The Synechocystis pilD *(*slr1120*) mutant accumulates two forms of PilA1 prepilin*

The pilin mutants used in this study (listed in Table 1) were derived from the glucose-tolerant *Synechocystis* WT-V

Table 1. Characteristics of *Synechocystis* strains used in this study.

Strain	Resistance	Mutation	Ref. for construct	Photoautotrophic growth
pilA1-2	Zeo	del[a]:89–782	This study	+
pilA2	Spec	ins[b]:57	Bhaya *et al.* (2000)	+
pilA4	Kan	del:206–528(+54)[c]	He and Vermaas (1999)	+
pilA5-8	Zeo	del:74–2190	This study	+
pilA9-11	Zeo	del:100–2479	This study	+
pilB1	Zeo	del:113–614	This study	+
pilQ	Cm	del:72–955	This study	+
pilD	Kan	del:4–570	Bhaya *et al.* (2000)	–
pilD/pilA1-2	Kan, Zeo		This study	+
pilD/pilA2	Kan, Spec		This study	–

a. Replacement of the indicated gene region (in base pairs) by the antibiotic-resistance cassette.
b. Insertion of the antibiotic-resistance cassette into the gene after nucleotide 57.
c. The deletion includes the first 54 bp down-stream of the *pilA4* gene.
Photoautotrophic growth was monitored by growing the mutant cells on BG11 plates under moderate-light conditions (40 $\mu E\ s^{-1}\ m^{-2}$) or high-light conditions (300 $\mu E\ s^{-1}\ m^{-2}$) for 2 weeks. + indicates that the proliferation of the strain was comparable to the WT under both tested conditions. The antibiotic-resistance genes conferred resistance to Zeo (zeocin), Spec (spectinomycin), Kan (kanamycin) or Cm (chloramphenicol).

sub-strain (Trautmann *et al.*, 2012). Unlike the original *Synechocystis* PCC strain, the WT-V sub-strain is non-motile because of a mutation in the SpkA signalling kinase (Kamei *et al.*, 2001); however, the biogenesis and the assembly of pilus fibres are not affected (Fig. S1). The use of the WT-V sub-strain (hereafter WT) genetic background eliminates the 'false-positive' phenotypes that might be observed if the immotile mutants were compared with a motile control.

The studied pilin mutants exhibited no obvious growth defects under moderate- and high-light conditions, with the exception of the *pilD* (*slr1120*) strain that lacks the putative prepilin peptidase. This strain was strictly mixotrophic and survived for a prolonged time (days) only on agar plates supplemented with glucose (Fig. 2A). Similarly, the *pilD* cells grew slowly in liquid culture with glucose, although they formed large aggregates; however, in media lacking glucose, the proliferation of this mutant ceased (not shown).

The PilA1 protein is the major structural component of thick pili in *Synechocystis* (Bhaya *et al.*, 2000) and is presumably the main substrate of the prepilin peptidase. Indeed, the *pilD* strain accumulated a PilA1 form with a lower electrophoretic mobility than the mature PilA1 (Fig. 3A), which corresponded well to the expected size of the prepilin molecule (pPilA1). Detection of this protein supported identity of the *slr1120* gene product as the Type IV prepilin peptidase. However, there was also a second PilA1 form with higher mobility than the mature PilA1 (Fig. 3A). Origin of this band was rather enigmatic and therefore we analysed it in detail by N-terminal sequencing and mass-spectrometry. The analyses showed that the protein contained the entire signal peptide (SP) with exception of the N-terminal methionine but it also contained the C-terminus including tri-methylated Lys residue (Fig. 3B), which excluded a truncation at the C-terminus of the protein. We further tested whether both prepilins contain a disulphide bridge, which is typical feature of the Type IV pilins (Giltner *et al.*, 2012). As shown in Fig. S2, the migration of both prepilins on SDS-PAGE gels was similarly shifted in the presence and absence of dithiothreitol (DTT), suggesting that both prepilins were present in the cells in an oxidized state (Motohashi *et al.*, 2001).

As the lower-mass form of prepilin contained all amino acid residues of the putative prepilin the most probable reason for its faster mobility was its insufficient post-translational modification. Indeed, the *Synechocystis* PilA1 protein has been reported to be *O*-glycosylated between residues 67 and 75 with Thr73 as the most probable residue binding the glycan composed of xylose and fucose (Kim *et al.*, 2009). An increased PilA1 glycosylation has resulted in the reduced electrophoretic mobility (Fig. 3A; Kim *et al.*, 2009), on the other hand insufficient post-translational modification of PilA1, most probably glycosylation, has led to the similar shift, which we observed between the prepilin forms (Kim *et al.*, 2004). Indeed, the mass-spectrometry analysis of the lower-mass prepilin showed no signals that would correspond to *O*-glycosylated peptide 67–75 (Fig. 3B) and therefore, we designated this protein as NpPilA1 (*N*on-glycosylated *p*repilin) and the slower migrating form as pPilA1.

The observed population of NpPilA1 indicated that either the process of prepilin glycosylation was very slow or, alternatively, a pool of prepilin escaped glycosylation. To discriminate between these possibilities we assessed the pPilA1 and NpPilA1 levels after 60 min incubation in the presence of the protein synthesis inhibitor chloramphenicol. As this treatment did not change the ratio

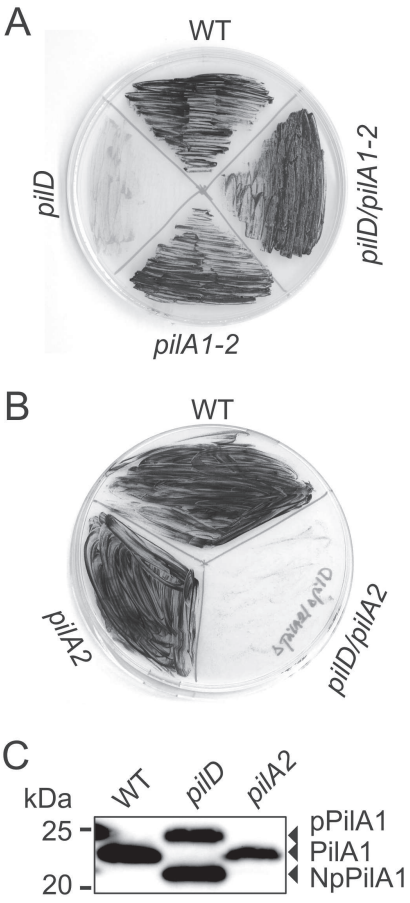

Fig. 2. Growth and complementation of the *pilD* mutant.
A and B. (A) Photoautotrophy of the *pilD* strain is rescued by deletion of the *pilA1-pilA2* chromosomal region (*pilA1-2*) but not by inactivation of the *pilA2* gene alone (B); see Table 1 for strain descriptions. Glucose-free BG11 plates were inoculated with similar amounts of cells and incubated in continuous moderate light (40 μE m^{-2} s^{-1}) for 10 days.
C. Immuno-detection of PilA1 in the *pilA2* strain grown under Glc– conditions; WT and *pilD* were included as controls and immunoblotting was performed as described for Fig. 3A.

between both proteins (Fig. S2), it implied that the *pilD* cells accumulated significant amount of non-glycosylated PilA1 prepilin that was neither additionally processed nor promptly degraded.

The PilD peptidase is essential for the function of the photosynthetic apparatus

The ability of *Synechocystis* cells to grow photoautotrophically apparently did not depend on the functional pilus biogenesis. *Synechocystis* mutants lacking factors essential for pilus assembly (*pilB* and *pilQ*) or the *pilA* genes/operons (*pilA1-2*, *pilA4*, *pilA5-8*, *pilA9-11*; Table 1) had no obvious growth defect (Table 1). Therefore, the presence of mature but unassembled pilin proteins in *pilB* and *pilQ* null mutants did not affect photoautotrophy. Similarly, the absence of either major (PilA1) or minor (pseudo)pilin proteins (PilA2, PilA4, PilA5-8, PilA9-11) had no significant effect on *Synechocystis* viability (Fig. 2, Table 1).

To understand the critical role of PilD in photosynthesis, we analysed the *pilD* strain grown in the presence of glucose (Glc+) and 24 h after its shifting to glucose–free medium (Glc–). The whole-cell spectra showed that the *pilD* cells grown in Glc+ contained virtually normal levels of photosynthetic pigments, except for a lower amount of carotenoids (Fig. 4A). This result was confirmed by the spectroscopic quantification of chlorophyll in the methanol extract (WT = 5.2, *pilD* = 5.5 μg chlorophyll ml^{-1} of cells at OD_{750} = 1). After shifting to Glc–, the total amount of chlorophyll in WT decreased (4.5 μg chlorophyll ml^{-1}; Fig. 4A) because of decreased PSI content, which is a characteristic response of the WT-V sub-strain to Glc– conditions (R. Sobotka and J. Komenda, unpublished data). No decrease in chlorophyll content was observed in the *pilD*, indicating that this regulatory mechanism does not work properly in the mutant (Fig. 4A; see *Discussion*). The PSII/PSI ratio was assessed by low-temperature (77K) chlorophyll emission spectra measured on intact cells. In principle, chlorophyll molecules bound to PSI and PSII complexes emit at characteristic wavelengths, which allows to compare photosystem stoichiometry *in vivo* (Fig. 4B). Most PSII chlorophylls emit at 685 nm except for one emitting at 695 nm which is quite specific for the active intact PSII complexes (Sinha *et al.*, 2012). The origin of the 685 peak is rather complex and includes also inactive PSII and its unassembled subunits (Sinha *et al.*, 2012), other chlorophyll-binding proteins like Hlips (Knoppová *et al.*, 2014) and an emission from phycobilisomes (Hernandez-Prieto *et al.*, 2011). On the other hand, PSI complexes are typical by the emission with maximum around 725 nm. The measurement showed that the mutant contained much less PSII complexes than WT when normalized to PSI level and also the PSI/PSII ratio in the mutant did not changed significantly in Glc– conditions (Fig. 4B), consistently to the whole-cell spectra (Fig. 4A). However, if the PSII level is low, the PSI and 685 peaks can contribute significantly to the 695 emission and, therefore, the evaluation of PSII/PSI ratio from 77K spectra should be made with caution. We therefore also compared levels of PSI (PsaD) and PSII (D1) subunits by immunoblotting using specific antibodies. In Glc+ condition the mutant cells contained higher levels of PsaD and a similar level of D1 relative to the control, but the D1 content decreased markedly after the shift to Glc– conditions whereas the PSI level remained rather constant (Fig. 4D). Finally, PSII activity was addressed directly by measuring oxygen evolution. This analysis revealed that

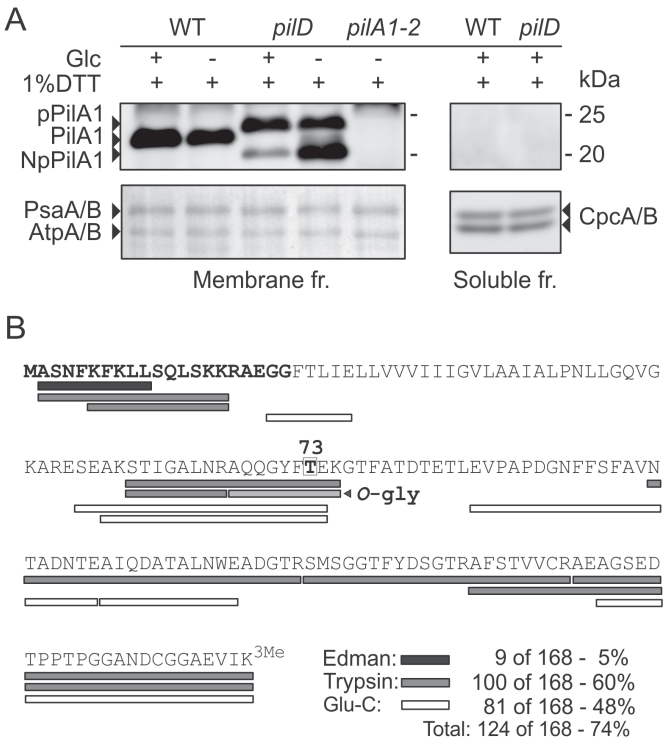

Fig. 3. A. Immuno-detection of the PilA1 prepilin in *Synechocystis pilD* cells. The *pilD* (*slr1120*) mutant lacks the mature form of PilA1 but accumulates the PilA1 prepilin (pPilA1) and a non-glycosylated form of the PilA1 prepilin (NpPilA1), both exclusively in the membrane fraction. Accumulation of the NpPilA1 form is increased after shifting of the *pilD* cells to glucose-free growth medium for 24 h (*pilD* Glc–). The PilA1 protein was detected using a specific antibody, and the membranes isolated from the *pilA1-2* strain were loaded as a control. The blotted proteins stained with Ponceau S are shown below as a loading control; the PsaA/B, AtpA/B and CpcA/B proteins are indicated. The same amount of chlorophyll (0.75 μg) was loaded in each line.
B. Peptide map of the NpPilA1 displaying sequence coverage and peptides generated by trypsin (grey bars, coverage 60%) and Glu-C protease (white bars, coverage 48%). The LC-MS analyses and Edman N-terminal sequencing (black bars, coverage 5%) data cover altogether 74% of the protein sequence. Apart from the absence of initial methionine and the tri-methylation of C-terminal lysine residue (3Me) the data show no other modification of the prepilin sequence. The trypsin peptide 67–75 shown previously to be *O*-glycosylated in the mature PilA1 protein (Kim *et al*., 2009) is highlighted (*O*-gly) including the candidate residue Thr73 (boxed).

the *pilD* cells (Glc+) had approximately half the PSII activity of the WT, and after the shift to Glc–, PSII activity in the mutant further decreased to approximately 20% of the WT (Fig. 4C). Together, these data demonstrated that the mutant maintained enough PSI complexes in both growth conditions tested but the number of functional PSII was low even in presence of glucose and further reduced under photoautotrophic conditions.

While the cell spectra did not suggest extensive changes in the thylakoid membrane system in the *pilD* mutant (Fig. 4A), inspection of the ultrastructure of *pilD* cells by electron microscopy unveiled abundance of abnormal membrane-like structures located in the vicinity of the cytoplasmic membrane (Fig. 5C–F). Vesicle-like and curled forms of membranes can be distinguished. Such structures were not observed in WT cells (Fig. 5A and B). Previously, formation of intracellular membranes has also been observed in *Escherichia coli* mutants lacking the signal recognition particle or SecE components of the translocation machinery (Herskovits *et al*., 2002).

We can conclude that the inactivation of the prepilin peptidase in *Synechocystis* impaired function of the photosynthetic apparatus to such extent that the *pilD* mutant was unable to grow photoautotrophically. Although the *pilD* mutant had capacity to build thylakoid membranes and contained a sufficient level of PSI, it had aberrant membrane ultrastructure and impaired activity of PSII. It appears that in the absence of an external source of reduced carbon, the *pilD* cells failed to maintain a critical number of functional PSII complexes and died.

Elimination of the pilA1 *gene restores the photosynthetic capacity of the* pilD *mutant*

Thick pili are assembled from hundreds of PilA1 subunits (Bhaya *et al*., 2000) hence the PilA1 proteins need to be produced in large quantities. Indeed, based on ^{35}S protein labelling, PilA1 is one of the most intensively synthesized membrane proteins in *Synechocystis* (Fig. 7) and the uncontrolled accumulation of the PilA1 prepilin could somehow impair the photosynthetic apparatus. On the *Synechocystis* chromosome, the *pilA1* gene is followed by *pilA2*, a pilin gene with no essential role in motility (Fig. 1; Yoshihara *et al*., 2001). Strikingly, the parallel deletion of the *pilA1-2* cluster and the *pilD* gene caused no defect in photoautotrophic growth compared to the WT (Fig. 2A), although cell aggregates were formed in liquid culture (not shown). We also generated a strain lacking only the *pilA2* gene (Table 1), and this mutation did not significantly affect the accumulation of the PilA1 protein (Fig. 2C) and did not rescue the *pilD* phenotype (Fig. 2B). These experiments demonstrated

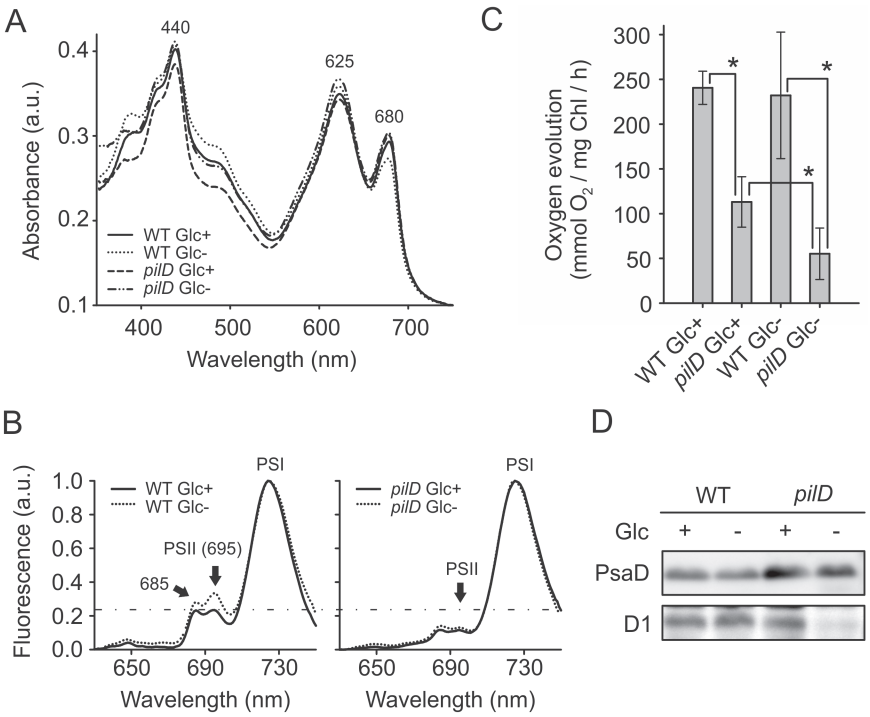

Fig. 4. Level and activity of PSII in the *Synechocystis pilD* strain.
A. Cell absorbance spectra of the WT and *pilD* strains under mixotrophic conditions (Glc+) and after shifting to the glucose-free medium for 24 h (Glc–). Chlorophyll is represented by the 440 and 680 nm peaks, phycobiliproteins by the 625 nm peak and carotenoids by the peaks in the range of 440–520 nm. The spectra were normalized to light scattering at 750 nm.
B. Low-temperature (77 K) fluorescence emission spectra of the WT and *pilD* cells grown under Glc+ and Glc– conditions. Peaks at 695 and 722 nm represent PSII and PSI complexes respectively. a.u., arbitrary units. The spectra were collected using excitation wavelength 435 nm to excite chlorophyll and were normalized to PSI peak.
C. The rate of oxygen evolution in the WT and *pilD* strains under conditions described in (A); the same numbers of cells normalized to light scattering at 750 nm were assayed. The values shown represent the means ± SD from three independent measurements, and asterisks indicate significant differences in oxygen levels as tested using a paired *t*-test ($P = 0.05$).
D. The level of the PSI subunit PsaD and PSII subunit D1 in the WT and *pilD* mutant. The membrane proteins were separated by SDS-PAGE, blotted and probed using specific antibodies; the same amount of chlorophyll (0.75 μg) was loaded in each lane.

that PilA1 prepilin was detrimental to *Synechocystis* cells and caused the *pilD* growth phenotype.

Accumulation of prepilin inhibits the synthesis of essential membrane complexes

To monitor the effect of the *pilD* mutation on protein synthesis/stability, we performed pulse-chase protein radiolabelling of *pilD* and WT strains grown in Glc– conditions. The labelled membrane proteins were separated by SDS-PAGE, and the gel was stained with Sypro Orange, dried and exposed to a phosphorimager plate (Fig. 6A). The autoradiograph demonstrated an inhibition of protein synthesis in the mutant, although the stability of the synthesized proteins was not altered. Significantly, the characteristic bands of the intensively labelled D1 subunit and the partly mature iD1 precursor (Komenda *et al.*, 2007) were practically undetectable in the mutant, suggesting that PSII synthesis and repair were drastically affected by the presence of prepilin. However, the synthesis of core PSI subunits PsaA/B appeared to be similar in the mutant and the WT (Fig. 6). This result suggested that the prepilin inhibited a subset of membrane proteins rather than had a global impact on the protein synthesis. We compared protein labelling pattern in the mutant (Fig. 6A) with a long (8 h) pulse-labelling of WT cells treated with a lethal concentration of chloramphenicol (50 mg l^{-1}; Fig. 6B). Indeed, chloramphenicol drastically reduced the total protein synthesis but the D1 protein synthesis could still be detected while signals of other membrane proteins disappeared completely (Fig. 6B). Given the very intensive labelling of D1 protein in the control (Fig. 6B), the pool of ribosomes translating D1 protein had to comprise a substantial portion of all ribosomes in the cell. If the translation machinery is

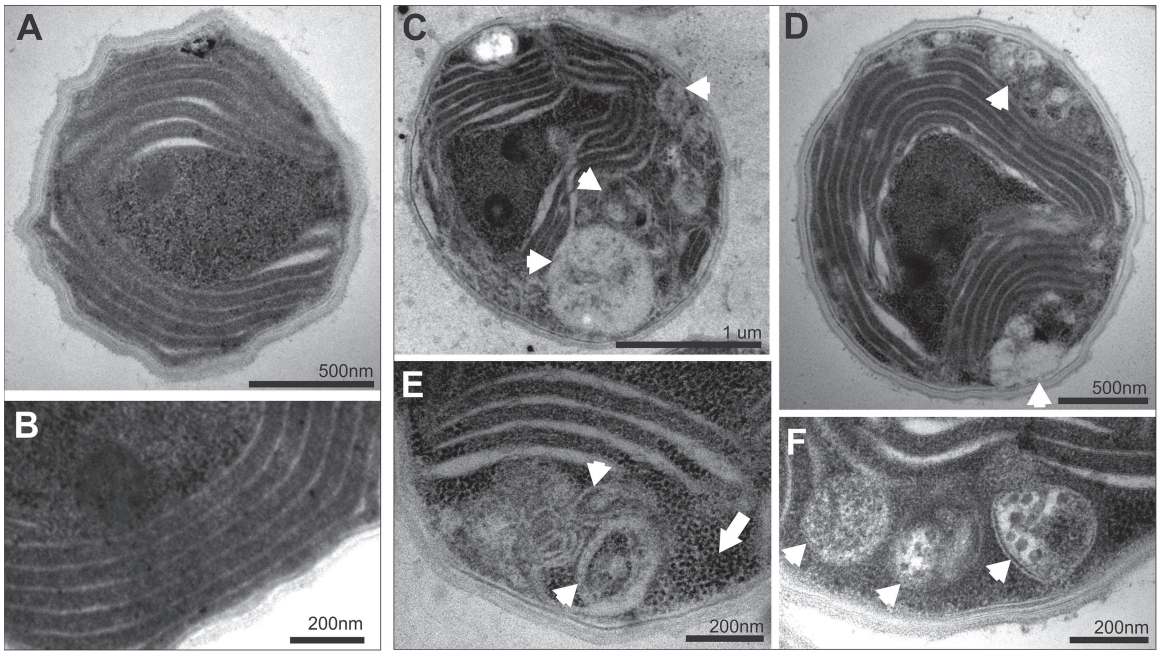

Fig. 5. Transmission electron microscopy of the *Synechocystis* WT and *pilD* cells. Representative stained ultra-thin sections of cells grown for 24 h in glucose-free medium (Glc–). (A) WT cells and (B) a detail of the WT thylakoid membranes. (C and D) *pilD* cells and (E and F) details of unusual membrane structures (marked by white arrowheads) observed in this strain. Note the high concentration of ribosomes in the vicinity of these structures (white arrow).

globally impaired, the D1 protein has certainly better chances to be synthesized, though with limited rate, than e.g. PSI core subunits. We concluded that the observed phenotype of the *pilD* mutant could not be caused by a global defect in protein synthesis but the accumulation of prepilin hit quite specifically otherwise intensive synthesis of PSII subunits.

The toxic effect of prepilin was further explored combining pulse-chase labelling and 2D protein electrophoresis. Similar amounts of WT and *pilD* membranes (based on chlorophyll content) were solubilized using dodecyl-*b*-maltoside (DDM) and subjected to Clear-Native electrophoresis (CN-PAGE, Fig. 7). Consistently with the above data, the native gel revealed significantly lower levels of dimeric and monomeric PSII complexes in the *pilD* sample (note the detection of chlorophyll fluorescence in Fig. 7). Separation of the CN-gel in the second dimension by SDS-PAGE confirmed the low content of individual PSII subunits in the mutant, and it also revealed a strongly reduced level of the NADH dehydrogenase complex (Fig. 7). However, the ATP synthase and the cytochrome b_6f complexes were still fairly abundant in the mutant; refer to (Herranen *et al.*, 2004) for a description of the identification of individual protein spots. The PilA1, pPilA1 and NpPilA1 spots were identified by mass-spectrometry (not shown). Furthermore, no membrane-bound ribosomes were visible in the *pilD* sample, which contrasted with abundance of ribosome subunits running at the top of the CN gel in the WT sample (Fig. 7) and with large numbers of ribosomes in *pilD* cells observed using electron microscopy (Fig. 5).

Notably, the 2D spots of pPilA1 and NpPilA1 were quite weak in the mutant sample, whereas PilA1 was among the most abundant membrane proteins in the WT (Fig. 7). This observation was inconsistent with the comparable levels of pPilA1, NpPilA1 and PilA1 detected by immunoblotting analysis of the completely denatured membrane fractions (Fig. 3A) and suggested that prepilins had limited solubility in DDM. In a separate experiment, we assessed the solubility of membrane proteins and observed that a fraction of pPilA1 and most of NpPilA1 remained insoluble after extraction of the membranes using DDM (Fig. S4). Therefore, it is likely that both forms of prepilins were prevalently localized in a compact structure(s) resistant to mild detergents. As a control, both photosystems were completely solubilized by DDM (Fig. S4); therefore, the analysis of PSII based on the 2D gel system was not biased by its partial solubility.

Exposing the 2D gels to a phosphorimager plate allowed us to assess the synthesis of membrane complexes during

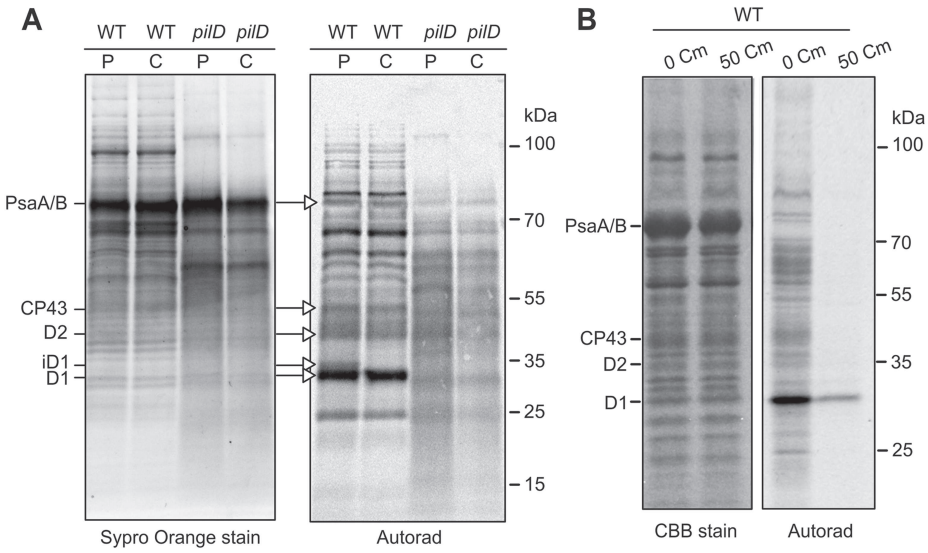

Fig. 6. Pulse-chase [^{35}S] labelling and SDS-PAGE analysis of membrane proteins from WT and *pilD* strains.
A. Cells (Glc–) were radiolabelled with a mixture of [^{35}S] methionine and cysteine for 60 min (line P) and then chased for 60 min in the presence of chloramphenicol (100 mg l^{-1}; line C) at irradiance of 100 μmol photons m^{-2} s^{-1}. Membrane proteins corresponding to 1 μg of chlorophyll were separated using denaturing SDS-PAGE, stained by Sypro Orange, dried and then exposed to a Phosphorimager plate for 7 days (Autorad). The PSI and PSII subunits are marked. The overall incorporation of radioactivity in the *pilD* sample did not exceed 70% of the WT (calculated using the ImageQuant 10 software, GE Healthcare Life Sciences).
B. Eight hours pulse-labelling of WT membrane proteins in presence of 50 mg l^{-1} chloramphenicol. The experiment was performed as described in A except the proteins were stained by Coomassie blue (CBB). A short, 30 min pulse-labelling without chloramphenicol, is shown as a control.

60 min pulse radiolabelling. As expected, PSII core subunits, PilA1 and the PSI subunits PsaA/B were among the most intensely labelled proteins in the WT (Fig. 7). Moreover, the PSII reaction centre assembly intermediate RC* (Knoppová *et al.*, 2014) was easily distinguished (see Fig. 8). In the mutant, all PSII subunits were labelled very weakly and detectable only as completely assembled PSII. It is worth to mention that pPilA1 was among the most strongly labelled proteins despite its limited solubility (Fig. 7, Fig. S4). The only mutant proteins labelled to the level comparable with WT were the PSI subunits assembled into trimeric PSI and the subunits of ATP synthase (quantification of selected spots is provided in Table S2). After the 60 min chase, the mutant cells incorporated more radioactivity into monomeric and dimeric PSII complexes (Fig. 8), showing that the process of PSII assembly was drastically limited by the lack of newly synthesized subunits but not completely inhibited. Intriguingly, most of the signal of labelled pPilA1 disappeared during the chase (Fig. 8). Based on the overall stability of pPilA1 and NpPilA1 after treatment with chloramphenicol (Fig. S2), we propose that the pPilA1 became less soluble in DDM during the chase rather than being degraded.

Together, these data provide evidence that the inactivation of the PilD peptidase has an adverse effect on the synthesis of PSII core subunits and on the accumulation of other essential membrane complexes like NADH dehydrogenase. The severe reduction in the levels of these complexes in the mutant cells was in sharp contrast to the continuous production of PSI and the ATP synthase (Fig. 7).

SecY translocons associate with NpPilA1 and undergo proteolytic degradation

The blocked synthesis of certain membrane proteins (Fig. 6), the formation of aberrant membrane structures (Fig. 5) and the low amount of membrane-bound ribosomes in the *pilD* mutant (Figs 7 and 9B) all indicated that prepilins interfered with the translocon machinery. Pilin synthesis requires SecY (Arts *et al.*, 2007; Francetic *et al.*, 2007), and the Sec translocon machinery is prone to degradation if it is jammed by a substrate (van Stelten *et al.*, 2009). *B. subtilis* cells depleted of Type I signal peptidases accumulated pre-proteins, which caused the jamming and inhibition of Sec translocons (Tjalsma *et al.*, 1998). Because this is analogous to the situation in the *pilD* strain, we asked whether there was an aberrant physical interaction between pPilA1 or NpPilA1 and components of the translocon apparatus. The SecY translocase was

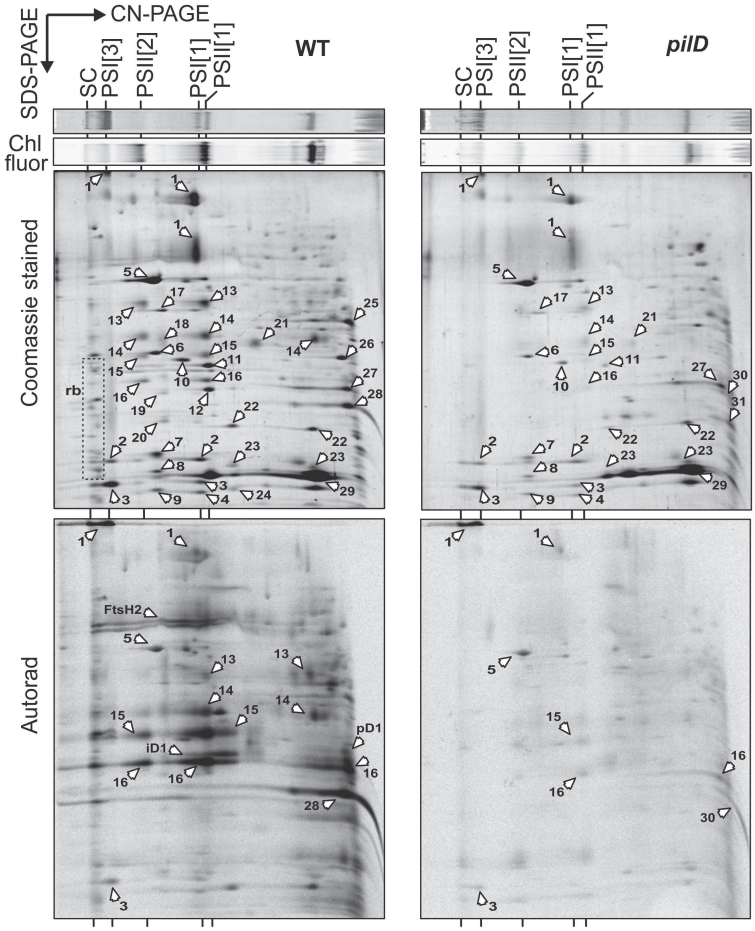

Fig. 7. 2D CN/SDS-PAGE and autoradiograph of membrane proteins from the WT and *pilD* strains. Cells grown under Glc– conditions were radiolabelled as described in the legend of Fig. 6. The isolated membranes were solubilized using DDM, and the obtained protein complexes were separated in the first dimension by clear-native electrophoresis (CN-PAGE). Approximately 4 μg of chlorophyll was loaded per each line. The CN gel was scanned using a LAS 4000 (Fuji) for chlorophyll fluorescence (Chl fluor) to visualize PSII complexes. After the second dimension (SDS-PAGE), the gel was stained with Coomassie blue, dried and then exposed to a Phosphorimager plate for seven days (Autorad). SC indicates high-molecular-mass supercomplexes; PSI[1] and PSI[3] indicate the monomeric and trimeric forms of PSI respectively; PSII[1] and PSII[2] indicate the monomers and dimers of PSII respectively. The individual proteins marked by arrows are 1 – PsaA/B, 2 – PsaD, 3 – PsaF, 4 – PsaL, 5 – AtpA/B, 6 – AtpC, 7 – AtpF, 8 – AtpD, 9 – AtpE, 10 – IlvC, 11 – CpcC1, 12 – CpcG1, 13 – CP47, 14 – CP43, 15 – D2, 16 – D1, 17 – NdhH, 18 – NdhB, 19 – NdhI, 20 – NdhJ, 21 – Amt1, 22 – PetA, 23 – PetB, 24 – PetD, 25 – PstA, 26 – PsbO, 27 – UrtA, 28 – PilA1, 29 – CpcA/B, 30 – pPilA1, 31 – NpPilA1, pD1 – precursor of D1, and iD1 – partially processed precursor of D1; rb indicates ribosome subunits.

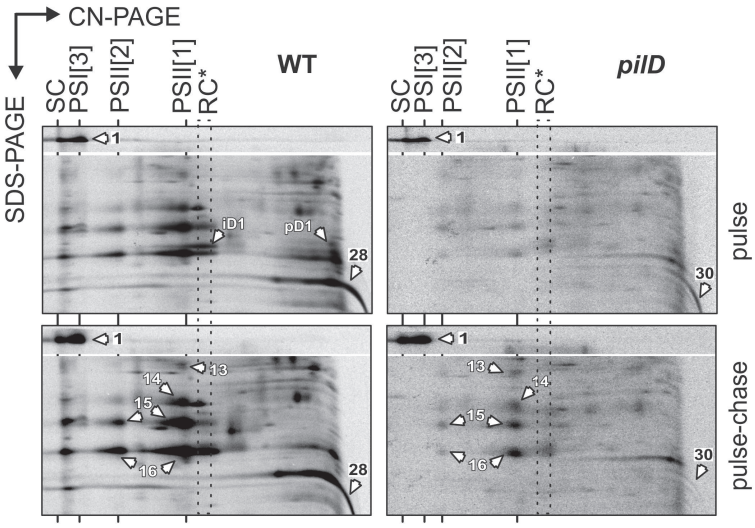

Fig. 8. Pulse-chase [^{35}S] labelling and 2D CN/SDS-PAGE of membrane proteins from the WT and *pilD* strains. Cells (Glc–) were radiolabelled as described for Fig. 6. Dried gels were exposed to a Phosphorimager plate for 7 days, and the *pilD* autoradiographs were further processed using ImageJ software (Knoppová *et al.*, 2014) to enhance the signal. For the same exposure time of the pulse-labelled strains, see Fig. 6. Only the top of the gel showing the PsaA/B proteins and the region between ~ 60 and ~ 20 kDa are shown. The protein complexes and individual proteins are labelled as in Fig. 7; RC* indicates a PSII assembly intermediate (see main text).

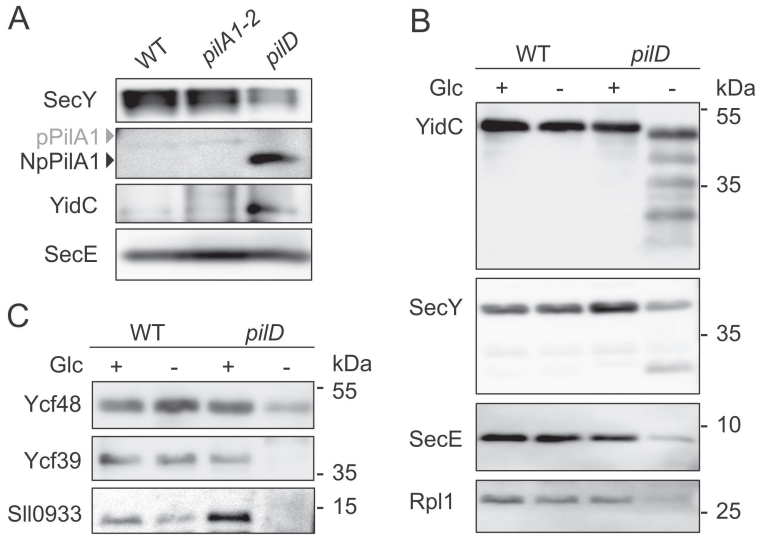

Fig. 9. Immuno-precipitation and immuno-detection of translocon components and PSII assembly factors.
A. Immuno-precipitation of the SecY translocase from solubilized membranes using the anti-SecY antibody and detection of the co-immunoprecipitated proteins. The antibody was incubated overnight with membrane proteins isolated from the WT, *pilA1-2* and *pilD* strains grown at Glc+, and then the antibody was immobilized on Protein A Sepharose 4B (Sigma, Germany). The resin was extensively washed, and the remaining proteins were eluted in a SDS buffer. The eluate was separated by SDS-PAGE, and the gel was blotted and probed with selected antibodies. Only NpPilA1 was detected in the eluate by anti-PilA1 antibody; the expected mobility of pPilA1 is indicated. The anti-SecE antibody was used to re-probe the blot as a control.
B. Immuno-detection of SecY, YidC, SecE and the ribosome subunit Rpl1. Isolated membrane fractions were denatured using 2% SDS and 1% DTT, separated by SDS-PAGE and blotted onto a PVDF membrane. The proteins were detected using specific antibodies as indicated.
C. Immuno-detection of the PSII assembly factors Ycf48, Ycf39 and Sll0933. The immunoblot was prepared essentially as described for (B).

immunoprecipitated from the DDM-solubilized membranes using the anti-SecY antibody, the immunoprecipitate was extensively washed, and the presence of pPilA1 and NpPilA1 was detected using antibodies. As shown in Fig. 9A, NpPilA1co-precipitated with SecY, although the yield of SecY was lower from the *pilD* membranes when compared to the WT (Fig. 9A). In addition to the SecYEG trimer, the YidC insertase/foldase also assists in the synthesis of membrane proteins (Sachelaru *et al.*, 2013) either independently or in a complex with SecY (Dalbey and Kuhn, 2012). Furthermore, YidC is most likely required for pilin synthesis (Saller *et al.*, 2009). Indeed, YidC co-precipitated with SecY specifically from the *pilD* cell membranes; neither PilA1 nor YidC was detected in the precipitate from WT or *pilA1-2* controls (Fig. 9A). As shown in the Fig. S4 the SecY, YidC and PilA1 antibodies are highly specific and it is very unlikely that the NpPilA1 and YidC were co-precipitated with other proteins than SecY.

If the *Synechocystis* major prepilin inhibited SecY, the stability of the translocon should be impaired. Notably, the total SecY level was strongly reduced in *pilD* cells under photoautotrophic conditions, and also a putative product of SecY degradation was detected using the anti-SecY antibody (Fig. 9B). Total SecE level and the pool of membrane-bound ribosomes were similarly reduced in the mutant (Fig. 9B). In addition, all detectable YidC in *pilD* (Glc–) cells appeared truncated and extensive degradation of this protein was evident from the number of YidC fragments (Fig. 9B). Because only residual PSII synthesis occurred in the mutant (Glc–) cells, we measured the levels of the auxiliary factors Ycf48, Ycf39 and Sll0933, which assist during synthesis of PSII core subunits (Rengstl *et al.*, 2013; Knoppová *et al.*, 2014). Consistent with levels of SecY and YidC, the amount of Ycf48 was strongly decreased, and Ycf39 and Sll0933 were completely absent in the mutant after shifting to photoautotrophic conditions (Fig. 9C).

The observed fast depletion of YidC and auxiliary factors involved in PSII synthesis prompted us to investigate putative interactions between these proteins and PilA1 or prepilins. Solubilized membranes from the WT and *pilD* strains were separated on a 2D gel, blotted and probed by selected antibodies. Interestingly, the PilA1 formed three higher-molecular-mass complexes (PilA1-A,B,C) and the A and B complexes co-migrated precisely with the Ycf48 protein. The origin of the Ycf48 spot co-migrating with A complex is unclear but the second Ycf48 signal around ~ 200 kDa indicates an early PSII assembly intermediate named RC*, which consists of D1 and D2 core subunits, several low-mass PSII subunits

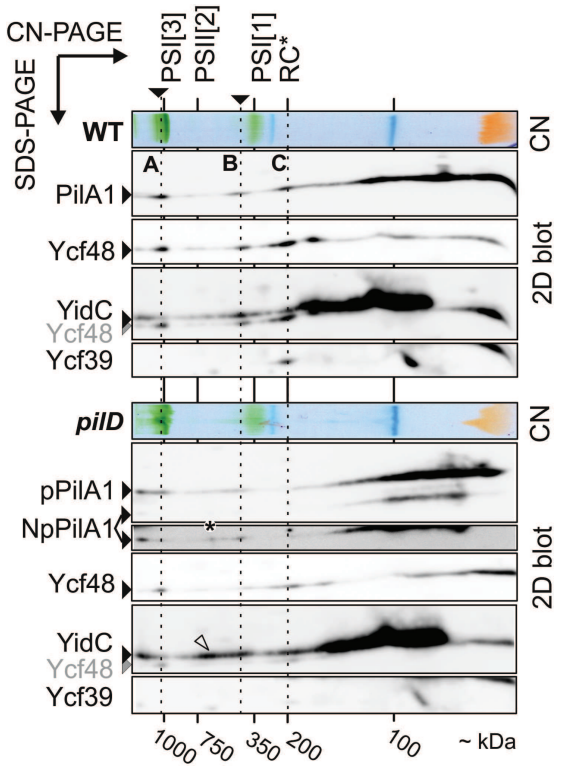

Fig. 10. Immuno-detection of PilA1 and PilA1 prepilins in high-molecular-mass membrane complexes using 2D CN/SDS-PAGE combined with immunoblotting. Membranes isolated from WT and *pilD* cells grown at Glc+ were solubilized by DDM, separated by 2D CN/SDS-PAGE essentially as described for Fig. 7 and blotted. The PVDF membrane was probed by PilA1 antibody and then successively re-probed with Ycf48, Ycf39 and YidC antibodies. In the WT strain, three high-molecular-mass PilA1 signals were detected (A–C, marked by dashed lines). RC* indicates position of the PSII assembly intermediate consisting D1 and D2 core subunits, several low-molecular-mass PSII proteins and Ycf48 and Ycf39 auxiliary factors. A NpPilA1-specific spot is marked by asterisk; the triangle highlights a YidC complex, which accumulates in the mutant strain. Approximate masses of photosynthetic complexes are also indicated.

and the Ycf48 and Ycf39 factors (Fig. 10). The RC* complex has been characterized recently in details and it is quite likely that is assembled in the vicinity of Sec translocon (Knoppová *et al.*, 2014). The PilA1-B complex seemed to co-migrate with a YidC spot (Fig. 10).

The same experiment performed on *pilD* (Glc+) cells showed a different pattern. First, a significant fraction of pPilA1 remained in a very large complex (> 1MDa) on the top of the native gel (Fig. 10). The putative PilA1-A complex was present but no pPilA1 co-migrated with RC* and the level of RC* was quite low (see the signal of Ycf39). The level of NpPilA1 was relatively weak as expected for Glc+ conditions (Fig. 3A); however, a longer exposition also revealed higher-molecular-mass NpPilA1 assemblies. Again, a significant portion of the NpPilA1 was found at the top of the native gel and also a NpPilA1 complex corresponding to PilA1-B was apparent, however practically no NpPilA1 co-migrated with the Ycf48. Interestingly, the immunodetection of YidC protein suggested formation of a relatively abundant YidC complex with size ~ 600 kDa accumulating specifically in the mutant (marked by a triangle in Fig. 10). The migration of this complex was very similar to a distinct NpPilA1 2D spot (marked by asterisk) completely absent in signals of PilA1 and pPilA1 proteins. It is tempting to speculate that the 600 KDa YidC complex is the aberrant structure associated with NpPilA1 co-precipitated from the *pilD* cells (Fig. 9A). It should be noted that prepilins lack competence for assembly into multimeric pilin structures and therefore the observed large complexes were hardly prepilin oligomers (Chen *et al.*, 2006).

Together, these data suggest that the NpPilA1 is physically attached to the Sec translocon and/or YidC. Because of their aberrant interactions, the translocons in the mutant most likely undergo extensive proteolytic degradation and this destructive process seems to include auxiliary factors involved in the synthesis of PSII core subunits. Consistently with the low stability of Ycf48 and Ycf39, the mature PilA1 as well as prepilins were shown to form large membrane complexes and might physically interact with the periplasmic/lumenal Ycf48 protein during formation of RC*.

Discussion

Type IV pilins are inserted into the membrane by the Sec translocase (Arvidson *et al.*, 1999; Arts *et al.*, 2007; Francetic *et al.*, 2007), and the positively charged N-terminus followed by a hydrophobic part (Fig. 1) is the critical feature for virtually any substrates of the Sec pathway (Dalbey and Kuhn, 2012). Although a detailed description of pilin synthesis is not available, knowledge of the synthesis of secreted bacterial proteins with the cleavable type I SP could help us to estimate how pilins are processed by the translocon machinery and why the absence of PilD results in the degradation of SecY and YidC. Unlike the prepilin SP, the cleavable part of the type I SP includes both the charged and hydrophobic parts; however, this makes hardly a fundamental difference in the mode by which the SP promotes translocation.

Once emerged from the ribosome, the hydrophobic residues of the type I SP interact with the signal recognition particle that guides the protein precursor to the Sec translocon. During the early stage of translocation, the nascent chain inside SecY adopts a loop topology and induces a conformational change to open the channel (Simon and Blobel, 1992; Gouridis *et al.*, 2009). As shown recently, the hydrophobic helix of the Type I SP occupies the lateral

gate, whereas the charged and more flexible leading stretch is already exposed to the cytoplasmic surface (Park *et al*., 2014). There, this charged part may interact with lipids, SecY and other components of the translocon machinery. The fate of the SP during the later stages of translation is unclear; however, at least for proteins with more membrane segments, the SP needs to be released from SecY. The SP might move to YidC because YidC attaches to SecY, where nascent membrane segments escape the translocon laterally (Sachelaru *et al*., 2013). Notably, the *E. coli* Type I peptidase has been cross-linked with the SecY-YidC complex but not with SecY alone (Sachelaru *et al*., 2013). This observation indicates that at least for the SecY/YidC-dependent proteins, the SP is cleaved by signal peptidase after it moves from SecY into YidC. This model is consistent with the observed critical length, typically > 80% of the total length the nascent chain has to attain to be processed by the Type I peptidase (Josefsson and Randall, 1981).

According to our current knowledge, the synthesis of pilins follows similar rules except that the charged N-terminus serves as the cleavable SP and that the hydrophobic helix remains a part of the mature pilin. Pilin synthesis requires an interaction with the signal recognition particle (Arvidson *et al*., 1999; Arts *et al*., 2007), and the conformational changes in SecY are most likely induced by the entire N-terminal part of the prepilin including the hydrophobic helix. Maturation of the major XcpT pilin in *P. aeruginosa* depends on functional Sec machinery (Arts *et al*., 2007), which implies that prepilins must be at least partly translocated to expose the SP to the PilD peptidase. However, the cleavage of the XcpT prepilin is very rapid; almost all radiolabelled XcpT is processed after 1 min (Arts *et al*., 2007). Therefore, it is likely that PilD is located near to and operates in parallel with pilin translocation. Arts *et al*. (2007) reported no effect of YidC deletion on the synthesis of XcpT in *E. coli*; however, this result should be considered carefully because it is based on a heterologous system. In *B. subtilis*, the major pilin ComGC was markedly reduced in the YqjG (YidC homologue) deletion strain (Saller *et al*., 2009), which argues for involving of YidC in pilin synthesis. Furthermore, the negatively charged residue in the hydrophobic segment seems to be a signature of YidC-dependence (Zhu *et al*., 2013), and the glutamic acid residue (+ 5) is highly conserved in all pilin proteins (Fig. 1; Giltner *et al*., 2012).

Here, we demonstrated that accumulation of the PilA1 prepilin inhibits the photoautotrophic growth of *Synechocystis* by a process accompanied by degradation of SecY and YidC (Fig. 9B). Based on the observed association of SecY, YidC and the NpPilA1 (Fig. 9A), we propose that pPilA1 is processed by PilD peptidase and most probably also glycosylated near to SecY. The interaction between SecY and YidC is weak (Scotti *et al*., 2000) and probably limited to active translocons (Boy and Koch, 2009). In contrast to the *pilD* mutant sample, in the WT membranes, YidC was not co-precipitated using the SecY antibody (Fig. 9A) and a plausible explanation could be that the inserted NpPilA1 spans both YidC and SecY and links them together. It is tempting to speculate that the charged prepilin SP is exposed and interacts with the cytoplasmic surface of SecY or YidC, and if not removed, it hampers the release of prepilin from the translocon and thereby triggers degradation of the whole translocon machinery.

It is intriguing how much the stability of Sec apparatus in the *pilD* mutant depended on the presence of glucose (Fig. 9B). The detrimental effect of prepilins cannot be completely eliminated by glucose, as documented by the low PSII oxygen evolution (Fig. 4C) and by the reduced content of the RC* complex (Fig. 10); however, the proteolytic degradation of translocons was obvious only under photoautotrophic conditions. Interestingly, the absence of glucose significantly elevated the level of NpPilA1 (Fig. 3A), which might signalize that rather than the total level of prepilin, an increase in the NpPilA1 content has fatal consequences for the cell viability. Glucose as a source of glycosylation substrate could suppress the harmful accumulation of NpPilA1 by increasing the efficiency of glycosylation reaction. Alternatively, glucose could simply provide energy needed for efficient glycosylation in the photosynthesis-deficient mutant cells. The glycosylation of prepilin can make this protein more flexible or less 'sticky' and thus prevent jamming of the translocon. Only a small fraction of NpPilA1 can be solubilized by DDM (Fig. S3), which argues for the formation of a rigid NpPilA1-containing domain in the membranes of mutated cells.

The accumulation of unprocessed Sec substrates is deleterious for bacteria (Dalbey and Wickner, 1985) because it induces the degradation of the jammed Sec translocons (van Stelten *et al*., 2009). Nonetheless, the induction of a similar process by the elimination of the PilD peptidase was rather unexpected because no growth defect has been reported for the well-studied *pilD* strains of *P. aeruginosa* (Pepe and Lory, 1998; Muller *et al*., 2010). This discrepancy could be explained in the following ways: (i) the *Synechocystis* PilA1 has a much longer and strongly charged SP than the major PAK pilin of *P. aeruginosa* (Fig. 1), which might make PilA1 more prone to blocking translocons; (ii) prepilins inhibit the synthesis of PSII, which makes cyanobacteria more sensitive to elimination of *pilD*; and (iii) non-glycosylated and potentially more toxic (lower-mass) prepilins such as NpPilA1 have not been observed in bacterial or archaeal *pilD* mutants (Marsh and Taylor, 1998; Bardy and Jarrell, 2003; Bode *et al*., 2009). Nonetheless, the inactivation of FlaK, a PilD homologue in the archaeon *Methanococcus voltae* that processes preflagellins, has strongly inhibited the cell proliferation (Bardy and Jarrell, 2003). It suggests that the harmful effect of

increased prepilin/pre-flagellin levels might not always be manifested under laboratory conditions.

The *Synechocystis pilD* null mutant has been previously characterized by Devaki Bhaya *et al.* (2000). Intriguingly, the *pilD* mutant in their study (named here *pilD*-DB) has been derived from the glucose-sensitive PCC WT, and although fully segregated, it grew photoautotrophically. The *pilD* strain described here was prepared in a glucose-tolerant background, and we isolated several photoautotrophic *pilD* revertants by growing the mutant on a plate without glucose for more than two weeks (M. Linhartová and R. Sobotka, in preparation). In order to clarify this point we obtained the *pilD*-DB strain directly from the Devaki Bhaya laboratory and found the PilA1 (pre)pilin completely missing (Fig. S5). We expect that the *pilD* segregation under photoautotrophic conditions generated a suppressor mutation(s) that minimized the synthesis of PilA1 prepilin. A point that also calls for an explanation is the constant PSII/PSI ratio observed in the *pilD* mutant shifted to Glc– conditions. The *Synechocystis* controls photosystem stoichiometry mostly by changing PSI level while the PSII cellular content is rather stable (Kopečná *et al.*, 2012). But rather than an active PSI degradation, the current model envisages that, if needed, the PSI synthesis is turned down and, as the cell proliferation continues, the existing pool of PSI complexes is 'diluted' due to the growth and cell division (Kopečná *et al.*, 2012). The proliferation of the *pilD* strain seems to be quickly inhibited after transfer to photoautotrophic conditions, which rules out this mechanism leaving the PSII/PSI ratio unchanged.

An interesting finding of this work is the completely different sensitivity of PSII and PSI synthesis to prepilin toxicity. The reaction centres of both photosystems are assembled from chlorophyll-binding subunits, and according to the current model, chlorophyll is delivered to apoproteins during their insertion into the membrane (Sobotka, 2014). Our work provides the first clue that photosystems are produced on different, perhaps more specialized or compartmented translocon complexes. The biogenesis of PSI also seems to be less sensitive to degradation of YidC. In cyanobacteria, YidC is strictly required for the biogenesis of the thylakoid membrane, and elimination of this protein is not possible (Spence *et al.*, 2004). However, it is not clear whether YidC is essential for the synthesis of all chlorophyll-binding proteins. Furthermore, there might be extrinsic components of the Sec apparatus required for the translocation of PSII subunits and pilins, but not critical for the biogenesis of PSI. Unprocessed prepilins were detected in the *secA* and *secD* mutants of *E. coli* (Francetic *et al.*, 2007), and SecA and SecDF could participate in the partitioning of large periplasmic/lumenal domains that are typical for the PSII core subunits.

In modern cyanobacteria the PSII is active in thylakoids; however, an overlap between pilin and PSII biogenesis is not completely surprising. Although the place at which the PSII subunits are synthesized and assembled is not clear yet, various indirect evidences place the PSII synthesis to a putative domain at the interface of thylakoid and cytoplasmic membrane ('PSII biogenesis centres') (Komenda *et al.*, 2012; Nickelsen and Rengstl, 2013). Moreover, the cyanobacterium *Gloeobacter violaceus* lacks internal thylakoid membranes and the photosynthetic apparatus has to be synthesized in the cytoplasmic membrane (Rexroth *et al.*, 2011). The genome of this living cyanobacterial fossil codes for seven pilin proteins (Table S1) and pilins thus probably coexist with PSII in the cytoplasmic membrane from the oldest cyanobacterial history.

The abovementioned PSII biogenesis centres can be defined by presence of translocons, PSII assembly factors like Ycf48, Ycf39 or Sll0933 (Komenda *et al.*, 2012), terminal enzymes of chlorophyll biosynthesis pathway (Chidgey *et al.*, 2014; Sobotka, 2014) and early PSII assembly intermediates (Knoppová *et al.*, 2014). Indeed, levels of assembly factors are decreased in the *pilD* mutant, and we suggest that these proteins are degraded along with the inhibited Sec-YidC complex. None of these auxiliary factors is essential in *Synechocystis*; however, their inactivation affects the synthesis of PSII core subunits rather than the assembly of PSII (Rengstl *et al.*, 2013). It is attractive to speculate that the abundant and large machinery engaged in PSII biogenesis also produces high levels of pilins when motility becomes important. Accumulation of PilA1 prepilin, or perhaps just its non-glycosylated form, induces destruction of this machinery, which results in lack of essential PSII subunits. This model would explain why the first detectable green complexes after the bleaching of *Synechocystis* are 'contaminated' by pilins (He and Vermaas, 1999). However, there is an alternative model, more consistent with the observed co-migration of PilA1 with RC* on the native gel (Fig. 10). Accumulating knowledge about (pseudo)pilins highlights the versatility and adaptability of these proteins in acquiring new functions (Giltner *et al.*, 2012). Our results leave open the possibility that a portion of pilins remains in contact with the proposed biosynthetic centre, most probably with the periplasmic/lumenal Ycf48 protein (Fig. 10), and plays a novel role in PSII biogenesis. The delayed re-greening in pilin mutants observed by He and Vermaas (1999) might be due to a missing part in this intricate protein factory.

Experimental procedures

Preparation of Synechocystis *mutants*

All experimental strains were derived from the non-motile glucose-tolerant WT-V sub-strain of the *Synechocystis* PCC 6803 (Trautmann *et al.*, 2012). To prepare the *pilD* strain, chromosomal DNA was isolated from the previously reported *pilD* mutant (Bhaya *et al.*, 2000), which was a generous gift

from Professor Devaki Bhaya (Carnegie Institution for Science, Stanford, USA). The chromosomal DNA was used to transform the WT-V sub-strain, and full segregation was achieved by re-streaking the transformants several times on plates with increasing concentrations of kanamycin. A similar approach was used to generate the *pilA4* strain using the construct provided by Professor Wim Vermaas (School of Life Sciences, Arizona, USA; He and Vermaas, 1999). To prepare the *pilA1*/*pilA2* (*pilA1-2*), *pilA5-8, pilA9-11, pilB1* and *pilQ* strains, the respective gene or operon was replaced with a zeocin- or chloramphenicol-resistance cassette using the megaprimer PCR method as described in (Kopečná *et al*., 2013; see Table 1 for a description of all the constructs used). To delete the *pilA2* gene, WT-V cells were transformed with the pGEM-T-*pilA2* vector obtained from Professor Devaki Bhaya, and the fully segregated strain was obtained using increasing concentrations of spectinomycin. Because inactivation of *pilD* or *pilA1* leads to loss of transformation competence (Bhaya *et al*., 2000; Yoshihara *et al*., 2001), to construct the *pilA1-2*/*pilD* double mutant, the non-segregated *pilA1-2* was transformed with the *pilD* chromosomal DNA, and then both alleles were fully segregated using increasing concentrations of zeocin and kanamycin simultaneously. Because the *pilA2* mutant is transformation-competent, it was possible to combine this allele with the *pilD* deletion by transformation of the *pilA2* strain with the *pilD* chromosomal DNA.

Growth conditions

Unless stated otherwise, the strains were grown mixotrophically in BG11 medium supplemented with 5 mM glucose on a rotary shaker under moderate light conditions (40 μmol photons m^{-2} s^{-1}) at 28°C. In this work, these conditions are called 'Glc+'. To study the effects of photoautotrophic conditions on the *pilD* strain, cells were harvested, washed, resuspended in fresh BG11 medium without glucose and then incubated in the same conditions for 24 h (Glc– conditions). The photosynthetic competence of pilin mutants was tested by incubating a similar amount of cells from the Glc+ liquid culture on a BG11 plate under moderate light (40 μmol photons m^{-2} s^{-1}) or under high light (300 μmol photons m^{-2} s^{-1}) at 28°C for 10 days.

Whole-cell absorption spectra and measurement of chlorophyll content

The absorption spectra of intact cells were measured using a Shimadzu UV-3000 spectrophotometer. To quantify the chlorophyll content per cell, cell cultures at OD_{750} ~ 0.4 were harvested, the pigments were extracted with methanol, and the chlorophyll concentration determined spectrophotometrically as previously described (Porra *et al*., 1989). For measurements based on the optical density of the culture, the cell aggregates were disintegrated using an IKA TP 18/10 Ultra-Turrax homogenizer (Janke & Kunkel IKA Werke, Germany).

Measurement of oxygen evolution

The rate of oxygen evolution was measured continuously at 28°C using a customized Clark-type oxygen sensor (OC 223-B atyp, Theta 90, Czech Republic). The measurements were performed in a double-jacketed, multiport electrode chamber with a working volume of 6 ml. Moderate light intensity was set and measured using a submersible spherical micro-quantum sensor US-SQS/L (Walz, Germany) connected to a ULM-500 light meter (Walz, Germany).

Enzymatic digestion and mass spectrometric analysis

Coomassie-stained protein bands were excised from the gel, cut into small pieces and destained using 50 mM 4-ethylmorpholine acetate (pH 8.1) in 50% acetonitrile (MeCN). The proteins were further reduced with 30 mM TCEP in 100 mM Tris-HCl (pH 8.0) at 65°C for 30 min and alkylated by 30 mM iodacetamide in 100 mM Tris-HCl (pH 8.0) for 60 min in the dark. The gel was washed with water, shrunk by dehydration in MeCN and reswelled again in water. The supernatant was removed and the gel was partly dried in a Speed-Vac concentrator. The protein samples were then digested overnight by 100 ng of trypsin (Promega) in 25 mM 4-ethylmorpholine acetate/5% MeCN (pH 8.1) at 37°C or by Glu-C protease (Roche) in 25 mM ammonium carbonate (pH 7.8) at 20°C.

In LC-MS and LC-MS/MS analyses the resulting peptides were separated using Ultimate 3000 RSLCnano system (Dionex) on an Acclaim PepMap RSLC column (75 μm × 150 mm, 2 μm, 100 Å; ThermoScientific) connected directly to an ESI source of SolariX XR FT-ICR mass spectrometer (Bruker Daltonics). The spectrometer was calibrated using lock mass calibration resulting in mass accuracy below 1 ppm. LC-MS data were processed using DataAnalysis software (Bruker Daltonics) and LC-MS/MS data were searched by MASCOT (MatrixScience) against a NCBI database.

Edman N-terminal sequencing

N-terminal amino acid analysis was performed using a Procise 491 protein sequencer (Applied Biosystems) according to the manufacturer's manual.

Electron microscopy

WT and *pilD* cells were harvested at OD_{750} ~ 0.4. For negative contrast, the cells were fixed in 1% glutaraldehyde, resuspended in fresh BG11, applied to grids, and then stained with 1% uranylacetate. For making sections, the cells were cryofixed using high-pressure freezing and freeze substitution as previously described (Kopečná *et al*., 2012). Negative contrast and ultra-thin sections were examined in a JEOL 1010 transmission electron microscope equipped with a Mega View III camera (Olympus – SIS).

Radioactive labelling of proteins and cell fractionation

Radioactive pulse–chase labelling with a mixture of [^{35}S]Met and [^{35}S]Cys was performed as previously described (Dobáková *et al*., 2009) at irradiance of 100 μmol photons

m^{-2} s^{-1}. The harvested cells were washed and broken by glass beads in buffer A containing 25 mM MES/NaOH, pH 6.5, 10 mM $MgCl_2$, 10 mM $CaCl_2$ and 25% glycerol. The mixture was pelleted at 30 000 *g* for 15 min yielding a soluble fraction containing the supernatant and a membrane fraction pellet, which was re-suspended in an excess volume of thylakoid buffer and then centrifuged to remove the soluble contaminants.

Electrophoresis and immunoblotting

Unless stated otherwise, the membranes or soluble proteins prepared as described above were denatured by incubation in 2% SDS and 1% dithiothreitol (DTT) for 30 min at room temperature and separated on a 12% SDS-gel (SDS-PAGE). The proteins were transferred to a PVDF membrane and incubated with specific primary antibodies and then with a secondary antibody conjugated with horseradish peroxidase (Sigma, Germany). The primary antibodies against the *Synechocystis* PilA1 and SecY proteins were raised in rabbits using the synthetic peptide fragments containing amino acids 147–160 and 4–14 respectively. The antibody raised against the recombinant fragment Arg117-Ser384 of *Synechocystis* YidC was kindly provided by Professor Jörg Nickelsen (Ludwig-Maximilians-University, Munich, Germany). The antibody against *Synechocystis* Ycf48 was kindly provided by Professor Peter Nixon (Imperial College, UK). The Rpl1 antibody was purchased from Agrisera (Sweden). To analyse membrane protein complexes under native conditions, the isolated membranes were resuspended in buffer A, solubilized by 1% n-dodecyl-ß-maltoside and separated on 4–14% Clear-Native electrophoresis gels (CN-PAGE) as described previously (Wittig *et al.*, 2007). Approximately 1 ml of cells at OD_{750} = 1 was loaded on a CN gel. The 'in gel' chlorophyll fluorescence of the photosynthetic complexes was quantified using a LAS 4000 imager (Fuji, Japan). Individual components of the protein complexes were resolved by incubation of the gel strip from the first dimension in 2% SDS and 1% DTT for 30 min at room temperature, and then the proteins were separated in the second dimension by SDS-PAGE in a denaturing 12–20% polyacrylamide gel containing 7 M urea (Dobáková *et al.*, 2009). The proteins were stained either with Coomassie Blue or by Sypro Orange (Sigma), and in the latter case the proteins were subsequently electro-blotted onto a PVDF membrane and probed with antibodies as described above. When radiolabelled samples were analysed, the gel was dried and exposed to a Phosphorimager plate (GE Healthcare).

Co-immunoprecipitation

The membrane fraction containing 20 µg of chlorophyll was solubilized with 1% n-dodecyl-ß-maltoside and incubated with the specified antibody overnight. Immunoglobulins were bound to Protein A-Sepharose 4B (Sigma) and released using a 25 mM Tris/HCl pH 7.5 buffer containing 1 M sucrose, 1% SDS, 1% DTT, 0.05% BFB at 50°C. The eluate was immediately separated by one-dimensional 12–20% SDS-PAGE, electro-blotted onto a PVDF membrane, which was probed repeatedly with primary antibodies.

Acknowledgements

We are grateful to Professor Devaki Bhaya (Carnegie Institution for Science, Stanford, USA) and Professor Wim Vermaas (School of Life Sciences, Arizona, USA) for various mutants and Professor Jörg Nickelsen (Ludwig-Maximilians-University, Munich, Germany) and Professor Peter Nixon (Imperial College, UK) for antibodies. We thank Eva Prachová for her technical assistance. R.S. and J.K. were supported by projects Algatech and by project 14-13967S of the Grant Agency of the Czech Republic. T.J. and P.T. were supported by Operational Program Prague – Competitiveness (CZ.2.16/3.1.00/24023).

References

Arts, J., van Boxtel, R., Filloux, A., Tommassen, J., and Koster, M. (2007) Export of the pseudopilin XcpT of the *Pseudomonas aeruginosa* type II secretion system via the signal recognition particle-Sec pathway. *J Bacteriol* **189:** 2069–2076.

Arvidson, C.G., Powers, T., Walter, P., and So, M. (1999) *Neisseria gonorrhoeae* PilA Is an FtsY homolog. *J Bacteriol* **181:** 731–739.

Bardy, S.L., and Jarrell, K.F. (2003) Cleavage of preflagellins by an aspartic acid signal peptidase is essential for flagellation in the archaeon *Methanococcus voltae*. *Mol Microbiol* **50:** 1339–1347.

Bhaya, D., Bianco, N.R., Bryant, D., and Grossman, A. (2000) Type IV pilus biogenesis and motility in the cyanobacterium *Synechocystis* sp PCC6803. *Mol Microbiol* **37:** 941–951.

Bhaya, D., Takahashi, A., Shahi, P., and Grossman, A.R. (2001) Novel motility mutants of *Synechocystis* strain PCC 6803 generated by *in vitro* transposon mutagenesis. *J Bacteriol* **183:** 6140–6143.

Bode, S., Quentmeier, C.C., Liao, P.N., Hafi, N., Barros, T., Wilk, L., *et al.* (2009) On the regulation of photosynthesis by excitonic interactions between carotenoids and chlorophylls. *Proc Natl Acad Sci USA* **106:** 12311–12316.

Boy, D., and Koch, H.-G. (2009) Visualization of distinct entities of the SecYEG translocon during translocation and integration of bacterial proteins. *Mol Biol Cell* **20:** 1804–1815.

Burrows, L.L. (2012) *Pseudomonas aeruginosa* twitching motility: type IV pili in action. *Annu Rev Microbiol* **66:** 493–520.

Carbonnelle, E., Helaine, S., Nassif, X., and Pelicic, V. (2006) A systematic genetic analysis in *Neisseria meningitidis* defines the Pil proteins required for assembly, functionality, stabilization and export of type IV pili. *Mol Microbiol* **61:** 1510–1522.

Chen, I., Provvedi, R., and Dubnau, D. (2006) A macromolecular complex formed by a pilin-like protein in competent *Bacillus subtilis*. *J Biol Chem* **281:** 21720–21727.

Chidgey, J.W., Linhartová, M., Komenda, J., Jackson, P.J., Dickman, M.J., Canniffe, D.P., *et al.* (2014) A cyanobacterial chlorophyll synthase-HliD complex associates with the Ycf39 protein and the YidC/Alb3 insertase. *Plant Cell* **26:** 1267–1279.

Dalbey, R.E., and Kuhn, A. (2012) Protein traffic in Gram-

negative bacteria – how exported and secreted proteins find their way. *FEMS Microbiol Rev* **36:** 1023–1045.
Dalbey, R.E., and Wickner, W. (1985) Leader peptidase catalyzes the release of exported proteins from the outer surface of the *Escherichia coli* plasma membrane. *J Biol Chem* **260:** 15925–15931.
Dobáková, M., Sobotka, R., Tichý, M., and Komenda, J. (2009) Psb28 protein is involved in the biogenesis of the photosystem II inner antenna CP47 (PsbB) in the cyanobacterium *Synechocystis* sp PCC 6803. *Plant Physiol* **149:** 1076–1086.
Francetic, O., Buddelmeijer, N., Lewenza, S., Kumamoto, C.A., and Pugsley, A.P. (2007) Signal recognition particle-dependent inner membrane targeting of the PulG pseudopilin component of a type II secretion system. *J Bacteriol* **189:** 1783–1793.
Giltner, C.L., Nguyen, Y., and Burrows, L.L. (2012) Type IV pilin proteins: versatile molecular modules. *Microbiol Mol Biol Rev* **76:** 740–772.
Gouridis, G., Karamanou, S., Gelis, I., Kalodimos, C.G., and Economou, A. (2009) Signal peptides are allosteric activators of the protein translocase. *Nature* **462:** 363–367.
He, Q., and Vermaas, W. (1999) Genetic deletion of proteins resembling Type IV pilins in *Synechocystis* sp. PCC 6803: their role in binding or transfer of newly synthesized chlorophyll. *Plant Mol Biol* **39:** 1175–1188.
Hernandez-Prieto, M.A., Tibiletti, T., Abasova, L., Kirilovsky, D., Vass, I., and Funk, C. (2011) The small CAB-like proteins of the cyanobacterium *Synechocystis* sp PCC 6803: their involvement in chlorophyll biogenesis for Photosystem II. *Biochim Biophys Acta* **1807:** 1143–1151.
Herranen, M., Battchikova, N., Zhang, P.P., Graf, A., Sirpio, S., Paakkarinen, V., *et al.* (2004) Towards functional proteomics of membrane protein complexes in *Synechocystis* sp PCC 6803. *Plant Physiol* **134:** 470–481.
Herskovits, A.A., Shimoni, E., Minsky, A., and Bibi, E. (2002) Accumulation of endoplasmic membranes and novel membrane-bound ribosome-signal recognition particle receptor complexes in *Escherichia coli*. *J Cell Biol* **159:** 403–410.
Holt, N.E., Zigmantas, D., Valkunas, L., Li, X.P., Niyogi, K.K., and Fleming, G.R. (2005) Carotenoid cation formation and the regulation of photosynthetic light harvesting. *Science* **307:** 433–436.
Josefsson, L.-G., and Randall, L.L. (1981) Different exported proteins in *E. coli* show differences in the temporal mode of processing *in vivo*. *Cell* **25:** 151–157.
Kamei, A., Yuasa, T., Orikawa, K., Geng, X.X., and Ikeuchi, M. (2001) A eukaryotic-type protein kinase, SpkA, is required for normal motility of the unicellular cyanobacterium *Synechocystis* sp. strain PCC 6803. *J Bacteriol* **183:** 1505–1510.
Kim, Y.H., Park, Y.M., Kim, S.J., Park, Y.I., Choi, J.S., and Chung, Y.H. (2004) The role of Slr1443 in pilus biogenesis in *Synechocystis* sp. PCC 6803: involvement in post-translational modification of pilins. *Biochem Biophys Res Commun* **315:** 179–186.
Kim, Y.H., Kim, J.Y., Kim, S.Y., Lee, J.H., Lee, J.S., Chung, Y.H., *et al.* (2009) Alteration in the glycan pattern of pilin in a nonmotile mutant of *Synechocystis* sp. PCC 6803. *Proteomics* **9:** 1075–1086.
Knoll, A.H. (2008) Cyanobacteria and earth history. In *The Cyanobacteria – Molecular Biology, Genomics and Evolution*. Herrero, A., and Flores, E. (eds). Norfolk: Caister Academic Press, pp. 1–19.
Knoppová, J., Sobotka, R., Tichý, M., Yu, J., Konik, P., Halada, P., *et al.* (2014) Discovery of a chlorophyll binding protein complex involved in the early steps of photosystem II assembly in *Synechocystis*. *Plant Cell* **26:** 1200–1212.
Komenda, J., Tichý, M., Prášil, O., Knoppová, J., Kuviková, S., de Vries, R., *et al.* (2007) The exposed N-terminal tail of the D1 subunit is required for rapid D1 degradation during photosystem II repair in *Synechocystis* sp PCC 6803. *Plant Cell* **19:** 2839–2854.
Komenda, J., Sobotka, R., and Nixon, P.J. (2012) Assembling and maintaining the Photosystem II complex in chloroplasts and cyanobacteria. *Curr Opin Plant Biol* **15:** 245–251.
Kopečná, J., Komenda, J., Bučinská, L., and Sobotka, R. (2012) Long-term acclimation of the cyanobacterium *Synechocystis* sp PCC 6803 to high light is accompanied by an enhanced production of chlorophyll that is preferentially channeled to trimeric photosystem I. *Plant Physiol* **160:** 2239–2250.
Kopečná, J., Sobotka, R., and Komenda, J. (2013) Inhibition of chlorophyll biosynthesis at the protochlorophyllide reduction step results in the parallel depletion of Photosystem I and Photosystem II in the cyanobacterium *Synechocystis* PCC 6803. *Planta* **237:** 497–508.
Li, X., Dang, S., Yan, C., Gong, X., Wang, J., and Shi, Y. (2013) Structure of a presenilin family intramembrane aspartate protease. *Nature* **493:** 56–61.
Marsh, J.W., and Taylor, R.K. (1998) Identification of the *Vibrio cholerae* type 4 prepilin peptidase required for cholera toxin secretion and pilus formation. *Mol Microbiol* **29:** 1481–1492.
Motohashi, K., Kondoh, A., Stumpp, M.T., and Hisabori, T. (2001) Comprehensive survey of proteins targeted by chloroplast thioredoxin. *Proc Natl Acad Sci USA* **98:** 11224–11229.
Mulkidjanian, A.Y., Koonin, E.V., Makarova, K.S., Mekhedov, S.L., Sorokin, A., Wolf, Y.I., *et al.* (2006) The cyanobacterial genome core and the origin of photosynthesis. *Proc Natl Acad Sci USA* **103:** 13126–13131.
Muller, M.G., Lambrev, P., Reus, M., Wientjes, E., Croce, R., and Holzwarth, A.R. (2010) Singlet energy dissipation in the photosystem II light-harvesting complex does not involve energy transfer to carotenoids. *Chemphyschem* **11:** 1289–1296.
Nickelsen, J., and Rengstl, B. (2013) Photosystem II assembly: from cyanobacteria to plants. *Annu Rev Plant Biol* **64:** 609–635.
Park, E., Menetret, J.F., Gumbart, J.C., Ludtke, S.J., Li, W., Whynot, A., *et al.* (2014) Structure of the SecY channel during initiation of protein translocation. *Nature* **506:** 102–106.
Pepe, J.C., and Lory, S. (1998) Amino acid substitutions in PilD, a bifunctional enzyme of *Pseudomonas aeruginosa*: effect on leader peptidase and n-methyltransferase activities *in vitro* and *in vivo*. *J Biol Chem* **273:** 19120–19129.
Porra, R.J., Thompson, W.A., and Kriedemann, P.E. (1989) Determination of accurate extinction coefficients and simul-

taneous equations for assaying chlorophylls a and b extracted with four different solvents: verification of the concentration of chlorophyll standards by atomic absorption spectroscopy. *Biochim Biophys Acta* **975:** 384–394.
Rengstl, B., Knoppová, J., Komenda, J., and Nickelsen, J. (2013) Characterization of a *Synechocystis* double mutant lacking the photosystem II assembly factors YCF48 and Sll0933. *Planta* **237:** 471–480.
Rexroth, S., Mullineaux, C.W., Ellinger, D., Sendtko, E., Rogner, M., and Koenig, F. (2011) The plasma membrane of the cyanobacterium *Gloeobacter violaceus* contains segregated bioenergetic domains. *Plant Cell* **23:** 2379–2390.
Sachelaru, I., Petriman, N.A., Kudva, R., Kuhn, P., Welte, T., Knapp, B., *et al*. (2013) YidC occupies the lateral gate of the SecYEG translocon and is sequentially displaced by a nascent membrane protein. *J Biol Chem* **288:** 16295–16307.
Saller, M.J., Fusetti, F., and Driessen, A.J. (2009) *Bacillus subtilis* SpoIIIJ and YqjG function in membrane protein biogenesis. *J Bacteriol* **191:** 6749–6757.
Scotti, P.A., Urbanus, M.L., Brunner, J., de Gier, J.W., von Heijne, G., van der Does, C., *et al*. (2000) YidC, the *Escherichia coli* homologue of mitochondrial Oxa1p, is a component of the Sec translocase. *EMBO J* **19:** 542–549.
Simon, S.M., and Blobel, G. (1992) Signal peptides open protein-conducting channels in *E. coli*. *Cell* **69:** 677–684.
Sinha, R.K., Komenda, J., Knoppová, J., Sedlářová, M., and Pospíšil, P. (2012) Small CAB-like proteins prevent formation of singlet oxygen in the damaged photosystem II complex of the cyanobacterium *Synechocystis* sp PCC 6803. *Plant Cell Environ* **35:** 806–818.
Sobotka, R. (2014) Making proteins green; biosynthesis of chlorophyll-binding proteins in cyanobacteria. *Photosynth Res* **119:** 223–232.
Spence, E., Bailey, S., Nenninger, A., Moller, S.G., and Robinson, C. (2004) A homolog of Albino3/Oxal is essential for thylakoid biogenesis in the cyanobacterium *Synechocystis* sp. PCC6803. *J Biol Chem* **279:** 55792–55800.
van Stelten, J., Silva, F., Belin, D., and Silhavy, T.J. (2009) Effects of antibiotics and a proto-oncogene homolog on destruction of protein translocator SecY. *Science* **325:** 753–756.
Takhar, H.K., Kemp, K., Kim, M., Howell, P.L., and Burrows, L.L. (2013) The platform protein is essential for type IV pilus biogenesis. *J Biol Chem* **288:** 9721–9728.
Tammam, S., Sampaleanu, L.M., Koo, J., Manoharan, K., Daubaras, M., Burrows, L.L., *et al*. (2013) PilMNOPQ from the *Pseudomonas aeruginosa* type IV pilus system form a transenvelope protein interaction network that interacts with PilA. *J Bacteriol* **195:** 2126–2135.
Tjalsma, H., Bolhuis, A., van Roosmalen, M.L., Wiegert, T., Schumann, W., Broekhuizen, C.P., *et al*. (1998) Functional analysis of the secretory precursor processing machinery of *Bacillus subtilis*: identification of a eubacterial homolog of archaeal and eukaryotic signal peptidases. *Genes Dev* **12:** 2318–2331.
Trautmann, D., Voss, B., Wilde, A., Al-Babili, S., and Hess, W.R. (2012) Microevolution in *Cyanobacteria*: re-sequencing a motile substrain of *Synechocystis* sp. PCC 6803. *DNA Res* **19:** 435–448.
Wittig, I., Karas, M., and Schagger, H. (2007) High resolution clear native electrophoresis for in-gel functional assays and fluorescence studies of membrane protein complexes. *Mol Cell Proteomics* **6:** 1215–1225.
Yoshihara, S., Geng, X., Okamoto, S., Yura, K., Murata, T., Go, M., *et al*. (2001) Mutational analysis of genes involved in pilus structure, motilityand transformation competency in the unicellular motile cyanobacterium *Synechocystis* sp. PCC6803. *Plant Cell Physiol* **42:** 63–73.
Zhu, L., Wasey, A., White, S.H., and Dalbey, R.E. (2013) Charge composition features of model single-span membrane proteins that determine selection of YidC and SecYEG translocase pathways in *Escherichia coli*. *J Biol Chem* **288:** 7704–7716.

Supporting information

Additional supporting information may be found in the online version of this article at the publisher's web-site.

9.2 Publication II: A cyanobacterial chlorophyll synthase-HliD complex associates with the Ycf39 protein and the YidC/Alb3 insertase.

Chidgey, J.W., Linhartová, M., Komenda, J., Jackson, P.J., Dickman, M.J., Canniffe, D.P., Koník, P., Pilný, J., Hunter, C.N., and Sobotka, R. (2014).
Plant Cell 26: 1267-1279.

The Plant Cell, Vol. 26: 1267 1279, March 2014, www.plantcell.org

A Cyanobacterial Chlorophyll Synthase-HliD Complex Associates with the Ycf39 Protein and the YidC/Alb3 Insertase[W][OPEN]

Jack W. Chidgey,[a,1] Markéta Linhartová,[b,c,1] Josef Komenda,[b,c] Philip J. Jackson,[a,d] Mark J. Dickman,[d] Daniel P. Canniffe,[a] Peter Koník,[c] Jan Pilný,[b] C. Neil Hunter,[a,2] and Roman Sobotka[b,c]

[a] Department of Molecular Biology and Biotechnology, University of Sheffield, Sheffield S10 2TN, United Kingdom
[b] Institute of Microbiology, Academy of Sciences, 37981 Třeboň, Czech Republic
[c] Faculty of Sciences, University of South Bohemia, 370 05 České Budějovice, Czech Republic
[d] ChELSI Institute, Department of Chemical and Biological Engineering, University of Sheffield, Sheffield S1 3JD, United Kingdom

Macromolecular membrane assemblies of chlorophyll-protein complexes efficiently harvest and trap light energy for photosynthesis. To investigate the delivery of chlorophylls to the newly synthesized photosystem apoproteins, a terminal enzyme of chlorophyll biosynthesis, chlorophyll synthase (ChlG), was tagged in the cyanobacterium Synechocystis PCC 6803 (Synechocystis) and used as bait in pull-down experiments. We retrieved an enzymatically active complex comprising ChlG and the high-light-inducible protein HliD, which associates with the Ycf39 protein, a putative assembly factor for photosystem II, and with the YidC/Alb3 insertase. 2D electrophoresis and immunoblotting also provided evidence for the presence of SecY and ribosome subunits. The isolated complex contained chlorophyll, chlorophyllide, and carotenoid pigments. Deletion of hliD elevated the level of the ChlG substrate, chlorophyllide, more than 6-fold; HliD is apparently required for assembly of FLAG-ChlG into larger complexes with other proteins such as Ycf39. These data reveal a link between chlorophyll biosynthesis and the Sec/YidC-dependent cotranslational insertion of nascent photosystem polypeptides into membranes. We expect that this close physical linkage coordinates the arrival of pigments and nascent apoproteins to produce photosynthetic pigment-protein complexes with minimal risk of accumulating phototoxic unbound chlorophylls.

INTRODUCTION

The photosystem I (PSI) and photosystem II (PSII) chlorophyll-protein complexes of cyanobacteria and plants absorb solar energy and use it for charge separation, which drives downstream processes such as NADPH formation and ATP synthesis. The structures of these complexes (Jordan et al., 2001; Umena et al., 2011) show how chlorophyll molecules are arranged to optimize the absorption of light and efficient energy transfer to the reaction center chlorophylls that act as primary electron donors (Renger and Schlodder, 2011). The biogenesis of PSI and PSII must involve close interplay between enzymes of the chlorophyll biosynthesis pathway and the machinery for synthesis and membrane insertion of the photosystem apoproteins. In vivo and in vitro studies provide circumstantial evidence for such a linkage, suggesting that chlorophyll has to be inserted into proteins cotranslationally, probably as a prerequisite for correct protein folding and for the stable incorporation of chlorophyll protein into membranes (Chua et al., 1976; Eichacker et al., 1996; Müller and Eichacker, 1999). As demonstrated using the DchlL mutant of the cyanobacterium Synechocystis PCC 6803 (hereafter, Synechocystis), which is unable to synthesize chlorophyll in the dark, the availability of de novo chlorophyll molecules is essential for the synthesis of all cyanobacterial chlorophyll proteins (Kopečná et al., 2013). By contrast, the absence of the carotenoid cofactor b-carotene has little effect on the synthesis of the PSI in Synechocystis, and although synthesis of PSII proteins is impaired, this complex nevertheless accumulates to some extent in the b-carotene-less mutant (Sozer et al., 2010).

A physical linkage between pigment and protein biosynthesis components is likely to be a prerequisite for tight mechanistic coupling between the production of chlorophylls and their attachment to nascent apoproteins, ensuring that there are no deleterious effects arising from unattached, phototoxic chlorophylls, such as the formation of destructive radical oxygen species (Apel and Hirt, 2004). Although there are reports of putative protein factors providing a connection between chlorophyll biosynthesis and PSII biogenesis (Dobáková et al., 2009; Schottkowski et al., 2009), the mechanisms that couple chlorophyll and protein biosynthesis remain unclear. The enzymes involved in the later steps of chlorophyll biosynthesis are considered to be associated with membranes (Masuda and Fujita, 2008), but chlorophyll synthase (ChlG), which attaches the phytol/geranylgeraniol tail to the chlorophyllide (Chlide) macrocycle, is known to be an intrinsic membrane protein (Addlesee et al., 2000). Given that the main chlorophyll binding subunits of

[1] These authors contributed equally to this work.
[2] Address correspondence to c.n.hunter sheffield.ac.uk.
The authors responsible for distribution of materials integral to the findings presented in this article in accordance with the policy described in the Instructions for Authors (www.plantcell.org) are: C. Neil Hunter (c.n.hunter sheffield.ac.uk) and Roman Sobotka (sobotka alga.cz).
[W] Online version contains Web-only data.
[OPEN] Articles can be viewed online without a subscription.
www.plantcell.org/cgi/doi/10.1105/tpc.114.124495

PSI (PsaA and PsaB) and PSII (D1, D2, CP43, and CP47) are relatively large and strongly hydrophobic transmembrane proteins synthesized on membrane-bound ribosomes, the use of ChlG in pull-down assays is a promising strategy to test the idea that this terminal enzyme of chlorophyll biosynthesis is closely associated with the protein synthesis/insertion machinery for the cotranslational attachment of chlorophylls to nascent photosystem apoproteins.

Here, we purified FLAG-tagged ChlG from Synechocystis as an enzymatically active pigment-protein complex. Analysis by electrophoresis, mass spectrometry (MS), gel filtration, and enzyme assay demonstrated that ChlG forms a functional complex with the high-light-inducible protein HliD (also named ScpE) and that larger assemblies involving the Alb3/YidC insertase and the Ycf39 protein, a putative assembly factor for PSII, can be isolated. These data provide evidence for the hitherto elusive link between chlorophyll and photosystem apoprotein synthesis.

RESULTS

FLAG-Tagged ChlG Is Purified in a Complex with HliD, Ycf39, and YidC Proteins

In order to identify putative protein partners of ChlG, we constructed a Synechocystis strain expressing chlG under control of the psbAII promoter and with a 3xFLAG-tag encoded at the N terminus of ChlG; subsequently, the original chlG gene was deleted. The resulting psbAII:Flag-chlG/DchlG (hereafter, Flag-chlG) strain exhibited a wild-type pigmentation (Supplemental Figure 1), indicating that the FLAG-tagged ChlG is functional. The cellular level of FLAG-ChlG was somewhat lower than of the native ChlG (Supplemental Figure 2A) but apparently sufficient to provide chlorophyll for maintaining normal levels of photosynthetic complexes.

A membrane fraction was prepared from the photoautotrophically grown Flag-chlG strain, solubilized with 1.5 b-dodecyl

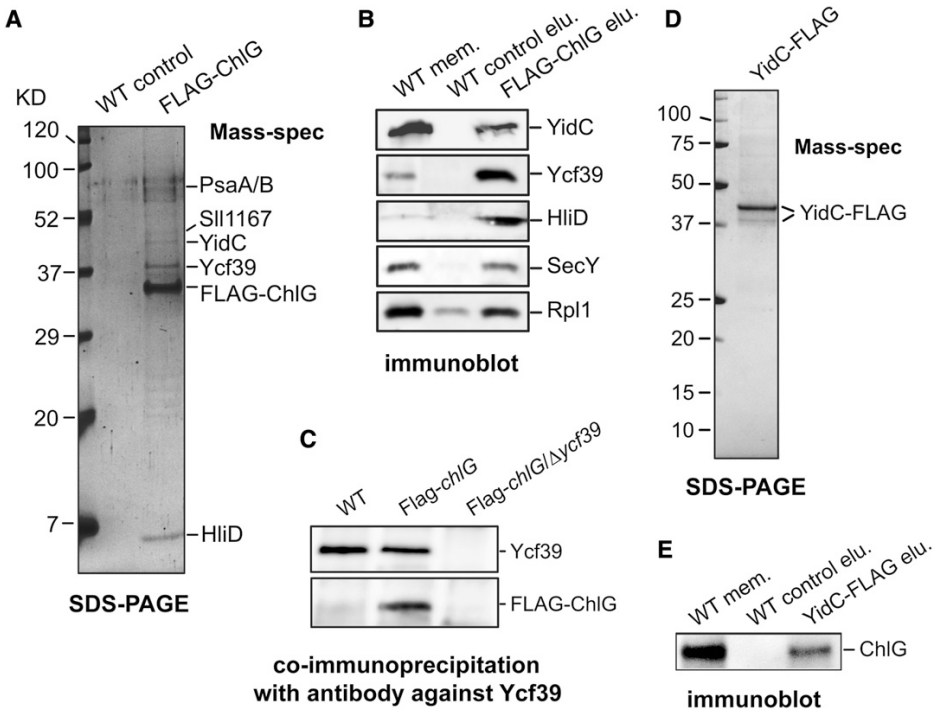

Figure 1. Purification of FLAG-ChlG and YidC-FLAG from Synechocystis Cells and Identification of Interacting Protein Partners.

(A) FLAG-ChlG was purified from the Flag-chlG strain under native conditions on the anti-FLAG affinity gel. Eluted proteins were separated by SDS-PAGE together with a control pull-down from the Synechocystis wild type and stained with Coomassie blue. The amount of protein loaded for each sample corresponded to one-tenth of the total eluate volume. Designated protein bands were identified by MS (see Supplemental Table 1 for detected peptides).

(B) Eluted proteins from the FLAG-ChlG pull-down were resolved by SDS-PAGE, transferred by immunoblot to a PVDF membrane and probed with selected antibodies.

(C) Immunoprecipitation of the Ycf39 protein by the anti-Ycf39 antibody from wild-type and Flag-ChlG strains. The FLAG-ChlG protein that co-immunoprecipitated with Ycf39 was detected by an anti-FLAG antibody.

(D) YidC-FLAG was purified from the yidC-Flag/DyidC strain and analyzed as described for FLAG-ChlG.

(E) Eluted proteins from the YidC-FLAG pull-down were resolved by SDS-PAGE, blotted, and probed with the anti-ChlG antibody.

maltoside, and the extract applied to an anti-FLAG affinity column. Following extensive washing, the eluted material was separated by SDS-PAGE (Figure 1A). The Coomassie blue stained bands were digested with trypsin and identified by MS. In addition to the FLAG-ChlG protein used as bait, we identified the Ycf39 homolog Slr0399, the Slr1471 protein belonging to the Alb3/Oxa1/YidC family (hereafter, YidC), the high-light-inducible protein HliD, the Sll1167 protein from the AmpH family, and the PsaA/B core proteins of PSI (see Supplemental Table 1 for identified peptides). Of these, SDS-PAGE of the control eluate resolved only weakly staining bands of PsaA/B (Figure 1A). Using specific antibodies, we confirmed the presence of Ycf39, YidC, and HliD in the FLAG-ChlG eluate, all of which were absent from the control pull-down (Figure 1B). In addition, we detected a specific signal for SecY for the FLAG-ChlG pull-down, as well as a signal for the Rpl1 ribosome subunit that is clearly stronger than in the control (Figure 1B). We also investigated the ChlG-Ycf39 interaction using an anti-Ycf39 antibody to immunoprecipitate Ycf39 from solubilized membrane proteins prepared from the Flag-ChlG strain; Figure 1C shows that the FLAG-ChlG protein was coimmunoprecipitated with Ycf39 from the Flag-chlG strain but not from the control Flag-chlG strain lacking Ycf39, providing further evidence for the complex between ChlG and Ycf39.

In order to confirm the association of YidC with ChlG, we constructed a yidC- Flag/DyidC strain that produced near-native amounts of the C-terminally FLAG-tagged YidC (Supplemental Figure 2B) and normal levels of photosynthetic complexes (Supplemental Figure 1). The YidC-FLAG pull-down was analyzed as for FLAG-ChlG; although the MS analysis of stained bands identified only the YidC-FLAG protein (Figure 1D), ChlG was clearly detected in the YidC-FLAG pull-down by the specific antibody (Figure 1E). Ycf39 and HliD were not detectable in this YidC-FLAG pull-down using the cognate antibodies (data not shown), consistent with the low amount of ChlG coeluted with YidC-FLAG, and shown by the lack of a Coomassie blue stained ChlG band in the gel in Figure 1D. The low ChlG content of the YidC-FLAG pull-down could arise from a weak YidC-ChlG interaction, possibly short-lived, given the transient presence of nascent protein chains within the YidC/Sec translocon. Clear-Native (CN) PAGE was used to examine the YidC-FLAG pull-down in more detail; the complexes were separated in the second dimension by SDS-PAGE (Supplemental Figure 3). Immunodetection of ChlG indicates that this protein comigrates with YidC-FLAG in specific oligomeric states confined to the lower range of YidC aggregates; the rest of the YidC population migrates as a continuum of oligomers ranging from tens to hundreds of kilodaltons in size.

The ChG-HliD Subcomplex Contains Chlorophyll, Chlide, and Carotenoids

The FLAG-ChlG eluate was green-orange in color, in contrast with the very pale-green elution from the wild-type membrane fraction control. Supplemental Figure 4A shows the very low absorption of the wild-type control and the 674-nm absorption maximum of the FLAG-ChlG eluate. The fluorescence emission spectrum recorded at 77K (Supplemental Figure 4B) resolves two emitting components; the major peak at 682 nm is expected to originate from the ChlG-HliD complex, and the 675-nm shoulder likely arises from free (dodecyl-b-maltoside bound) chlorophyll. The presence of some PSI complexes gives rise to the lower 720-nm emission peak. In order to examine the association of these pigments with the ChlG, HliD, Ycf39, and YidC components, which would imply the presence of a hitherto uncharacterized pigment-protein complex, the FLAG-ChlG eluate was concentrated ; 5-fold using a 100-kD cutoff ultrafilter and analyzed using CN-PAGE. Two yellow-orange bands, CN1 and CN2, were resolved, each with a mass 100 kD as suggested from migration of the CpcA/B hexamer (107 kD) in the control lane (Figure 2A). In addition, a green band with no correspondence to any abundant chlorophyll-protein complex in Synechocystis was present in the FLAG-ChlG pull-down (Figure 2A). As this band exhibited an absorption spectrum typical for the PSI complex (Figure 2C) but it migrated more slowly than monomeric PSI, this complex was designated as PSI[1] . The green band near the top of the gel corresponded to the trimeric PSI in solubilized membranes (Figure 2A, left lane). Absorption spectra of the CN1 and CN2 bands excised from the gel showed that both bands are associated with Chl(ide) a (absorbance at 674 nm) and carotenoids (absorbance at 484 to 514 nm) (Figure 2B). The only difference between CN1 and CN2 complexes seems to be a slightly higher chlorophyll/carotenoid ratio in CN2 (Figure 2B).

Complexes resolved on CN-PAGE were further separated in the second dimension by SDS-PAGE and stained either by Coomassie blue prior to in-gel tryptic digestion and MS analysis or by Sypro Orange for blotting and immunodetection (Figure 3). The CN1 and CN2 bands both contained FLAG-ChlG and HliD, providing clear evidence for the association of this complex with pigments. However, a very faint complex above CN1 can be recognized (white dashed line, left, Figure 3) containing FLAG-ChlG, Ycf39, and Sll1167. Although YidC was not detected on the 2D gels by protein staining, immunoblotting with the anti-YidC antibody shows that it also comigrated with this faint band above CN1. FLAG-ChlG, HliD, and Sll1167 are present in the CN1 band, although not YidC (white dashed line, right, Figure 3). The CN2 band appears to consist only of FLAG-ChlG and HliD, and the fastest migrating FLAG-ChlG spot (white asterisk) was not associated with pigments and probably arose from free ChlG (Figure 3). CN/SDS-PAGE also resolved the ribosome subunits (Figure 3; Supplemental Figure 5), and the immunoblot showed that SecY was bound to the large ribosome subunit. The green PSI[1] band remained mostly stacked on the top of the resolving gel, which is a characteristic behavior of PSI complexes due to the high stability of PSI core proteins (Komenda et al., 2012b).

Gel filtration was used to further characterize the composition, molecular masses, and spectral properties of FLAG-ChlG assemblies within the FLAG-ChlG eluate. Several complexes were resolved by this method (Figure 4) with the largest one eluting in the void volume (peak GF1). The typical red shift in chlorophyll absorbance seen for the GF1 and GF2 fractions indicated that they consist mainly of PSI complexes (Supplemental Figure 6). Immunoblot analysis of the column fractions corresponding to peaks GF1-4 showed that most of the YidC and Ycf39 eluted

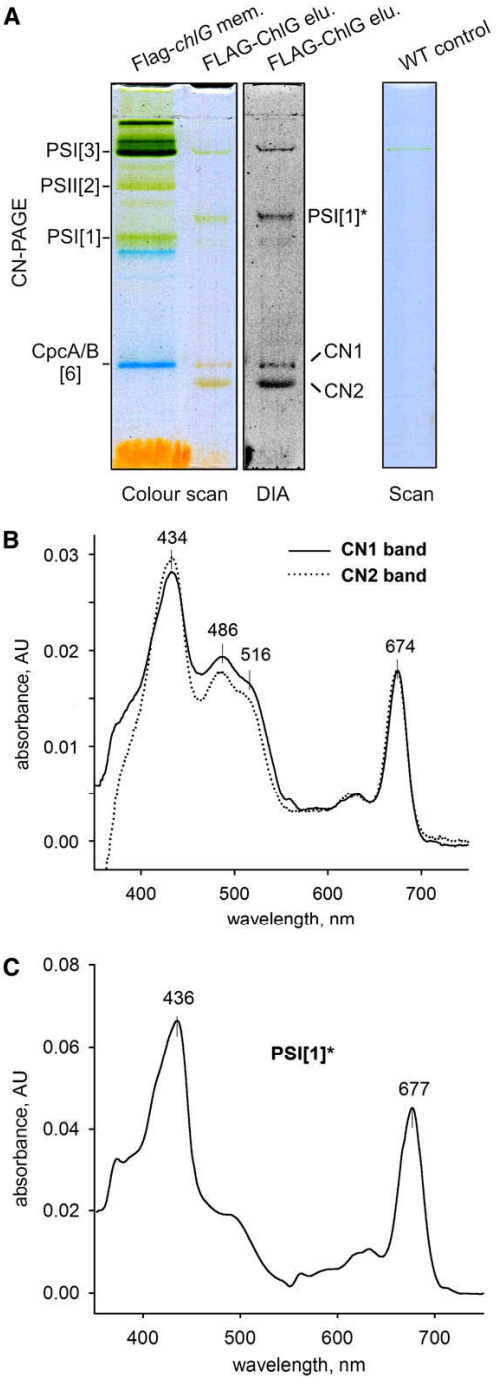

Figure 2. Separation of the Purified FLAG-ChlG Complex by CN-PAGE and Spectroscopy Analysis of Pigmented Bands.

(A) CN-PAGE of the purified FLAG-ChlG complex and a control eluate from wild-type cells, the loading of which corresponded to ; 75 of the total eluates. Solubilized membranes (3 mg of chlorophyll) from the Flag-chlG strain were used to demonstrate the mobility of photosynthetic complexes: PSI[1] and PSI[3], monomer and trimer of PSI, respectively; PSII[2], dimer of PSII; CpcA/B[6], 107-kD heterohexamer of CpcA and CpcB phycobiliproteins. After separation, the gel was scanned in color by an office scanner and in transmittance mode (DIA) using a LAS 4000 imager (Fuji). CN1, CN2, and PSI[1] mark protein complexes identified in FLAG-ChlG elution (line 2) but not in the total membrane fraction (line 1).

(B) The orange-yellow CN1 and CN2 bands were excised from the CN-PAGE gel, and absorption spectra were recorded as described in Methods. AU, absorbance units.

(C) Absorption spectra of the PSI[1] complex; the red shifted absorbance of the chlorophyll Q_y peak is typical for PSI complexes.

slightly later than peak GF1 (; 5.7 mL), whereas most of the HliD eluted either in the GF3 peak containing FLAG-ChlG or in the GF4 peak containing neither FLAG-ChlG nor Ycf39 (Figure 4). This analysis showed that YidC and Ycf39 tend to become detached from ChlG but remain in a large complex with molecular mass higher than 400 kD, although small amounts of YidC and Ycf39 retain an association with ChlG. This behavior of YidC might be related to a tendency of this protein to form high-mass oligomers (Supplemental Figure 3). HliD associated preferentially with ChlG forming a complex with an apparent molecular mass of ; 70 kD. Given the molecular masses of FLAG-ChlG and HliD, at 38.5 and 6.5 kD, respectively, the complex likely represents ChlG with several bound copies of HliD. A substantial proportion of the HliD in the eluate became detached from FLAG-ChlG and migrated as an ; 40-kD aggregate probably consisting of several copies of the protein associated with lipids, detergents, and pigments. In conclusion, gel filtration yielded a pattern of complexes somewhat different from the CN-PAGE analysis, as the FLAG-ChlG-HliD interaction was apparently less stable during this separation method, resulting in an abundant free HliD peak (GF4). On the other hand, this approach validated the conclusion derived from the 2D electrophoresis (Figure 3) showing that the FLAG-ChlG eluate consists of an abundant ChlG-HliD core and less tightly attached Ycf39/YidC components.

In order to obtain a detailed insight into the pigment composition of the FLAG-ChlG-HliD complex, we constructed another strain expressing FLAG-ChlG in a Synechocystis mutant lacking PSI due to deletion of the psaA/B operon. We purified FLAG-ChlG and then performed a gel filtration separation experiment analogous to the one described above. Elimination of PSI simplified the elution profile without affecting the ChlG-HliD complex, which eluted at 6.8 mL as before (Figure 5A). After elimination of PSI, a significant 5.8 mL elution peak was found with absorption detection at 280 nm (Figure 5A), which corresponded to the elution volume of Ycf39 and YidC in Figure 4. The absorption spectra of peaks GF3 (ChlG-HliD) and GF4 (HliD) in Figure 5B demonstrate the relatively high carotenoid content of HliD-containing fractions, particularly in the ChlG-HliD complex. We noted that the absorption spectrum of the GF3 peak was practically identical to that of the CN1 band (Figure 2B) from the native gel. The pigments in ChlG-HliD complex (GF3 peak), free of any contaminating PSI pigments, were extracted from the collected fractions

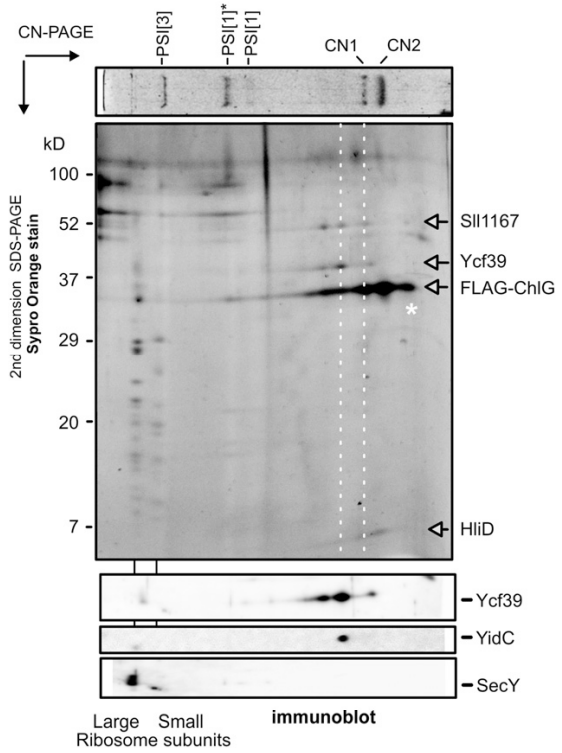

Figure 3. 2D Electrophoresis of the Purified FLAG-ChlG Complex and Identification of Individual Protein Spots.

A gel strip from CN-PAGE with separated FLAG-ChlG complexes (see Figure 2A) was further separated in a second dimension by SDS-PAGE. The gel was stained by Sypro Orange and then blotted onto a PVDF membrane. The identity of designated spots on the stained gel was assigned by MS and further verified by specific antibodies (see Results). PSI[1] is a form of monomeric PSI migrating slower than a typical PSI[1] (Figures 2A and 2D). YidC, SecY, and Ycf39 were detected using specific antibodies. For identification of individual ribosome subunits migrating close to the top of CN gel, see Supplemental Figure 5.

and analyzed by HPLC. The results (Figure 5C) showed a complex spectrum of pigments associated with the ChlG-HliD complex. In addition to chlorophyll, we also detected Chlide and three carotenoids: zeaxanthin, b-carotene, and myxoxanthophyll. The molar ratio between chlorophyll and carotenoids was estimated to be: Chl(ide) (6): zeaxanthin (3):b-carotene (1): myxoxanthophyll (1) (Figure 5C). The amount of Chlide was rather low, only reaching ; 20 of the chlorophyll level.

ChlG Activity of the Purified FLAG-ChlG Complex

Oster et al. (1997) showed that an Escherichia coli cell extract containing recombinant ChlG from Synechocystis catalyses the attachment of geranylgeraniol or phytol tails to the Chlide macrocycle. In this work, we examined the ChlG activity of purified, native ChlG preparations, initially by assaying the capacity of the FLAG-ChlG eluate to use the endogenous Chlide pool as a source of substrate. Geranylgeranyl-diphosphate was added to the FLAG-ChlG eluate, the stopped assay was terminated at various times during the 32-min time period, and then the geranylgeranyl-chlorophyll product was quantified using HPLC (Figure 6A). The data showed the concomitant increase in geranylgeranyl-chlorophyll and the decrease in Chlide, indicating that the FLAG-ChlG-HliD-Ycf39-YidC complex possesses ChlG activity and the coeluting Chlide is accessible to the ChlG. Furthermore, the subsequent addition of exogenous geranylgeranyl-diphosphate and Chlide stimulated continued ChlG activity (Figures 6B and 6C).

The HliD-Less Strain of Synechocystis Lacks ChlG Subcomplexes and Accumulates Chlide

Based on data already presented, we can conclude that a stable, active pigment binding ChlG-HliD core is integrated into larger complexes that also contain Ycf39 and YidC. In order to observe the in vivo effects of genetic removal of HliD on the composition of this complex, the hliD gene was deleted from the Flag-chlG strain. Detergent-solubilized membrane proteins from the Flag-chlG and Flag-chlG/DhliD strains were separated by 2D CN/SDS-PAGE, blotted, and probed with an anti-FLAG antibody (Figure 7A). The pattern of FLAG-ChlG spots in the case of the Flag-chlG resembled that of the separated FLAG-ChlG pull-down on CN-PAGE (Figure 3) with putative CN1 and CN2 bands (marked by asterisks in Figure 7A) and with a higher mass complex containing Ycf39 (black arrowhead in Figure 7A). By contrast, the total FLAG-ChlG signal in the DhliD sample (Figure 7A,

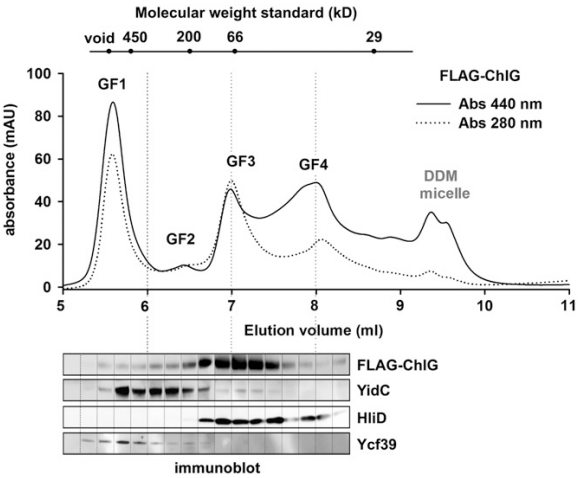

Figure 4. Separation of the Purified FLAG-ChlG Complexes by Gel Filtration Chromatography and Immunodetection of Eluted Proteins.

The FLAG-ChlG pull-down was loaded on a BioSec 3000 column, and eluted protein/complexes were detected by absorbance at 280 and 440 nm. Eluted fractions were collected and subjected to immunoblot analysis; each band corresponds to the 0.2-mL chromatograph fraction with which it is aligned. DDM, dodecyl-b-maltoside.

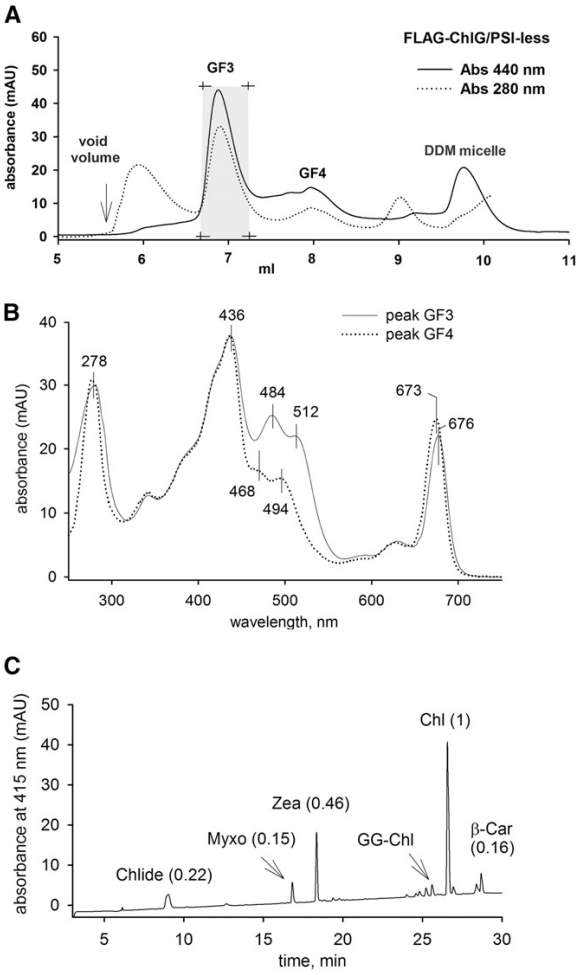

Figure 5. Analysis of Pigments Associated with the FLAG-ChlG-HliD Complex.

(A) FLAG-ChlG pull-down obtained from the PSI-less background was separated on a gel filtration column essentially as described for Figure 4 and the GF3 peak collected (gray box). DDM, dodecyl-b-maltoside.

(B) Absorption spectra of the GF3 and GF4 peaks were recorded by a HPLC diode array detector.

(C) Pigments were extracted from the pooled fractions representing the GF3 peak (gray box in [A]), separated by HPLC and detected at 415 nm. The area of each peak was integrated and the molar stoichiometry of individual pigments estimated. Myxo, myxoxanthophyll; Zea, zeaxanthin; GG-Chl, geranylgeranyl chlorophyll; b-Car, b-carotene.

bottom right-hand panel) was much weaker and rather smeared with no apparent spots. Furthermore, reprobing the immunoblot with anti-Ycf39 showed that Ycf39 was undetectable in membranes isolated from the Flag-chlG/DhliD mutant (Figure 7A, bottom right-hand panel). Despite repeated efforts, we were unable to isolate FLAG-tagged ChlG from the HliD-less strain, indicating that the protein is most probably destabilized and degraded during the isolation procedure. Thus, the inherent pigment binding capacity of ChlG could not be determined in the absence of HliD.

As different native electrophoretic systems can provide different pattern of separated complexes (Wittig et al., 2007), we repeated the analysis of Flag-chlG membranes using Blue-Native instead of CN/SDS-PAGE (Supplemental Figure 7). In this case, the pattern of FLAG-ChlG complexes detected in Flag-chlG membranes was simpler with three clearly separated signals visible in the immunoblot, and only the lowest molecular mass spot retained in the hliD mutant (Supplemental Figure 7). In contrast with separation of the same sample on CN-PAGE, Ycf39 seems to be detached from ChlG-HliD and migrates as an oligomer, consistent with a weaker association of Ycf39 with a more stable ChlG-HliD core. Interestingly, Blue-Native electrophoresis resolved a minor fraction of FLAG-ChlG that migrated close to PSII as a large, 400-kD complex that was not affected by the absence of HliD (Supplemental Figure 7, black arrows).

It is intriguing that the hliD deletion affected neither cell growth nor the accumulation of photosystems (compared with first dimension CN gel strips in Figure 7A), despite the large decrease in ChlG level, the rearrangement of its complexes and the significant decrease in the amount of Ycf39. Previously, no phenotype has been observed for the Synechocystis DhliD strain (Funk and Vermaas, 1999; He et al., 2001), although multiple deletions of Hli family members including HliD do affect chlorophyll metabolism (Xu et al., 2002). In order to identify a selective effect of hliD deletion on chlorophyll biosynthesis, we compared levels of chlorophyll precursors in the DhliD and wild-type strains (Figure 7B). Interestingly, even under moderate light intensity, the Chlide level was elevated more than 6-fold in the DhliD mutant, and there was only a very low level (10 of the wild type) of protoporphyrin IX (Figure 7B); chlorophyll biosynthesis intermediates such as protochlorophyllide were also lowered, but to a smaller extent. For comparison, we also analyzed chlorophyll biosynthesis intermediates in another mutant that lacks the HliC protein, the amino acid sequence of which is very similar to HliD (Supplemental Figure 8). No significant changes in chlorophyll precursor levels were found in this strain (Figure 7C), suggesting that the disturbances in chlorophyll biosynthesis observed in Figure 7B were specifically induced by elimination of HliD.

A reciprocal experiment assessed the effect of deleting the ycf39 gene on HliD and ChlG. We observed a significant decrease in the HliD level in the Dycf39 strain and elevated levels of ChlG (Figure 8). Levels of chlorophyll precursors were not perturbed by elimination of the Ycf39 protein (data not shown). We conclude that the absence of Ycf39 has a negative impact on synthesis/stability of HliD and that HliD is important for accumulation of both Ycf39 and ChlG in the cell and for maintaining low levels of Chlide.

DISCUSSION

The BchG/ChlG (bacterio)chlorophyll synthases are integral membrane proteins that attach the geranylgeraniol tail to the

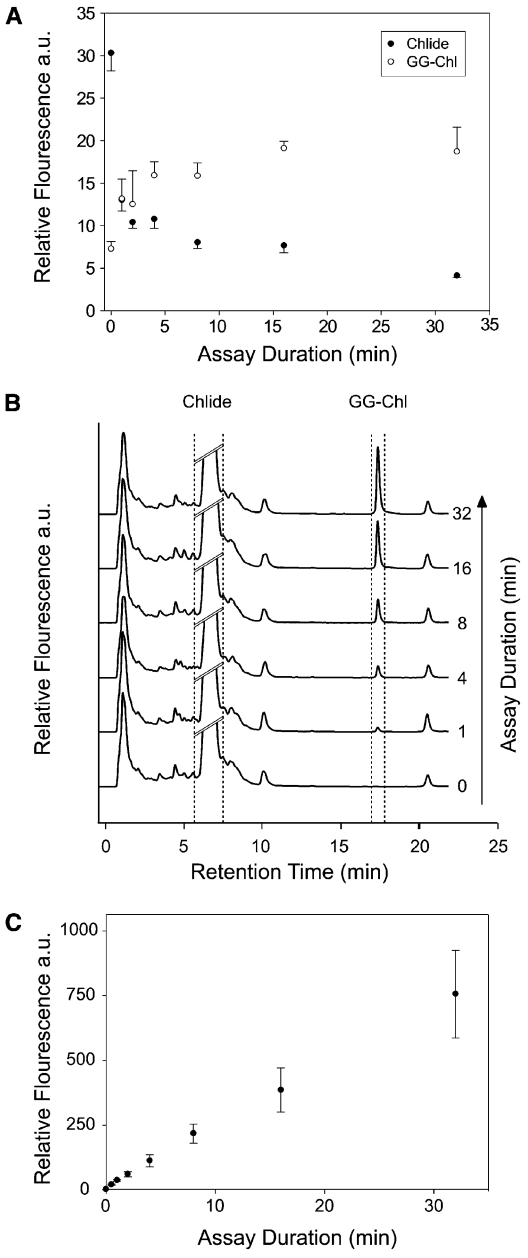

Figure 6. ChlG Activity of the Purified FLAG-ChlG Complex.

(A) Conversion of the endogenous Chlide pool and exogenous Chlide to geranylgeranyl-chlorophyll (GG-Chl). Stopped assays were performed in the presence of 20 mM geranylgeranyl diphosphate. Assays were performed in triplicate and each time point was analyzed by reverse-phase HPLC.

(B) Utilization of exogenously added Chlide by FLAG-ChlG. Assays were performed as in (A) but with the addition of 20 mM Chlide. Each chromatography trace is representative of one of three replicates.

(C) Evolution of the geranylgeranyl-chlorophyll product in the exogenous Chlide assays in (B).

(bacterio)chlorophyll macrocycle (Oster et al., 1997), a process that increases the hydrophobicity of (bacterio)chlorophyll pigments and commits them to insertion within the many binding sites within the photosystem apoproteins. Given that photosystem formation requires a supply of chlorophylls, which must be tightly synchronized with synthesis of nascent apoproteins to avoid accumulation of unused pigments, it was reasonable to hypothesize that the (bacterio)chlorophyll synthases are in close proximity to the protein synthesis/insertion/assembly apparatus for the photosystem biogenesis. Such a close connection between biosynthetic components would minimize the time for pigment transfer from the synthase to the translocon channel containing nascent polypeptides and therefore reduce the risk of photooxidative damage to chlorophylls and their surroundings. One way to establish a fully concerted biosynthetic/assembly mechanism would involve a protein supercomplex comprising ChlG and translocon components, as recently suggested (Sobotka, 2014). Here, we used the Synechocystis ChlG as bait in pull-down experiments to show that the ChlG forms a relatively stable pigment-protein complex primarily with HliD, a member of CAB-like protein family. More loosely attached are Ycf39, a member of short chain dehydrogenases (Kallberg et al., 2002), and the YidC insertase. Nevertheless, both proteins remain attached to ChlG-HliD during membrane solubilization, affinity chromatography on the anti-FLAG column, and CN-PAGE (Figure 3). Although YidC, as a general insertase, is probably involved in the synthesis of ChlG, it is very unlikely that miniscule amounts of nascent FLAG-ChlG would pull down enough of the YidC involved in ChlG assembly to be detectable by Coomassie blue staining (Figure 1A). We show that FLAG-tagged YidC migrates in CN/SDS-PAGE as a series of oligomers, with a subpopulation of smaller assemblies associating with ChlG (Supplemental Figure 3). There is therefore strong experimental support for indirect association of ChlG, HliD, and YidC with the SecY translocase and ribosome subunits, forming a continuous link from chlorophyll biosynthesis to cotranslational insertion of nascent photosystem polypeptides and their folding and assembly to form functional photosystems.

The HliD Component

HliD is a small, one-helix protein belonging to the high-light-induced protein (Hlip) family that shares a significant sequence similarity to plant chlorophyll a/b binding proteins and possesses a highly conserved chlorophyll binding (CAB) motif (Supplemental Figure 8). Genes encoding Hlips are common in cyanobacterial genomes and are strongly expressed under various stress conditions (Bhaya et al., 2002). The Synechocystis chromosome encodes four small Hlip members called HliA-D, and another Hlip is fused with ferrochelatase as a C-terminal CAB domain, which is a typical feature of cyanobacterial and chloroplast ferrochelatases (Sobotka et al., 2011). A Synechocystis mutant lacking all five Hlips is photosensitive and has markedly reduced levels of chlorophyll and all major carotenoids (Xu et al., 2004). Individual Hlips seem to fulfill distinct although overlapping roles, which is reflected in their different patterns of regulation (He et al., 2001). Deletion of the ferrochelatase CAB domain resulted in an aberrant accumulation

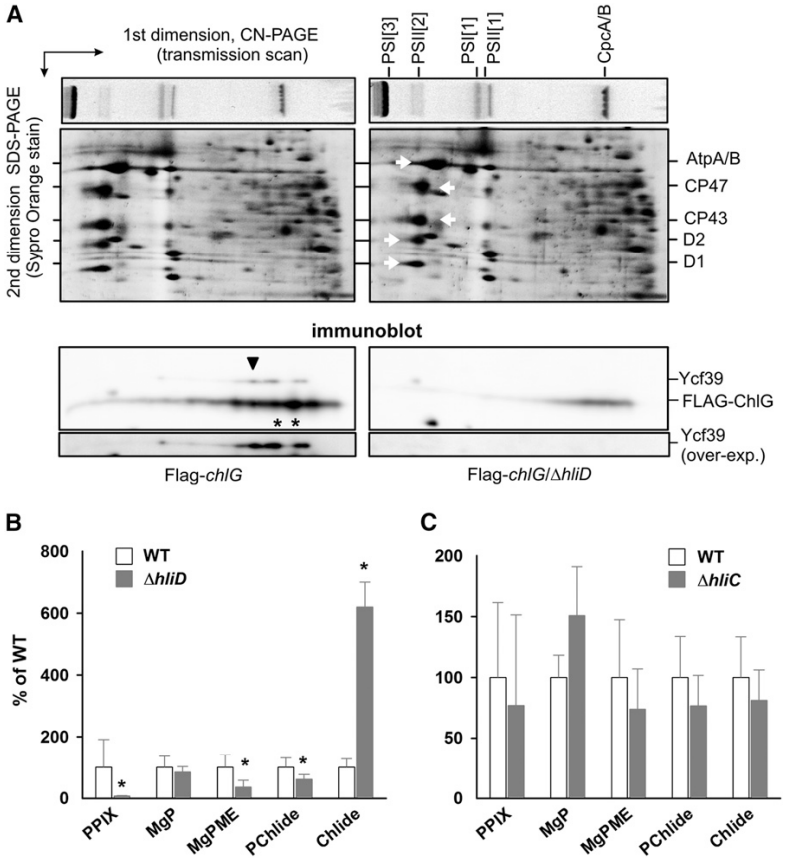

Figure 7. Characterization of Synechocystis DhliD Strains.

(A) Deletion of the hliD gene affects abundance of FLAG-ChlG and Ycf39 proteins as well as the formation of higher mass FLAG-ChlG complexes in the membrane. Membrane fractions isolated from the Synechocystis Flag-chlG (left) and Flag-chlG/DhliD (right) strains were separated by 2D CN/SDS-PAGE, stained by Sypro Orange, and finally blotted onto a PVDF membrane. Only the part of the SDS gel between ; 25 and ; 70 kD is presented; spots representing PSII core subunits and AtpA/B proteins are marked by white arrows. FLAG-ChlG and Ycf39 were detected by anti-FLAG and anti-Ycf39 antibodies, respectively. Black asterisks indicate the positions of the CN1 and CN2 bands (see Figure 3); the black arrowhead indicates a putative complex between FLAG-ChlG and Ycf39. In the lowest immunoblot panel, the Ycf39 signal was overexposed.

(B) Analysis of chlorophyll precursors in the wild-type and DhliD strains grown photoautotrophically at 40 mmol of photons m^{-2} s^{-1}. Precursors were extracted with 70 methanol from cells at OD_{750} 0.4 and analyzed by HPLC equipped with a diode array detector and a pair of fluorescence detectors (Hollingshead et al., 2012). PPIX, protoporphyrin IX; MgP, Mg-protoporphyrin IX; MgPME, Mg-protoporphyrin IX monomethylester; PChlide, protochlorophyllide. Values shown represent means 6 SD from three independent measurements. Asterisks indicate statistically significant differences in precursor levels as tested using a paired t test (P 0.05).

(C) An identical measurement of chlorophyll precursors as in (B) performed on the DhliC strain.

of chlorophyll-protein complexes under high light, a phenotype not observed for other Hlip mutants (Sobotka et al., 2011). HliA, HliB, and HliC were found to interact with the PSII subunit CP47, likely to photoprotect the PSII assembly machinery and stabilize chlorophylls released during the process of PSII repair (Promnares et al., 2006; Yao et al., 2007). In contrast, HliD does not colocalize with PSII (Yao et al., 2007) but rather, as shown in this work, HliD copurifies with FLAG-ChlG (Figure 1). A distinct role for HliD is in line with our finding that the hliD null mutant, but not a hliC mutant, accumulates Chlide under nonstress conditions, and this accumulation is accompanied by significantly lowered levels of precursors earlier in the chlorophyll pathway (Figure 7). The observed disturbance of the whole tetrapyrrole pathway in the hliD mutant is consistent with previous analyses of Hlip-less Synechocystis strains that exhibit impaired synthesis of chlorophyll proteins due to a chlorophyll deficiency (Hernandez-Prieto et al., 2011; Yao et al., 2012).

The increased pool of Chlide could be the consequence of lowered ChlG activity but could also arise from a defect in chlorophyll recycling. The half-life of chlorophyll in Synechocystis is

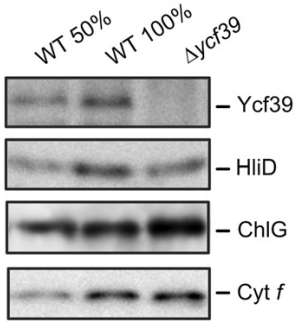

Figure 8. Immunodetection of HliD and ChlG in the Synechocystis Dycf39 Strain.

Membrane fractions prepared from wild-type and Dycf39 strains were separated by SDS-PAGE and blotted, and the HliD and ChlG proteins were detected by specific antibodies. The level of cytochrome f detected though its peroxidase activity was included as a loading control.

much shorter when all Hlips are deleted (Yao et al., 2012) and Chlide was demonstrated to be an intermediate of chlorophyll reutilization (Vavilin et al., 2005). How exactly Hlips assist the process of chlorophyll recycling is not known; however, our data show that the ChlG-HliD complex binds chlorophyll, carotenoids, and Chlide, possibly released from degraded chlorophyll-proteins in the vicinity of ChlG. This complex is enzymatically active and is able to convert its endogenous Chlide pool, as well as exogenous Chlide, to chlorophyll in the presence of added geranylgeranyl-diphosphate (Figure 6). Thus, we suggest that Chlide could be channeled to HliD from degraded proteins, perhaps via a network of other Hlips, then phytylated by ChlG in its HliD-bound state prior to loading into apoproteins. Associated carotenoids would operate as energy scavengers to prevent formation of oxygen radicals following excitation of Chl(ide). The total carotenoid to Chl (ide) ratio found in the FLAG-ChlG-HliD complex is relatively high (; 1:1), and the unexpected presence of three different carotenoids (Figure 5C) suggests that carotenoids play an important protective role during chlorophyll phytolation. It is noteworthy that the absorption spectrum of FLAG-ChlG-HliD suggests a higher carotenoid content in comparison with the putative HliD oligomer detected as peak GF4 (Figure 5B), indicating that some carotenoid(s) might be located at the interface between ChlG and HliD, but this requires further study. Although HliD is not essential for ChlG activity, its absence decreased the cellular ChlG level, and this protein is needed for assembly of FLAG-ChlG into larger complexes with other proteins such as Ycf39 (Figure 7A).

Similar molecular mechanisms are expected to underpin the synthesis of chlorophyll-proteins in cyanobacteria and chloroplasts. Plants are likely to contain a ChlG associated with a light-harvesting complex (LHC)-like protein resembling HliD. The situation in plants is made more complex by the presence of broader spectrum of LHC-like proteins, which includes single-helix (OHP), double-helix (SEP and LIL), and triple-helix (ELIP) proteins. However, strong evidence already exists that implicates plant LHC-like proteins in chlorophyll biosynthesis; overexpression of the Arabidopsis thaliana ELIP2 gene reduced the levels of chlorophyll precursors and chlorophyll-protein complexes (Tzvetkova-Chevolleau et al., 2007), and LIL3, which physically interacts with geranylgeranyl reductase, is critical for the accumulation of this enzyme in the chloroplast (Tanaka et al., 2010). Geranylgeranyl reductase cooperates with ChlG for chlorophyll phytolation (Rüdiger et al., 2005) and so the association of terminal enzymes of the chlorophyll pathway with HLIPs/LHC-like proteins might be a common theme.

The YidC Component

YidC (Slr1471), which belongs to the evolutionarily conserved YidC/Oxa1/Alb3 protein family involved in biogenesis of membrane proteins in bacteria, mitochondria, and chloroplasts, is thought to be involved in assisting partitioning of transmembrane segments into the lipid bilayer and folding of nascent membrane proteins (Beck et al., 2001; Nagamori et al., 2004). In E. coli, YidC binds to the SecY component of the SecYEG protein conducting channel, where nascent transmembrane segments laterally escape the translocon (Sachelaru et al., 2013). The critical role of YidC/Alb3 for biogenesis of cyanobacterial and plant thylakoid membranes is well documented (Spence et al., 2004; Göhre et al., 2006). Replacement of YidC with YidC-GFP in Synechocystis resulted in a photosensitive strain accumulating only limited amounts of both photosystems (Ossenbühl et al., 2006). Like the bacterial YidC, the chloroplast Alb3 associates with the SecY translocase (Klostermann et al., 2002), and in a current model, the core photosystem subunits are synthesized on Sec translocon associated with YidC/Alb3 (Sobotka, 2014). Moreover, various techniques have revealed the interaction between Alb3 and chlorophyll binding proteins (Pasch et al., 2005; Göhre et al., 2006). However, the interaction between SecY and YidC is relatively weak (Scotti et al., 2000) and dynamically responds to the binding of ribosomes (Sachelaru et al., 2013), which might explain why SecY is detectable in the FLAG-ChlG pull-down only using antibodies and not by MS or protein staining as with YidC (Figure 1).

Regarding the foldase activity of YidC (Nagamori et al., 2004), we expect that the YidC/Alb3 assists chlorophyll loading into nascent apoproteins. Interestingly, ribosomal pausing occurs at distinct sites during the elongation of the D1 subunit of PSII, and this pausing seems to be intimately associated with chlorophyll binding (Kim et al., 1994). It is tempting to speculate that the YidC/Alb3 fixes growing polypeptides in a series of programmed configurations amenable for chlorophyll insertion and that ribosome pausing provides the time for attachment of chlorophyll molecules, provided by nearby ChlG. In this context, it is noteworthy that the posttranslational targeting of LHCs into chloroplast membranes is mediated by Alb3 alone with no assistance from the Sec translocon (Moore et al., 2003). Since pigments are loaded into LHCs very probably during integration into the membrane, it is reasonable to expect that the posttranslational insertion of chlorophyll into LHCs is also mediated by an Alb3-ChlG complex.

Our model of a ChlG-HliD complex physically associated with YidC/Sec translocon is in line with accumulating evidence that the translocon machinery can be extended by various factors

involved in postprocessing of the translocated polypeptide. In the endoplasmic reticulum, oligosaccharyl transferase and signal peptidase are components of the translocon (Rapoport, 2007). The bacterial translocon was shown to interact with chaperones such as PpiD (Antonoaea et al., 2008) and with FtsH proteases ensuring quality control of translated proteins or the integrity of translocon itself (van Bloois et al., 2008). It appears that, in addition to its role for protein translocation, the SecYEG/YidC core serves as a platform for accessory proteins devoted to nascent protein modification, cofactor binding, or early steps of complex assembly. We show that whereas ChlG interacts with HliD, Ycf39, and YidC, tagged YidC retrieves only low levels of ChlG, reflecting a possibly transient interaction between these proteins and a wider role for YidC as part of a translocon for many types of membrane complex insertion and assembly. The existence of an extensive machinery for membrane integration, cofactor attachment, and protein folding is consistent with the proposed biogenesis center (Stengel et al., 2012), speculated to be responsible for the early steps of PSII assembly in cyanobacteria (Komenda et al., 2012a). The monomeric PSI[1] complex, which seems to specifically coelute with FLAG-ChlG (Figures 1 and 2), could be another structural and functional component of the biogenesis center. We can only speculate that the PSI[1] complex could serve as a scaffold for some other components or/and as an efficient energy scavenger.

The Ycf39 and Sll1167 Components

An interaction between Ycf39 and the ChlG-HliD subcomplex was demonstrated by its purification with FLAG-ChlG and by coimmunoprecipitation (Figure 1). Ycf39 belongs to family of atypical short-chain alcohol dehydrogenase/reductases, which have an NAD(P)H binding motif near the N terminus but lack the canonical Tyr residue critical for activity of typical short-chain alcohol dehydrogenase/reductases (Kallberg et al., 2002). The function of Ycf39 in Synechocystis has not been established; deletion of the cognate slr0399 gene had no effect on cell viability, but it did complement mutations near to the Q_A quinone acceptor of PSII (Ermakova-Gerdes and Vermaas, 1999). This observation led to speculation that Ycf39 is a chaperone-like protein involved in quinone insertion into the PSII complex (Ermakova-Gerdes and Vermaas, 1999). Inactivation of the Arabidopsis Ycf39 homolog Hcf244 greatly decreased accumulation of PSII core proteins, and although the mechanism of Hcf244 action was not explained, it appears to be connected to the synthesis of the D1 protein (Link et al., 2012). The association of the cyanobacterial Ycf39 with ChlG and HliD suggests its role in pigment insertion or modification. Indeed, our recent data confirm the involvement of Ycf39 in the delivery of chlorophyll to the newly synthesized D1 protein and stabilization of the PSII reaction center complex (Knoppová et al., 2014).

The Sll1167 protein is related to the AmpH family of bacterial enzymes expected to assist in remodeling of peptidoglycan layer (González-Leiza et al., 2011); its enigmatic occurrence in the vicinity of chlorophyll-protein biosynthesis components raises the possibility that Sll1167 plays a structural or functional role in photosystem biogenesis.

METHODS

Growth Conditions

Synechocystis PCC 6803 (hereafter, Synechocystis) strains were grown in a rotary shaker under moderate light conditions (40 mmol of photons m^{-2} s^{-1}) at 30 C in liquid BG11 medium. For purification of protein complexes, 4 liters of cells were grown photomixotrophically in a 10-liter flask under 100 mmol of photons m^{-2} s^{-1} light in BG11 medium supplemented with 5 mM Glc. The cell culture was agitated with magnetic stirrer and bubbled with air.

Construction of Synechocystis Strains

To prepare Synechocystis strains expressing ChlG with a 3xFLAG (hereafter, FLAG) tag at the N terminus, the chlG gene (slr0056) was cloned into the pPD-NFLAG plasmid and the construct transformed into the wild type. pPD-NFLAG contains the Synechocystis psbAII promoter, a sequence encoding the 3xFLAG tag, and flanking sequences for homologous recombination that allow insertion of tagged constructs into the Synechocystis genome in place of the psbAII gene (Hollingshead et al., 2012). The Flag-yidC strain was constructed using pPD-CFLAG plasmid to place the 3xFLAG tag at the YidC C terminus. The only difference between pPD-NFLAG and pPD-CFLAG plasmids is in the position of the tag. The chlG, yidC (slr1471), and ycf39 (slr0399) genes were deleted using the megaprimer PCR method essentially as described (Kopečná et al., 2013). The Flag-chlG strain lacking the Ycf39 protein was prepared using genomic DNA isolated from the Dycf39 strain, and the PSI-less variant of the Flag-chlG strain was constructed using DNA isolated from the $psaAB^{-}$ strain described by Shen et al. (1993). The DhliC and DhliD mutants were obtained by the transformation of Synechocystis wild-type strain using genomic DNA isolated from previously described Hlip mutants (Xu et al., 2004). In all cases, transformants were selected on a BG11 agar plate containing 5 mg mL^{-1} of appropriate antibiotic and fully segregated by restreaking transformants on plates with increasing concentration of the antibiotic.

Preparation of Solubilized Membrane Fraction and Anti-FLAG Pull-Down

Synechocystis cells expressing genes for FLAG-tagged proteins were grown to an OD_{750} of 0.5 to 0.7. Cells were pelleted, washed, and resuspended with buffer A (25 mM MES/NaOH, pH 6.5, 10 mM $CaCl_2$, 10 mM $MgCl_2$, 25 glycerol, and EDTA-free Protease Inhibitor [Roche]). Cells were mixed in equal proportions with glass beads and broken in a Mini-Beadbeater-16 (BioSpec), and the soluble proteins and membranes were separated by centrifugation (65,000g, 45 min). The membrane fraction was washed once with an excess of buffer A, then resuspended in buffer A and solubilized for 30 min at 10 C with 1.5 dodecyl-b-maltoside (Applichem). Finally, insoluble contaminants were removed by centrifugation (65,000g, 25 min).

FLAG-ChlG and FLAG-YidC complexes were purified from membrane fraction using an anti-FLAG-M2 agarose column (Sigma-Aldrich). To remove contaminants, the anti-FLAG-resin was washed with 20 resin volumes of buffer A containing 0.25 dodecyl-b-maltoside. The FLAG-tagged proteins were eluted with 2.5 resin volumes of buffer A containing 150 mg/mL 3xFLAG peptide (Sigma-Aldrich) and 0.04 dodecyl-b-maltoside.

Denaturing and 2D Electrophoresis and Protein Immunodetection

The protein composition of the purified complexes was analyzed by electrophoresis in a denaturing 12 to 20 linear gradient polyacrylamide gel containing 7 M urea (Dobáková et al., 2009). Proteins were stained

either by Coomassie Brilliant Blue or subsequently transferred onto a polyvinylidene fluoride (PVDF) membrane for immunodetection (see below). For native electrophoresis, the FLAG-ChlG pull-down was concentrated 5-fold on a 100-kD cutoff microconcentrator (Millipore) and separated on 4 to 12 clear native gel (Wittig et al., 2007). Individual components of protein complexes were resolved by incubating the gel strip from the first dimension in 2 SDS and 1 DTT for 30 min at room temperature, and proteins were separated in the second dimension by SDS-electrophoresis in a denaturing 12 to 20 polyacrylamide gel containing 7 M urea (Dobáková et al., 2009). Proteins were stained either by Coomassie Brilliant Blue or Sypro Orange, and in the latter case, they were subsequently transferred onto a PVDF membrane. Membranes were incubated with specific primary antibodies and then with secondary antibody conjugated with horseradish peroxidase (Sigma-Aldrich). Primary antibodies against SecY, Ycf39, and ChlG were raised in rabbit against synthetic peptides 4-14, 311-322, and 89-104, respectively. The antibody raised against the recombinant fragment Arg-117 Ser-384 of the Synechocystis YidC was kindly provided by Jörg Nickelsen (Ludwig-Maximilians-University, Munich, Germany). Antibodies against the HliD and Rpl1 were purchased from Agrisera (Sweden)

Measurement of Absorption and Fluorescence Spectra

Absorption spectra of protein bands cut from CN-PAGE were measured at room temperature with a Shimadzu UV-3000 spectrophotometer. The 77K fluorescence emission spectra were measured in liquid nitrogen with an Aminco spectrofluorimeter (Spectronic Unicam) using an excitation wavelength of 435 nm to excite chlorophyll a.

MS

After SDS-PAGE, Coomassie Brilliant Blue stained protein bands/spots were excised and subjected to in-gel digestion with trypsin (porcine, modified, proteomics grade; Sigma-Aldrich). The tryptic peptides were analyzed by nanoflow liquid chromatography coupled to MS using instrument systems comprising an UltiMate 3000 nano-LC (Dionex) installed with PepMap C_{18} 5 mm 3 300-mm (trapping) and 150 mm 3 75-mm (analytical) columns (Dionex) operating at flow rates of 30 mL/min and 300 nL/min, respectively, with the same solvents and elution gradient detailed above. Data were acquired online using a Maxis UHR-TOF mass spectrometer (Bruker) with line MS and automated dependent MS/MS scans. For protein identification, mass spectra were converted to Mascot Generic File format using a processing script provided by Bruker and submitted to Mascot Daemon v. 2.1.3 running with Mascot Server v. 2.2.01 against the Synechocystis complete proteome database (http://www.uniprot.org/uniprot/ query organism:1111708).

Gel Filtration and Pigment Analysis

The FLAG-ChlG eluate prepared from 4 liters of cells was immediately injected onto an Agilent-1200 HPLC machine and separated on Bio-sep 3000 column (Phenomenex) using 25 mM HEPES buffer, pH 7.5, containing 0.25 dodecyl-b-maltoside at a flow rate of 0.2 mL min^{-1} at 10 C. Fractions were collected using an Agilent-1200 fraction collector. To analyze the pigments coeluted with the major FLAG-ChlG peak from the gel filtration column, fractions representing the GF3 peak were pooled and concentrated ; 10 times on 30-kD cutoff microconcentrators (Millipore). This solution was extracted with an excess of methanol and the extract injected onto an Agilent-1200 HPLC. Separation was performed on a reverse-phase column (Kinetex C8, 2.6-mm particle size, 3.9 3 150 mm; Phenomenex) with 35 methanol and 15 acetonitrile in 0.25 M pyridine (solvent A) and 20 methanol and 20 acetone in acetonitrile as solvents B. Pigments were eluted with a linear gradient of solvent B (30 to 95 in 25 min) followed by 95 of solvent B at a flow rate of 0.8 mL min^{-1} at 40 C. Pigment stoichiometries were estimated using published extinction coefficients for chlorophyll and b-carotene (Eijckelhoff and Dekker, 1997); the extinction coefficient for myxoxanthophyll in methanol (e412 66 mM^{-1} cm^{-1}) was calculated using an authentic standard prepared from Synechocystis membranes.

ChlG Activity Assay

FLAG-ChlG eluate from 4 liters of cells was incubated at 30 C with 20 mM geranylgeranyl-pyrophosphate (Sigma-Aldrich) and, where appropriate, 20 mM Chlide (kindly provided by D.J. Heyes, University of Manchester, UK). Assays were stopped at the appropriate time point by the addition of excess methanol and subsequently analyzed on an Agilent-1200 HPLC. Separation was performed on a reverse-phase column (Nova-Pak C18, 4-mm particle size, 3.9 3 150 mm; Waters) with 350 mM ammonium acetate and 30 methanol as solvent A and 100 methanol as solvent B. Pigments were eluted with a linear gradient of solvent B (65 to 100 , 15 min) followed by 100 solvent B at a flow rate of 0.9 mL min^{-1} at 40 C. Pigment content was continuously monitored by the HPLC fluorescence detector (440 nm excitation; 670 nm emission). Relative quantification was performed by integration of relevant chromatograph peaks. All assays were performed in triplicate.

Quantification of Chlorophyll Precursors

For quantitative determination of chlorophyll precursors, 50 mL of culture at OD_{750} 0.4 was filtered through a 4-mm cellulose filter to remove precipitated pigments in the growth medium and harvested. Pigments were extracted with an excess of 80 methanol/20 water and measured essentially as described previously (Hollingshead et al., 2012).

Accession Numbers

Sequence data from this article can be found in the Arabidopsis Genome Initiative or GenBank/EMBL databases under accession number BAA10281.2 (chlG).

Supplemental Data

The following materials are available in the online version of this article.

Supplemental Figure 1. Whole-Cell Absorption Spectra of Synechocystis Wild Type and Flag-chlG/DchlG (Hereafter Flag-chlG) and yidC-Flag/DyidC Strains Grown Photoautotrophically.

Supplemental Figure 2. Immunodetection of ChlG and YidC Native Proteins and Their Tagged Derivatives Expressed under the psbAII Promoter.

Supplemental Figure 3. 2D Electrophoresis of the Purified YidC-FLAG and Immunodetection of ChlG.

Supplemental Figure 4. Absorption and Fluorescence Spectroscopy of FLAG-ChlG and Control Pull-Downs.

Supplemental Figure 5. Identification of Individual Ribosomal Subunits by 2D CN/SDS-PAGE.

Supplemental Figure 6. Absorbance Spectra of GF1 and GF2 Gel Filtration Peaks Measured by a Diode-Array Detector.

Supplemental Figure 7. 2D Electrophoresis of Membrane Complexes from Flag-chlG and Flag-chlG/DhliD Strains and Immunodetection of FLAG-ChlG and Ycf39.

Supplemental Figure 8. Amino Acid Sequence Alignment of Synechocystis Hli Proteins and the Third Transmembrane Helix of the Arabidopsis Lhca2 Protein.

Supplemental Table 1. Identification of Proteins in the FLAG-ChlG Pull-Down Eluate.

ACKNOWLEDGMENTS

We thank Lenka Moravcová for her excellent technical assistance. R.S. and J.K. were supported by project Algatech and by project P501/10/1000 of the Grant Agency of the Czech Republic. J.W.C. gratefully acknowledges a doctoral studentship from the Biotechnology and Biological Sciences Research Council (BBSRC; UK). P.J.J., D.P.C., M.J.D., and C.N.H. were supported by a research grant from the BBSRC.

AUTHOR CONTRIBUTIONS

J.W.C., M.L., P.J.J., J.P., M.J.D., J.K., R.S., and C.N.H. designed experiments. J.W.C., M.L., P.J.J., D.P.C., P.K., J.P., and R.S. performed experiments. R.S., J.K., and C.N.H. wrote the article.

Received February 18, 2014; revised February 18, 2014; accepted February 28, 2014; published March 28, 2014.

REFERENCES

Addlesee, H.A., Fiedor, L., and Hunter, C.N. (2000). Physical mapping of bchG, orf427, and orf177 in the photosynthesis gene cluster of Rhodobacter sphaeroides: Functional assignment of the bacteriochlorophyll synthetase gene. J. Bacteriol. 182: 3175 3182.

Antonoaea, R., Fürst, M., Nishiyama, K., and Müller, M. (2008). The periplasmic chaperone PpiD interacts with secretory proteins exiting from the SecYEG translocon. Biochemistry 47: 5649 5656.

Apel, K., and Hirt, H. (2004). Reactive oxygen species: Metabolism, oxidative stress, and signal transduction. Annu. Rev. Plant Biol. 55: 373 399.

Beck, K., Eisner, G., Trescher, D., Dalbey, R.E., Brunner, J., and Müller, M. (2001). YidC, an assembly site for polytopic Escherichia coli membrane proteins located in immediate proximity to the SecYE translocon and lipids. EMBO Rep. 2: 709 714.

Bhaya, D., Dufresne, A., Vaulot, D., and Grossman, A. (2002). Analysis of the hli gene family in marine and freshwater cyanobacteria. FEMS Microbiol. Lett. 215: 209 219.

Chua, N.H., Blobel, G., Siekevitz, P., and Palade, G.E. (1976). Periodic variations in the ratio of free to thylakoid-bound chloroplast ribosomes during the cell cycle of Chlamydomonas reinhardtii. J. Cell Biol. 71: 497 514.

Dobáková, M., Sobotka, R., Tichý, M., and Komenda, J. (2009). Psb28 protein is involved in the biogenesis of the photosystem II inner antenna CP47 (PsbB) in the cyanobacterium Synechocystis sp. PCC 6803. Plant Physiol. 149: 1076 1086.

Eichacker, L.A., Helfrich, M., Rüdiger, W., and Müller, B. (1996). Stabilization of chlorophyll a-binding apoproteins P700, CP47, CP43, D2, and D1 by chlorophyll a or Zn-pheophytin a. J. Biol. Chem. 271: 32174 32179.

Eijckelhoff, C., and Dekker, J.P. (1997). A routine method to determine the chlorophyll a, pheophytin a and b-carotene contents of isolated photosystem II reaction center complexes. Photosynth. Res. 52: 69 73.

Ermakova-Gerdes, S., and Vermaas, W. (1999). Inactivation of the open reading frame slr0399 in Synechocystis sp. PCC 6803 functionally complements mutations near the $Q_{(A)}$ niche of photosystem II. A possible role of Slr0399 as a chaperone for quinone binding. J. Biol. Chem. 274: 30540 30549.

Funk, C., and Vermaas, W. (1999). A cyanobacterial gene family coding for single-helix proteins resembling part of the light-harvesting proteins from higher plants. Biochemistry 38: 9397 9404.

Göhre, V., Ossenbühl, F., Crèvecoeur, M., Eichacker, L.A., and Rochaix, J.D. (2006). One of two alb3 proteins is essential for the assembly of the photosystems and for cell survival in Chlamydomonas. Plant Cell 18: 1454 1466.

González-Leiza, S.M., de Pedro, M.A., and Ayala, J.A. (2011). AmpH, a bifunctional DD-endopeptidase and DD-carboxypeptidase of Escherichia coli. J. Bacteriol. 193: 6887 6894.

He, Q., Dolganov, N., Bjorkman, O., and Grossman, A.R. (2001). The high light-inducible polypeptides in Synechocystis PCC6803. Expression and function in high light. J. Biol. Chem. 276: 306 314.

Hernandez-Prieto, M.A., Tibiletti, T., Abasova, L., Kirilovsky, D., Vass, I., and Funk, C. (2011). The small CAB-like proteins of the cyanobacterium Synechocystis sp. PCC 6803: Their involvement in chlorophyll biogenesis for photosystem II. Biochim. Biophys. Acta 1807: 1143 1151.

Hollingshead, S., Kopecná, J., Jackson, P.J., Canniffe, D.P., Davison, P.A., Dickman, M.J., Sobotka, R., and Hunter, C.N. (2012). Conserved chloroplast open-reading frame ycf54 is required for activity of the magnesium protoporphyrin monomethylester oxidative cyclase in Synechocystis PCC 6803. J. Biol. Chem. 287: 27823 27833.

Jordan, P., Fromme, P., Witt, H.T., Klukas, O., Saenger, W., and Krauss, N. (2001). Three-dimensional structure of cyanobacterial photosystem I at 2.5 A resolution. Nature 411: 909 917.

Kallberg, Y., Oppermann, U., Jörnvall, H., and Persson, B. (2002). Short-chain dehydrogenases/reductases (SDRs). Eur. J. Biochem. 269: 4409 4417.

Kim, J., Klein, P.G., and Mullet, J.E. (1994). Synthesis and turnover of photosystem II reaction center protein D1. Ribosome pausing increases during chloroplast development. J. Biol. Chem. 269: 17918 17923.

Klostermann, E., Droste Gen Helling, I., Carde, J.P., and Schünemann, D. (2002). The thylakoid membrane protein ALB3 associates with the cpSecY-translocase in Arabidopsis thaliana. Biochem. J. 368: 777 781.

Knoppová, J., Sobotka, R., Tichý, M., Yu, J., Koník, P., Halada, P., Nixon, P.J., and Komenda, J. (2014). Identification of a novel chlorophyll binding protein complex involved in the early steps of photosystem II assembly. Plant Cell, in press.

Komenda, J., Knoppová, J., Kopečná, J., Sobotka, R., Halada, P., Yu, J.F., Nickelsen, J., Boehm, M., and Nixon, P.J. (2012b). The Psb27 assembly factor binds to the CP43 complex of photosystem II in the cyanobacterium Synechocystis sp. PCC 6803. Plant Physiol. 158: 476 486.

Komenda, J., Sobotka, R., and Nixon, P.J. (2012a). Assembling and maintaining the Photosystem II complex in chloroplasts and cyanobacteria. Curr. Opin. Plant Biol. 15: 245 251.

Kopečná, J., Sobotka, R., and Komenda, J. (2013). Inhibition of chlorophyll biosynthesis at the protochlorophyllide reduction step results in the parallel depletion of photosystem I and photosystem II in the cyanobacterium Synechocystis PCC 6803. Planta 237: 497 508.

Link, S., Engelmann, K., Meierhoff, K., and Westhoff, P. (2012). The atypical short-chain dehydrogenases HCF173 and HCF244 are jointly involved in translational initiation of the psbA mRNA of Arabidopsis. Plant Physiol. 160: 2202 2218.

Masuda, T., and Fujita, Y. (2008). Regulation and evolution of chlorophyll metabolism. Photochem. Photobiol. Sci. 7: 1131 1149.

Moore, M., Goforth, R.L., Mori, H., and Henry, R. (2003). Functional interaction of chloroplast SRP/FtsY with the ALB3 translocase in thylakoids: Substrate not required. J. Cell Biol. 162: 1245 1254.

Müller, B., and Eichacker, L.A. (1999). Assembly of the D1 precursor in monomeric photosystem II reaction center precomplexes precedes chlorophyll a-triggered accumulation of reaction center II in barley etioplasts. Plant Cell 11: 2365 2377.

Nagamori, S., Smirnova, I.N., and Kaback, H.R. (2004). Role of YidC in folding of polytopic membrane proteins. J. Cell Biol. 165: 53 62.

Ossenbühl, F., Inaba-Sulpice, M., Meurer, J., Soll, J., and Eichacker, L.A. (2006). The synechocystis sp PCC 6803 oxa1 homolog is essential for membrane integration of reaction center precursor protein pD1. Plant Cell 18: 2236 2246.

Oster, U., Bauer, C.E., and Rüdiger, W. (1997). Characterization of chlorophyll a and bacteriochlorophyll a synthases by heterologous expression in Escherichia coli. J. Biol. Chem. 272: 9671 9676.

Pasch, J.C., Nickelsen, J., and Schünemann, D. (2005). The yeast split-ubiquitin system to study chloroplast membrane protein interactions. Appl. Microbiol. Biotechnol. 69: 440 447.

Promnares, K., Komenda, J., Bumba, L., Nebesarova, J., Vacha, F., and Tichy, M. (2006). Cyanobacterial small chlorophyll-binding protein ScpD (HliB) is located on the periphery of photosystem II in the vicinity of PsbH and CP47 subunits. J. Biol. Chem. 281: 32705 32713.

Rapoport, T.A. (2007). Protein translocation across the eukaryotic endoplasmic reticulum and bacterial plasma membranes. Nature 450: 663 669.

Renger, T., and Schlodder, E. (2011). Optical properties, excitation energy and primary charge transfer in photosystem II: Theory meets experiment. J. Photochem. Photobiol. B Biol. 104: 126 141.

Rüdiger, W., Böhm, S., Helfrich, M., Schulz, S., and Schoch, S. (2005). Enzymes of the last steps of chlorophyll biosynthesis: Modification of the substrate structure helps to understand the topology of the active centers. Biochemistry 44: 10864 10872.

Sachelaru, I., Petriman, N.A., Kudva, R., Kuhn, P., Welte, T., Knapp, B., Drepper, F., Warscheid, B., and Koch, H.G. (2013). YidC occupies the lateral gate of the SecYEG translocon and is sequentially displaced by a nascent membrane protein. J. Biol. Chem. 288: 16295 16307.

Schottkowski, M., Ratke, J., Oster, U., Nowaczyk, M., and Nickelsen, J. (2009). Pitt, a novel tetratricopeptide repeat protein involved in light-dependent chlorophyll biosynthesis and thylakoid membrane biogenesis in Synechocystis sp. PCC 6803. Mol. Plant 2: 1289 1297.

Scotti, P.A., Urbanus, M.L., Brunner, J., de Gier, J.W., von Heijne, G., van der Does, C., Driessen, A.J., Oudega, B., and Luirink, J. (2000). YidC, the Escherichia coli homologue of mitochondrial Oxa1p, is a component of the Sec translocase. EMBO J. 19: 542 549.

Shen, G.Z., Boussiba, S., and Vermaas, W.F.J. (1993). Synechocystis sp PCC 6803 strains lacking photosystem I and phycobilisome function. Plant Cell 5: 1853 1863.

Sobotka, R. (2014). Making proteins green; biosynthesis of chlorophyll-binding proteins in cyanobacteria. Photosynth. Res. 119: 223 232.

Sobotka, R., Tichy, M., Wilde, A., and Hunter, C.N. (2011). Functional assignments for the carboxyl-terminal domains of the ferrochelatase from Synechocystis PCC 6803: The CAB domain plays a regulatory role, and region II is essential for catalysis. Plant Physiol. 155: 1735 1747.

Sozer, O., Komenda, J., Ughy, B., Domonkos, I., Laczkó-Dobos, H., Malec, P., Gombos, Z., and Kis, M. (2010). Involvement of carotenoids in the synthesis and assembly of protein subunits of photosynthetic reaction centers of Synechocystis sp. PCC 6803. Plant Cell Physiol. 51: 823 835.

Spence, E., Bailey, S., Nenninger, A., Møller, S.G., and Robinson, C. (2004). A homolog of Albino3/Oxal is essential for thylakoid biogenesis in the cyanobacterium Synechocystis sp. PCC6803. J. Biol. Chem. 279: 55792 55800.

Stengel, A., Gügel, I.L., Hilger, D., Rengstl, B., Jung, H., and Nickelsen, J. (2012). Initial steps of photosystem II de novo assembly and preloading with manganese take place in biogenesis centers in Synechocystis. Plant Cell 24: 660 675.

Tanaka, R., Rothbart, M., Oka, S., Takabayashi, A., Takahashi, K., Shibata, M., Myouga, F., Motohashi, R., Shinozaki, K., Grimm, B., and Tanaka, A. (2010). LIL3, a light-harvesting-like protein, plays an essential role in chlorophyll and tocopherol biosynthesis. Proc. Natl. Acad. Sci. USA 107: 16721 16725.

Tzvetkova-Chevolleau, T., Franck, F., Alawady, A.E., Dall Osto, L., Carrière, F., Bassi, R., Grimm, B., Nussaume, L., and Havaux, M. (2007). The light stress-induced protein ELIP2 is a regulator of chlorophyll synthesis in Arabidopsis thaliana. Plant J. 50: 795 809.

Umena, Y., Kawakami, K., Shen, J.R., and Kamiya, N. (2011). Crystal structure of oxygen-evolving photosystem II at a resolution of 1.9 . Nature 473: 55 60.

van Bloois, E., Dekker, H.L., Fröderberg, L., Houben, E.N., Urbanus, M.L., de Koster, C.G., de Gier, J.W., and Luirink, J. (2008). Detection of cross-links between FtsH, YidC, HflK/C suggests a linked role for these proteins in quality control upon insertion of bacterial inner membrane proteins. FEBS Lett. 582: 1419 1424.

Vavilin, D., Brune, D.C., and Vermaas, W. (2005). ^{15}N-labeling to determine chlorophyll synthesis and degradation in Synechocystis sp. PCC 6803 strains lacking one or both photosystems. Biochim. Biophys. Acta 1708: 91 101.

Wittig, I., Karas, M., and Schägger, H. (2007). High resolution clear native electrophoresis for in-gel functional assays and fluorescence studies of membrane protein complexes. Mol. Cell. Proteomics 6: 1215 1225.

Xu, H., Vavilin, D., Funk, C., and Vermaas, W. (2002). Small Cab-like proteins regulating tetrapyrrole biosynthesis in the cyanobacterium Synechocystis sp. PCC 6803. Plant Mol. Biol. 49: 149 160.

Xu, H., Vavilin, D., Funk, C., and Vermaas, W. (2004). Multiple deletions of small Cab-like proteins in the cyanobacterium Synechocystis sp. PCC 6803: Consequences for pigment biosynthesis and accumulation. J. Biol. Chem. 279: 27971 27979.

Yao, D., Kieselbach, T., Komenda, J., Promnares, K., Prieto, M.A. H., Tichy, M., Vermaas, W., and Funk, C. (2007). Localization of the small CAB-like proteins in photosystem II. J. Biol. Chem. 282: 267 276.

Yao, D.C.I., Brune, D.C., Vavilin, D., and Vermaas, W.F.J. (2012). Photosystem II component lifetimes in the cyanobacterium Synechocystis sp. strain PCC 6803: small Cab-like proteins stabilize biosynthesis intermediates and affect early steps in chlorophyll synthesis. J. Biol. Chem. 287: 682 692.

10. Unpublished manuscript

10.1 Mutations suppressing the lack of prepilin peptidase provide insights into the maturation of the major pilin protein in cyanobacteria.

Linhartová, M., Skotnicová, P., Hakkila, K., Tichý, M., Komenda, J., Knoppová, J., Gilabert, J. F., Guallar, V., Tyystjärvi, T., Sobotka, R.

Mutations suppressing the lack of prepilin peptidase provide insights into the maturation of the major pilin protein in cyanobacteria

Markéta Linhartová,[a,b] Petra Skotnicová,[a] Kaisa Hakkila,[c] Martin Tichý,[a] Josef Komenda,[a,b] Jana Knoppová,[a] Joan F. Gilabert,[d] Victor Guallar,[d,e] Taina Tyystjärvi,[c] and Roman Sobotka[a,b,#]

[a]Institute of Microbiology of the Czech Academy of Sciences, Opatovický mlýn, 37981 Třeboň, The Czech Republic

[b]Faculty of Science, University of South Bohemia, Branišovská 31, 37005 České Budějovice, The Czech Republic

[c]Biochemistry/Molecular Plant Biology, University of Turku, FI-20014 Turku, Finland

[d]Barcelona Supercomputing Center, Jordi Girona 29, E-08034 Barcelona, Spain.

[e]ICREA: Institucio Catalana de Recerca i Estudis Avançats Passeig Lluis Companys 23, 08010 Barcelona (Spain).

Running Head: Suppressing the prepilin toxicity in cyanobacteria

#Address correspondence to Roman Sobotka, sobotka@alga.cz.

KEYWORDS Type IV pili, *Synechocystis*, Photosystem II, PilD peptidase

Abstract

Type IV pili are bacterial surface-exposed filaments that are built up by small monomers called pilin proteins. Pilins are synthesized as longer precursors (prepilins), the N-terminal signal peptide of which must be removed by the processing protease PilD. A mutant of the cyanobacterium *Synechocystis* sp. PCC 6803 lacking the PilD protease is not capable of photoautotrophic growth because of the impaired function of Sec translocons. Here, we isolated phototrophic suppressor strains of the original *pilD* mutant and, by sequencing their genomes, we identified mutations in the SigF sigma factor, the γ subunit of RNA polymerase, the signal peptide of major pilin PilA1, and in the *pilA1-pilA2* intergenic region. Characterization of suppressor strains suggests that, rather than the total prepilin level in the cell, the presence of non-glycosylated PilA1 prepilin is specifically harmful. We propose that the restricted lateral mobility of the non-glycosylated PilA1 prepilin causing its accumulation in the translocon-rich membrane domains, which attenuates the synthesis of membrane proteins.

Introduction

Type IV pili are appendages on the cell surface that belong to the most versatile prokaryotic nano-machines mediating diverse functions including adhesion, aggregation, motility, secretion or DNA uptake (Giltner et al., 2012). The key building block of the Type IV pili is a so-called major pilin protein, which is synthesized as an integral cell membrane protein but later is extracted from the membrane bilayer and assembled into long helical polymers protruding from the cell. In Gram-negative bacteria, the assembly (and disassembly) of pili is driven by ATP hydrolysis and requires a large molecular machinery anchored in the cytoplasmic and outer membranes, spanning the whole periplasmic space (Craig et al., 2019).

The highly conserved feature of Type IV pilins is their process of maturation. Pilin monomers are produced as precursors called prepilins with an N-terminal signal sequence required for the insertion of prepilins into the membrane followed by a conserved transmembrane segment (Giltner et al., 2012). The N-terminal signal segment is then removed by the integral membrane peptidase PilD that cleaves prepilin roughly proximal to the cytoplasmic membrane surface (Strom et al., 1993; LaPointe and Taylor, 2000).

Analysis of various bacterial species lacking the PilD peptidase has demonstrated that removal of the signal peptide is essential for pilus assembly (Goosens et al., 2017); non-matured prepilins remain anchored in the membrane (Strom et al., 1993). *O*-glycosylation of major pilins has been reported in many bacterial strains and this post-translational modification probably facilitates pilus assembly or its stability (Marceau et al., 1998).

Cyanobacteria are a unique group of Gram-negative bacteria with the ability to perform oxygenic photosynthesis and fix carbon dioxide into organic compounds. In contrast to other prokaryotes, many cyanobacteria contain an endogenous membrane system, which is very abundant in photosystem I (PSI) and photosystem II (PSII) complexes – large, membrane-embedded, oxidoreductases powered by light. PSI and PSII are essential for all oxygenic phototrophs as they use the energy of photons to generate highly oxidizing/reducing species that are needed for the oxidation of water and the reduction of $NADP^+$. Although cyanobacteria evolved this metabolic strategy not used by other prokaryotes, they possess many typical bacterial structures including Type IV pili (Schuergers and Wilde, 2015).

In our previous study, we revealed an intimate and unexpected link between the maturation of pilins and the biogenesis of photosynthetic membrane complexes (Linhartová et al., 2014). We found that the elimination of the PilD protease and the consequent accumulation of prepilins in the cyanobacterium *Synechocystis* sp. PCC 6803 (hereafter *Synechocystis*) triggered degradation of the SecY translocase and the YidC insertase. The latter protein is known to associate with the SecYEG heterotrimer forming a component of the bacterial holo-translocon, – molecular machinery promoting the insertion of most membrane proteins into the lipid bilayer (Sachelaru et al., 2017). Disturbing the holo-translocon drastically reduces the synthesis of membrane proteins including all core subunits of PSII (Linhartová et al., 2014). Due to the toxicity of prepilins, the *pilD* strain was no longer able to grow photoautotrophically though proliferation under mixotrophic conditions (in the presence of glucose) was possible (Linhartová et al., 2014). Interestingly, deletion of the *pilA1* gene coding for the major PilA1 pilin completely rescued the photosynthetic capacity of the *pilD* strain (Linhartová et al., 2014). It led us to a prediction that spontaneous mutations reducing the synthesis of PilA1 prepilin (pPilA1), or its harmful impact on the activity of translocons, will improve the photoautotrophic growth of the *pilD* mutant.

Here, we identified five mutations in four different photoautotrophic *pilD* suppressor (revertant) strains. Two mutations were located in the SigF sigma factor and the remaining

three mutations were located in the γ subunit of the RNA polymerase (RNAP), the *pilA1-pilA2* intergenic region, and the *pilA1* gene. Effects of these mutations as well as the suppressor effect of mixotrophic growth conditions were analyzed in detail. Our results suggest that there is a link between the PilA1 prepilin (pPilA1) toxicity and the lagged glycosylation of this protein. We propose that the accumulation of the non-glycosylated pPilA1 in the biosynthetically active membrane zones is responsible of the growth arrest of the *pilD* mutant.

Results

Spontaneous mutations suppressing the lack of PilD

To generate mutations suppressing the deletion of *Synechocystis* PilD peptidase we incubated the *pilD* strain under photoautotrophic conditions on a BG-11 agar plate (40 μmol of photons m^{-2} s^{-1}; hereafter normal light) for three weeks. However, the mutant cells bleached completely in a few days without forming any colonies. In contrast to photoautotrophic conditions, *pilD* grew initially well on agar plates supplemented with 5 mM glucose (Glc^+ conditions) but after several days the cell pigmentation turned pale (Fig. S1) and cells died in two weeks if not restreaked on a fresh Glc^+ plate. Interestingly, many *pilD* suppressor colonies appeared after two weeks on Glc^+ plates (Fig. S1; see also Fig. 3A) and virtually all of them were able to grow also photoautotrophically. We selected four colonies (rev1-4), that differed markedly in size and pigmentation, for an in-depth analysis.

To identify suppressor mutations in rev1-4 strains, we performed their whole genome re-sequencing using an Illumina HiSeq platform. Obtained reads were mapped on the GT-S reference genome (Tajima et al., 2011) and, after subtraction of mutations that had been identified previously to occur in our WT laboratory substrain (GT-W; Tichý et al., 2016), we revealed mutations specific for the *pilD* revertants (Fig. 1, Table 1). The point mutation in rev1 causes the amino-acid substitution H45P in the SigF sigma factor (Fig. 1A) and the mutation in rev2 leads to the S3G substitution in a signal peptide of the major pilin, PilA1 (Fig. 1B). The mutation in rev3 is located in the *pilA1-pilA2* intergenic region (Fig. 1C), specifically in the predicted terminator of the *pilA1* gene (Hess, W., personal communication). The rev4 strain contained two mutations; an R221C substitution in SigF (Fig. 1A) and an E95K substitution in the RNAP γ subunit.

The RNAP-SigF holoenzyme is responsible for the transcription of the specific regulon involving the *pilA1* gene (Asayama and Imamura, 2008) and potentially also other *pilA* genes in *Synechocystis* (Flores et al., 2019). The histidine (H45) residue, mutated to proline in the rev1 strain, is conserved in cyanobacterial SigF and SigJ factors (Fig. S2) and it is probably in a contact with the TATA element of the *pilA1* gene (Fig. 2A). The effect of the R221C mutation in SigF is less clear but the substituted arginine residue might facilitate the contact with the RNAP core protein (Fig. 2B; see discussion for details).

Growth phenotype of the pilD suppressor strains

Although neither of the four rev strains exhibited such a fast bleaching phenotype on the Glc^+ agar plates as the original *pilD* strain, rev2 and rev3 strains grew into a much thinner layer and the rev2 strain visibly bleached after 3 weeks (Fig. 3A). The viability of rev2 and rev3 appeared opposite under photoautotrophic conditions, particularly under longer incubation on agar plates. Rev2 and rev3 strains proliferated only for a few first days and the rev3 mutant visibly faded showing a poorer phenotype than rev2 (Fig. 3B). Rev1 and rev4 strains resembled again the WT control, which was further confirmed in liquid (Glc^-) culture. Consistent with the growth on the agar plate both rev2 and rev3 suffered from a growth defect (Fig. 3C); however, their phenotypes were distinct. In contrast to constant, albeit slow growth of the rev2 (Fig. 3C), and its stable level of chlorophyll (Fig. S1B), the initial proliferation of rev3 was similar to WT. However, at higher culture density the mutant growth was arrested (OD_{730nm} >1.5; Fig. 3C), which was accompanied by a sharp decrease in cellular chlorophyll (Fig. S1B).

The fast depletion of PSII in the *pilD* mutant after its shift from Glc^+ to photoautotrophic conditions has been reported previously (Linhartová et al., 2014). We, therefore, analyzed the content of PSII in revertants at 48 hours after changing the growth media from Glc^+ to Glc^- conditions. Indeed, *pilD* cells lost most of the PSII complexes and particularly the dimeric PSII form disappeared almost completely (Fig. 3D). In contrast, all four suppressor mutants were capable to maintain dimeric PSII although only rev1 and rev4 had the level comparable to WT (Fig. 3D). As shown by a more detailed analysis of membrane proteins by 2D clear-native/SDS electrophoresis (CN/SDS-PAGE), rev3 cells were visibly defective in the accumulation of membrane proteins as the total levels of many of them were reduced (Fig. S3).

A striking characteristic of *Synechocystis pilD* and *pilA1/pilA2* mutants is very compact cell aggregation under mixotrophic (Glc^+) growth conditions (Fig. S4). This type of aggregation persists a vigorous shaking at 120 rpm and thus differs from cell flocculation characteristic of large flocs formed by cells settled down at the bottom of the cultivation flask (Conradi et al., 2019). Interestingly, the rev1 and rev4 strains, harbouring mutations in the *sigF* gene, exhibited almost no tendency to form aggregates and the *sigF* deletion strain also did not aggregate (Fig. S4) in contrast to Flores et al. (2019). Aggregation of rev2 cells was weaker than that of the *pilD* mutant and a portion of cells remained fully dispersed, whereas the rev3 aggregated comparably to the parental strain (Fig. S4). None of these strains aggregated under photoautotrophic conditions (Fig. S4).

We conclude that suppressor mutations in the rev1 and rev4 strains almost completely restored the viability of the *pilD* mutant in our standard laboratory conditions. The remaining two strains (rev2, rev3) were only partially complemented. Although the rev3 strain proliferated better if supplemented with glucose than rev2, it appeared phenotypically closest to the original *pilD* mutant based on the poor accumulation of membrane proteins (Fig. S3), a compact cell aggregation (Fig. S4), and the growth inhibition and loss of chlorophyll during the prolonged cultivation on plates (Fig. 3B) as well as in liquid cultures (Fig. 3C).

Effect of suppressor mutations on the expression of pilA1 gene

As all suppressor mutations could potentially affect the expression of the *pilA1* gene, we quantified the *pilA1* transcripts by Northern blotting both in Glc^- and Glc^+ conditions. Note, that the glucose itself had a strong suppressor effect on the prepilin toxicity (Fig. 3A, B). The *pilA1* transcript was found to be monocistronic (Fig. 4A, B), consistent with previous reports (He and Vermaas, 1999; Asayama and Imamura, 2008), and the *pilA1* mRNA was 4 to 5 times more abundant in the *pilD* mutant than in WT (Fig. 4C, D). As expected no *pilA1* transcript was detected in the *sigF* mutant.

In the rev1 strain, the H45P mutation in the SigF protein reduced significantly the content of *pilA1* mRNA to the level in WT both in Glc^- and Glc^+ (Fig. 4). On the other hand, in the rev4 strain, that contains mutated SigF and an additional mutation in the RNAP γ subunit, the *pilA1* transcript level dropped to the WT level only in Glc^- but remained similar as in

the *pilD* strain in mixotrophic conditions (Fig. 4). The amount of *pilA1* mRNA in rev2 (mutation in the *pilA1* gene) was high (Fig. 4) indicating that the suppressor effect does not stem from the weakened *pilA1* expression. In the rev3 strain, the point mutation in *pilA1-pilA2* intergenic region lowered the amount of *pilA1* transcript to the WT level only in Glc^- conditions; the situation was thus opposite to rev4. Interestingly, we detected also a longer *pilA1* transcript (~1300 bp) only in rev3 and specifically under the photoautotrophic conditions (Fig. 4A, B); this result was observed in three biological replicates (Fig. S5). The length of this transcript corresponds to *pilA1-pilA2* mRNA (see Fig. 1C) suggesting that the rev3 mutation might affect the *pilA1* terminator.

Based on transcriptomic data, Kopf and co-workers (Kopf et al., 2014) identified a *Synechocystis* transcription unit (TU1331) coding for a putative *pilA1* anti-sense RNA with length ~100 bp longer than the 'sense' *pilA1* mRNA. The rev3 mutation is located in the promoter region of the expected anti-sense gene between -10 and -35 elements (Fig. 1C). However, we did not detect such an antisense transcript on the Northern blot, which suggests that its level is much lower than that of *pilA1* (Fig. 4A, B).

This transcript analysis revealed a complex regulation of the *pilA1* gene regarding the trophic mode. Since the pPilA1 protein is connected with lethality under Glc^- conditions (Fig. 3B), low levels of *pilA1* transcript in rev1 and rev4 (both having suppressor mutation in SigF) after 48h without glucose could explain the ability of these strains to grow photoautotrophically. On the other hand, the very strong expression of *pilA1* in the rev2 and rev3 strains in Glc^- (Fig. 4D) implies that the remaining two mutations suppress the prepilin toxicity by a different mechanism than does the mutated sigma factor SigF.

Accumulation of PilA1 prepilin and the stability of translocon machinery

The level of PilA1 protein in the isolated cellular membrane fraction was assessed using immunoblotting. The newly synthesized PilA1 protein (prepilin) is matured by the PilD protease and further glycosylated (Kim et al., 2009; Linhartová et al., 2014). In *Synechocystis* WT cells, we detected only the mature PilA1 protein, whereas the prepilin or the non-glycosylated pilin were below the detection limits (Fig. 5). On the contrary, a high amount of prepilin accumulated in the *pilD* strain, circa 50% of which was non-glycosylated pPilA1 ($pPilA1^n$) and 50% glycosylated pPilA1 ($pPilA1^g$; Fig. 5). It is notable

that in WT cells the PilA1 content greatly increased after shifting cells from Glc^+ to Glc^- conditions, which did not happen in the *pilD* mutant or any of the revertant strains (Fig. 5B). This increase in PilA1 level in WT has not been observed previously after 24 h of incubation under Glc^- conditions (Linhartová et al., 2014) indicating that the higher accumulation of PilA1 requires longer (48 h) incubation in the absence of glucose or it is stimulated with higher cell density.

Consistently with the low level of *pilA1* mRNA, the rev1 cells contained almost no $pPilA1^n$ and less of $pPilA1^g$ than the *pilD* mutant regardless of the growth conditions used. The rev2 and rev4 strains contained much less $pPilA1^n$ than the *pilD* mutant and supplementation with external glucose further promoted the prepilin glycosylation in these revertant strains (Fig. 5). The amount of $pPilA1^g$ was even higher in the rev3 strain compared to the *pilD* mutant and the strain still exhibited a high level of $pPilA1^n$ when cultivated without glucose. However, the ratio of both forms was shifted from about half of the glycosylated form in Glc^+ to ~ 75 % of the glycosylated prepilin over ~ 25 % of the non-glycosylated in Glc^-.

Accumulation of pPilA1 in the *pilD* mutant in photoautotrophic conditions was previously shown to cause degradation of the SecY translocase and the YidC insertase (Linhartová et al., 2014) as well the lumenal Ycf48 protein, which forms a complex with YidC and facilitates the insertion of chlorophyll molecules into PSII subunits (Bučinská et al., 2018; Yu et al., 2018). This process was accompanied by abolished production of PSII subunits (Linhartová et al., 2014). The proteolytic degradation of YidC and Ycf48 in the *pilD* mutant in Glc^- (Fig. 5) is in agreement with the earlier results. Notably, the content and stability of YidC insertase and Ycf48 did not appear affected in any of the suppressor strain including rev3 that is deficient in the content of membrane proteins (Fig. S3).

Synthesis and glycosylation of pPilA1 prepilin in pilD suppressor strains

We have previously speculated that the $pPilA1^n$ form of prepilin, rather than the glycosylated $pPilA1^g$, is responsible for the deleterious effect on the membrane-protein synthesis (Linhartová et al., 2014). Although the $pPilA1^n$ was less abundant in rev2 and rev3 than in the *pilD* mutant, there was indeed a question whether the observed decrease in

pPilA1^{n} can account for the improved PSII biogenesis (Fig. 3D) and for the restored stability of YidC/Ycf48 in these strains (Fig. 5B).

To better understand prepilin toxicity, we assessed the synthesis of membrane proteins in cells grown under Glc^{-} conditions by radioactive pulse labelling (20 min) using a [^{35}S]Met/Cys mixture. Labelled membrane proteins were separated in SDS-PAGE (Commassie stained gels are shown in Fig. S6) and autoradiographed (Fig. 6). As shown previously, the synthesis of membrane proteins in the *pilD* strain under Glc^{-} conditions is extremely weak (Linhartová et al., 2014) and we, therefore, compared the proteins labelling of rev1-4 strains with WT (all 48 h in Glc^{-}) and with the *pilD* (Glc^{+}) sample. Intriguingly, even in a (fresh) Glc^{+} culture, the overall labelling of membrane proteins in *pilD* was much less intensive than in WT (Glc^{-}; Fig. 6A). On the contrary, in rev1, rev2 and rev4 strain the total synthesis of membrane proteins was similar to WT. Consistent with the lowered amount of membrane proteins in rev3 in Glc^{-} conditions (Fig. S3), the total protein labelling in this strain is < 50 % of the WT including D1 and D2 core subunits of PSII (Fig. 6B).

The signal of newly synthesized pPilA1^{g} was clearly much weaker in all rev strains than in the *pilD* (Glc^{+}) sample and also less intensive than that of PilA1 in WT (Fig. 6A). Given this low intensity, we cannot exclude a 'contribution' of other weakly labelled proteins with a similar gel mobility. Moreover, the labelling of pPilA1^{n} also cannot be resolved on 1D-gel as it comigrates with an unknown intensively labelled protein (marked by an asterisk in Fig. 6A; see also later). To obtain a better resolution of labelled pPilA1^{g} and pPilA1^{n}, the identical samples as in Fig. 6A were separated by 2D CN/SDS-PAGE and blotted. The radioactivity of the blotted proteins was visualized by phosphorimaging. We found that the synthesis of prepilin in rev1 and rev4 is very low since we were not able to detect the characteristic signals of pPilA1^{g} or pPilA1^{n} in these strains (Fig. 6B). Both forms of pPilA1 in these strains thus probably slowly accumulate to the level detected by immunoblotting (Fig. 5B). In contrast to rev1 and rev4, the pulse labelled forms of prepilin were well detectable in rev2 and rev3. In rev3, about a half of the labelled prepilins is non-glycosylated, whereas it is the majority in rev2. It should be noted that in the previous study we were not able to detect PilA1^{n} in WT even by radiolabelling (Linhartová et al., 2014). The glycosylation of PilA1 in WT must therefore be very fast (in a few minutes) but the glycosylation of prepilin is dramatically slowed down.

Two-dimensional (2D) separation of radiolabelled proteins allowed us to inspect the process of PSII biogenesis. As expected, the labelling of D1 and D2 subunits incorporated into the new PSII complexes was much weaker in rev3 than in other rev strains (Fig. 6B). However, the process of PSII assembly was not restored in rev2 either (note the signal of labelled D1 and D2 in monomeric and dimeric PSII) although the synthesis of D1 and D2 subunits in this strain appeared as intensive as in WT (Fig. 6A). The partially blocked biogenesis of PSII correlated with the lowered level of PSII in rev2 and rev3 (Fig. 3D).

Minor PilA2 pilin promotes the glycosylation of PilA1

Rev2 and rev3 strains with poor phototrophic performance (Fig. 3B,C) exhibit a strong transcription of the *pilA1* gene (Fig. 4D) and a high rate of pPilA1 synthesis (Fig. 6B). As it is very likely that the intensive synthesis of prepilin is directly connected to the impaired PSII biogenesis (Linhartová et al., 2014; see discussion), the greatly reduced expression of *pilA1* in rev1 and rev4 under Glc^- offers a straightforward explanation of how the SigF and RNAP mutations suppress the loss of *pilD*. The mechanism of rev2 and rev3 mutations was, however, enigmatic.

The rev3 mutation is located in the predicted terminator of the *pilA1* gene and might thus increase the expression of the downstream located *pilA2* gene (Fig. 1C). We immunodetected the PilA1 protein in *pilA2* (Glc^-) and *pilD*/*pilA2* (Glc^+) strains to see any potential effect of the absence of PilA2 on the stability/biogenesis of PilA1. Interestingly, another form of PilA1 was detected in the *pilA2* strain, which would correspond to the non-glycosylated PilA1 ($PilA1^n$; Fig. 7A). Moreover, in the *pilD*/*pilA2* strain, the glycosylated pPilA1 was almost completely absent while the level of $pPilA1^n$ remained high (Fig. 7B). These data suggest that the PilA2 protein is required for the modification of PilA1 and also support the model that, rather than the $pPilA1^g$, the $pPilA1^n$ inhibits protein synthesis; note that the deletion of *pilA2* does not complement the *pilD* (Linhartová et al., 2014). Indeed, if compared to the original *pilD* strain, the $pPilA1^n$ in rev3 (Glc^-) appears specifically depleted (Fig. 5B; see also Fig. 7C).

S3G mutation in the signal peptide weakens the interaction of pPilA1 with the membrane

The S3G mutation (rev2) is located in the signal peptide that is cleaved out by the PilD protease during the pPilA1 maturation. In our previous work, the pPilA co-

immunoprecipitated with SecY showing an aberrant interaction between the prepilins and the translocon (Linhartová et al., 2014). To check the potential effect of the *pilA1* gene mutation (S3G) on the interaction with translocons, we repeated this experiment involving the rev2 and rev3 strains. We immunoprecipitated SecY and detected the co-purified pPilA1. In the *pilD* mutant the pPilA1^{g} and a smaller amount of pPilA1^{n} co-eluted with SecY but the pPilA1^{g} was only detected in the rev3 sample; most likely because the level of pPilA1^{n} is much reduced in rev3 cells. In contrast, no detectable pPilA1-S3G protein was co-isolated with SecY from the rev2 strain (Fig. 7). Although the pPilA1was less abundant in rev2 membranes than in *pilD* (Fig. 7), no detectable pPilA1 in the SecY precipitate signalized that the S3G mutation makes the association with translocons less likely.

According to available structures of the PilD-related aspartyl proteases (3S0X; 4HYC), the charged prepilin signal peptide is cleaved by PilD after being exposed to the cytosolic/stromal surface of the cell membrane (Hu et al., 2011; Li et al., 2013). To understand how the replacement of Ser3 with Gly in the signal peptide prevents the aberrant association of the prepilin to SecY, we performed molecular dynamics (MD) simulations of the pPilA1^{n} protein in a model thylakoid membrane (TM) (Daskalakis, 2018). As a starting position, the signal peptide was exposed in the cytosol (Fig. 8A). Interestingly, the charged signal peptide almost immediately (6 ns) attached to the membrane surface, forming several hydrogen bonds between hydroxyl groups of galactolipids and Met1, Ser3 and Arg17 residues (Fig. S8A). Thereafter, the signal peptide remained attached to lipid sugars through the entire 0.5 μs MD simulation, just becoming deeply buried into the membrane (Fig. 8A; see Supplementary video S1).

Although the association of the signal peptide with the model TM appears very robust, the SecY translocase is known to associate specifically with anionic lipids, such as phosphatidylglycerol or cardiolipin (reviewed in Crane and Randall, 2017). However, the total content of phosphatidylglycerol in *Synechocystis* cells is low (~10 %; Kopečná et al., 2015), and such a low content was used in our model TM (Daskalakis, 2018). To evaluate the effect of phospholipids on the interaction between the signal peptide and the membrane, we run the same simulation in the model phosphatidylcholine (POPC) membrane bilayer. In this case, the formation of stable contact between the signal peptide and POPC phosphate groups took longer (~0.25 μs; Fig. S8B), but the peptide remained firmly embedded in the membrane later on (Fig. 8B; Supplementary video S2). Again, the network of hydrogen

bonds between the signal peptide and lipids included the hydroxyl group of S3 residue (Fig. S8B).

We performed simulations of the mutated pPilA1-S3G and compared the strength of interaction between the signal peptide and lipids with the simulation of WT pPilA1 (see Fig. S8C,D for initial positions). In both TM and POPC membranes, the number of hydrogen bonds per frame was higher for the WT protein (Fig. 8C). Notably, the interaction of the WT pPilA with POPC membrane surface specifically strengthened (8.6 H-bonds per frame) after the formation of a stable contact with phospholipids. In contrast, the interaction of the mutated signal peptide with POPC remained transient (2.8 H-bonds per frame; Fig. 8C) as documented also by the final position of the N-terminus extended above the membrane surface (Fig. 8D; Supplementary video S3,4).

Discussion

The lack of PilD protease is lethal for *Synechocystis* cells grown under photoautotrophic conditions (Fig. 3B), due to the inhibition of protein synthesis on membranes (Linhartová et al., 2014). It contrasts to no observable growth defects in heterotrophic bacteria with the inhibited activity of PilD (Pepe and Lory, 1998; Berry et al., 2019). Similarly, the accumulation of other types of prepilins involved in adhesion (Tomich et al., 2006), secretion (Pugsley, 1993), or in the formation of T- and F-pili (Lai et al., 2002; Jain et al., 2011) do not appear to be detrimental for the bacterial cell.

In heterotrophic bacteria, Type IV pilins are synthesized and located in the plasma membrane before they are extracted from the membrane and assembled into long pili fibres (Craig et al., 2019). However, the *Synechocystis* major pilin PilA1 was identified both in plasma and TMs (Pisareva et al., 2011; Selão et al., 2016). Molecular machinery dedicated for the maturation (PilD) and *O*-glycosylation of PilA1 should also be located in both the TM and plasma membrane; otherwise, these processes would not be fast enough to result in no detectable prepilin or PilA1^{n} in WT cells (Fig. 5). It is thus very unlikely that the presence of PilA1 in TMs results from a mistargeting into the plasma membrane. We speculate that the cyanobacterial Type IV pilins acquired a new function related to the photosynthetic membrane. This hypothesis is supported by specific defects in chlorophyll biosynthesis observed in *Synechocystis pilA1*/*pilA2* mutant (He and Vermaas, 1999).

The synthesis and maturation of major pilin in TM domains active in the biogenesis of photosynthetic apparatus could be the main reason, why the elimination of PilD is not tolerated in *Synechocystis*. In our previous work, we proposed that the pPilA1 protein, and particularly its non-glycosylated form, jams the SecY-YidC holotranslocons thereby triggering their degradation (Linhartová et al., 2014). As illustrated also in this work, the omission of glucose (suppressor effect of which is discussed later) from the growth medium of *pilD* has fast and destructive impact on the synthesis of membrane proteins. Complexes with a very fast turnover such as PSII are quickly depleted (Fig. 3C).

In the present work, we confirmed that the high rate of pPilA1 synthesis is responsible for the lethality of the *pilD* deletion. In rev1 and rev4 strains, the secondary mutations were localized in the alternative SigF sigma factor; rev4 contains also another mutation in the RNAP (Fig. 1). Interestingly, by lowering the content of *pilA1* mRNA to the WT level, as observed in rev1 and rev4 strains (Fig. 4B), the protein synthesis as well as the biogenesis of PSII, appears fully restored (Fig. 6B). Nonetheless, despite the comparable level of *pilA1* mRNA in rev1 and rev4 with WT, the radiolabelling or the accumulation of pPilA1 is quite low when compared with PilA1 (Fig. 5B; 6B). These data indicate that the fraction of the synthesized pPilA1 is quickly degraded, in line with our previous pulse-chase experiments (Linhartová et al., 2014). We assume that due to very intensive expression of the *pilA1* gene, the *pilD* mutant fails to degrade the synthesized prepilin fast enough to prevent the growth inhibition phenotype.

The suppressor mutations in SigF are worth a detailed description as the mutated SigF variants are functional (Fig. 4B). Because the structure of the cyanobacterial SigF has not been resolved yet, we constructed a SigF model using the *E. coli* RpoS-RNAS structure as a template (PDB code 5IPL; Liu et al., 2016; Fig. 2) The predicted structure of SigF resembles closely the structure of RpoS except the N-terminal σ 1.2 domain of RpoS, that is missing in group 3 sigma factors to which the SigF belongs (see Srivastava et al., 2020 for a recent review). The histidine (H45) residue in SigF is located at the position of Arg or Lys conserved in most sigma factors including RpoS (Fig. S2). This particular R/K charged residue (R107) is in contact with the DNA chain two nucleotides before the -10 element (Fig. 2; Liu et al., 2016). In contrast to the consensus cyanobacterial and *E. coli* -10 elements, the *pilA1* promoter contains a distinct -12 element (Asayama and Imamura, 2008). We, therefore, speculate that the H45P mutation impairs either the recognition of the *pilA1* promoter or the transcription initiation.

The arginine residue R211 in RpoS (R221C mutation in rev4), conserved in all types of bacterial sigma factors, is located in the domain σ4 which binds to the −35 element. Structural data for the contacts between RpoS and the −35 element are not available; nonetheless, it has been solved recently for the extracytoplasmic function (ECF) sigma factors SigH (Li et al., 2019). Structural alignment between SigF and SigH suggests that the R211 residue does not interact with DNA but might provide a contact with the RNAP core. In the rev4 strain, the other mutation is located in the γ subunit of RNAP core, close to the predicted interaction site (Fig. 2). Based on this *in silico* analysis, we propose that the rev4 mutations might lower the affinity of SigF to RNAP core. Intriguingly, rev4 mutations show no effect on the *pilA1* mRNA level in the presence of glucose (Fig. 4A). This finding implies an important effect of the trophic mode on the control over the *pilA1* expression.

Rev2 and rev3 mutations suppress the *pilD* deletion by a different mechanism than via inhibition of the *pilA1* expression (Fig. 4). The location of the rev3 mutation in the *pilA1* terminator (Fig. 1C) and the detection of a longer *pilA1* transcript in this strain (Fig. S4) prompted us to check the effect of the *pilA2* deletion on the PilA1 biosynthesis. The observed requirement of the PilA2 protein for the PilA1 glycosylation was unexpected since minor pilins have not been linked with the pilin glycosylation yet. Even more intriguing is the fact that the PilA2 prepilin is a functional protein in *pilD* (Fig. 7B); given the presence of highly conserved signal peptide in PilA2 (Linhartová et al., 2014), this protein is almost for sure matured by PilD.

The glycosylation of pPilA1 is very slow (Fig. 6B) and the pPilA1^{n} accumulates in the cell (Fig. 5). The recognition of pPilA1 as a substrate for *O*-glycosylation may be weak or the pPilA2 is much less efficient in promoting the pPilA glycosylation. We prefer the model that the rev3 mutation increases the level of pPilA2 thereby improving the rate of pPilA1 glycosylation. In rev3 about half of the pulse-labelled pPilA1 was glycosylated, while in the rev2 strain the pPilA1^{g} form was hardly detectable (Fig. 6B). Altogether our results suggest that the non-glycosylated pPilA1 is more deleterious than the pPilA1^{g}. In *Neisseria gonorrhoeae*, the lack of glycosylation of the major pilin protein causes a growth arrest and authors speculated that the unassembled (non-glycosylated) pilin protein disrupts essential processes in plasma membrane (Vik et al., 2012).

Our MD simulations show that the charged signal peptide of the prepilin interacts tightly with the membrane surface (Fig. 8) and the lateral diffusion of prepilin is likely much more restricted than that of the PilA1. As the mobility of membrane proteins can be facilitated by glycosylation (Hartel et al., 2016), we hypothesize that the pPilA1^{n} has an even stronger tendency than the pPilA1^{g} to accumulate in translocon-rich membrane domains. Nonetheless, the aberrant interaction between pPilA1 and SecY/YidC might not be so crucial to trigger translocon degradation as we proposed before (Linhartová et al., 2014). The pPilA1 is copurified with SecY from rev3 (Fig. 7C) and, although the protein synthesis in this strain is impaired (Fig. 6A), there is no sight of YidC degradation (Fig. 5B). More likely, just the high concentration of prepilins in biogenic membrane zones can attenuate the activity of translocons, the proteolytic degradation may be detectable only after a very high degree of inactivation. The S3G mutation in pPilA1 should facilitate the mobility of pilin within the membrane, particularly in phospholipid-rich domains (Fig. 8C). The mutated S3G prepilin seems also less stable, which further improves the viability of the rev2 strain.

The suppressor effect of glucose is probably pleiotropic. The external source of glucose seems to downregulate the *pilA1* expression in the *pilD* mutant (if judged from the ratio of *pilA1* mRNA in WT and *pilD*; Fig. 4) and accessible glucose may promote the prepilin glycosylation. In addition, mixotrophic metabolism enables to better cope with the lower content of membrane proteins; note that the protein labelling in *pilD* cells is weak even under Glc^{+} conditions (Fig. 6A).

Strong aggregation of pilin mutants under mixotrophic conditions is an interesting phenotype with a potential value for the cyanobacterial biotechnology. Aggregation disappeared in rev1 and rev4 strains harbouring the mutated *sigF* and the *sigF* deletion strain, used for this work, does not aggregate despite it does not produce the PilA1 protein (Fig. S3, Barker et al., 2006). Although the non-aggregation phenotype of *sigF* is inconsistent with the report of Flores et al. (2019); authors admit that their *sigF* mutant is derived from an aggregation-prone *Synechocystis* substrain. We can conclude that the absence of major pilin protein causes cell aggregation by a SigF-dependent mechanism, perhaps via secreted compounds (Flores et al., 2019).

Materials and methods

463 ***Synechocystis strains and cultivation***

464 Strains used in this study were derived from the *Synechocystis* GT-W substrain, *pilD* and
465 *pilA1*/*pilA2* mutant strains were described in (Linhartová et al., 2014) and the *sigF* mutant
466 in Barker et al. (2006). Photoautotrophic suppressor mutants of the *pilD* strain were
467 generated by cultivation on a BG-11 plate with 5 mM glucose for two weeks at normal light
468 intensity (40 μmol of photons m^{-2} s^{-1}) at 28 °C. For mixotrophic conditions (Glc^+), the BG-
469 11 medium was supplemented with 5 mM glucose. Liquid cultures were grown in
470 Erlenmeyer flasks under normal light at 28 °C on a rotary shaker (120 rpm). Mixotrophic
471 cultures were diluted daily with fresh Glc^+ medium and collected at OD_{730nm} of ~ 0.4. To
472 study the effects of photoautotrophic conditions (Glc^-), the cells grown in Glc^+ conditions
473 were harvested at 6000 rpm, washed, and diluted into fresh BG-11 medium without glucose
474 and then incubated at normal light for 48 h.

475

476 ***Whole-genome re-sequencing and variant detections***

477 DNA for genomic sequencing was isolated as described by Ermakova-Gerdes and Vermaas
478 (1999), with slight modifications. Briefly, the cells were washed by saturated NaI solution
479 and lysed by lysozyme and SDS. The lysate was treated with proteinase K, extracted with
480 phenol, phenol-chloroform (1:1) and chloroform and treated with RNase. The DNA was
481 precipitated with sodium acetate and ethanol, air-dried and resuspended in water.
482 *Synechocystis* re-sequencing was performed commercially at the Gene Profiling Facility,
483 Princess Margaret Hospital, Toronto. 100 bp paired-end sequencing was performed on an
484 Illumina HiSeq 2000 platform. The average sequencing depth was around 70. Reads were
485 mapped to the *Synechocystis* GT-S sequence (NC_017277) and the variants were called
486 using default settings of the Geneious 11.0 software (http://www.geneious.com). Only
487 variants with a higher than 60% frequency were considered.

488

489 ***Extraction of RNAs and Northern blotting***

490 Total RNA was isolated from cells (40 ml cultures at OD_{750nm} ~ 0.5) using a hot phenol
491 method according to Tyystjärvi et al. (2001), except that cell pellets were resuspended in
492 0.3 M sucrose and 10 mM sodium acetate (pH 4.5). Samples containing 3.75 μg total RNA
493 were denatured with glyoxal and separated on a 1.2% agarose gel in phosphate buffer and

transferred to Hybond-N membrane (Tyystjärvi et al., 2001). The *pilA1* and 16S rRNA genes were amplified from genomic DNA using *pilA1-f/pilA1-r* and *rrn-f* /*rrn-r* primers, respectively (Table S1). DNA fragments were labelled with α-dCTP 10 mCi/ml (Perkin Elmer) using the Prime-a-Gene Labeling System (Promega, USA) according to the manufacturer's instructions. The probes were purified using Illustra ProbeQuant G-50 Micro Columns (GE Healthcare). Membranes were prehybridized in 6 x SSC, 1 x Denhardt's , 0.1% SDS, 100 µl/ml herring sperm DNA at 67 °C for 1 h. A denatured *pilA* probe was added and hybridized at 67 °C overnight. Membranes were rinsed twice with 3 x SSC, 0.1% SDS and then washed twice for 10 min at 60 °C in 3 x SSC, 0.1% SDS and autoradiographed. The *pilA* probe was removed by washing the membrane three times with 0.5% SDS at 95 °C for 10 min and then reprobed with the 16S rRNA probe.

Protein isolation, electrophoresis, immunoblotting, and co-immunoprecipitation

About 100 mL of cells at an OD_{730nm} of ~0.4 were harvested by centrifugation at 6000 x *g* for 10 min at 4°C and pelleted cells were first washed with and then resuspended in buffer A (25 mM MES/NaOH, pH 6.5, 10 mM $MgCl_2$, 10 mM $CaCl_2$ and 25 % glycerol). Cells were mixed with 100-200 µm diameter glass beads in 1:1 ratio (1 volume of dense cell solution with 1 volume of glass beads) and broken (6 x 40 seconds) using a MiniBeadbeater 16 (Biospec, USA). To separate soluble and membrane fractions, samples were centrifuged at 30 000 x *g* for 15 min at 4 °C. Pelleted membranes were washed once with an excess of buffer A and then resuspended in 250 µL of buffer A. Chlorophyll concentration in the isolated membranes was measured spectrophotometrically according to Porra et al. (1989).

To detect the amount of PilA1 protein by immunoblotting, membrane proteins (contained 1 µg of chlorophyll) were solubilized with 2% SDS and 1% dithiothreitol (DTT) for 30 min at room temperature and separated on a 12 - 20% or 16 - 20% linear gradient SDS-PAGE gel containing 7 M urea (Komenda et al., 2019). The proteins were transferred to a PVDF membrane and the PilA1 protein was detected with a specific primary antibody raised against amino acids 147-160 of the PilA1 (prepared commercially by GenScript, USA). The antibody raised against the recombinant fragment R117-S384 of *Synechocystis* YidC was kindly provided by Prof. Jörg Nickelsen (Ludwig-Maximilians-University, Munich, Germany). The antibody against *Synechocystis* Ycf48 was kindly provided by Professor Peter Nixon (Imperial College, UK). The secondary antibody was conjugated with

horseradish peroxidase (Sigma, Germany) and the signal detected using Immobilon Crescendo substrate (Millipore, USA). Membrane proteins (each sample contained 1 or 4 µg of chlorophyll if not indicated otherwise) were solubilized with 2% SDS and 1% DTT for 30 min at room temperature and separated on a 16 - 20% linear gradient SDS-PAGE gel containing 7 M urea.

Analysis of membrane proteins (contained 4 µg of chlorophyll) under native conditions was performed by CN-PAGE as described by Komenda et al. (2019). Individual components of protein complexes were resolved by incubating the gel stripe from the first dimension in 2% (w/v) SDS and 1% (w/v) DTT for 30 min at room temperature, and proteins were separated along the second dimension by a gradient SDS-PAGE described above. Proteins were in-gel stained by SYPRO Orange (Sigma, Germany).

Co-immunoprecipitation was performed essentially as described in Linhartová et al. (2014). Briefly, the anti-SecY antibody was incubated overnight with membrane proteins isolated from the WT, *pilD* mutant and rev2 and rev3 strains grown with glucose, and then the antibody was immobilised on Protein A - Sepharose (Sigma, Germany). The resin was extensively washed and the remaining proteins were eluted in 1% SDS/DTT and 0,05% BFB Tris/sucrose buffer and separated by 12 - 20% linear gradient SDS-PAGE. The gel was blotted and probed with selected antibodies. The primary antibody against the *Synechocystis* SecY and SecE proteins were raised in rabbits using the synthetic peptide fragments containing amino acids 4-14 and 1-19, respectively.

Protein radiolabelling

For protein labelling, cell cultures containing 75 µg of chlorophyll mL^{-1} were incubated with a mixture of [35S]-Met and [35S]-Cys (Hartmann Analytics) at moderate light intensity (40 µmol of photons m^{-2} s^{-1}) at 28 °C; further details of the labelling procedure are described in Dobáková et al. (2009). 2D protein separation was performed as described above. The 2D gel was stained with SYPRO Orange, blotted onto a PVDF membrane and exposed to a phosphorimager plate (GE Healthcare, Austria) overnight and scanned by Storm 860 (GE Healthcare, Austria).

Molecular dynamics

The model of the thylakoid membrane, fully hydrated, with ions and equilibrated for 200 ns, has been described previously (Daskalakis, 2018). The structure of pPilA1 protein was modelled using iTASSER (Yang et al., 2015) with a C-score of = -1.3. Molecular dynamics simulations using the thylakoid membrane were performed using GROMACS version 2018.2 (SoftwareX, 2015, 1-2, 19-25), the AMBER03 protein forcefield (Duan et al., 2003) and the SPC water model. The protein was inserted into the membrane using Schrodinger's Maestro software, and the remaining preparation steps (solvent box generation and ion placement) were carried out with GROMACS. The system was minimized using steep descent until the maximum force in the system was below 400 kJ/mol/nm. Next, NVT equilibration was performed at 303 K for 20 ns followed by NPT equilibration at 303 K and 1 atm for 40 ns. Finally, 500 ns production simulations were performed with frames saved every 1 ns. In both equilibration phases, as well as the subsequent production simulation, the time step was 2 fs, since h-bonds were constrained using the LINCS algorithm. The temperature was controlled using a V-rescale thermostat in the NVT equilibration and Nose-Hoover thermostat in NPT and production phases. The pressure was controlled with a Parrinello-Rahman barostat. Electrostatics were taken into account using PME with 1.2 nm electrostatic and van der Waals cut-offs.

MD simulations with the POPC membrane were run using Desmond 2015.4, (Bowers et al., 2006) the OPLS2005 force field and the SPC water model. The protein was inserted into the membrane using Schrodinger's Maestro software, and the remaining preparation steps were performed with Desmond. The equilibration set-up was the default protocol for Desmond, consisting of: 1) Brownian Dynamics simulation in NVT at 10 K with restraints on solute heavy atoms for 100 ps, 2) NVT simulation at 10 K with restraints on solute heavy atoms for 12 ps, 3) NPT simulation at 10 K with restraints on solute heavy atoms for 12 ps, 4) NPT simulation at 300 K and 1 atm with restraints on solute heavy atoms for 12 ps, 5) NPT simulations at the same conditions with no restraints for 24 ps and 6) production NPT simulation at the same conditions with no restraints for 500 ns.

Acknowledgments

This work was supported by the Czech Science Foundation (project 19-29225X), T.T was supported by the Academy of Finland (265807).

Contribution

M.L., J.K. and R.S. were involved in the design of this study. M.L., P.S., K.H., M.T., J.K., J.Kn., J.F.G., V.G., T.T. and R.S. were involved in data acquisition and analysis. M.L., T.T. and R.S. wrote the manuscript.

We declare no competing interests.

596 **Table 1.** List of mutations identified by sequencing of *pilD* revertants. The nucleotide
597 position refers to the GT-S sequence (NC_017277) and gene ID corresponds to CyanoBase
598 (http://genome.microbedb.jp/cyanobase).

Strain	Start	Size	NT change	AA change	Gene ID	Gene product
rev1	3370196	1	A → C	H45P	*slr1564*	Sigma factor SigF
rev2	1296310	1	T → C	S3G	*sll1694*	Major pilin protein PilA1
rev3	1295748	1	G → A	-	*sll1694-sll1695* intergenic region	-
rev4	3370693	1	C → T	R211C	*slr1564*	Sigma factor SigF
rev4	1853201	1	G → A	E95K	*slr1265*	The γ subunit of the RNA polymerase

599

600

601

Figures

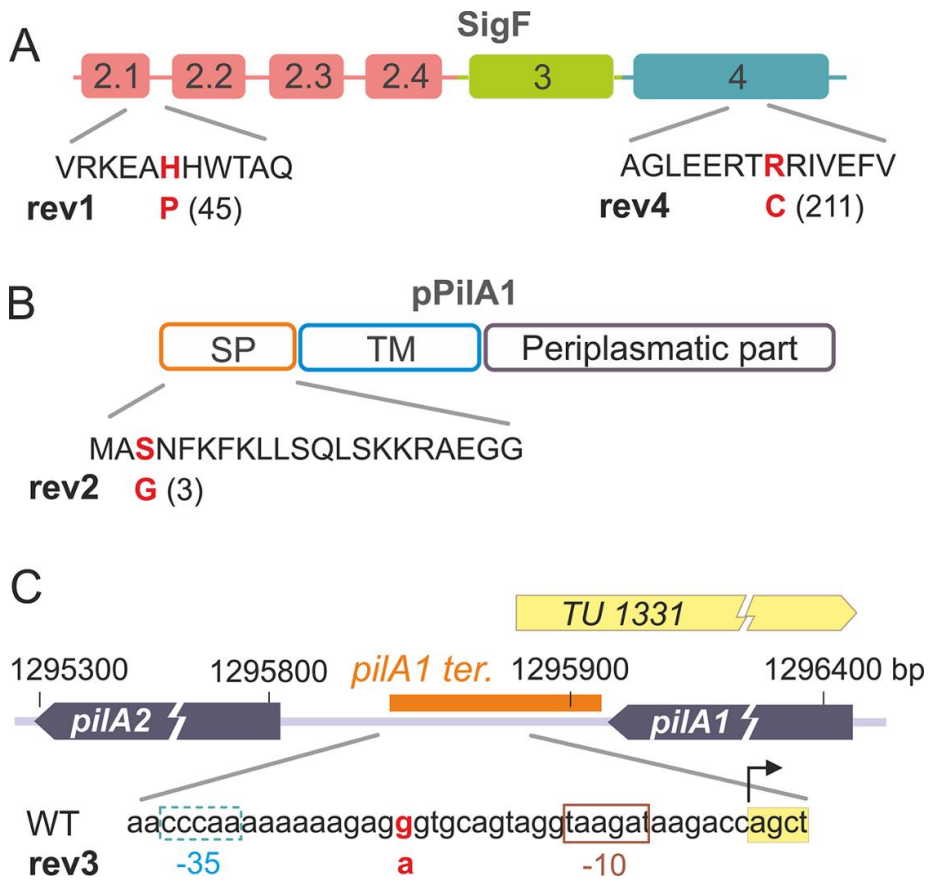

Figure 1. Overview of mutations that restore photoautotrophic growth of the *pilD* strain. A) Sigma factor SigF contains three main domains (σ2, σ3, σ4); the suppressor mutation in rev1 is located in the σ2.1 region, which interacts with TATA box of recognized genes. The SigF mutation found in rev4 strain is located in domain σ4, which typically interacts with the -35 segment of the promoter (see Fig. 2 for a structural model). Note that the rev4 strain contains another suppressor E95K mutation in the RNAP γ subunit. B) The mutation identified in the rev2 strain causes the S3G amino-acid substitution in the signal peptide of the PilA1 protein. C) The rev3 strain contains a point nucleotide substitution in the intergenic region between genes coding for the pilin proteins PilA1 and PilA2. Transcription unit TU1331 including its promoter (-10 and -35 elements) is depicted (Kopf et al., 2014) together with the predicted *pilA1* terminator (orange box; Hess, W. personal communication).

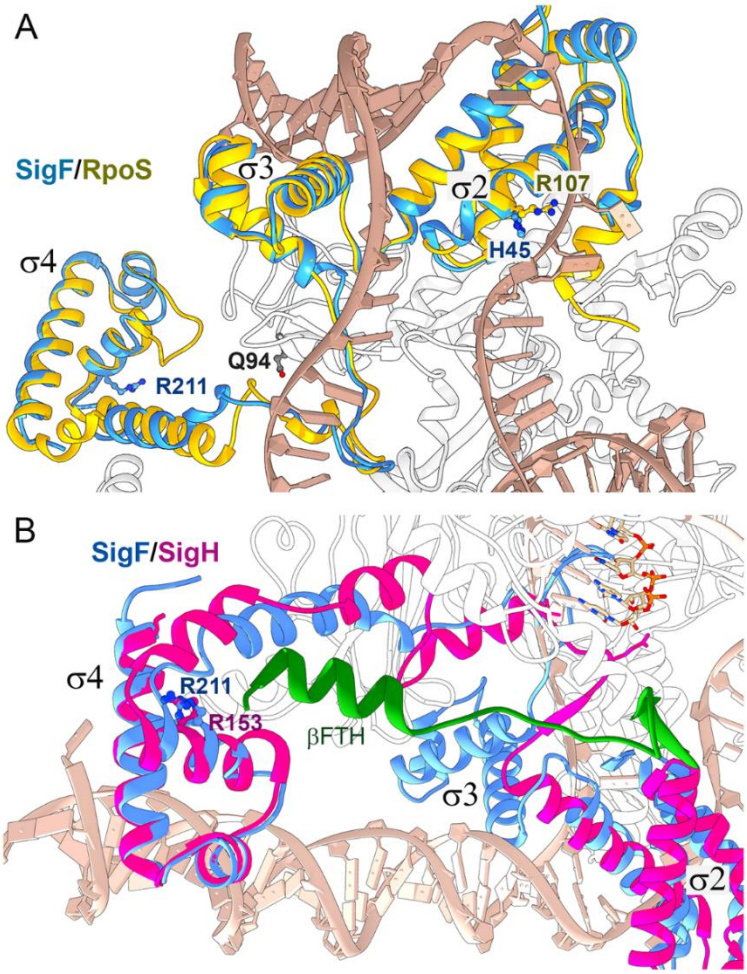

Figure 2. Structure alignment of the *Synechocystis* SigF with group 2 and ECF sigma factors bound in RNAP holoenzymes. A) The structure of *Synechocystis* SigF was predicted using I-TASSER (C-score = 0.98; Yang et al. 2015) and aligned with the crystal structure of the transcription initiation complex from *E. coli* containing RpoS (PDB code 5IPL; Liu et al., 2016) using Chimera software (Pettersen et al., 2004). RpoS is depicted in gold, SigF in blue, DNA in tan and the RNAP β' subunit in white. Residues in SigF that are mutated in rev1 and rev4 strains are shown in dark blue; Q94 corresponds to the E95 residue in the *Synechocystis* RNAP γ subunit. B) The predicted structure of SigF was aligned with the crystal structure of the RNAP-SigH transcription initiation complex from *Mycobacterium tuberculosis* (PDB code 6DV9; Li et al. 2019). ECF sigma factors lack the σ3 domain, however, the SigF R211 residue mutated in rev4 is highly conserved in ECF sigma factors (R153 in SigH, Li et al. 2019). SigH is depicted in magenta, SigF in blue, RNAP subunit β in white and the C-terminal flap-tip helix of the RNAP-β subunit (βFTH) in green (see Discussion for details).

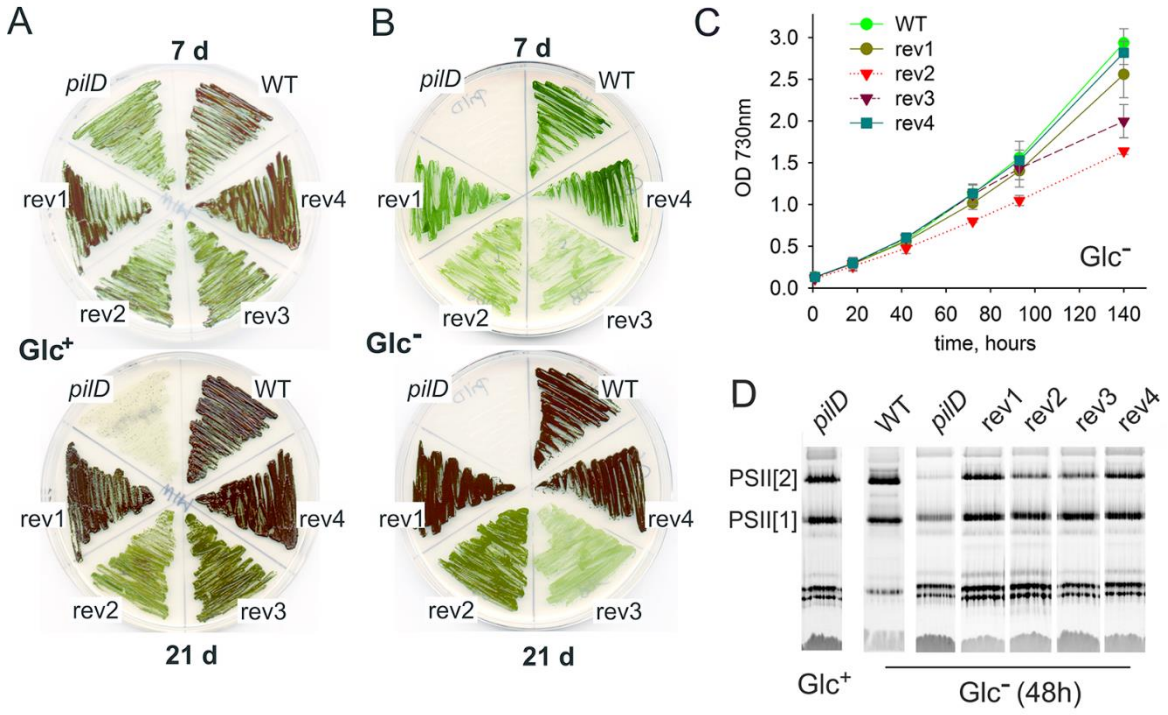

Figure 3. Characterization of spontaneous revertants derived from the *pilD* strain. A) Growth on agar plates was assessed for the WT, *pilD* mutant and the four isolated *pilD* revertants (rev1-4) at the 7th and 21st day of cultivation under mixotrophic conditions and (B) under photoautotrophic conditions. C) Photoautotrophic growth of the WT and rev1-4 strains. Cells were grown in liquid culture and optical density was monitored spectroscopically (see Fig. S1B for chlorophyll content). D) Membrane protein complexes, isolated from the WT and mutant strains grown for 48 h in Glc$^-$, were solubilized and separated by CN-PAGE. The loading corresponds to the same number of cells per lane based on OD_{730}; 4 µg of chlorophyll for WT. After separation, the gel was scanned (see Fig. S3) and PSII complexes were detected by chlorophyll fluorescence after excitation by blue light in LAS 4000 (Fuji). PSII[1] and PSII[2] indicates the monomeric and dimeric PSII, respectively.

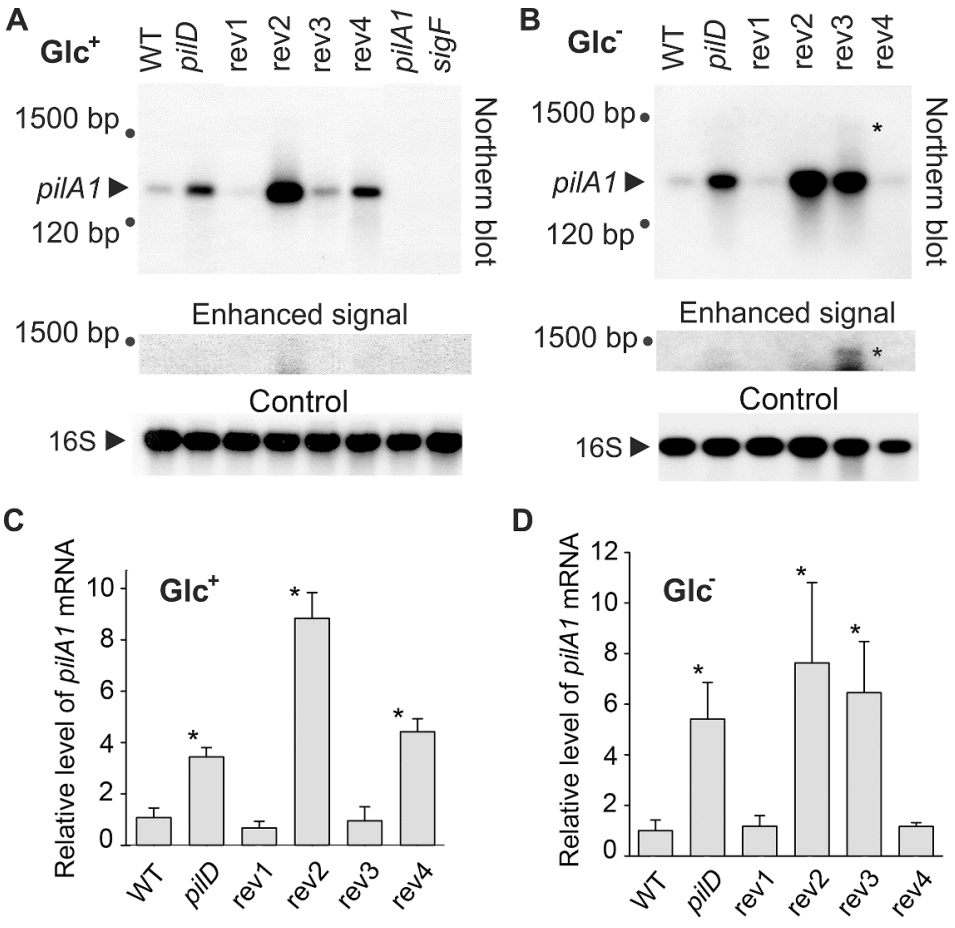

649

650 **Figure 4. Cellular levels of *pilA1* mRNA in WT, *pilD* mutant, and *pilD* revertant**
651 **strains.** RNA was isolated from WT and mutant cells that were grown for 2 days in the
652 presence (A) or absence (B) of glucose. RNA was blotted and hybridized sequentially with
653 radiolabeled probes against *pilA1* mRNA and 16S rRNA. An unknown larger transcript,
654 detected with the *pilA1* probe, is indicated by an asterisk. As the signal of this longer
655 transcript is much weaker than the signal of *pilA1*, an enhanced image of the upper part of
656 the membrane is also shown (see Fig. S5 for biological triplicate). *pilA1* and *sigF* mutants
657 were included as negative controls; 3.75 µg of total isolated RNA was loaded in each lane.
658 C) and D) Hybridization was repeated using independent cell cultures, the density of the
659 signals were quantified using ImageQuant TL 10 (GE Healthcare), normalized to the signal
660 of 16S RNA and plotted. The values represent means ± SD from three independent
661 measurements. Asterisks indicate statistically significant differences in the *pilA1* mRNA
662 levels between WT and other strains as tested using a paired Student's t-test (* $P < 0.05$).

663

664

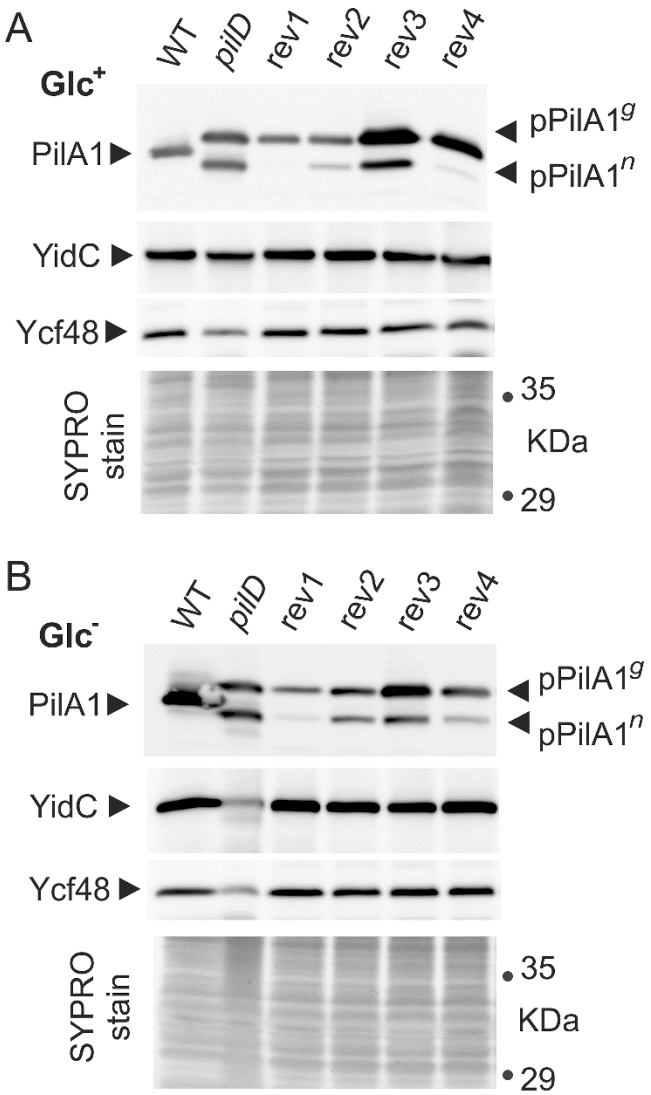

665

666 **Figure 5. Cellular levels of pPilA1^g and pPilA1^n proteins and the stability of YidC and**
667 **Ycf48 in the WT, *pilD* mutant, and *pilD* revertant strains.** Membrane proteins were
668 isolated from Glc^+ (A) and Glc^- conditions (B), separated by SDS electrophoresis and
669 blotted; the loading corresponded to the same number of cells based on OD_{730}. Pilin and
670 prepilin forms of PilA1, YidC insertase, and Ycf48 were immunodetected by specific
671 antibodies. The gel stained with SYPRO Orange before blotting is shown below the blot as
672 a loading control. pPilA1^g, pPilA1^n designate glycosylated and non-glycosylated prepilins,
673 respectively.

674

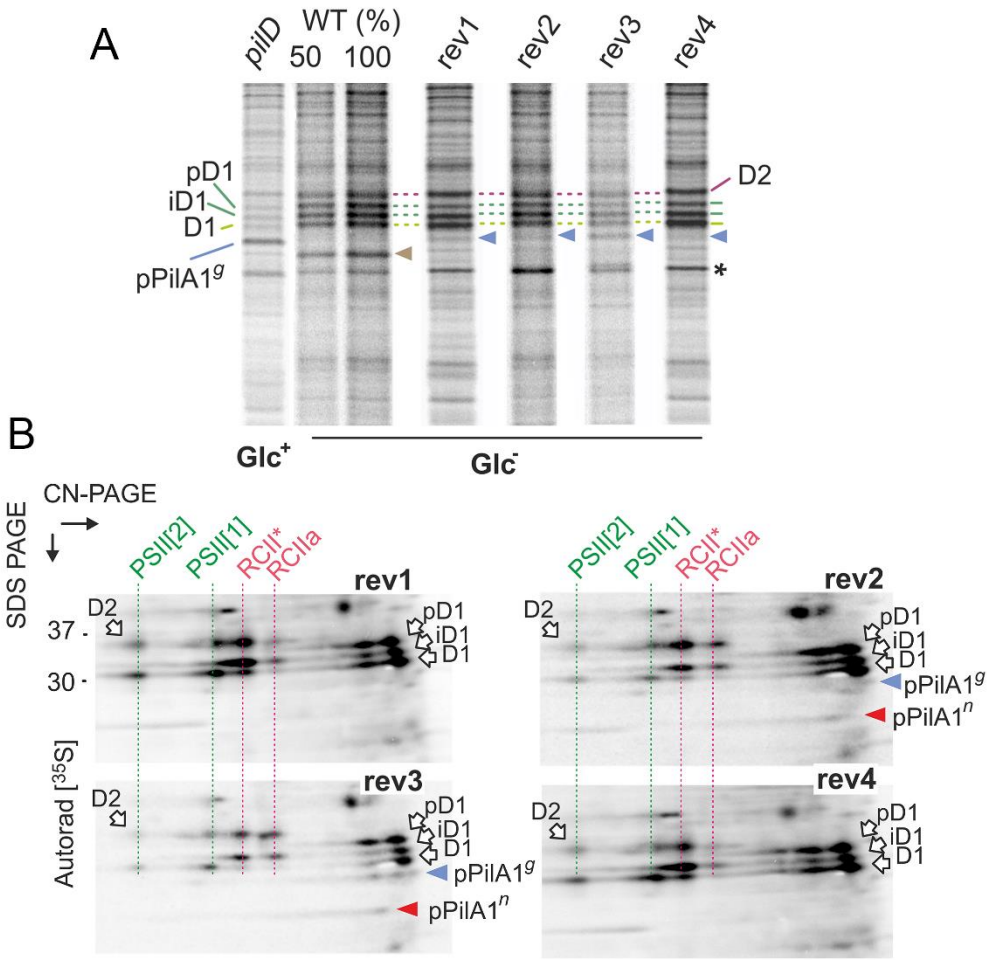

675

676 **Figure 6. Synthesis of prepilin and PSII complexes in WT, *pilD* mutant and *pilD***
677 **revertant strains**. A) WT and rev strains from Glc$^-$ conditions and the *pilD* (Glc$^+$) were
678 radiolabelled with a mixture of [^{35}S]Met/Cys using a 20-min pulse. Isolated membrane
679 proteins were separated by 16-20 % SDS-PAGE; 1 µg of chlorophyll was loaded for each
680 strain. The gels were stained with Coomassie Blue (Fig. S6), dried, and the labelled proteins
681 were detected by phosphorimaging. The signal of pPilA^g is indicated by a blue arrowhead,
682 all three forms of radiolabelled D1 subunit are marked by green dashed lines; pD1 and iD1
683 indicate unprocessed and partially processed forms of the D1 subunit. D2 subunit is marked
684 by a purple dashed line; brown arrowhead indicates the signal of radiolabelled PilA1
685 proteins in WT. Asterisk indicates an intensively labelled band that has the same mobility
686 in the gel as the pPilA^n. B) The radiolabelled rev1-4 samples (4 µg of chlorophyll) were
687 separated by 2D CN/SDS-PAGE, stained by SYPRO Orange stain (see Fig. S7 for the
688 stained gels) and blotted onto a PVDF membrane. The labelled proteins were detected by
689 phosphorimaging. Dashed red lines highlight PSII assembly intermediates RCIIa and
690 RCII* (Bečková et al., 2017), green lines highlight labelled PSII subunits assembled into

monomeric and dimeric PSII. The signals of pPilA^{g} and pPilA^{n} are indicated by blue and red arrowheads, respectively.

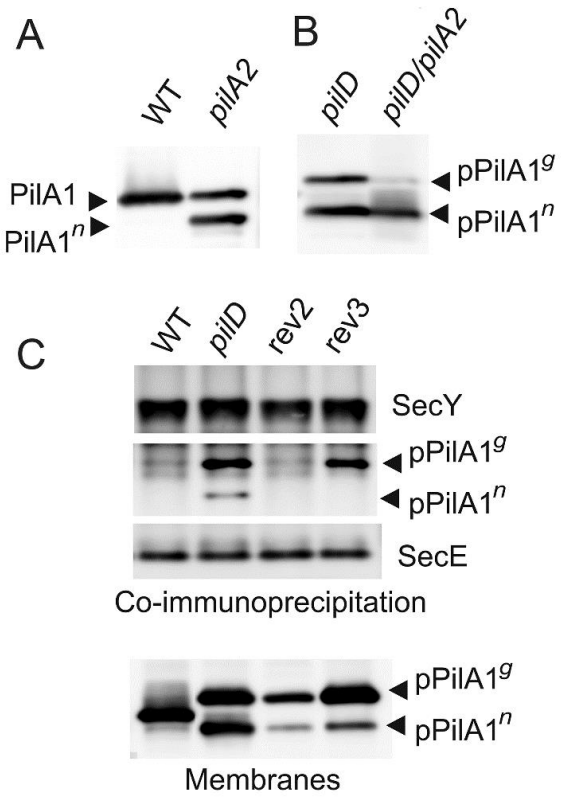

Figure 7. The role of PilA2 in the PilA1 biogenesis and the co-immunoprecipitation of the SecY translocase with prepilin. A) Immunodetection of PilA1 in membrane proteins isolated from WT and *pilA2* cells grown under Glc^{-} conditions. Membrane proteins were separated by SDS-PAGE and blotted; PilA1^{n} indicates a putative non-glycosylated form of PilA1. B) Immunodetection of pPilA1 in separated membrane proteins from *pilD* and *pilD*/*pilA2* cells. Both strains were grown in Glc^{+} conditions. C) The anti-SecY antibody was incubated with membrane proteins isolated from the WT, *pilD* mutant and rev2 and rev3 strains grown in Glc^{+} conditions and then immobilised on Protein A - Sepharose (Sigma, Germany), eluted in SDS buffer, and separated by SDS-PAGE. The gel was blotted and probed with anti-SecY and anti-PilA1 antibodies; the anti-SecE antibody was re-probed as a control. The level of PilA1 forms is also shown for the identical membrane samples to those used for the co-immunoprecipitation.

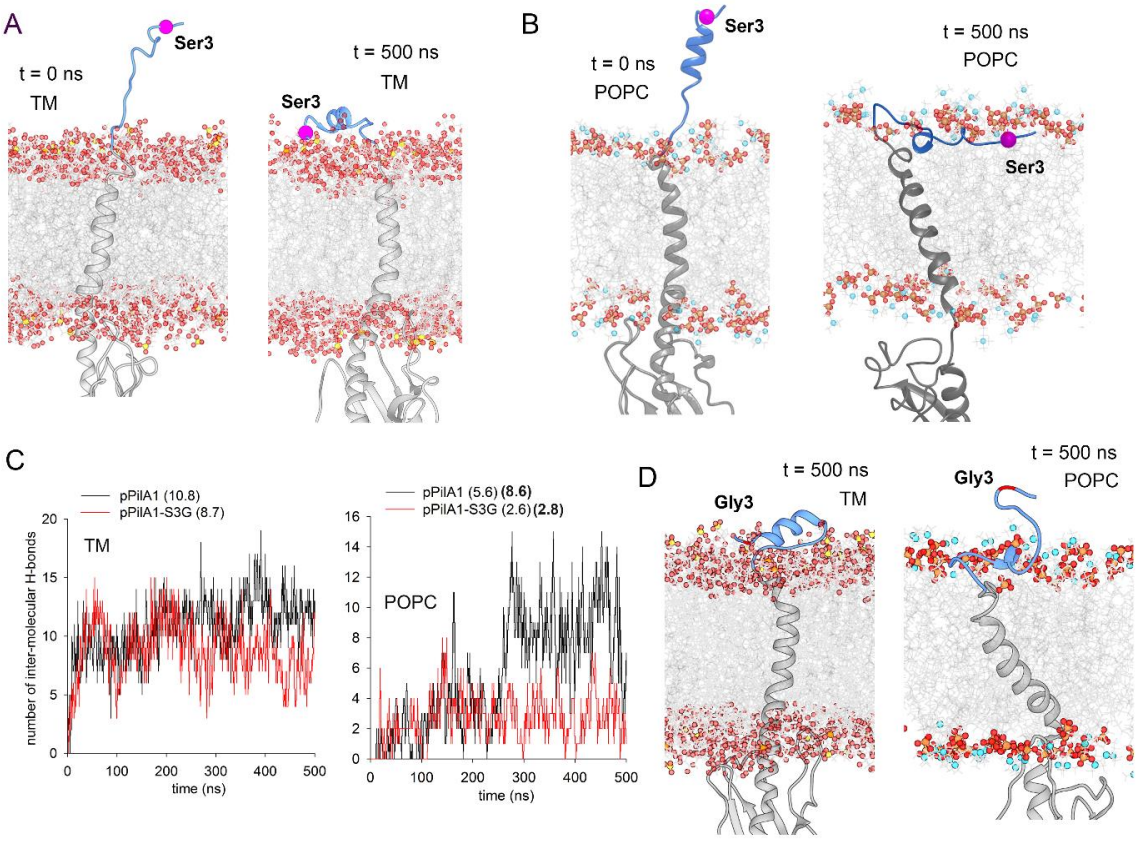

Figure 8. **MD simulations of the *Synechocystis* pPilA1 and pPilA1-S3G proteins in a membrane bilayer**. A) Snapshots of the initial (0 ns) and the representative final (500 ns) conformation of pPilA1 in the TM (video S1). The signal peptide of pPilA1 is depicted in blue, the rest of the protein in grey. Oxygen atoms in lipid molecules are shown as red spheres, sulphur (in SQDG) as yellow spheres, phosphate atoms as orange spheres and nitrogen atoms (in POPC) as blue spheres. The position of Ser3 is highlighted by a magenta ball. Water molecules were omitted for clarity. B) A snapshot of the initial (0 ns) and representative final (500 ns) positions of pPilA1 in the POPC bilayer (video S2). C) Number of intermolecular hydrogen bonds between the pPilA1 signal peptide and TM or POPC lipid molecules for each frame (0-500 ns) of the MD simulation compared with the pPilA1-S3G**.** Numbers in parentheses indicate an average number of hydrogen bonds per frame formed during the simulation, numbers in bold show the number of hydrogen bonds for the period between 250-500 ns. See Fig. S8A, B for the description of hydrogen bonds between the lipid polar region and the pPilA1 signal peptide. D) A representative final

positions of PilA1-SG3 in the TM and POPC bilayer (video S3 and S4); see also Fig. S8C,D for the initial positions of the pPilA-S3G mutant protein.

Literature

Asayama, M., and Imamura, S. (2008). Stringent promoter recognition and autoregulation by the group 3 sigma-factor SigF in the cyanobacterium *Synechocystis* sp. strain PCC 6803. Nucleic Acids Res **36:** 5297-5305.

Barker, M., de Vries, R., Nield, J., Komenda, J., and Nixon, P.J. (2006). The Deg proteases protect *Synechocystis* sp PCC 6803 during heat and light stresses but are not essential for removal of damaged D1 protein during the photosystem two repair cycle. J Biol Chem **281:** 30347-30355.

Bečková, M., Gardian, Z., Yu, J., Koník, P., Nixon, P.J., and Komenda, J. (2017). Association of Psb28 and Psb27 proteins with PSII-PSI supercomplexes upon exposure of *Synechocystis* sp. PCC 6803 to high light. Mol Plant **10:** 62-72.

Berry, J.L., Gurung, I., Anonsen, J.H., Spielman, I., Harper, E., Hall, A.M.J., Goosens, V.J., Raynaud, C., Koomey, M., Biais, N., Matthews, S., and Pelicic, V. (2019). Global biochemical and structural analysis of the type IV pilus from the Gram-positive bacterium *Streptococcus sanguinis*. J Biol Chem **294:** 6796-6808.

Bowers, K.J., Chow, E., Xu, H., Dror, R.O., Eastwood, M.P., Gregersen, B.A., Klepeis, J.L., Kolossvary, I., Moraes, M.A., Sacerdoti, F.D., Salmon, J.K., Shan, Y., and Shaw, D.E. (2006). Scalable algorithms for molecular dynamics simulations on commodity clusters. In International conference for high performance computing, networking, storage and analysis (Tampa, Florida: Machinery, New York, USA), pp. 84-es.

Bučinská, L., Kiss, E., Koník, P., Knoppová, J., Komenda, J., and Sobotka, R. (2018). The ribosome-bound protein Pam68 promotes insertion of chlorophyll into the CP47 subunit of photosystem II. Plant Physiol **176:** 2931-2942.

Conradi, F.D., Zhou, R.Q., Oeser, S., Schuergers, N., Wilde, A., and Mullineaux, C.W. (2019). Factors controlling floc formation and structure in the cyanobacterium *Synechocystis* sp. strain PCC 6803. J Bacteriol **201:** e00344-00319.

Craig, L., Forest, K.T., and Maier, B. (2019). Type IV pili: dynamics, biophysics and functional consequences. Nat Rev Microbiol **17:** 429-440.

Crane, J.M., and Randall, L.L. (2017). The Sec system: protein export in *Escherichia coli*. EcoSal Plus **7**.

Daskalakis, V. (2018). Protein-protein interactions within photosystem II under photoprotection: the synergy between CP29 minor antenna, subunit S (PsbS) and zeaxanthin at all-atom resolution. Phys Chem Chem Phys **20:** 11843-11855.

Dobáková, M., Sobotka, R., Tichý, M., and Komenda, J. (2009). Psb28 protein is involved in the biogenesis of the photosystem II inner antenna CP47 (PsbB) in the cyanobacterium *Synechocystis* sp. PCC 6803. Plant Physiol **149:** 1076-1086.

Duan, Y., Wu, C., Chowdhury, S., Lee, M.C., Xiong, G., Zhang, W., Yang, R., Cieplak, P., Luo, R., Lee, T., Caldwell, J., Wang, J., and Kollman, P. (2003). A point-charge force field for molecular mechanics simulations of proteins based on condensed-phase quantum mechanical calculations. J Comput Chem **24:** 1999-2012.

Ermakova-Gerdes, S., and Vermaas, W.F.J. (1999). Inactivation of the open reading frame *slr0399* in *Synechocystis* sp. PCC 6803 functionally complements mutations near the Q(A) niche of photosystem II. A possible role of Slr0399 as a chaperone for quinone binding. J Biol Chem **274:** 30540-30549.

Flores, C., Santos, M., Pereira, S.B., Mota, R., Rossi, F., De Philippis, R., Couto, N., Karunakaran, E., Wright, P.C., Oliveira, P., and Tamagnini, P. (2019). The alternative sigma factor SigF is a key player in the control of secretion mechanisms in *Synechocystis* sp. PCC 6803. Environ Microbiol **21:** 343-359.

Giltner, C.L., Nguyen, Y., and Burrows, L.L. (2012). Type IV pilin proteins: versatile molecular modules. Microbiol Mol Biol Rev **76:** 740-772.

Goosens, V.J., Busch, A., Georgiadou, M., Castagnini, M., Forest, K.T., Waksman, G., and Pelicic, V. (2017). Reconstitution of a minimal machinery capable of assembling periplasmic type IV pili. Proc Natl Acad Sci U S A **114:** E4978-E4986.

Hartel, A.J., Glogger, M., Jones, N.G., Abuillan, W., Batram, C., Hermann, A., Fenz, S.F., Tanaka, M., and Engstler, M. (2016). N-glycosylation enables high lateral mobility of GPI-anchored proteins at a molecular crowding threshold. Nat Commun **7:** 12870.

He, Q., and Vermaas, W.F.J. (1999). Genetic deletion of proteins resembling Type IV pilins in *Synechocystis* sp. PCC 6803: their role in binding or transfer of newly synthesized chlorophyll. Plant Mol Biol **39:** 1175-1188.

Hu, J., Xue, Y., Lee, S., and Ha, Y. (2011). The crystal structure of GXGD membrane protease FlaK. Nature **475:** 528-531.

Jain, S., Kahnt, J., and van der Does, C. (2011). Processing and maturation of the pilin of the type IV secretion system encoded within the gonococcal genetic island. J Biol Chem **286:** 43601-43610.

Kim, Y.H., Kim, J.Y., Kim, S.Y., Lee, J.H., Lee, J.S., Chung, Y.H., Yoo, J.S., and Park, Y.M. (2009). Alteration in the glycan pattern of pilin in a nonmotile mutant of *Synechocystis* sp. PCC 6803. Proteomics **9:** 1075-1086.

Komenda, J., Krynická, V., and Zakar, T. (2019). Isolation of thylakoid membranes from the cyanobacterium *Synechocystis* sp. PCC 6803 and analysis of their photosynthetic pigment-protein complexes by clear native-PAGE. Bio-protocol **9:** e3126.

Kopečná, J., Pilný, J., Krynická, V., Tomčala, A., Kis, M., Gombos, Z., Komenda, J., and Sobotka, R. (2015). Lack of phosphatidylglycerol inhibits chlorophyll biosynthesis at multiple sites and limits chlorophyllide reutilization in the cyanobacterium *Synechocystis* 6803. Plant Physiol **169:** 1307-1317.

Kopf, M., Klähn, S., Scholz, I., Matthiessen, J.K.F., Hess, W.R., and Voß, B. (2014). Comparative analysis of the primary transcriptome of *Synechocystis* sp. PCC 6803. DNA Research **21:** 527-539.

Lai, E.M., Eisenbrandt, R., Kalkum, M., Lanka, E., and Kado, C.I. (2002). Biogenesis of T pili in *Agrobacterium tumefaciens* requires precise VirB2 propilin cleavage and cyclization. J Bacteriol **184:** 327-330.

LaPointe, C.F., and Taylor, R.K. (2000). The type 4 prepilin peptidases comprise a novel family of aspartic acid proteases. J Biol Chem **275:** 1502-1510.

Li, L., Fang, C., Zhuang, N., Wang, T., and Zhang, Y. (2019). Structural basis for transcription initiation by bacterial ECF sigma factors. Nat Commun **10:** 1153.

Li, X., Dang, S., Yan, C., Gong, X., Wang, J., and Shi, Y. (2013). Structure of a presenilin family intramembrane aspartate protease. Nature **493:** 56-61.

Linhartová, M., Bučinská, L., Halada, P., Ječmen, T., Šetlík, J., Komenda, J., and Sobotka, R. (2014). Accumulation of the Type IV prepilin triggers degradation of SecY and YidC and inhibits synthesis of Photosystem II proteins in the cyanobacterium *Synechocystis* PCC 6803. Mol Microbiol **93:** 1207-1223.

Liu, B., Zuo, Y., and Steitz, T.A. (2016). Structures of *E. coli* sigmaS-transcription initiation complexes provide new insights into polymerase mechanism. Proc Natl Acad Sci U S A **113:** 4051-4056.

Marceau, M., Forest, K., Béretti, J.-L., Tainer, J., and Nassif, X. (1998). Consequences of the loss of O-linked glycosylation of meningococcal type IV pilin on piliation and pilus-mediated adhesion. Mol Microbiol **27:** 705-715.

Pepe, J.C., and Lory, S. (1998). Amino acid substitutions in PilD, a bifunctional enzyme of *Pseudomonas aeruginosa*: Effect on leader peptidase and n-methyltransferase activities in vitro and in vivo. J Biol Chem **273:** 19120-19129.

Pettersen, E.F., Goddard, T.D., Huang, C.C., Couch, G.S., Greenblatt, D.M., Meng, E.C., and Ferrin, T.E. (2004). UCSF Chimera--a visualization system for exploratory research and analysis. J Comput Chem **25:** 1605-1612.

Pisareva, T., Kwon, J., Oh, J., Kim, S., Ge, C.R., Wieslander, A., Choi, J.S., and Norling, B. (2011). Model for membrane organization and protein sorting in the cyanobacterium *Synechocystis* sp PCC 6803 inferred from proteomics and multivariate sequence analyses. J Proteome Res **10:** 3617-3631.

Porra, R.J., Thompson, W.A., and Kriedemann, P.E. (1989). Determination of accurate extinction coefficients and simultaneous equations for assaying chlorophylls *a* and *b* extracted with four different solvents: verification of the concentration of chlorophyll standards by atomic absorption spectroscopy. Biochim Biophys Acta **975:** 384-394.

Pugsley, A.P. (1993). Processing and methylation of PulG, a pilin-like component of the general secretory pathway of *Klebsiella oxytoca*. Mol Microbiol **9:** 295-308.

Sachelaru, I., Winter, L., Knyazev, D.G., Zimmermann, M., Vogt, A., Kuttner, R., Ollinger, N., Siligan, C., Pohl, P., and Koch, H.-G. (2017). YidC and SecYEG form a heterotetrameric protein translocation channel. Scientific Reports **7:** 101.

Schuergers, N., and Wilde, A. (2015). Appendages of the cyanobacterial cell. Life **5:** 700-715.

Selão, T.T., Zhang, L., Knoppova, J., Komenda, J., and Norling, B. (2016). Photosystem II assembly steps take place in the thylakoid membrane of the cyanobacterium *Synechocystis* sp. PCC6803. Plant Cell Physiol **57:** 95-104.

Srivastava, A., Summers, M.L., and Sobotka, R. (2020). Cyanobacterial sigma factors: Current and future applications for biotechnological advances. Biotechnol Adv **40:** 107517.

Strom, M.S., Nunn, D.N., and Lory, S. (1993). A single bifunctional enzyme, PilD, catalyzes cleavage and N-methylation of proteins belonging to the type IV pilin family. Proc Natl Acad Sci USA **90:** 2404-2408.

Tajima, N., Sato, S., Maruyama, F., Kaneko, T., Sasaki, N.V., Kurokawa, K., Ohta, H., Kanesaki, Y., Yoshikawa, H., Tabata, S., Ikeuchi, M., and Sato, N. (2011). Genomic structure of the cyanobacterium *Synechocystis* sp. PCC 6803 strain GT-S. DNA Research **18:** 393-399.

Tichý, M., Bečková, M., Kopečná, J., Noda, J., Sobotka, R., and Komenda, J. (2016). Strain of *Synechocystis* PCC 6803 with aberrant assembly of photosystem II contains tandem duplication of a large chromosomal region. Front Plant Sci **7:** 648.

Tomich, M., Fine, D.H., and Figurski, D.H. (2006). The TadV protein of *Actinobacillus actinomycetemcomitans* is a novel aspartic acid prepilin peptidase required for maturation of the Flp1 pilin and TadE and TadF pseudopilins. J Bacteriol **188:** 6899-6914.

Tyystjärvi, T., Herranen, M., and Aro, E.M. (2001). Regulation of translation elongation in cyanobacteria: membrane targeting of the ribosome nascent‐chain complexes controls the synthesis of D1 protein. Mol Microbiol **40:** 476-484.

Vik, Å., Aspholm, M., Anonsen, J.H., Børud, B., Roos, N., and Koomey, M. (2012). Insights into type IV pilus biogenesis and dynamics from genetic analysis of a C-terminally tagged pilin: a role for O-linked glycosylation. Mol Microbiol **85:** 1166-1178.

Yang, J., Yan, R., Roy, A., Xu, D., Poisson, J., and Zhang, Y. (2015). The I-TASSER Suite: protein structure and function prediction. Nat Methods **12:** 7-8.

Yu, J., Knoppová, J., Michoux, F., Bialek, W., Cota, E., Shukla, M.K., Strašková, A., Pascual Aznar, G., Sobotka, R., Komenda, J., Murray, J.W., and Nixon, P.J. (2018). Ycf48 involved in the biogenesis of the oxygen-evolving photosystem II complex is a seven-bladed beta-propeller protein. Proc Natl Acad Sci USA **115:** E7824-E7833.

SUPPLEMENTARY FIGURES

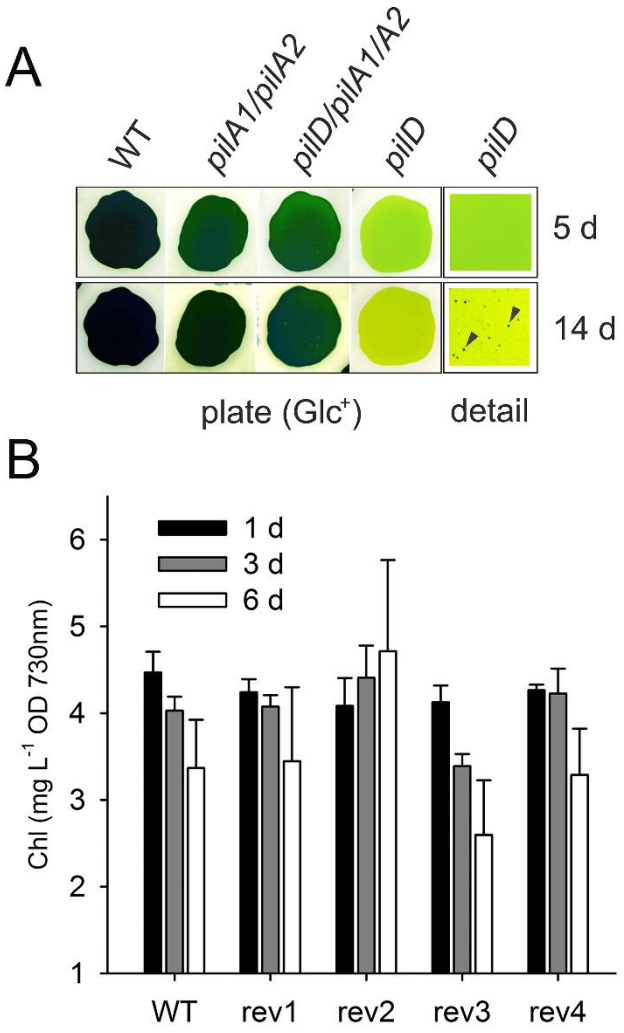

Figure S1. **Generation of *pilD* suppressor mutations and chlorophyll content in suppressor strains.** A) The originally isolated *pilD* mutants together with the WT, *pilA1/pilA2* and, *pilD/pilA1/pilA2* strain (Linhartová et al. 2014) were streaked onto BG-11 plate and cultivated under mixotrophic conditions. Pictures of the strains were taken on the 5th (5 d) and 14th (14 d) day of cultivation; arrowheads indicate suppressor mutants. B) Cellular chlorophyll content was measured during photoautotrophic cultivation of WT and rev1-4 strains (see also Fig. 3B). The chlorophyll content was measured spectrophotometrically at days 1, 3, and 6 and normalized to optical density at 730 nm.

Figure S2. Amino-acid sequence alignment of the N-terminal part of cyanobacterial group 3 sigma factors (SigF and SigJ). The red triangle shows the position of the rev1 mutation in *Synechocystis* SigF (*slr1564*). The asterisks designate fully conserved amino acid residues and double and single dots strongly and weakly-conserved residues, respectively *E. coli* RpoS is included as an example of group 2 sigma factors. Gene sources: *alr0277*, *all3853* - *Anabaena* PCC 7120; *ava_3085*, *ava_1844* - *Anabaena variabilis* ATCC 29413; *Npun_R1337*, *Npun_F4811* - *Nostoc punctiforme* ATCC 29133; *Synpcc7942_1784*, *Synpcc7942_1510* - *Synechococcus elongatus* PCC 7942; *MAE52920* - *Microcystis aeruginosa* NIES-843; *SYNPCC7002_A1924* - *Synechococcus elongatus* PCC 7002; *tlr0738* - *Thermosynechococcus elongatus* BP-1.

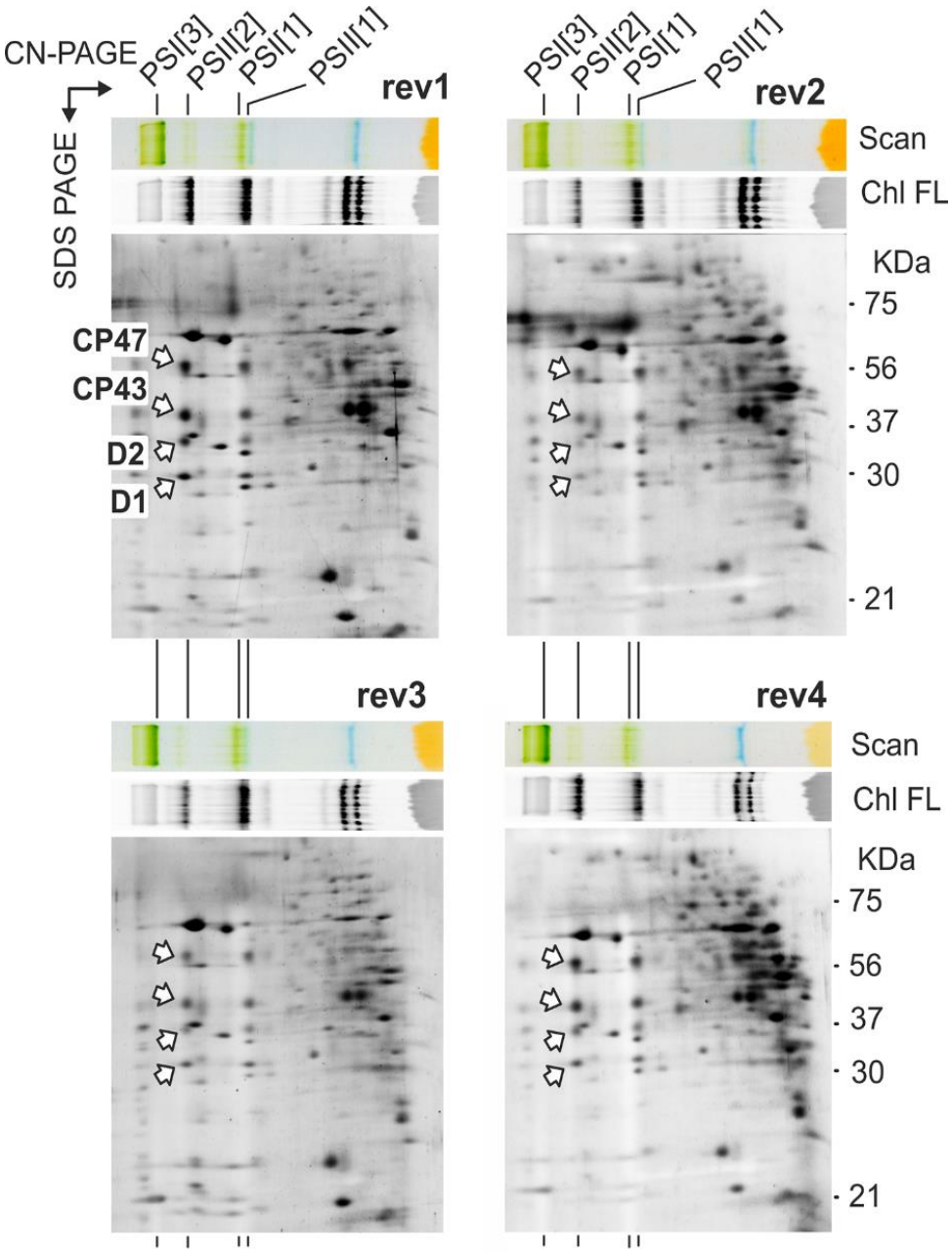

Figure S3. **2D CN/SDS-PAGE of membrane protein complexes isolated from *pilD* suppressor strains.** Suppressor strains (rev1-4) were grown for 48 h in the absence of Glc. Isolated membranes were solubilized and separated by CN-PAGE on the same gel (see Fig. 3C); 4 µg of Chl was loaded for each strain, and then the gel stripes were cut individually and separated in pairs (rev1 and rev2, rev3 and rev4) in the same gels in the second dimension by 12-20 % SDS-PAGE. The gel was stained with SYPRO Orange; core large subunits of PSII in dimeric complexes are indicated. PSI[3] is the trimer of PSI, PSI[1] is the monomer of PSI, PSII[2] is the dimer of PSII and PSII[1] is the monomer of PSII. White arrows indicate CP47, CP43, D2, and D1 subunits of PSII.

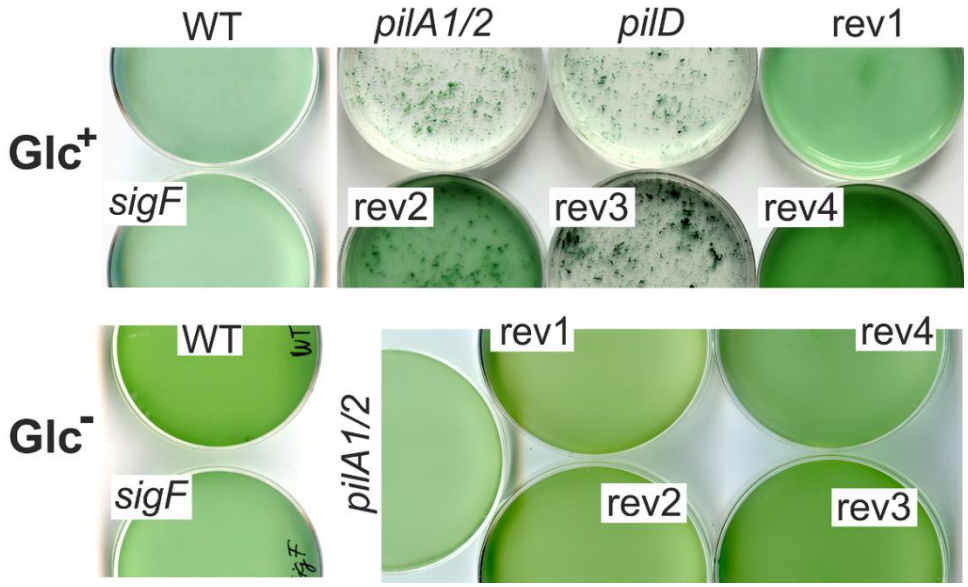

Figure S4. **Aggregation of pilin lacking cells and *pilD* suppressor strains.** Cells were grown in liquid cultures in Erlenmeyer flasks on a rotary shaker at 120 rpm in mixotrophic (Glc^+) and photoautotrophic (Glc^-) conditions. Cultures were then transferred to Petri dishes only for taking documentation.

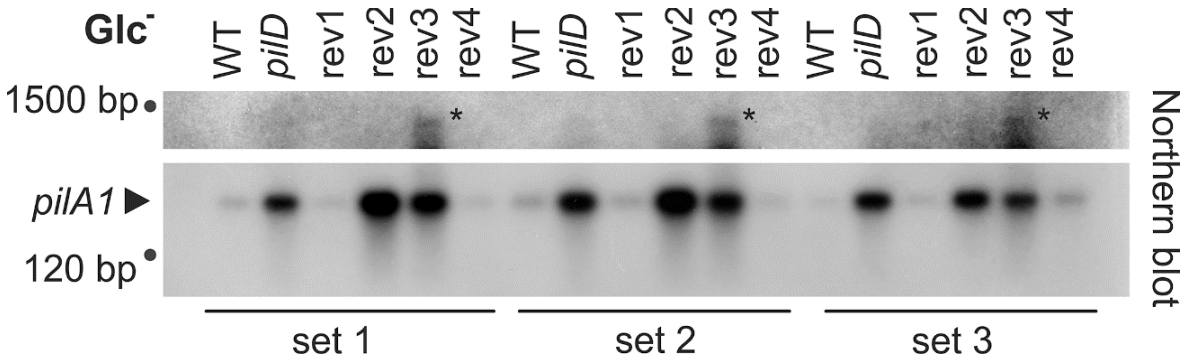

Figure S5. **Cellular levels of *pilA1* mRNA in the *pilD* revertant strains.** A) RNA was isolated from WT and mutant cells which were grown for 2 days in the absence of glucose (Glc^-); sets 1-3 represent three independent biological replicates. RNA was blotted and hybridized with a radiolabeled probe against *pilA1* mRNA. The intensity of the upper part of the radiogram was enhanced to visualize the signal of a longer RNA molecule hybridizing with the *pilA1* probe. See Fig. 3 for further details.

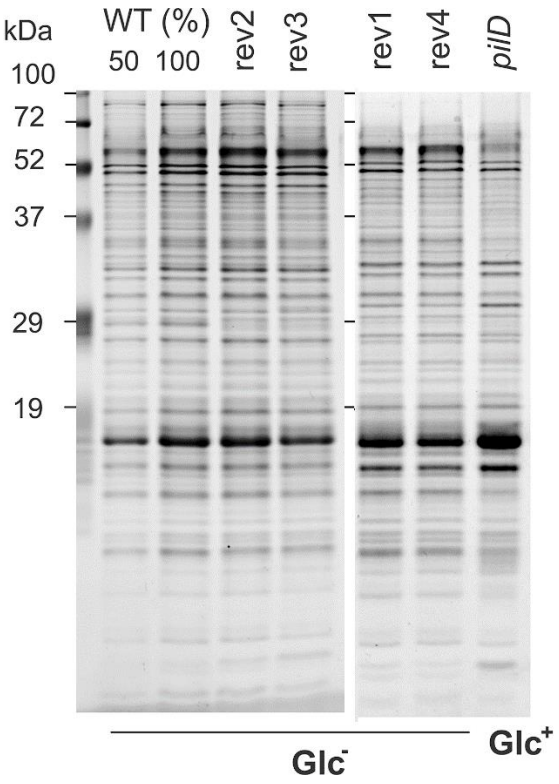

Figure S6. **SDS-PAGE of membrane proteins isolated from WT, the *pilD* mutant, and the *pilD* suppressor strains**. All strains were grown under Glc^- conditions except *pilD* that was grown mixotrophically. Cells were radiolabeled with a mixture of [^{35}S]Met/Cys using a 20-min pulse (see Fig. 6A). Isolated membranes were solubilized and proteins corresponding to 1 µg of Chl separated in 16-20 % SDS-PAGE gels. The gel was stained with Commassie blue. Please note that the order of samples is different than is presented in Fig. 6A.

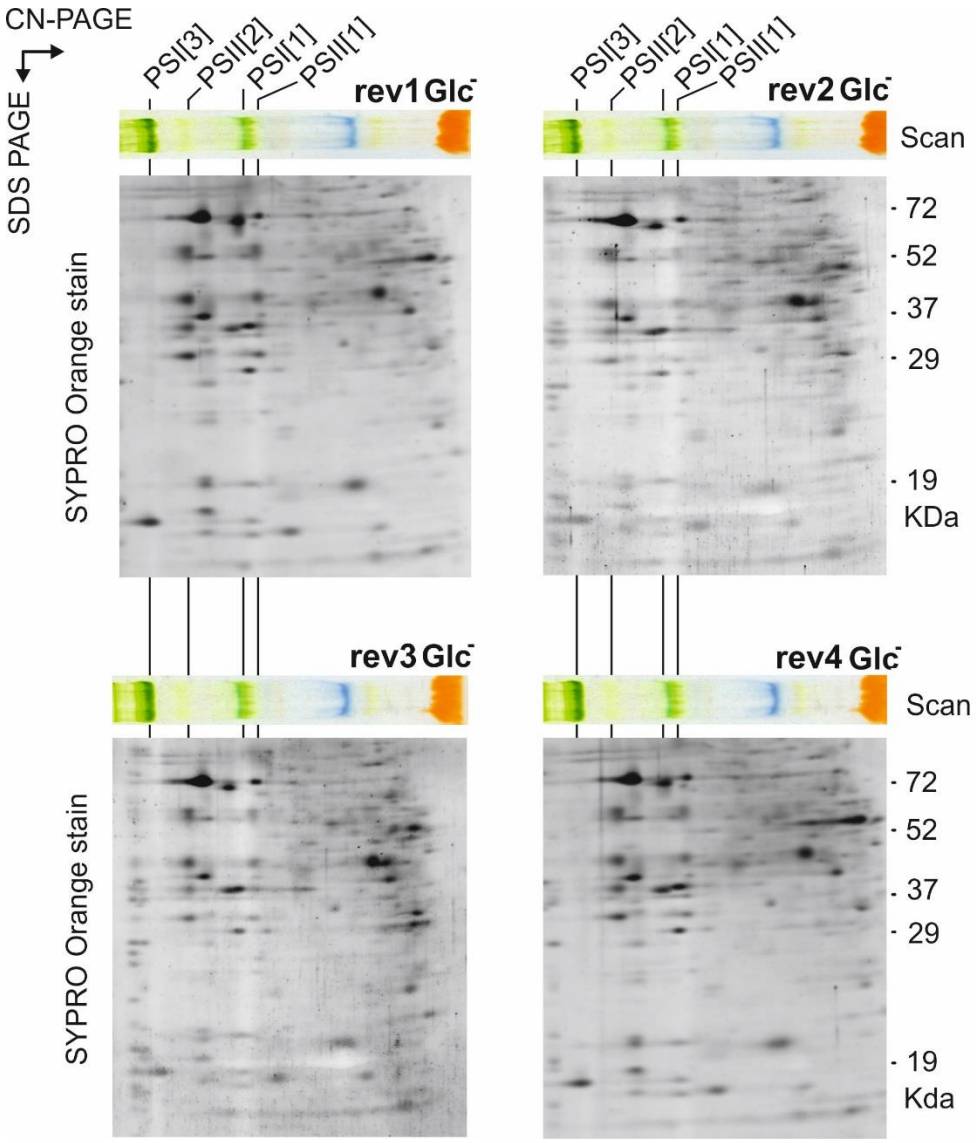

Figure S7. **2D CN/SDS-PAGE of membrane proteins isolated from the radiolabelled *pilD* suppressor strains**. Cells, grown under Glc$^-$ conditions, were radiolabeled with a mixture of [^{35}S]Met/Cys using a 20-min pulse (see Fig. 6B). Isolated membranes were solubilized and separated by CN-PAGE; 4 µg of Chl was loaded for each strain. The gel stripes from the first dimension were cut and separated in the second dimension on two 16-20 % SDS-PAGE gels, each combining a pair of stripes (rev1 and rev4, rev2 and rev3). Gels were stained with SYPRO Orange. PSI[3] is the trimer of PSI, PSI[1] is the monomer of PSI, PSII[2] is the dimer of PSII and PSII[1] is the monomer of PSII.

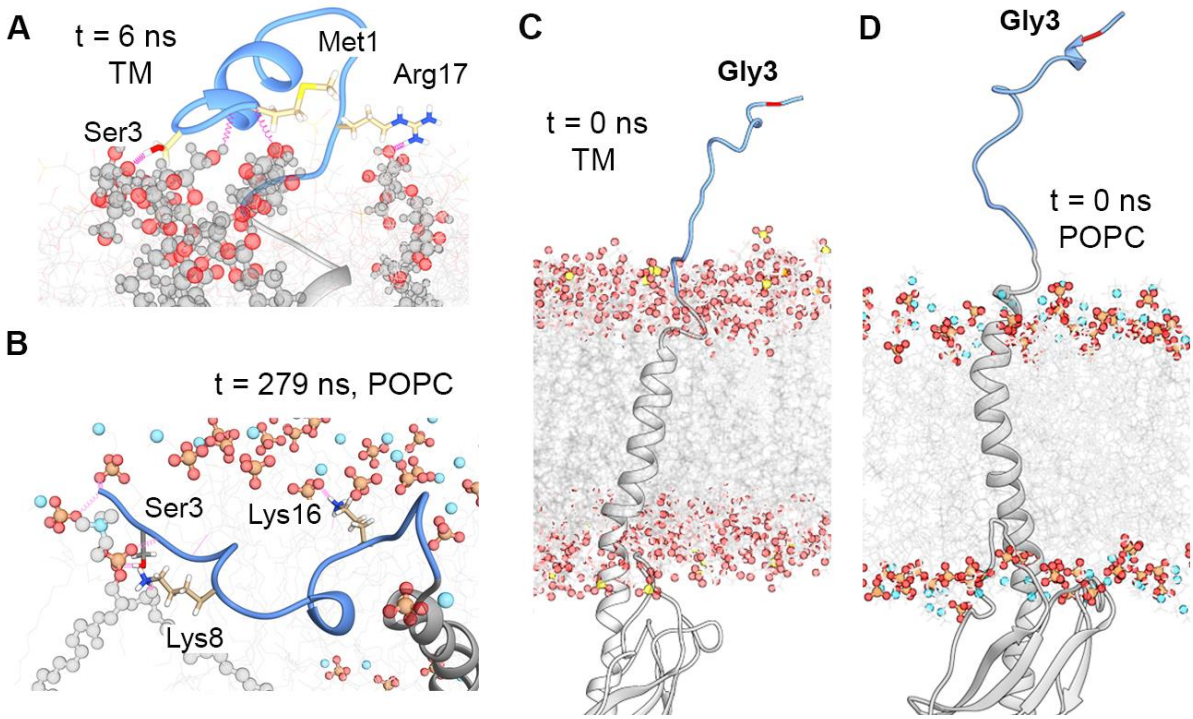

Figure S8. **MD simulations of the *Synechocystis* pPilA1 and pPilA1-S3G proteins in membrane bilayers**. A) A snapshot (6 ns) showing the first stable interaction between the pPilA1 signal peptide and the lipid polar region of TM; established hydrogen bonds are highlighted as purple springs. B) A first stable interaction (279 ns) between pPilA1 signal peptide and POPC lipids. C) and D) Snapshots of the initial (0 ns) conformation of pPilA-S3G in the thylakoid membrane (TM) and the POPC membrane.

SUPPLEMENTARY TABLE

Table S1. A list of oligonucleotides used in this study.

Oligonucleotide	Sequence
pilA1-f	5'-GACAATCATATGGCTAGTAATTTTAAATTC-3'
pilA1-r	5'-GACAATGCTAGCTTTAATTACTTCAGCACCAC-3'
rrn-f	5'-AGCGTCCGTAGGTGGTTATG-3'
rrn-r	5'-CACATACTCCACCGCTTGTG-3

References

Linhartová, M., Bučinská, L., Halada, P., Ječmen, T., Šetlík, J., Komenda, J., and Sobotka, R. (2014). Accumulation of the Type IV prepilin triggers degradation of SecY and YidC and inhibits synthesis of Photosystem II proteins in the cyanobacterium *Synechocystis* PCC 6803. Mol Microbiol **93:** 1207-1223.

linhartova@alga.cz
Function of the Type IV pili proteins in the cyanobacterium *Synechocystis* sp. PCC 6803.
Ph.D. Thesis, 2021

University of South Bohemia in České Budějovice
Faculty of Science
Branišovská 1760
CZ-37005 České Budějovice, The Czech Republic
Phone: +420 387 776 201
www.prf.jcu.cz, e-mail: sekret-fpr@prf.jcu.cz